MICROALGAE FOR METABOLITE PRODUCTION UNDER STRESS CONDITIONS

EDITED BY: Changhong Yao, Wei Xiong and Chengwei Liang
PUBLISHED IN: Frontiers in Bioengineering and Biotechnology

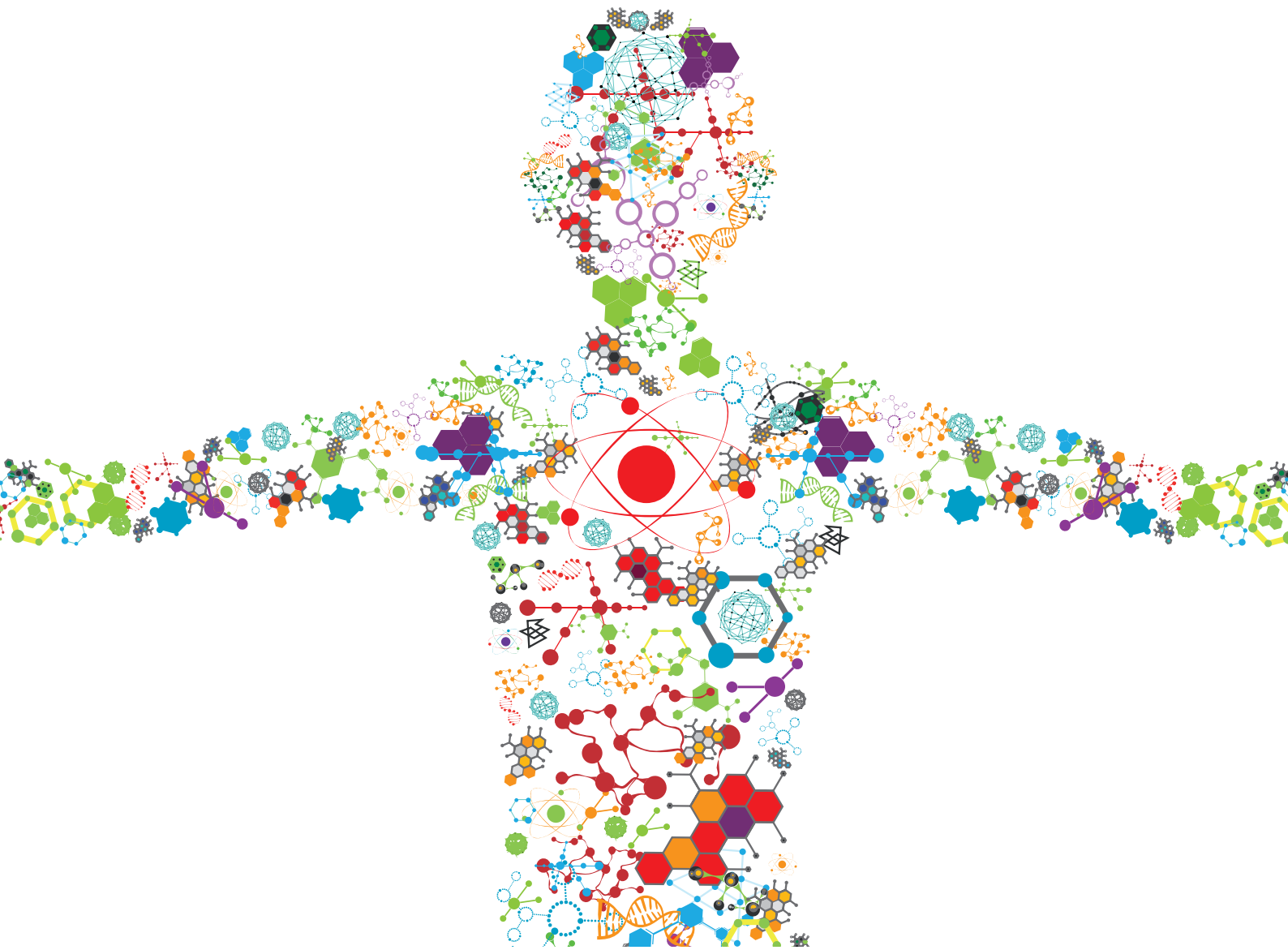

frontiers Research Topics

frontiers

ISSN 1664-8714
ISBN 978-2-88974-401-5
DOI 10.3389/978-2-88974-401-5

About Frontiers

Frontiers is more than just an open-access publisher of scholarly articles: it is a pioneering approach to the world of academia, radically improving the way scholarly research is managed. The grand vision of Frontiers is a world where all people have an equal opportunity to seek, share and generate knowledge. Frontiers provides immediate and permanent online open access to all its publications, but this alone is not enough to realize our grand goals.

Frontiers Journal Series

The Frontiers Journal Series is a multi-tier and interdisciplinary set of open-access, online journals, promising a paradigm shift from the current review, selection and dissemination processes in academic publishing. All Frontiers journals are driven by researchers for researchers; therefore, they constitute a service to the scholarly community. At the same time, the Frontiers Journal Series operates on a revolutionary invention, the tiered publishing system, initially addressing specific communities of scholars, and gradually climbing up to broader public understanding, thus serving the interests of the lay society, too.

Dedication to Quality

Each Frontiers article is a landmark of the highest quality, thanks to genuinely collaborative interactions between authors and review editors, who include some of the world's best academicians. Research must be certified by peers before entering a stream of knowledge that may eventually reach the public - and shape society; therefore, Frontiers only applies the most rigorous and unbiased reviews.
Frontiers revolutionizes research publishing by freely delivering the most outstanding research, evaluated with no bias from both the academic and social point of view. By applying the most advanced information technologies, Frontiers is catapulting scholarly publishing into a new generation.

What are Frontiers Research Topics?

Frontiers Research Topics are very popular trademarks of the Frontiers Journals Series: they are collections of at least ten articles, all centered on a particular subject. With their unique mix of varied contributions from Original Research to Review Articles, Frontiers Research Topics unify the most influential researchers, the latest key findings and historical advances in a hot research area! Find out more on how to host your own Frontiers Research Topic or contribute to one as an author by contacting the Frontiers Editorial Office: frontiersin.org/about/contact

MICROALGAE FOR METABOLITE PRODUCTION UNDER STRESS CONDITIONS

Topic Editors:
Changhong Yao, Sichuan University, China
Wei Xiong, National Renewable Energy Laboratory (DOE), United States
Chengwei Liang, Qingdao University of Science and Technology, China

Dr. Wei Xiong is employed by the National Renewable Energy Laboratory, USA. All other Topic Editors declare no competing interests with regards to the Research Topic subject.

Citation: Yao, C., Xiong, W., Liang, C., eds. (2022). Microalgae for Metabolite Production Under Stress Conditions. Lausanne: Frontiers Media SA.
doi: 10.3389/978-2-88974-401-5

Table of Contents

frontiers in Bioengineering and Biotechnology

EDITORIAL
published: 06 January 2022
doi: 10.3389/fbioe.2021.812425

Editorial: Microalgae for Metabolite Production Under Stress Conditions

*Chengwei Liang**

College of Marine Science and Biological Engineering, Qingdao University of Science and Technology, Qingdao, China

Keywords: microalga, microalga biomass, high-value added products, stress condition, molecular mechanism

Editorial on the Research Topic

Microalgae for Metabolite Production Under Stress Conditions

Microalgae are found in marine and freshwater environments and convert carbon dioxide into potential biofuels (carbohydrates, lipids), foods and high-value products such as lutein, chlorophyll, and zeaxanthin driven by solar energy, normally under certain stressful cultivation conditions. The past 20 years have seen a flood of patents related to microalgal biofuels as shown in the article by Li et al. Briefly, the majority of patents are related to strains and their cultivation under different conditions, especially some stress conditions, the introduction of regulating reagents, the combination of different downstream treatments and bio-refinery methods or processes. In general, there are no natural microalgae suitable for high value-added production directly. Therefore, in the last 2 decades, the artificial modification of natural strains is concerning, especially with the development of gene engineering.

In most instances, the accumulation of high value-added products occurs under stress conditions, which adversely affects the growth of microalgae. Thus, the industrial production of microalgae may have been limited by biomass supply. Therefore, studying the mechanism of accumulation of high additive products under stress conditions may solve this problem. In this field of research, several articles reported the molecular mechanism of microalgae from different aspects. Xi et al. reported that reactive oxygen species may serve as mediators or second messengers to trigger the fine-tuning of key genes that are involved in photosynthesis and β-carotene biosynthesis in *Dunaliella salina* under stress conditions. The changes in photosynthesis efficiency and energy metabolism will be useful for β-carotene accumulation in *D. salina* under stress conditions. Wang et al. examined six transcription factors (TFs) belonging to the MYB, MYB_related, NF-YC, Nin-like, and C3H families involved in the transcription regulation of 27 astaxanthin synthesis-related genes according to the regulatory network which will help to understand the transcription regulatory mechanism of astaxanthin synthesis in *Haematococcus pluvialis* under stress conditions. These TFs could affect astaxanthin synthesis by directly regulating the β-carotene ketolase gene (CrtO) which is the key gene involved in astaxanthin biosynthesis. Polyunsaturated fatty acids (PUFAs) compositions in serine/threonine kinases (STKs) gene spkD and spkG knockout mutant *Synechocystis* sp. PCC6803 are lower than those in the wild-type, which showed that STKs play important roles in regulating PUFA biosynthesis in *Synechocystis* sp. PCC6803 (Chen et al.). These results may also have implications for other algae.

In the past decades, various cultivation strategies including heterotrophic cultivation, photoautotrophy-to-heterotrophy cultivation and heterotrophy-to-photoautotrophy cultivation modes in addition to photoautotrophic cultivation have emerged to enhance microalgal lipid production in order to balance the costs. Heterotrophy-to-photoautotrophy cultivation takes advantages of both cultivation modes, which produce high-quality biomass via heterotrophy and induce biosynthesis of particular end-products under photoautotrophic conditions. Hu Zhang et al. studied the mechanisms underlying the enhanced biomass and lipid production of *Scenedesmus*

OPEN ACCESS

Edited and reviewed by:
Manfred Zinn,
HES-SO Valais-Wallis, Switzerland

***Correspondence:**
Chengwei Liang
liangchw117@126.com

Specialty section:
This article was submitted to Nanobiotechnology, a section of the journal Frontiers in Bioengineering and Biotechnology

Received: *10 November 2021*
Accepted: *13 December 2021*
Published: *06 January 2022*

Citation:
Liang C (2022) Editorial: Microalgae for Metabolite Production Under Stress Conditions. Front. Bioeng. Biotechnol. 9:812425. doi: 10.3389/fbioe.2021.812425

acuminatus during trophic transition from heterotrophy to photoautotrophy under stress conditions (high light and N limited conditions). Carbon metabolism was deduced to provide sufficient energy to sustain vigorous growth of *S. acuminatus* cells under stress. Enhanced lipid production may be attributable to the upregulation of acetyl-CoA carboxylase (ACCase) and diacylglycerol acyltransferase 2(DGAT2)at the gene expression level.

Microalgae-bacteria co-cultivation systems are another new avenue that can be investigated to improve the mass production of microalgae. Ouyang et al. employed metabolomics to gain a better understanding of the underlying causes of improvements in growth and paramylon production in *Euglena gracilis* when co-cultivated with *Vibrio natriegens*. Some differential metabolites including economically important metabolites such as choline, ectoine, 4R-aminopentanoic acid, methyl N-methylanthranilate and methyl carbamate were found in the co-cultivation group which may provide clues for the industrial application of *E. gracilis*.

More knowledge on the molecular mechanisms of high-value products in microalgae can guide utilization of key molecules to solve the problems that limit the commercial application of microalgae. In this area of research, the chloroplast glyceraldehyde-3-phosphate dehydrogenase (cGAPDH) overexpressed strain *Chlamydomonas reinhardtii* P3-GAPDH reported in the article (Zhu et al.) demonstrated higher carbon fixation and PUFA synthesis efficiency. The overexpression of chloroplast GAPDH gene enabled the P3-GAPDH to maintain high photosynthetic activity and promote biomass production, i.e., the carbohydrate and lipid content increased by 96.6 and 93. 4%, respectively, under normal cultivation conditions. Thus, it is hoped that this will lead to simultaneous high production of biomass and energy storage compounds.

Microalgae are also good organisms for bioremediation applications due to their strong acclimation to changing metal ion concentrations in the environment via metal homeostasis. Metabolomics and proteomic analysis were used in two studies (He et al. and Zhen et al.), to examine the mechanism of acclimatization of microalgae to metal ions. The results showed that in order to meet the intracellular requirements of ions, metals can be transferred into the cell via the uptake system and macromolecular metabolites such as proteins, pigments, and lipids were regulated to adapt to stress conditions.

Microalgae have great application potential as they can accumulate high-value products under stress conditions. However, stress conditions usually suppress the growth of microalgae which limit their commercial application. The information on this topic will provide clues to achieve two-win between the production of high microalgal biomass and high value compounds.

AUTHOR CONTRIBUTIONS

CL drafted the manuscript.

FUNDING

This work was supported by National Natural Science Foundation of China grant (31770393).

Conflict of Interest: The author declares that the research was conducted in the absence of any commercial or financial relationships that could be construed as a potential conflict of interest.

Publisher's Note: All claims expressed in this article are solely those of the authors and do not necessarily represent those of their affiliated organizations, or those of the publisher, the editors and the reviewers. Any product that may be evaluated in this article, or claim that may be made by its manufacturer, is not guaranteed or endorsed by the publisher.

frontiers in Bioengineering and Biotechnology

MINI REVIEW
published: 26 August 2020
doi: 10.3389/fbioe.2020.01035

A Quick Look Back at the Microalgal Biofuel Patents: Rise and Fall

Dongzi Li[1], Wei Du[2], Wantao Fu[1] and Xupeng Cao[2,3,4,5]**

[1] Marine College of Science-Technology and Environment, Dalian Ocean University, Dalian, China, [2] Dalian Institute of Chemical Physics, Chinese Academy of Sciences, Dalian, China, [3] State Key Laboratory of Catalysis, Dalian Institute of Chemical Physics, Chinese Academy of Sciences, Dalian, China, [4] Dalian National Laboratory of Clean Energy, Division of Solar Energy, Dalian Institute of Chemical Physics, Chinese Academy of Sciences, Dalian, China, [5] Dalian Key Laboratory of Energy Biotechnology, Dalian Institute of Chemical Physics, Chinese Academy of Sciences, Dalian, China

Microalgae is a promising organism as the feedstock of the next generation biofuels, as well as high value nature products, such as astaxanthin, normally under certain stress cultivation conditions. With the clear industrialization targets, there have been two waves of microalgae R&D from the last century and showed obvious energy-driven trends. The overall R&D came into a valley now, however, the promising is still there. So here, from the industrialization point of view, the patent evolution concerning the microalgae for biofuels in the second wave were reviewed and summarized. These technology information will help the scientists to join together with industry to drive the next boost.

Keywords: microalgae, patent, industrialization, stress cultivation, biofuel

OPEN ACCESS

Edited by:
Chengwei Liang,
Qingdao University of Science and Technology, China

Reviewed by:
Xinqing Zhao,
Shanghai Jiao Tong University, China
Qiang Wang,
Institute of Hydrobiology (CAS), China

****Correspondence:***
Wantao Fu
fuwantao@dlou.edu.cn
Xupeng Cao
c_x_p@dicp.ac.cn

Specialty section:
This article was submitted to Bioprocess Engineering, a section of the journal Frontiers in Bioengineering and Biotechnology

Received: *21 July 2020*
Accepted: *10 August 2020*
Published: *26 August 2020*

Citation:
Li D, Du W, Fu W and Cao X (2020) A Quick Look Back at the Microalgal Biofuel Patents: Rise and Fall. Front. Bioeng. Biotechnol. 8:1035. doi: 10.3389/fbioe.2020.01035

INTRODUCTION

Microalgae are found in both marine and freshwater environments and convert carbon dioxide to potential biofuels (carbohydrates, lipids), foods and high-value products, driven by solar energy, as well as are good organisms for bioremediation applications (Sheehan et al., 1998; Chisti, 2007; Hu et al., 2008; Mata et al., 2010; Wijffels and Barbosa, 2010; Chen et al., 2018; Khan et al., 2018; Shuba and Kifle, 2018). With the afraid of fossil fuel crisis, it's officially considered as a solution at 1978 under the program funded by the US Department of Energy's Office of Fuels Development, known as the Aquatic Species Program (or ASP), which main focus was the production of biodiesel from high lipid-content algae grown in ponds, utilizing waste CO_2 from coal fire power plants (Sheehan et al., 1998). Over the nearly two decades (from 1978 to 1996), ASP stopped far from the industrialization of microalgae as fuels stocks, one reason for which was the high life-span cost comparing with the relative low price of the fuels. However, ASP promoted the R&D of microalgae from the collection and evaluation of thousand species, the science of manipulating the genes and metabolism, to the engineering of production systems. The detailed contributions of ASP was well-documented Sheehan et al. (1998).

While the oil price dramatically increased from the beginning of the twenty-first century, microalgae come back the visual field again with the support from governments, the industries and the venture capitals all over the world, but cooled down after 2015 till now, indicated by the takeover of Solazyme by TerraVia in US and retreat of ENN in China. The rise and fall of it was the result of multi factors, which was not only the affair of science and technology. As one of the key components of the innovation, the patent bridges the lab and the factory. Here, after the second wave of microalgae R&D, the patent evolution during the last 20 years were quickly reviewed for the reference to the next boost of microalgae industrialization.

THE ANALYSIS OF MICROALGAE BIOFUELS RELATED PATENTS FROM LAST 20 YEARS

Patents Collection and Refinement

The patents data used here were mainly from Patsnap® patent database and Derwent World Patents Index was used as an amendment. The keywords used for index were provided in **Supplementary Data File**. More than ten thousand patents were further refined, considering the fact that microalgae biofuels production is the process to convert solar energy to chemical energy by photosynthesis in a direct or indirect manner, the photosynthesis related information should be shown in the claims, such as autotrophic growth, or with light, etc.

Differing to normal research publications, the patent is a kind of legal documents and a collection of patent applications covering the same or similar technical content were defined as a family, which can help us to focus on the technical part of patents, other than the different legal status. After refine, 3,393 items from 730 families were extracted for the further analysis. To verify the coverage of the index, 11 patents from authors were used as a reference, which covers the strain screening and application to the downstream bio-refinery to biofuels, and all of them were included by above index.

The Patent Application Amount Change With Crude Oil Price

The aim of the development of biofuels is the makeup or replacement of traditional fossil fuels, especially the oil, for the reason of the final products of the biofuels. So the difference between the cost of biofuels to oil should be a driving force of the R&D development of microalgae.

The crude oil prices per barrel of West Texas Intermediate (WTI) with the adjustment for inflation using the headline CPI were collected from Macrotrends database[1]. For simplification, the average price of January of each were used to compared with the yearly patent application status. In **Figure 1**, the overall correlation of oil price to the number of patent application is about 0.86 before 2015 and 0.84 till now.

Although only a little changes in the correlation factors shown in the last 5 years, serious effects on the direction of microalgae R&D existed. It will detailed discussed in the "Discussion" section.

Global and Technical Distributions

Nearly 25% patents were held by United States (975) followed by Japan (541), China (289), Australia (164), Canada (155), and South Korea (119). The validated patent number was shown in **Supplementary Figure 1**, briefly, more than half of them are validated till the end of June, 2020.

As an intellectual property (IP) tools, it's reasonable that most top player of patent applications were companies, such as Solazyme Inc. (now is acquired by Corbion) with 313 items and nearly 10% of the patent pool analyzed (see **Supplementary Table 1**). However, the Scripps Research Institute also holds 46 items and ranked first among research institutes.

To obtain an overall technical view of these patent, International Patent Classification (IPC[2]) information was used to classify and summarize the patents in the pool. The top related IPC classes were listed in **Supplementary Table 2** and the IPC class distribution in different countries or organizations were shown in **Supplementary Figure 1**. The yearly distribution of major IPC was shown in **Supplementary Figure 2**. Briefly, the majority of patents are related to strains and their cultivation under different condition, especially some stress conditions, the introduction of some regulating reagents, the combination of different downstream treatment and bio-refinery methods or processes.

The most related class is C12N, which is directly related to microalgae itself, including compositions, propagating, preserving, or maintaining, and also including mutation or genetic engineering of microalgae as well as novel culture media. In the patent pool, 58% patents were concerned with this class. The second hot class is C12P, which relates to the processes to synthesis a desired chemical compound or composition or to separate optical isomers from a racemic mixture. It consisted with the aim of these patent to produce biofuels, which are mostly in the form of fatty acids or lipids, or carbohydrates. Among them, some multifunctional compounds, other than the feedstock to biofuels, such as special carbohydrates, pigments or medium chain fatty acids, were drawing more attentions.

After more than thousands of strains, there was no natural microalga suitable for the biofuel production directly. So in the last two decades, the artificial modification of natural strains was also concerned, especially with the development of gene engineering, such as CRISPR technology in US20160208243A1 family. So the IPC A01H reached the third rank in the second wave.

Core Techniques Within Patents for Microalgae Biofuels Based on Citation Relationships

The citation of the patent usually represented the core techniques in the field and direction of the knowledge flow (Alcácer and Gittelman, 2006). The citation in the patent is not as strict as scientific publications, however, the core techniques cannot be ignored due to their potential legal risks. In the patent pool, the citation relationship were summarized by using Cytoscape (version 3.8.0). Some important knots were significantly shown with concentrated links (**Supplementary Figure 3**).

The most cited validated patents, with cited number over 100, were listed in the **Table 1**. Among them, only US20160208243A1 was applied in 2015, and other are almost older than 10 years and close to the edge of patent term. In this 16 top cited patents, five of them were about the gene manipulation of microalgae, eight of them were about the cultivation to promote the biofuel production and three of them were concerned with the downstream bio-refinery. Bio-refinery has the advantages

[1]https://www.macrotrends.net/1369/crude-oil-price-history-chart

[2]https://www.wipo.int/classifications/ipc/en/

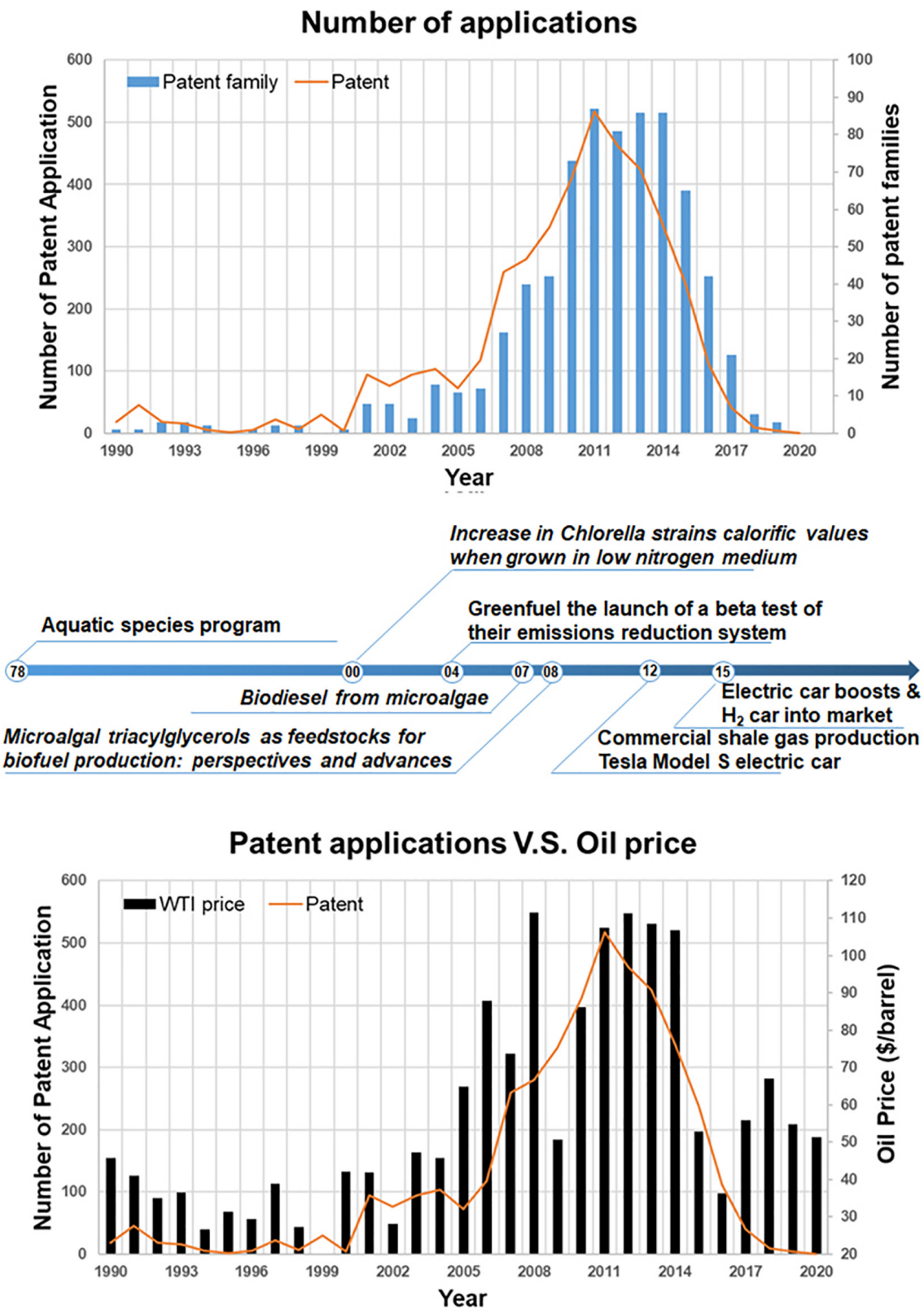

FIGURE 1 | The patent application changes in last 30 years. The upper figure is the application in terms of single patent and patent family. The bottom figure is the application changes with the crude oil prices. The timeline in the middle marks some milestones for microalgae biofuel R&D development.

TABLE 1 | Valid patents with more than 100 cites.

No.	Patent number	Year	Cited number	Title	Patent Owner	Description
1	US6750048	2001	361	Solventless extraction process	OMEGA TECHNOLOGIES	A method for extracting lipids from microorganisms without using organic extraction solvent.
2	US20080160593A1	2007	354	Two-stage process for producing oil from microalgae	GENIFUEL CORPORATION	By promoting sequential photoautotrophic and heterotrophic growth, a biofuels production process from cultivating an oil-producing algae.
3	US20040019927A1	2003	276	Polynucleotides and polypeptides in plants	MENDEL BIOTECHNOLOGY, INC.	About plant transcription factors and using to produce transgenic plants with advantageous properties.
4	US20090148918A1	2008	220	Glycerol feedstock utilization for oil-based fuel manufacturing	CORBION BIOTECH, INC.	Methods of manufacturing biodiesel and other oil-based compounds using glycerol and its combinations as an energy source in fermentation of oil-bearing microorganisms.
5	US20050009049A1	2004	216	Expanding the eukaryotic genetic code	SCRIPPS RESEARCH INSTITUTE	Compositions and methods for producing translational components that expand the number of genetically encoded amino acids in eukaryotic cells.
6	US20080160591A1	2007	204	Diffuse light extended surface area water-supported photobioreactor	COLORADO STATE UNIVERSITY RESEARCH FOUNDATION	A scalable photobioreactor system for efficient production of photosynthetic microorganisms such as microalgae and cyanobacteria.
7	US7883882	2009	196	Renewable chemical production from novel fatty acid feedstocks	CORBION BIOTECH, INC.	Methods of manufacturing renewable chemicals through the manufacture of novel triglyceride oils followed by chemical modification of the oils.
8	US20090047721A1	2008	186	Renewable diesel and jet fuel from microbial sources	CORBION BIOTECH, INC.	Methods of manufacturing alkanes from triglyceride oils produced through fermentation of oil-bearing microbes.
9	US20090011480A1	2009	185	Use of cellulosic materials for cultivation of microorganisms	CORBION BIOTECH, INC.	Methods of cultivating oil-bearing microbes using cellulosic material.
10	US20040265952A1	2004	163	Unnatural reactive amino acid genetic code additions	ENERGY, UNITED STATES DEPARTMENT OF	Compositions and methods for producing translational components that expand the number of genetically encoded amino acids in eukaryotic cells.
11	US20160208243A1	2015	162	Novel CRISPR enzymes and systems	THE BROAD INSTITUTE INC.; PRESIDENT AND FELLOWS OF HARVARD COLLEGE; MASSACHUSETTS INSTITUTE OF TECHNOLOGY	Systems, methods, and compositions for targeting nucleic acids, including microalgae.
12	US20110092726A1	2011	137	System for cultivation and processing of microorganisms, processing of products therefrom, and processing in drillhole reactors	WINWICK BUSINESS SOLUTIONS PTY LTD	Cultivating autotrophic microorganisms, particularly microalgae, in a bioreactor to enable laminar flow which in cross section is closed and which has transparent walls through which the culture is irradiated to enable photosynthesis.
13	US20030037355A1	2001	131	Methods and compositions to modulate expression in plants	SCRIPPS RESEARCH INSTITUTE; SYNGENTA PARTICIPATIONS AG	The use of zinc finger proteins and fusions of said proteins to regulate gene expression and metabolic pathways.
14	US20110086386A1	2010	124	Algae biomass fractionation	TRUCENT, INC.	A method of fractionating biomass, and recovering cell and cell derived products from the non-polar solvent solution and polar biomass solution.
15	US20080118964A1	2006	117	Continuous-batch hybrid process for production of oil and other useful products from photosynthetic microbes	CELLANA, INC.	Cultivating photosynthetic microbes in closed systems for continuous cultivation and open systems for batch cultivation.
16	US20100151538A1	2009	107	Cellulosic cultivation of oleaginous microorganisms	CORBION BIOTECH, INC.	Cultivation of oleaginous microorganisms on feedstocks including depolymerized cellulosic material such as corn stover, Miscanthus, forage sorghum, sugar beet pulp, and sugar cane bagasse.

of high atomic economy and was expected as an integrated solution for energy, wastewater treatment, food and nutrient supply (Suganya et al., 2016). However, maybe limited by the biomass supply, except on the health-related approaches, there was few reports on the stable industrialization of bio-refinery or co-production established.

DISCUSSION

The Driving Force for the Future Microalgae R&D Changes

As shown in **Figure 1**, at the beginning, the afraid of depletion of fossil fuels drove the first wave of microalgae R&D, mostly under the support of ASP by the US DOE and more likely a pure scientific affair to produce bio hydrogen or bio transportation fuels. The higher cost of microalgae cultivation and relative low oil price caused the cease of the first wave in 1995 (Sheehan et al., 1998). But, the accumulation on strains and numerous technologies helps the form of the second wave while the crude oil price dramatically increased in the early of 21 century.

The stress condition cultivation became the sign of the second wave, mostly started by Illman et al.'s (2000) work on the low nitrogen cultivation for high calorific value biomass to develop renewable energy resource. Differed to the first wave, with the increase of oil price, the microalgae biofuel R&D became a move by both scientists and venture capitals (VCs), which was marked by the launch of the beta test of CO_2 and NO_x emission reduction system by Greenfuel in MIT in 2004. Following Chisti and Hu et al.'s direction in 2007–08 (Chisti, 2007; Hu et al., 2008), around the stressed cultivation of microalgae, a large amount patents were applied and covered the whole processes of microalgae biofuel production. The driving force of this period was still the high crude oil price.

Things changed from 2012, when commercial shale gas realized and Tesla Model S electric car came into the market, which caused the energy production and consuming structure reformed. With less progress in the cut of production cost or significant increase in production efficiency, the VCs and big companies turned their focus. Without enough support, the patent application decrease rapidly.

After 2015, although the oil price increased a little bit, the popularization of electric car and the development of other renewable energy resources caused the traditional driving force of microalgae R&D lost.

New Driving Force From Synthetic Biology and Customized Natural Products Production

The development of biotechnology brings the hope to meet the next wave of microalgae R&D. Due to its fast growth, unicellular form, high photosynthesis capacity and diverse secondary metabolisms, the microalgae based CO_2 and NO_x capture will be a new driving force for the innovation of a new gene manipulation, cell or organelle factory building, non-meat protein production, medium length chain fatty acids synthesis. And above targets also consisted with the major technical classes, including C12N15, C12P7, and C12N1.

AUTHOR CONTRIBUTIONS

DL and XC collected and manually classified the patents and drafted the manuscript. WD organized and guided the analysis. WF analyzed the collected patents and drafted the manuscript. All authors contributed to the article and approved the submitted version.

FUNDING

This work was supported by the DMTO grant (DMTO201409) from Dalian Institute of Chemical Physics, Chinese Academy of Sciences, Dalian Key Laboratory of Energy Biotechnology and NSFC grant (21878285) from National Natural Science Foundation of China.

ACKNOWLEDGMENTS

We thank Dr. Xue Song from Dalian University of Technology for her comments and suggestion on microalgae biotechnology development.

SUPPLEMENTARY MATERIAL

The Supplementary Material for this article can be found online at: https://www.frontiersin.org/articles/10.3389/fbioe.2020.01035/full#supplementary-material

REFERENCES

Alcácer, J., and Gittelman, M. (2006). Patent citations as a measure of knowledge flows: the influence of examiner citations. *Rev. Econ. Stat.* 88, 774–779. doi: 10.1162/rest.88.4.774

Chen, H., Wang, J., Zheng, Y., Zhan, J., He, C., and Wang, Q. (2018). Algal biofuel production coupled bioremediation of biomass power plant wastes based on *Chlorella* sp. C2 cultivation. *Appl. Energy* 211, 296–305. doi: 10.1016/j.apenergy.2017.11.058

Chisti, Y. (2007). Biodiesel from microalgae. *Biotechnol. Adv.* 25, 294–306. doi: 10.1016/j.biotechadv.2007.02.001

Hu, Q., Sommerfeld, M., Jarvis, E., Ghirardi, M., Posewitz, M., Seibert, M., et al. (2008). Microalgal triacylglycerols as feedstocks for biofuel production: perspectives and advances. *Plant J.* 54, 621–639. doi: 10.1111/j.1365-313x.2008.03492.x

Illman, A. M., Scragg, A. H., and Shales, S. W. (2000). Increase in *Chlorella* strains calorific values when grown in low nitrogen medium. *Enzyme Microb. Technol.* 27, 631–635. doi: 10.1016/s0141-0229(00)00266-0

Khan, M. I., Shin, J. H., and Kim, J. D. (2018). The promising future of microalgae: current status, challenges, and optimization of a sustainable and renewable industry for biofuels, feed, and other products. *Microb. Cell. Fact.* 17:36. doi: 10.1186/s12934-018-0879-x

Mata, T. M., Martins, A. A., and Caetano, N. S. (2010). Microalgae for biodiesel production and other applications: a review. *Renew. Sust. Energ. Rev.* 14, 217–232. doi: 10.1016/j.rser.2009.07.020

Sheehan, J., Dunahay, T., Benemann, J., and Roessler, P. (1998). *Look Back at the U.S. Department of Energy's Aquatic Species Program: Biodiesel from Algae; Close-Out Report*. Golden, CO: National Renewable Energy Lab, doi: 10.2172/15003040

Shuba, E. S., and Kifle, D. (2018). Microalgae to biofuels: 'Promising' alternative and renewable energy, review. *Renew. Sust. Energ. Rev.* 81, 743–755. doi: 10.1016/j.rser.2017.08.042

Suganya, T., Varman, M., Masjuki, H. H., and Renganathan, S. (2016). Macroalgae and microalgae as a potential source for commercial applications along with biofuels production: a biorefinery approach. *Renew. Sust. Energ. Rev.* 55, 909–941. doi: 10.1016/j.rser.2015.11.026

Wijffels, R. H., and Barbosa, M. J. (2010). An outlook on microalgal biofuels. *Science* 329, 796–799. doi: 10.1126/science.1189003

Conflict of Interest: The authors declare that the research was conducted in the absence of any commercial or financial relationships that could be construed as a potential conflict of interest.

frontiers in Bioengineering and Biotechnology

ORIGINAL RESEARCH
published: 12 January 2021
doi: 10.3389/fbioe.2020.603513

A Carbon Fixation Enhanced *Chlamydomonas reinhardtii* Strain for Achieving the Double-Win Between Growth and Biofuel Production Under Non-stressed Conditions

Zhen Zhu[1,2,3,4†], Huijiao Cao[1,2,3,4†], Xu Li[5], Junfeng Rong[5], Xupeng Cao[2,3,4*] and Jing Tian[1*]*

[1] School of Bioengineering, Dalian Polytechnic University, Dalian, China, [2] State Key Laboratory of Catalysis, Dalian Institute of Chemical Physics, Chinese Academy of Sciences, Dalian, China, [3] Division of Solar Energy, Dalian National Laboratory of Clean Energy, Dalian Institute of Chemical Physics, Chinese Academy of Sciences, Dalian, China, [4] Dalian Key Laboratory of Energy Biotechnology, Dalian Institute of Chemical Physics, Chinese Academy of Sciences, Dalian, China, [5] Research Centre of Renewable Energy, Research Institute of Petroleum Processing, Sinopec, Beijing, China

The stressed cultivations are widely used in microalgae R&D for the biofuel production with the repress on growth to a certain degree, which limits the overall productivity. The balance between the growth and energy storage compounds accumulation is a target needing the combination of both strain selection or construction and culture optimization. Here, an engineered strain of *Chlamydomonas reinhardtii*, in which the chloroplast type glyceraldehyde-3-phosphate dehydrogenase (cGAPDH) was overexpressed and named as P3-GAPDH, was cultured on the Algal Station platform. Compared with wild type (WT), *C. reinhardtii* CC137c, in Tris-acetate-phosphate (TAP) medium, the highest density of WT and P3-GAPDH were 1.23 ± 0.13 and 1.74 ± 0.09 g L^{-1} within 96 h, and the maximum biomass productivity was 24.30 ± 1.65 and 28.54 ± 1.43 mg L^{-1} h^{-1}, respectively. In terms of the energy storage compounds, both carbohydrate and fatty acids content doubled in P3-GAPDH, from 0.13 ± 0.02 to 0.26 ± 0.04 g L^{-1} for carbohydrate and from 0.08 ± 0.01 to 0.16 ± 0.01 g L^{-1} for fatty acids, among which poly unsaturated fatty acids increased by 65.8%. Together with the continuous monitor of the chlorophyll fluorescence dynamics parameters F_v/F_m and F_v'/F_m' and pH of culture, enhanced Calvin cycle by overexpressed cGAPDH promoted the carbon conversion and subsequent energy storage compounds accumulation. *C. reinhardtii* P3-GAPDH strain showed the potential as a good chassis with high carbon conversion ability.

Keywords: biofuel, *Chlamydomonas reinhardtii*, nitrogen depletion, carbon fixation, photosynthesis, algal station, fatty acids

OPEN ACCESS

Edited by:
Chengwei Liang,
Qingdao University of Science and Technology, China

Reviewed by:
Noppol Leksawasdi,
Chiang Mai University, Thailand
Ankush Karemore,
Georgia Institute of Technology, United States

****Correspondence:***
Junfeng Rong
rongjf.ripp@sinopec.com
Xupeng Cao
c_x_p@dicp.ac.cn
Jing Tian
tianjing@dlpu.edu.cn

† These authors have contributed equally to this work

Specialty section:
This article was submitted to Bioprocess Engineering, a section of the journal Frontiers in Bioengineering and Biotechnology

Received: *07 September 2020*
Accepted: *11 December 2020*
Published: *12 January 2021*

Citation:
Zhu Z, Cao H, Li X, Rong J, Cao X and Tian J (2021) A Carbon Fixation Enhanced Chlamydomonas reinhardtii Strain for Achieving the Double-Win Between Growth and Biofuel Production Under Non-stressed Conditions. Front. Bioeng. Biotechnol. 8:603513. doi: 10.3389/fbioe.2020.603513

INTRODUCTION

The green algae *Chlamydomonas reinhardtii* is a model organism that has been systematically studied for more than 50 years (Fields et al., 2018). It has the most abundant physiological and biological information among microalgae with well-annotated genome information, and its genome of chloroplasts and mitochondria has also been sequenced (Harris, 2001). It's a good candidate for biohydrogen and biofuels development under certain stressed conditions, such as sulfur or nitrogen depletion condition (Faraloni et al., 2011; Gargouri et al., 2017). As a photosynthetic unicellular model organism, it has the advantage of both plant and microbial expression systems, providing the most abundant gene engineering operation possibilities in synthetic biology (Merchant et al., 2007).

As a single cell photosynthetic organism, *C. reinhardtii* provides a platform for the production of a wide range of complex proteins, pigments, and energy storage compounds, and is increasingly recognized as a cheap, scalable, and safe "cell factory" of high-value products as well as bioenergy (Carrera Pacheco et al., 2018). Till now, on the bioenergy and carbon sequestration aspect, *C. reinhardtii* has been investigated on the mechanism and application in hydrogen production (Degrenne et al., 2010; Scoma et al., 2012; Chen et al., 2014), biodiesel production (Fan and Zheng, 2017; Yang et al., 2018) and wastewater treatment (Faraloni et al., 2011), etc.

Like other microalgae, nitrogen depletion stress is a popular method to improve the carbohydrate and triacylglycerols (TAG) content of *C. reinhardtii*. However, the overall biomass productivity was limited due to the inhibition of the growth under stress conditions. Aiming the carbon sequestration and biofuel production, it is necessary to formulate cultivate strategies to balance the energy storage compounds and cell growth to achieve sustainable production with the maximum time-space yield (Moon et al., 2013). By selecting the appropriate cultivation mode and medium, the synchronized proteins, starch, and oils production with cell growth were also achieved in microalgae (Duong et al., 2015a,b; Wang et al., 2015; Zhang et al., 2019; Kim et al., 2020). Besides optimization of the cultivation, screening, or constructing new strains, which are more suitable for guided production under the controlled conditions is a fundamental solution. Because some intrinsic metabolism consumption for stress response is not necessary furthermore in the controlled cultivation and the recycle of this part of carbon and energy could provide the biomass accumulation 20–50% more, such as shift the carbon of photorespiration to carbon fixation in tobacco resulting a 40% increase in biomass productivity (South, 2019). In our previous work, by overexpression of chloroplast glyceraldehyde-3-phosphate dehydrogenase (cGAPDH) in *C. reinhardtii*, the continuous energy storage compounds accumulation was achieved in the flask cultivation (Zhu et al., 2019). cGAPDH is the key enzyme in the Calvin cycle and the joint of carbon fixation and carbon metabolism in the chloroplast. However, the mechanism underlying is unknown. Especially, the previous evaluations were carried out in the flasks with seldom shakes, in which the CO_2 supply was mostly based on the diffusion from the air and the performance under CO_2 sufficient conditions was unknown.

Here, the above *C. reinhardtii* strain, P3-GAPDH, was investigated by continuously monitoring its chlorophyll fluorescence dynamics, together with the fatty acids profiling changes to make a deeper understanding of physiological and biochemical aspects. Briefly, the *C. reinhardtii* CC137c (WT) and the dominant P3-GAPDH were parallelly evaluated by self-developed the Algal Station (AS) platform (Cao et al., 2019) in 1.5 L bubbling flat-plate bioreactors under the mixotrophic cultivation modes in TAP medium. AS platform was developed by the Dalian Institute of Chemical Physics, Chinese Academy of Sciences, and it's the first commercial system to use the maximum quantum yield of photosynthesis II, F_v/F_m, as an online control parameter for microalgae cultivation together with light intensity, optical density (OD), pH, etc., and meets the requirement from lab to industry by South China University of Technology, Clean Energy Development Center of ENN Group and Microalgae Biotechnology Center of SDIC. The online monitoring of chlorophyll fluorescence dynamics, pH and OD, together with offline measurement of fatty acids profile were carried out to make a detailed evaluation.

MATERIALS AND METHODS

Microalgal Strains and Medium

Microalgal strain *C. reinhardtii* CC137c (wild type, WT) was provided by the Chlamydomonas Resource Center at Duke University. The chloroplast Glyceraldehyde-3-phosphate dehydrogenase (cGAPDH) overexpressed strain *C. reinhardtii* P3-GAPDH was obtained in our previous work (Zhu et al., 2019). Both strains were cultured in TAP media (Kosourov et al., 2007). The seed cells were first cultured in 100 mL conical flasks with 50 mL media. After 3 days, the cells were transferred into 3 L conical flasks with 1 L medium, respectively, under a 14/10 h light/dark cycle with the illumination of the white fluorescent lights at 50 μmol m^{-2} s^{-1} as seeds for bioreactor culture. The temperature was maintained at 25 ± 1°C.

Cultivation and Sampling

Both WT and P3-GAPDH were cultured for 96 h in a 1.5 L flat-plate poly (polymethyl methacrylate) (PMMA) photobioreactor (15.2 × 3.5 × 30 cm in length, width, and height) on Algal Station (AS) system, which was aired with 2% CO_2 compressed air as described previously (Cao et al., 2019). The aeration rate was 0.4 vvm and supplied throughout the culture. The light intensity on the front surface of the flat-plate was 300 μmol m^{-2} s^{-1} under the 14/10 h light/dark cycle, in which the illumination started at 8:00 am and ended at 10:00 pm. The culture temperature was 25 ± 1°C. The inoculation was at 3:00 pm at Day 0 and the samples were taken at 9:00 am and 9:00 pm every day for offline verification of OD and F_v/F_m, as well as for F_v'/F_m', carbohydrate and fatty acid profile determination after the centrifugation. Three batches experiments were carried out. The online monitoring of OD and F_v/F_m were taken with a 20 min interval.

To make it easily to understand the effect of light cycle during the culture, the time scale used here were based on light/dark cycle, which caused the inoculation started at the point of 7 h relatively, and similarly hereinafter without specification.

Optical Density and Dry Weight

To ensure the OD detection by non-diluted measurement with AS, the offline verification was carried out by a UV/VIS spectrophotometer (Jasco V-650, JASCO Corporation, Japan) at 750 nm. For the detection by Jasco V-650, the samples were diluted to keep a reliable OD_{750} under 1.0.

The specific growth rate (μ) was calculated in terms of the Equation (1):

$$\mu = (lnOD_2 - lnOD_1)/12 \quad (1)$$

The OD_1 and OD_2 are the absorbances by the AS with a 12 h's interval at the same time as the offline sampling, respectively.

The dry weight was measured by filtering a certain volume (5–10 mL) of cultures by pre-dried and pre-weighed Whatman GF/C filters dried at 60°C for 24 h as previous report (Meng et al., 2015). The dry weight was calculated in terms of the Equation (2) with three replicates:

$$DW = (w_2 - w_1)/v \quad (2)$$

where w_1 is the weight of pre-dried GF/C filter in g, w_2 is the weight of filter with dried algal culture in g, and v is the initial volume of the sample in L.

The productivity was calculated by the equation:

$$P = 1000 * (DW_2 - DW_1)/12 \quad (3)$$

where DW_1 and DW_2 are the corresponding dry weight in g L^{-1} with a 12 h's interval, respectively, and P is the productivity in mg L^{-1} h^{-1}.

Chlorophyll Fluorescence Dynamics Parameters Detection

The online monitoring of F_v/F_m by AS with 20 min interval showed a continuous change pattern and it was also verified by a chlorophyll fluorometer (Water-PAM Heinz Walz GmbH, Effeltrich, Germany) following the procedure in previous reports (Yao et al., 2012, 2013) during for the offline sampling. The effective photochemical quantum yield, F_v'/F_m' was simultaneously detected by Water-PAM together with F_v/F_m.

Carbohydrate Analysis

Carbohydrate content was determined by the colorimetric method of anthrone-sulfuric acid as described previously (Zhu et al., 2019). In brief, about 5 mg of dried biomass was weighed and ultrasonic crushing followed by treatment in boiling water for 10 min with pre-prepared anthrone-sulfuric acid (74%). The quantifications were carried out on UV/VIS spectrophotometer mentioned before against the standard curve of "glucose concentration—absorbance," which was shown in **Supplementary Material**.

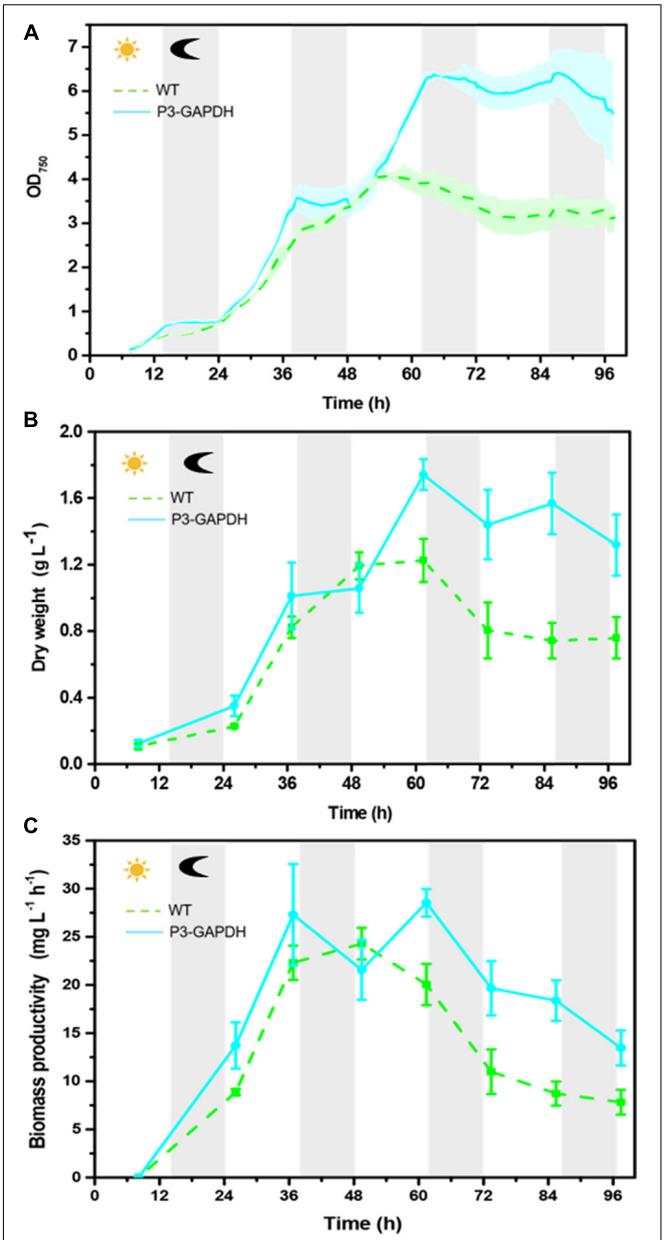

FIGURE 1 | The growth difference between two strains. **(A)** Growth curve by Algal Station, **(B)** Dry weight curve, **(C)** Biomass productivity curve of WT and P3-GAPDH during light-dark cycles. The productivity is the biomass per unit time. Line represents P3-GAPDH, dot line represents WT, and shaded areas (in **A**) or error bars (in **B**,**C**) of each line indicate the standard error of the line values. The gray background marked with a dark moon represents the dark time, while the white background marked with a sun represents illumination during the cultivation. The time scale used here were based on light/dark cycle, which caused the inoculation started at the point of 7 h in the time scale.

Fatty Acid Analysis

The fatty acid profile based on fatty acid methyl esters (FAMEs) were detected by GC after a quick transesterification with methanol following previous report (Yang et al., 2017). In brief, about 5 mg dried biomass was transesterification in

5 mL methanol with 2% H_2SO_4 at 70°C for 1 h. Then 2 mL hexane together with 0.75 mL deionized water were used to extract FAMEs and the obtained hexane mixture was further dewatered by about 0.5 g anhydrous Na_2SO_4. Then the mixture was analyzed on an Agilent 7890 GC with a DB-23 capillary column (30 mm × 0.32 mm × 0.25 μm, Agilent Technology) and a flame ionization detector (FID). The injector temperature was 270℃ with a split ratio of 50:1. The column was heated at 130°C for 1 min, then increased to 170℃ at a rate of 10℃ min^{-1}, and then increased at a rate of 2.8°C min^{-1} to 215°C where it was maintained for 1 min. After the determination of FA profiling, the group of saturated/monounsaturated/polyunsaturated FAs were summing up and the percentage of them in the total FAs were calculated.

Statistical Analysis

All data were presented as the averages ± *SD* for three biological replicates from three batches. The One-way ANOVA analyses were performed in Excel (version 2016, Microsoft) to make the significance analysis for the fatty acid content. The *P*-value was obtained through data analysis in Excel. The level of statistical significance was set to a significant difference ($p < 0.05$) and an extremely significant difference ($p < 0.01$).

RESULTS

Growth and Biomass Accumulation

The growth in P3-GAPDH was monitored and compared with WT on the AS platform for 4 days (**Figure 1A** and **Supplementary Table S1**). There was no significant difference in the growth during the first 2 days, while P3-GAPDH showed a clear step like day-night change pattern. P3-GAPDH's OD was almost flat in the dark, whereas increased rapidly with illumination. The maximum OD of WT reached 4.08 at 50 h and there were no difference in OD between WT and P3-GAPDH before it. The WT turned into the steady phase then. However, P3-GAPDH kept growing to 60 h and its maximum OD reached 6.37, which increased more than 50% than that of WT. The maximum specific growth rates (μ_{max}) reached at 30 h for both P3-GAPDH and WT, were 0.13 and 0.09 h^{-1}, respectively. By the way, the data for **Figure 1A** were collected directly from AS with a 20 min intervals, and the variation between batches were indicated by shadows for each strain.

The dry weights showed a similar trend to OD and were shown in **Figures 1B,C**. The maximum DW of WT and P3-GAPDH were 1.23 ± 0.13 and 1.74 ± 0.09 g L^{-1}, respectively, with biomass productivity of 24.30 ± 1.65 and 28.54 ± 1.43 mg L^{-1} h^{-1}. Compared with previous reports of the mixotrophic cultivation of *C. reinhardtii* in **Table 1**, P3-GAPDH had the highest productivity in biomass under similar conditions.

F_v/F_m and F_v'/F_m' Patterns

The chlorophyll fluorescence dynamics parameters, the maximum quantum of PSII, F_v/F_m, and the effective photochemical quantum yield of PSII, F_v'/F_m', changes were shown in **Figure 2** (**Supplementary Table S2**). The F_v'/F_m' of P3-GAPDH were higher and more stable than that of WT in almost all the whole cultivation, which indicated the higher photochemical conversion in P3-GAPDH. The F_v'/F_m' of WT showed a more fluctuation pattern with the light cycle, increasing with the illumination and decreasing in the dark after day 1, and

TABLE 1 | Comparison of *C. reinhardtii* mixotrophy cultivation among this study and other reports.

C. reinhardtii strains	Bioreactor	Light intensity (μ $molm^{-2}$ s^{-1})	Photoperiod (h)	Medium	Dry biomass per culture (g L^{-1})	Biomass productivity (mg L^{-1} h^{-1})	References
UTEX-90	100 L flat-vertical photobioreactor	n.r	Outdoor cultivation	TAP+2%CO_2	1.45	20.13	Kim et al., 2006
137C	1.5 L torus PBR/5-L cylindrical PBR	500	n.r	TAP	1.1/0.9	4.6	Degrenne et al., 2010
CC124	0.5 L glass columns	70 (both sides)	24	TAP+3%CO_2	1.7	26	Faraloni et al., 2011
CC124	Outdoor 50 L horizontal tubular photobioreactor	500 (both sides)	Outdoor cultivation	TAP+3%CO_2	1.6	9.5	Scoma et al., 2012
CC124	250 mL flasks	180–200	n.r	TAP+10 g/L acetate	2.15	18	Moon et al., 2013
CC124/CC125 mutant	250 mL flasks	180–200	6/18	TAP	1.1/2.1	9.16	Carrera Pacheco et al., 2018
CC137c	1.5 L flat-plate poly(polymethyl merthacrylate) PBR	300	14/10	TAP+2%CO_2	1.23	24.3	This study
P3-GAPDH	1.5 L flat-plate poly(polymethyl merthacrylate) PBR	300	14/10	TAP+2%CO_2	1.74	28.54	This study

n.r not reported.

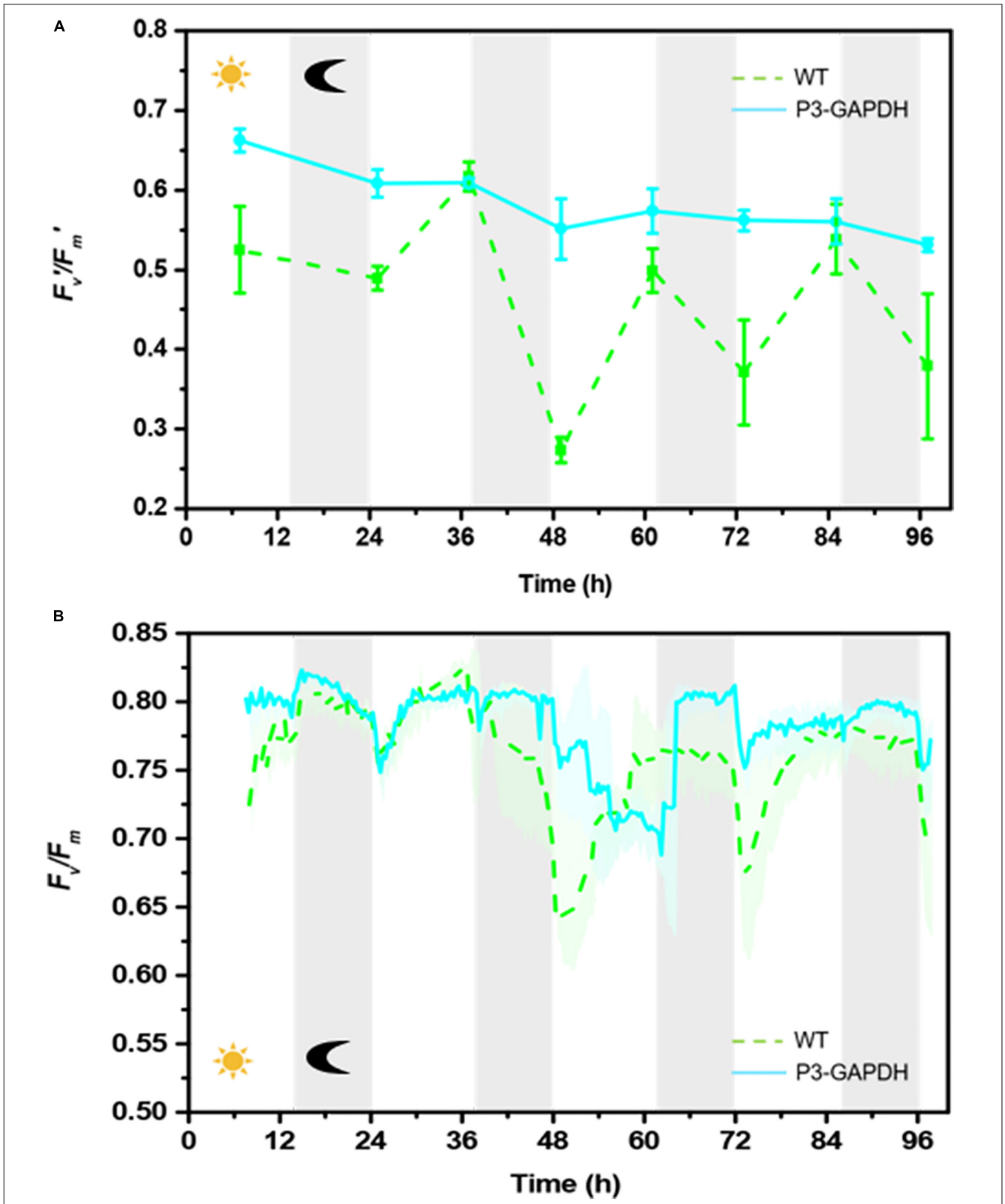

FIGURE 2 | The F_v'/F_m' and F_v/F_m change patterns difference. **(A)** F_v'/F_m' of WT and P3-GAPDH by water-PAM, **(B)** F_v/F_m of WT and P3-GAPDH by Algal Station. Line represents P3-GAPDH, dot line represents WT, and shaded areas (in **B**) or error bars (in **A**) of each line indicate the standard error of the values. The gray background marked with a dark moon represents the dark time, while the white background marked with a sun represents illumination during the cultivation.

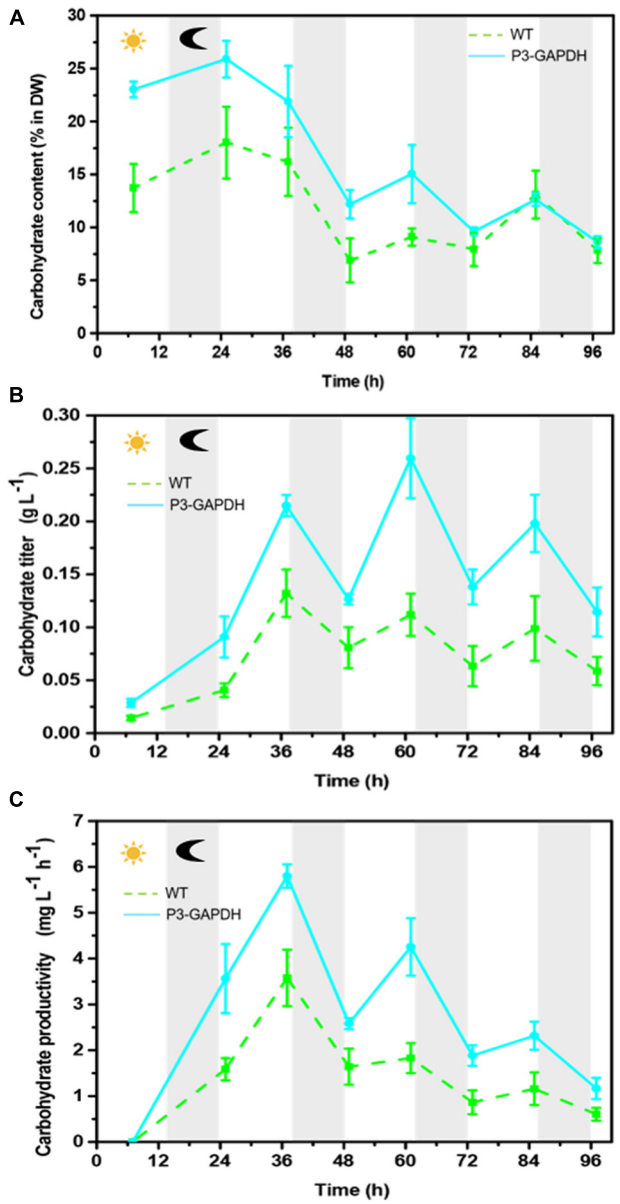

FIGURE 3 | The difference in carbohydrate content and production. **(A)** Carbohydrate content, **(B)** carbohydrate yield, **(C)** carbohydrate productivity of WT and P3-GAPDH. Carbohydrate productivity is the yield per unit time. Line represents P3-GAPDH, dot line represents WT, and error bars indicate the standard error of the values. The gray background marked with a dark moon represents the dark time, while the white background marked with a sun represents illumination during the cultivation.

lowed to 0.27 after the second dark period. On the contrary, the F_v'/F_m' kept above 0.5 throughout the P3-GAPDH's cultivation and there was less correlation to the light cycle as WT.

The overall pattern of F_v/F_m in both strains showed obvious light dependent pattern with the help of continuously monitoring by AS in **Figure 2B**. Without light, the F_v/F_m kept stable in the dark. While the illumination started, it dropped quickly followed by a relatively slow recovery in both two strains except in the third light period. As the OD curves in **Figure 1A**, the F_v/F_m data were collected by AS and the variations were shown as shadows.

From both **Figures 2A,B**, the obviously fluctuation happened in the third light period, which may link to the change of mixtrophic cultivation to autotrophic cultivation and will be discussed later.

Carbohydrate Content Changes

The carbohydrate content and production of P3-GAPDH kept higher than those of WT, with a large fluctuation ranges with the illumination cycle (**Figure 3**). On average, the carbohydrate content in WT was 16.2% of dry weight, with the highest titer of 0.13 ± 0.02 g L^{-1} and a maximum productivity of 3.58 mg L^{-1} h^{-1}. Comparing to WT, carbohydrate accounted for 25.9% of the dry weight in P3-GAPDH at time point 25 h, and the maximum titer was 0.26 ± 0.04 g L^{-1}, with a maximum productivity of 5.80 mg L^{-1} h^{-1}. The high carbohydrate titer in P3-GAPDH in the bioreactor cultivation was consistent with the previous report in the flask (Zhu et al., 2019). By the overexpression of cGAPDH, the carbohydrate productivity nearly doubled under the light within the third and the forth cycle.

Fatty Acid Content and Profiling Changes

By the sum of each FA's content detected by GC (**Table 2**), both the fatty acid (FA) content and production were compared between WT and P3-GAPDH and shown in **Figure 4**. Although the total FA (TFA) content of WT was higher than P3-GAPDH at the inoculation, the TFA content in WT decreased from 12.1 to nearby 7.0% in the steady phase. The TFA content maintained a relatively stable level in P3-GAPDH nearby 10.0%, except a drop to 7.3% at time point 25 h (**Figure 4A**). However, due to more biomass produced in P3-GAPDH, the P3-GAPDH's TFA yield nearly doubled while compared to that in WT, 0.16 ± 0.01 and 0.08 ± 0.01 g L^{-1}, and with the maximum productivity of 2.58 ± 0.15 and 1.93 ± 0.07 mg L^{-1} h^{-1}, respectively (**Figures 4B,C**).

In *C. reinhardtii*, polyunsaturated fatty acids (PUFAs), such as C18:3, construct the majority of the membrane of the chloroplast and thylakoid and contribute to the photosynthesis process (Yang et al., 2017). The contents and titers of saturated fatty acids (SFA), monounsaturated fatty acids (MUFA), and PUFA in WT and P3-GAPDH, which changed significantly different (**Figure 5**). In P3-GAPDH, more PUFA, such as C16:4, C18:2, C18:3, C18:4, were produced and a stable content were maintained. The maximum titer of SFA and PUFA were 0.02 ± 0.00 and 0.04 ± 0.00 g L^{-1}, respectively, in WT, while the maximum titer of SFA and PUFA were 0.04 ± 0.00 and 0.09 ± 0.01 g L^{-1} in P3-GAPDH, which was twofold and 2.25-fold to WT, respectively. The percentage of SFA, MUFA, PUFA in TFA was shown in **Table 2**. It was clear that PUFA was predominant in TFA. The detailed increment of fatty acids in P3-GAPDH compared with WT was summarized in **Table 3**. The increased in PUFA production was also consisted with the start of the second growth wave of P3-GAPDH after time point 36 h.

TABLE 2 | Fatty acid composition and the proportion of SFA, MUFA, PUFA in TFA of WT and P3-GAPDH grown in TAP medium after 96 h.

	7 h		24 h		36 h		48 h		60 h		72 h		84 h		96 h	
	WT	**P3-GAPDH**	**WT**	**P3-GAPDH**	**WT**	**P3-GAPDH**	**WT**	**P3-GAPDH**	**WT**	**P3-GAPDH**	**WT**	**P3-GAPDH**	**WT**	**P3-GAPDH**	**WT**	**P3-GAPDH**
C16:0	2.33 ± 0.10	2.00 ± 0.05	1.90 ± 0.05	1.82 ± 0.03	1.73 ± 0.16	2.00 ± 0.05	1.64 ± 0.18	2.11 ± 0.11	1.57 ± 0.03	2.22 ± 0.02	1.59 ± 0.04	2.29 ± 0.15	1.75 ± 0.08	2.19 ± 0.09	1.69 ± 0.11	2.03 ± 0.10
C16:1n9	0.66 ± 0.04	0.49 ± 0.02	0.27 ± 0.04	0.21 ± 0.01	0.33 ± 0.00	0.33 ± 0.02	0.25 ± 0.02	0.34 ± 0.04	0.33 ± 0.03	0.37 ± 0.07	0.44 ± 0.07	0.42 ± 0.01	0.45 ± 0.04	0.49 ± 0.03	0.46 ± 0.09	0.47 ± 0.01
C16:1n7	0.23 ± 0.02	0.21 ± 0.01	0.20 ± 0.02	0.17 ± 0.01	0.44 ± 0.10	0.18 ± 0.01	0.81 ± 0.10	0.28 ± 0.07	0.67 ± 0.04	0.32 ± 0.14	0.48 ± 0.02	0.20 ± 0.02	0.38 ± 0.02	0.21 ± 0.01	0.36 ± 0.04	0.24 ± 0.04
C16:2n6	0.35 ± 0.01	0.21 ± 0.00	0.08 ± 0.01	0.04 ± 0.00	0.09 ± 0.00	0.04 ± 0.01	0.03 ± 0.00	0.05 ± 0.01	0.07 ± 0.00	0.12 ± 0.03	0.08 ± 0.02	0.15 ± 0.03	0.14 ± 0.02	0.18 ± 0.03	0.11 ± 0.00	0.12 ± 0.01
C16:3n6	0.30 ± 0.04	0.17 ± 0.01	0.14 ± 0.01	0.08 ± 0.00	0.11 ± 0.01	0.08 ± 0.01	0.06 ± 0.01	0.07 ± 0.01	0.07 ± 0.01	0.07 ± 0.02	0.09 ± 0.02	0.09 ± 0.01	0.13 ± 0.02	0.13 ± 0.01	0.11 ± 0.02	0.10 ± 0.01
C16:3n3	0.20 ± 0.02	0.14 ± 0.00	0.14 ± 0.02	0.11 ± 0.01	0.16 ± 0.05	0.20 ± 0.03	0.06 ± 0.02	0.13 ± 0.01	0.07 ± 0.02	0.16 ± 0.04	0.06 ± 0.01	0.15 ± 0.01	0.10 ± 0.01	0.18 ± 0.03	0.09 ± 0.03	0.16 ± 0.03
C16:4n3	1.61 ± 0.20	1.35 ± 0.04	0.95 ± 0.06	0.86 ± 0.03	1.10 ± 0.11	1.27 ± 0.07	0.65 ± 0.12	1.19 ± 0.08	0.68 ± 0.14	1.14 ± 0.24	0.74 ± 0.05	1.26 ± 0.02	0.89 ± 0.08	1.39 ± 0.06	0.87 ± 0.26	1.19 ± 0.18
C18:0	0.31 ± 0.01	0.33 ± 0.02	0.27 ± 0.02	0.23 ± 0.01	0.24 ± 0.03	0.26 ± 0.00	0.21 ± 0.03	0.27 ± 0.01	0.19 ± 0.04	0.28 ± 0.02	0.20 ± 0.03	0.33 ± 0.05	0.19 ± 0.03	0.27 ± 0.03	0.21 ± 0.04	0.26 ± 0.03
C18:1n9	0.24 ± 0.02	0.20 ± 0.01	0.60 ± 0.02	0.38 ± 0.02	0.58 ± 0.03	0.39 ± 0.10	0.30 ± 0.03	0.31 ± 0.06	0.20 ± 0.06	0.22 ± 0.02	0.13 ± 0.02	0.18 ± 0.02	0.12 ± 0.01	0.11 ± 0.01	0.12 ± 0.02	0.10 ± 0.01
C18:1n7	0.54 ± 0.01	0.33 ± 0.02	0.49 ± 0.03	0.34 ± 0.01	0.49 ± 0.03	0.43 ± 0.00	0.86 ± 0.04	0.51 ± 0.05	0.80 ± 0.04	0.55 ± 0.07	0.65 ± 0.02	0.46 ± 0.05	0.62 ± 0.08	0.55 ± 0.04	0.60 ± 0.10	0.51 ± 0.08
C18:2n6	1.68 ± 0.03	1.13 ± 0.02	0.69 ± 0.02	0.59 ± 0.03	0.69 ± 0.06	0.59 ± 0.10	0.41 ± 0.08	0.52 ± 0.06	0.37 ± 0.03	0.66 ± 0.05	0.43 ± 0.07	0.71 ± 0.07	0.58 ± 0.09	0.62 ± 0.09	0.48 ± 0.06	0.43 ± 0.05
C18:3n6	0.72 ± 0.02	0.63 ± 0.17	0.66 ± 0.03	0.61 ± 0.12	0.57 ± 0.04	0.73 ± 0.23	0.38 ± 0.06	0.63 ± 0.01	0.36 ± 0.04	0.52 ± 0.09	0.39 ± 0.00	0.64 ± 0.05	0.42 ± 0.02	0.67 ± 0.03	0.40 ± 0.08	0.62 ± 0.07
C18:3n3	2.80 ± 0.30	2.35 ± 0.06	1.95 ± 0.11	1.89 ± 0.04	2.03 ± 0.23	2.53 ± 0.10	1.17 ± 0.25	2.30 ± 0.11	1.16 ± 0.24	2.24 ± 0.45	1.23 ± 0.08	2.35 ± 0.01	1.47 ± 0.14	2.48 ± 0.12	1.37 ± 0.41	2.08 ± 0.35
C18:4n3	0.19 ± 0.01	0.16 ± 0.01	0.20 ± 0.02	0.17 ± 0.01	0.16 ± 0.02	0.24 ± 0.01	0.10 ± 0.02	0.25 ± 0.01	0.13 ± 0.03	0.20 ± 0.05	0.16 ± 0.02	0.24 ± 0.02	0.19 ± 0.03	0.31 ± 0.01	0.18 ± 0.06	0.31 ± 0.05
	7 h		**24 h**		**36 h**		**48 h**		**60 h**		**72 h**		**84 h**		**96 h**	
	WT	**P3-GAPDH**	**WT**	**P3-GAPDH**	**WT**	**P3-GAPDH**	**WT**	**P3-GAPDH**	**WT**	**P3-GAPDH**	**WT**	**P3-GAPDH**	**WT**	**P3-GAPDH**	**WT**	**P3-GAPDH**
SFA	21.8 ± 0.7	24.0 ± 0.4	25.5 ± 0.5	27.3 ± 0.7	22.5 ± 0.5	24.4 ± 0.8	26.6 ± 0.6	26.6 ± 0.8	26.4 ± 0.6	27.7 ± 2.4	26.8 ± 0.3	27.6 ± 1.3	26.1 ± 0.7	25.1 ± 1.3	27.1 ± 1.9	26.6 ± 1.0
MUFA	13.8 ± 0.8	12.6 ± 0.3	18.2 ± 0.2	14.8 ± 0.4	21.3 ± 2.3	14.3 ± 1.0	32.5 ± 5.2	16.0 ± 1.2	30.3 ± 3.2	16.4 ± 3.1	25.6 ± 0.4	13.4 ± 0.9	21.1 ± 1.2	13.9 ± 0.1	22.5 ± 4.2	15.4 ± 1.0
PUFA	64.4 ± 1.3	63.4 ± 0.7	56.3 ± 0.5	57.9 ± 0.9	56.2 ± 1.8	61.3 ± 1.7	40.8 ± 4.6	57.4 ± 2.0	43.3 ± 3.8	55.9 ± 5.2	47.6 ± 0.1	59.0 ± 1.4	52.7 ± 1.9	61.0 ± 1.2	50.4 ± 6.1	58.0 ± 1.9

Data expressed as a percentage of dry weight (% in DW) and were shown as means−x ± SD (n = 3). Data expressed as a percentage of SFA, MUFA, PUFA in TFA (%) and were shown as means−x ± SD (n = 3).

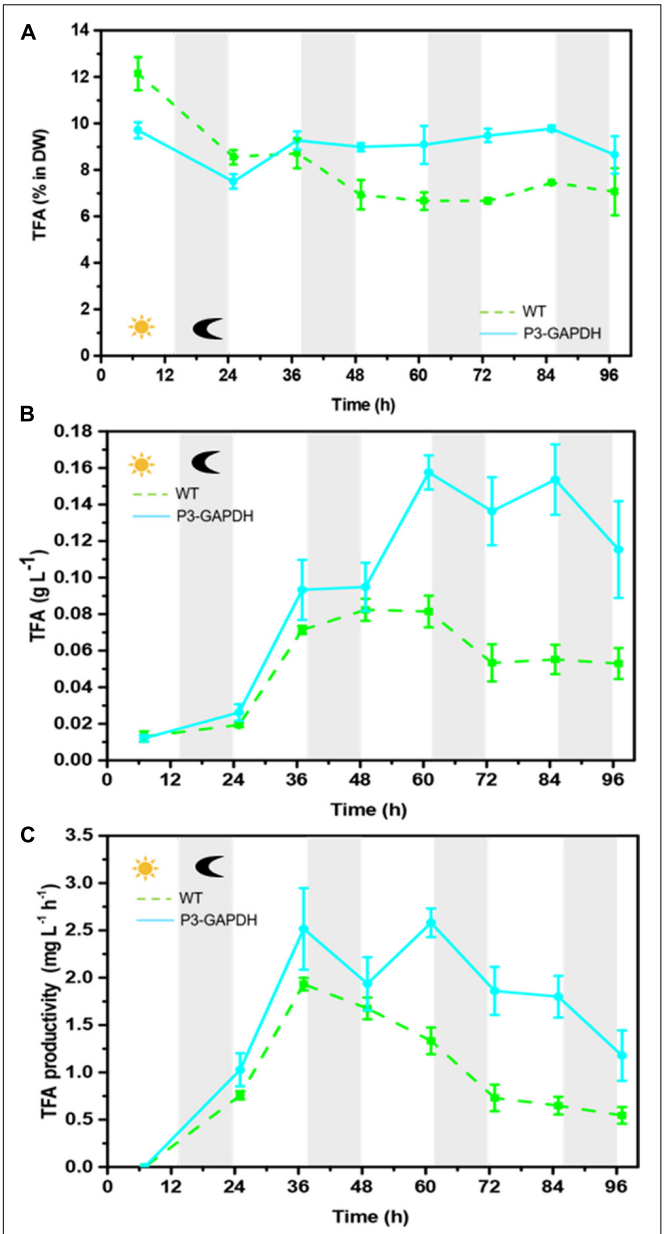

FIGURE 4 | The difference in TFA content and production. **(A)** TFA content, **(B)** TFA yield, **(C)** TFA productivity of WT and P3-GAPDH. TFA productivity is the yield per unit time. Line represents P3-GAPDH, dot line represents WT, and error bars indicate the standard error of the values. The gray background marked with a dark moon represents the dark time, while the white background marked with a sun represents illumination during the cultivation.

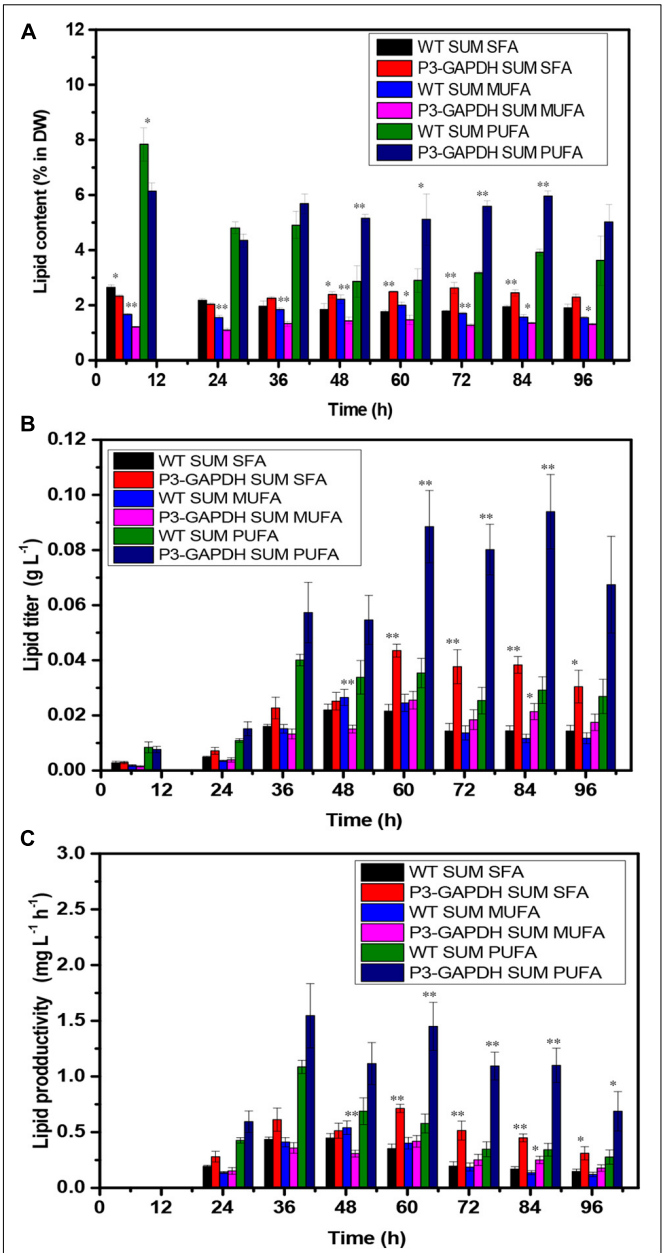

FIGURE 5 | The difference in FAs composition. **(A)** FAs content, **(B)** FAs yield, **(C)** FAs productivity of WT and P3-GAPDH. FAs productivity is the yield per unit time. These fatty acids were classified into three categories: SFA, MUFA, PUFA, and compared with the content for each kind of fatty acid, respectively. For each point, the mean is given, $n = 3$. * and ** denote significant difference ($p < 0.05$) and extremely significant difference ($p < 0.01$) between WT and P3-GAPDH, respectively.

pH Changes of WT and P3-GAPDH During Cultivation

The pH-values of two microalgae were monitored by AS was significantly different (**Figure 6**). It's was notable that between time point 48–62 h, the pH-value of WT showed a bigger fluctuation than that in P3-GAPDH. The change of pH here indicated the depletion of acetate in the TAP and the loss of some buffer ability from it.

TABLE 3 | Increment of fatty acids in P3-GAPDH compared with WT.

Fatty acid	61 h	73 h	85 h	97 h
Total fatty acid (TFA)	93%	155%	178%	118%
Saturated (SFA)	102%	164%	166%	113%
Monounsaturated (MUFA)	4%	35%	84%	49%
Polyunsaturated (PUFA)	150%	216%	222%	151%

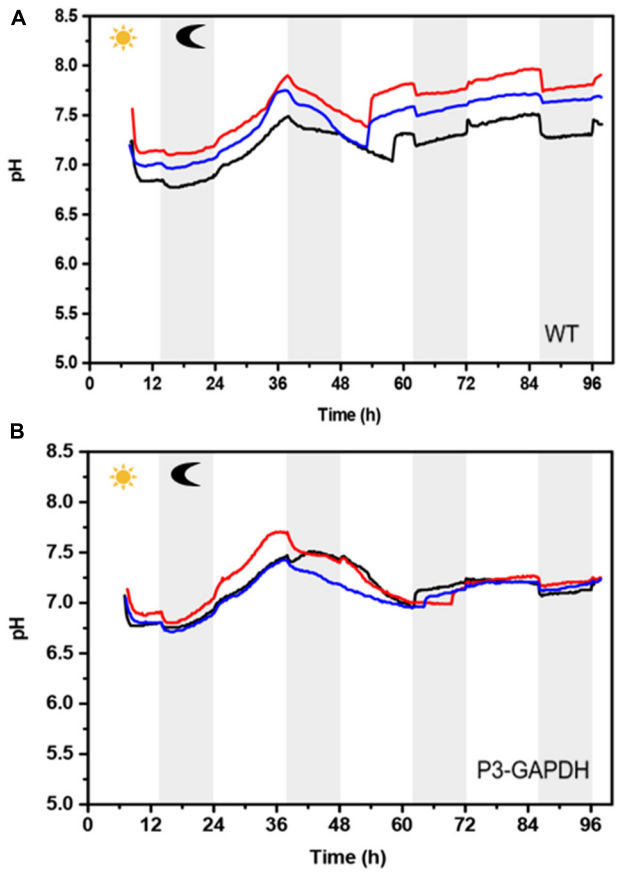

FIGURE 6 | pH changes during the cultivation | pH curve of **(A)** WT and **(B)** P3-GAPDH. Three lines represent three batches.

DISCUSSION

GAPDH is the key enzyme in the glycolysis and Calvin cycle. Most studies were focused on the cytoplasm type GAPDH, and the chloroplast GAPDH's contribution to the carbon metabolism was rarely studied. It has been postulated to play an important role in the supramolecular complexes in the Calvin cycle in the *C. reinhardtii* based on structure biology studies (Emmanuelle et al., 2004; Erales et al., 2009). In *Chlamydomonas*, glycolysis is divided into a chloroplastidic and a cytosolic part with the enzymes GAPDH/ phosphoglycerate kinase (PGK) being located in the chloroplast stroma and its activity depends onNADPH mediated complex dissociation under the regulation of the light (Wedel and Soll, 1998). After the identification the significant changes of cGAPDH during the nitrogen starvation in *C. reinhardtii*, the strain with overexpressed cGAPDH in the chloroplast was constructed to evaluate its contribution to carbon fixation previously (Zhu et al., 2019) and results showed a better carbon conversion in the P3-GAPDH strain. However, in the flask cultivation with TAP media, the mixtrophic condition with low CO_2 supply limited the understanding of the effect of cGAPDH on the carbon fixation. So, a more detailed comparison of P3-GAPDH with WT was carried out in the bioreactor with enriched CO_2 supply, in which both the mixtrophic and autotrophic cultivation existed. Based on the continuously monitoring of OD and pH, the switch of above two cultivation modes happened nearby the time point 50 h (**Figures 1A**, **6**). To simplify, the culture before 50 h was treated as mixtrophic mode (Mix) and the left as autotrophic mode (Auto).

With the existence of acetate, P3-GAPDH only showed a little help in the growth (OD), However, a more than 50% increase in carbohydrate productivity still achieved (**Figure 3C**) in the Mix mode and resulted in the highest productivity under the similar cultivation conditions (**Tables 1**, **4**). It's postulated that overexpressed cGAPDH contributed to more carbon fixation from two aspects: (1) Due to cGAPDH converts the products of carbon fixation in the Calvin cycle, the overexpression of it will also help to reduce the energy or electron accumulation in the electron transfer chain of the light reaction part in the photosynthesis, which was indicated by the relative higher and stable F_v'/F_m' (**Figure 2A**). The overexpression might break the light regulation of cGAPDH's activity with extra free enzymes from the GAPDH/PGK complex. It'll be verified by the proteomics analysis in our further work. (2) The maintenance of the photosynthesis system, and was indicated by the continuously monitoring of F_v/F_m (**Figure 2B**). As the major components in the thylakoid membrane, where the photosynthesis carries out, glycolipids [monogalactosyldiacylglycerol (MGDG), digalactosyldiacylglycerol (DGDG), and sulphoquinovosyldiacylglycerol (SQDG)], which are mostly formed with PUFAs (Yang et al., 2018), and P3-GAPDH strain was proved to produced more PUFAs (**Figure 5** and **Table 2**; Zhu et al., 2019).

Combined both the physiological and biochemical analysis, cGAPDH is postulated to play an important role in the regulation

TABLE 4 | The comparison among this study and Faraloni et al. (2011).

C. reinhardtii strains	Temperature	Light intensity	Dry biomass per culture (g L^{-1})	The time of max dry biomass (h)	Biomass productivity (mg L^{-1} h^{-1})	The time of max biomass productivity (h)	Specific growth rates (h^{-1})
CC124	28°C	70 μmol m^{-2} s^{-1} (supplied on both sides)	1.70	65 (24 h light)	26.0	65	0.08
CC137c	25°C	300 μmol m^{-2} s^{-1} (supplied on one side)	1.23	54 (14/10 h light)	24.3	42	0.09
P3-GAPDH	25°C	300 μmol m^{-2} s^{-1} (supplied on one side)	1.74	54 (14/10 h light)	28.5	54	0.13

of carbon fixation in the chloroplast. Here, without the repletion of other nutrients, the overexpression of chloroplast GAPDH gene enables the P3-GAPDH to maintain high photosynthetic activity and promote biomass production, i.e. the carbohydrate and lipid content increased by 96.6 and 93.4%, respectively, which were mostly from the Auto mode cultivation. The results indicated that overexpressed cGAPDH increased the carbon fixation capacity of *C. reinhardtii* not only by push the carbon to downstream metabolisms, such as carbohydrates and FAs, but also promote the photochemical conversion in the photosynthesis, liking a self-inspiring cycle: overexpressed cGAPDH producing more C3 metabolite for PUFAs synthesis, while more PUFAs maintaining a more robust photosynthesis and resulting more fixed carbon for cGAPDH to use. It brings the hope to achieve the two-win between growth and energy storage compounds production other than traditional nitrogen depletion stress with the suppress of the growth, i.e., to achieve both higher biomass and higher energy storage compounds production simultaneously.

Here only the physiological and content analysis was carried out. Detailed molecular biology studies, such as—omics analysis, were needed to understand the carbon fixation improvement by overexpressing the cGAPDH to aid the future synthetic biology development by using a microalgae cell factory.

CONCLUSION

The cGAPDH overexpressed strain P3-GAPDH was verified in the bioreactor and it higher carbon fixation than previously reported under similar conditions was confirmed. The overexpress cGAPDH not only promoted the carbon conversion from photosynthesis, but also formed a self-inspiring cycle by promoting the PUFAs synthesis, which are important to the maintenance high photosynthesis activity.

DATA AVAILABILITY STATEMENT

The original contributions presented in the study are included in the article/**Supplementary Material**, further inquiries can be directed to the corresponding author/s.

AUTHOR CONTRIBUTIONS

XC, JT, and JR designed the research. ZZ, HC, and XC wrote the manuscript and analyzed the data. ZZ, HC, and XL performed the research and provided technical support. All authors read and approved the final manuscript.

FUNDING

This work was supported by the National Natural Science Foundation of China (Nos. 31771914 and 21878285), the State Key Laboratory of Catalytic Materials and Reaction Engineering (RIPP, SINOPEC), and the Dalian Key Laboratory of Energy Biotechnology.

ACKNOWLEDGMENTS

We hope to thank Senior Engineer Yadong Chu for the technique support in Energy Biotechnology Platform of Dalian Institute of Chemical Physics, CAS.

SUPPLEMENTARY MATERIAL

The Supplementary Material for this article can be found online at: https://www.frontiersin.org/articles/10.3389/fbioe.2020.603513/full#supplementary-material

REFERENCES

Cao, X., Xi, Y., Liu, J., Chu, Y., Wu, P., Yang, M., et al. (2019). New insights into the CO2-steady and pH-steady cultivations of two microalgae based on continuous online parameter monitoring. *Algal Res.* 38:101370. doi: 10.1016/j.algal.2018.11.021

Carrera Pacheco, S. E., Hankamer, B., and Oey, M. (2018). Optimising light conditions increases recombinant protein production in *Chlamydomonas reinhardtii* chloroplasts. *Algal Res.* 32, 329–340. doi: 10.1016/j.algal.2018.04.011

Chen, M., Zhang, L., Li, S., Chang, S., Wang, W., Zhang, Z., et al. (2014). Characterization of cell growth and photobiological H2 production of *Chlamydomonas reinhardtii* in ASSF industry wastewater. *Int. J. Hydrogen Energy* 39, 13462–13467. doi: 10.1016/j.ijhydene.2014.03.132

Degrenne, B., Pruvost, J., Christophe, G., Cornet, J. F., Cogne, G., and Legrand, J. (2010). Investigation of the combined effects of acetate and photobioreactor illuminated fraction in the induction of anoxia for hydrogen production by *Chlamydomonas reinhardtii*. *Int. J. Hydrogen Energy* 35, 10741–10749. doi: 10.1016/j.ijhydene.2010.02.067

Duong, V. T., Ahmed, F., Thomas-Hall, S. R., Quigley, S., Nowak, E., and Schenk, P. M. (2015a). High protein- and high lipid-producing microalgae from northern Australia as potential feedstock for animal feed and biodiesel. *Front. Bioeng. Biotechnol.* 3:53. doi: 10.3389/fbioe.2015.00053

Duong, V. T., Thomas-Hall, S. R., and Schenk, P. M. (2015b). Growth and lipid accumulation of microalgae from fluctuating brackish and sea water locations in South East Queensland-Australia. *Front. Plant Sci.* 6:359. doi: 10.3389/fpls.2015.00359

Emmanuelle, G., Guillermo, M., Sandrine, L., and Brigitte, G. (2004). Involvement of two positively charged residues of *Chlamydomonas reinhardtii* glyceraldehyde-3-phosphate dehydrogenase in the assembly process of a bi-enzyme complex involved in CO2 assimilation. *Eur. J. Biochem.* 271, 4737–4744. doi: 10.1111/j.1432-1033.2004.04437.x

Erales, J., Lorenzi, M., Lebrun, R., Fournel, A., Etienne, E., Courcelle, C., et al. (2009). A new function of GAPDH from *Chlamydomonas reinhardtii*: a thiol-disulfide exchange reaction with CP12. *Biochemistry* 48, 6034–6040. doi: 10.1021/bi900569h

Fan, J., and Zheng, L. (2017). Acclimation to NaCl and light stress of heterotrophic *Chlamydomonas reinhardtii* for lipid accumulation. *J. Biosci. Bioeng.* 124, 302–308. doi: 10.1016/j.jbiosc.2017.04.009

Faraloni, C., Ena, A., Pintucci, C., and Torzillo, G. (2011). Enhanced hydrogen production by means of sulfur-deprived *Chlamydomonas reinhardtii* cultures grown in pretreated olive mill wastewater. *Int. J. Hydrogen Energy* 36, 5920–5931. doi: 10.1016/j.ijhydene.2011.02.007

Fields, F. J., Ostrand, J. T., and Mayfield, S. P. (2018). Fed-batch mixotrophic cultivation of *Chlamydomonas reinhardtii* for high-density cultures. *Algal Res.* 33, 109–117. doi: 10.1016/j.algal.2018.05.006

Gargouri, M., Bates, P. D., Park, J. J., Kirchhoff, H., and Gang, D. R. (2017). Functional photosystem I maintains proper energy balance during nitrogen depletion in *Chlamydomonas reinhardtii*, promoting triacylglycerol accumulation. *Biotechnol. Biofuels.* 10:89. doi: 10.1186/s13068-017-0774-4

Harris, E. H. (2001). *Chlamydomonas* as a model organism. *Annu. Rev. Plant Physiol. Plant Mol. Biol.* 52, 363–406. doi: 10.1146/annurev.arplant.52.1.363

Kim, E. J., Kim, S., Choi, H. G., and Han, S. J. (2020). Co-production of biodiesel and bioethanol using psychrophilic microalga *Chlamydomonas* sp. KNM0029C isolated from Arctic sea ice. *Biotechnol. Biofuels* 13:20. doi: 10.1186/s13068-020-1660-z

Kim, M. S., Baek, J. S., Yun, Y. S., Jun Sim, S., Park, S., and Kim, S. C. (2006). Hydrogen production from *Chlamydomonas reinhardtii* biomass using a two-step conversion process: anaerobic conversion and photosynthetic fermentation. *Int. J. Hydrogen Energy* 31, 812–816. doi: 10.1016/j.ijhydene.2005.06.009

Kosourov, S., Patrusheva, E., Ghirardi, M. L., Seibert, M., and Tsygankov, A. (2007). A comparison of hydrogen photoproduction by sulfur-deprived *Chlamydomonas reinhardtii* under different growth conditions. *J. Biotechnol.* 128, 776–787. doi: 10.1016/j.jbiotec.2006.12.025

Meng, Y., Jiang, J., Wang, H., Cao, X., Xue, S., and Yang, Q. (2015). The characteristics of TAG and EPA accumulation in *Nannochloropsis oceanica* IMET1 under different nitrogen supply regimes. *Bioresour. Technol.* 179, 483–489. doi: 10.1016/j.biortech.2014.12.012

Merchant, S. S., Prochnik, S. E., Vallon, O., Harris, E. H., Karpowicz, S. J., Witman, G. B., et al. (2007). The Chlamydomonas genome reveals the evolution of key animal and plant functions. *Science* 318, 245–250.

Moon, M., Kim, C. W., Park, W. K., Yoo, G., Choi, Y. E., and Yang, J. W. (2013). Mixotrophic growth with acetate or volatile fatty acids maximizes growth and lipid production in *Chlamydomonas reinhardtii*. *Algal Res.* 2, 352–357. doi: 10.1016/j.algal.2013.09.003

Scoma, A., Giannelli, L., Faraloni, C., and Torzillo, G. (2012). Outdoor H2 production in a 50-L tubular photobioreactor by means of a sulfur-deprived culture of the microalga *Chlamydomonas reinhardtii*. *J. Biotechnol.* 157, 620–627. doi: 10.1016/j.jbiotec.2011.06.040

South, P. F. (2019). Synthetic glycolate metabolism pathways stimulate crop growth and productivity in the field. *Science* 365, 768–768.

Wang, X., Ruan, Z., Sheridan, P., Boileau, D., Liu, Y., and Liao, W. (2015). Two-stage photoautotrophic cultivation to improve carbohydrate production in *Chlamydomonas reinhardtii*. *Biomass Bioenergy* 74, 280–287. doi: 10.1016/j.biombioe.2015.01.024

Wedel, N., and Soll, J. (1998). Evolutionary conserved light regulation of Calvin cycle activity by NADPH-mediated reversible phosphoribulokinase/CP12/glyceraldehyde-3-phosphate dehydrogenase complex dissociation. *Proc. Natl. Acad. Sci. U.S.A.* 95, 9699–9704. doi: 10.1073/pnas.95.16.9699

Yang, M., Fan, Y., Wu, P., Chu, Y., Shen, P., and Xue, S. (2017). An extended approach to quantify triacylglycerol in microalgae by characteristic fatty acids. *Front. Plant Sci.* 8:1949. doi: 10.3389/fpls.2017.01949

Yang, M., Meng, Y., Chu, Y., Fan, Y., Cao, X., and Xue, S. (2018). Triacylglycerol accumulates exclusively outside the chloroplast in short-term nitrogen-deprived *Chlamydomonas reinhardtii*. *Biochim. Biophys. Acta* 1863, 1478–1487. doi: 10.1016/j.bbalip.2018.09.009

Yao, C., Ai, J., Cao, X., Xue, S., and Zhang, W. (2012). Enhancing starch production of a marine green microalga *Tetraselmis subcordiformis* through nutrient limitation. *Bioresour. Technol.* 118, 438–444. doi: 10.1016/j.biortech.2012.05.030

Yao, C. H., Ai, J. N., Cao, X. P., and Xue, S. (2013). Characterization of cell growth and starch production in the marine green microalga *Tetraselmis subcordiformis* under extracellular phosphorus-deprived and sequentially phosphorus-replete conditions. *Appl. Microbiol. Biotechnol.* 97, 6099–6110. doi: 10.1007/s00253-013-4983-x

Zhang, Z., Tan, Y., Wang, W., Bai, W., Fan, J., and Huang, J. (2019). Efficient heterotrophic cultivation of *Chlamydomonas reinhardtii*. *J. Appl. Phycol.* 31, 1545–1554. doi: 10.1007/s10811-018-1666-0

Zhu, Z., Cao, X., Yuan, G., Liu, J., Xue, S., and Tian, J. (2019). Studies on the effect of overexpressed chloroplast glyceraldehyde-3-phosphate dehydrogenase on carbohydrate and fatty acid contents of *Chlamydomonas reihardtii*. *Periodical Ocean Univ. China* 49, 050–058.

Conflict of Interest: The authors declare that the research was conducted in the absence of any commercial or financial relationships that could be construed as a potential conflict of interest.

frontiers in Bioengineering and Biotechnology

ORIGINAL RESEARCH
published: 15 January 2021
doi: 10.3389/fbioe.2020.613768

ROS Induce β-Carotene Biosynthesis Caused by Changes of Photosynthesis Efficiency and Energy Metabolism in *Dunaliella salina* Under Stress Conditions

Yimei Xi, Fantao Kong and Zhanyou Chi*

School of Bioengineering, Dalian University of Technology, Dalian, China

The unicellular alga *Dunaliella salina* is regarded as a promising cell factory for the commercial production of β-carotene due to its high yield of carotenoids. However, the underlying mechanism of β-carotene accumulation is still unclear. In this study, the regulatory mechanism of β-carotene accumulation in *D. salina* under stress conditions was investigated. Our results indicated that there is a significant positive correlation between the cellular ROS level and β-carotene content, and the maximum quantum efficiency (F_v/F_m) of PSII is negatively correlated with β-carotene content under stress conditions. The increase of ROS was found to be coupled with the inhibition of F_v/F_m of PSII in *D. salina* under stress conditions. Furthermore, transcriptomic analysis of the cells cultivated with H_2O_2 supplementation showed that the major differentially expressed genes involved in β-carotene metabolism were upregulated, whereas the genes involved in photosynthesis were downregulated. These results indicated that ROS induce β-carotene accumulation in *D. salina* through fine-tuning genes which were involved in photosynthesis and β-carotene biosynthesis. Our study provided a better understanding of the regulatory mechanism involved in β-carotene accumulation in *D. salina*, which might be useful for overaccumulation of carotenoids and other valuable compounds in other microalgae.

Keywords: *Dunaliella salina*, ROS, β-carotene, carotenogenesis, transcriptomic analysis

OPEN ACCESS

Edited by:
Changhong Yao,
Sichuan University, China

Reviewed by:
Jin Liu,
Peking University, China
Yulin Cui,
Chinese Academy of Sciences (CAS), China

****Correspondence:***
Fantao Kong
kongfantao@dlut.edu.cn

Specialty section:
This article was submitted to Bioprocess Engineering, a section of the journal Frontiers in Bioengineering and Biotechnology

Received: *03 October 2020*
Accepted: *25 November 2020*
Published: *15 January 2021*

Citation:
Xi Y, Kong F and Chi Z (2021) ROS Induce β-Carotene Biosynthesis Caused by Changes of Photosynthesis Efficiency and Energy Metabolism in Dunaliella salina Under Stress Conditions. Front. Bioeng. Biotechnol. 8:613768. doi: 10.3389/fbioe.2020.613768

INTRODUCTION

Carotenoids are light-harvesting pigments that act as antioxidant molecules. Among the carotenoids, β-carotene is a high-value carotenoid that can be produced in many marine animals, higher plants, and microorganisms including microalgae. Due to its strong pigmentation function, powerful antioxidative activity, and broad beneficial effects on human health, β-carotene possesses a wide range of applications in feed, food, and nutraceutical and pharmaceutical industries, which has attracted great attention (Jin and Melis, 2003; Combe et al., 2015; Liang et al., 2019). However, humans cannot synthesize β-carotene and must obtain it through diet. In 2015, the global β-carotene market was approximately estimated to be US$ 432 million with 36% revenues from microalga-derived natural β-carotene (Nethravathy et al., 2019).

Microalgae are a group of photosynthetic microorganisms and are sources of numerous value-added products, such as lipids, carbohydrates, and carotenoids (Chew et al., 2017). The green microalga *Dunaliella salina* (thereafter *D. salina*) can synthesize an extremely large amount of β-carotene (up to 10% of the dry weight) (Harvey and Xu, 2019). The high carotene contents in *D. salina* make it a promising cell factory for the large-scale production of natural β-carotene. Nevertheless, *D. salina* has inherent limitations such as slow growth rate and low biomass yield. Moreover, the regulatory mechanism of β-carotene production in *D. salina* is not clear, which hinders the economically feasible production of β-carotene at industrial level.

It has been reported that an increase in intracellular β-carotene content is often accompanied by a high level of reactive oxygen species (ROS) in microalgal cells which are suffering from abiotic stresses, such as high light, high salinity, and nutrient deprivation (Cowan et al., 1992; Lamers et al., 2008; Ye et al., 2008). ROS mainly include hydrogen peroxide (H_2O_2), superoxide ($O2^-$), and hydroxyl radical ($OH^·$). It was reported that ROS can act as signals to trigger various cellular events, i.e., activation of many metabolic pathways through phosphorylation cascades and the oxidation of key signaling molecules (Shi et al., 2017; Zhang L. et al., 2019). As signaling molecules, the moderate level of ROS is beneficial for the cells to regulate gene expression and initiate self-protective mechanisms in response to environmental changes (Cowan and Rose, 1991; Liu et al., 2012). However, a high level of ROS accumulated during stress will damage DNA, proteins, lipids, and photosynthetic pigments in microalgae (Liu et al., 2012).

ROS are generally generated from chloroplast and mitochondrial electron transport flows due to excitation of O_2 by excessive electrons in microalgae. The chloroplast is the primary compartment for β-carotene formation (Cowan et al., 1992; Kamalanathan et al., 2017). ROS were produced accompanied with β-carotene formation under stress conditions, which can alleviate the oxidative damage to the photosynthetic system in microalgae (Henriquez et al., 2016). Shaish et al. (1993) reported that the photosynthetically produced ROS are involved in triggering massive β-carotene accumulation in *D. bardawil*. However, the molecular mechanism is still not clear. Under abiotic stress conditions, e.g., high light (HL), nitrogen deprivation (N–) and high salinity (HS), and β-carotene overaccumulation accompanied with high level of ROS were found in *D. salina*, respectively (Liu et al., 2012; Mirshekari et al., 2019; Zhao et al., 2019). However, there is also still a lack of understanding regarding the regulatory mechanism of ROS on β-carotene accumulation in *D. salina* under these stress conditions. Moreover, the relationship between photosynthesis activity and β-carotene accumulation is still poorly understood.

Here we investigated the relationship between ROS content and β-carotene accumulation in *D. salina* under different stress conditions (i.e., high light, high salinity, and nitrogen starvation), and the correlation between photosynthesis activity and β-carotene accumulation was also analyzed using Spearman correlation analysis. Additionally, the differential expression of key genes involved in photosynthesis and β-carotene biosynthesis pathways of the cells cultivated with H_2O_2 supplementation was also examined through transcriptomic analysis. In this work, we found that ROS play an important role in β-carotene metabolism through fine-tuning the key genes that are involved in photosynthesis and β-carotene biosynthesis in *D. salina* under stress conditions. Our work might shed light on future research aiming to enhance β-carotene accumulation in *D. salina* and other microalgae.

MATERIALS AND METHODS

Algal Strain and Culture Conditions

Dunaliella salina strain (CCAP 19/18) was purchased from the Culture Collection of Algae and Protozoa (Windermere, United Kingdom). The strain was previously maintained in the medium of modified Artificial Sea Water (ASW), which was composed of 1.5 M NaCl, 5 mM KNO_3, 0.45 mM $MgCl_2{\cdot}6H_2O$, 0.05 mM $MgSO_4{\cdot}7H_2O$, 0.3 mM $CaCl_2{\cdot}2H_2O$, 0.13 mM K_2HPO_4, 0.02 mM $FeCl_3$, 0.02 mM EDTA, and 1 mL of trace element stock containing 50 mM H_3BO_3, 10 mM $MnCl_2{\cdot}4H_2O$, 0.8 mM $ZnSO_4{\cdot}7H_2O$, 0.8 mM $CuSO_4{\cdot}5H_2O$, 2 mM $NaMoO_4{\cdot}2H_2O$, 1.5 mM $NaVO_3$, and 0.2 mM $CoCl_2{\cdot}6H_2O$, and the pH was adjusted to 7.5 (Doddaiah et al., 2013). This strain was maintained in 500-mL conical flasks at 50 μmol photons$\cdot m^{-2}\cdot s^{-1}$ light intensity in this study. To test the effect of H_2O_2 supplementation on β-carotene accumulation in cells, different concentrations of H_2O_2 (0, 0.5, 1.0, 1.5, and 2.0 mM) were added to algal cultures in ASW medium.

The cells were cultivated in air-lift laboratory-scale flat photobioreactors (0.22 × 0.22 × 0.025 m) filled with 1.0 L of culture medium under the following five different culture conditions: nitrogen starvation (N–, ASW medium without KNO_3), high light (HL, 2,000 μmol photons$\cdot m^{-2}\cdot s^{-1}$), high salinity (HS, 3.0 M NaCl), and optimal growth condition (N+, control). Unless otherwise noted, all the cells were cultured in ASW medium at 25°C aerated with filter-sterilized air at 0.5 vvm and illuminated at 100 μmol photons$\cdot m^{-2}\cdot s^{-1}$. The different culture conditions were shown in **Table 1**.

Biomass and β-Carotene Determination

Dry weight was determined as previously described (Chi et al., 2016). Briefly, 10.0-mL cultures were filtered using pre-weighed Whatman GF/C filters (47 mm diameter) and washed three times with 2.0 mL 0.5 M ammonium bicarbonate and then were dried at 60°C for 16 h in an incubator. The dried biomass ($g{\cdot}L^{-1}$) of the microalgal cells was then gravimetrically measured.

TABLE 1 | The different culture conditions used in this study.

Culture conditions	Abbreviations	Light intensity (μmol$\cdot m^{-2}\cdot s^{-1}$)	NaCl (M)	KNO_3 (mM)
Control	N+	100.0	1.5	5.0
Nitrogen starvation	N–	100.0	1.5	0.0
High salinity	HS	100.0	3.0	5.0
High light	HL	2000.0	1.5	5.0

β-Carotene Extraction and Determination

β-Carotene was extracted and measured following the method previously described (Zhu et al., 2018, Kleinegris et al., 2010). Briefly, 1.0 mL of cell culture at exponential phase was harvested at 10,000 g for 2 min and resuspended in 3.0 mL dodecane and 9.0 mL of methanol. After centrifugation for 2 min at 10,000 g, the dodecane-containing lipophilic carotenoids (upper layer) were obtained and measured with a spectrophotometer (Jasco V-530, JASCO Corporation, Japan) at 453 and 665 nm with dodecane as a reference. The carotene concentration was calculated as Equation (1):

$$C_{\beta-car}(mg \cdot L^{-1}) = (A_{453} - A_{665}/3.91) \times 3.657 \times 3 \times X \quad (1)$$

where (A_{453}-A_{665}/3.91) is the absorbance of β-carotene corrected for chlorophyll contamination, 3.657 is the calibration factor derived from HPLC analysis of β-carotene concentration, 3 is the amount of milliliters of dodecane added for extraction, and X is the dilution factor to measure absorbance on spectrophotometer (Kleinegris et al., 2010, 2011).

The amount of β-carotene in the algal biomass was calculated according to Equation (2).

$$\beta - \text{carotene}(\%) = \frac{C_{\beta-car} \times 10}{DW} \quad (2)$$

where $C_{\beta-car}$ is the β-carotene content ($mg \cdot L^{-1}$), and DW is the cell dry weight ($g \cdot L^{-1}$) (Zhu et al., 2018).

Determination of ROS and H_2O_2 Levels

The ROS levels were determined using the ROS assay kit (Beyotime Institute of Biotechnology, China) as previously reported (Kong et al., 2018). Briefly, 10 μM of 2′,7′-dichlorofluorescein diacetate (DCFH-DA) was added to 1.0 mL samples containing 1.0×10^6 cells and incubated for 20 min in the dark. The samples were washed twice and resuspended in 1.0 mL fresh medium. The fluorescence emission spectra were read at 525 nm (with excitation at 500 nm) using a fluorescence spectrophotometer (F-4500, Hitachi, Japan) (Liu et al., 2012).

The H_2O_2 content was measured using a commercial H_2O_2 assay kit (NJJCBIO, China) as previously described (Zhang L. et al., 2019). Briefly, 1.0×10^6 fresh algal cells were homogenized in an ice bath and centrifuged at 10,000 g for 3 min, and H_2O_2 concentration was measured following the manufacturer's protocols.

Chlorophyll Fluorescence Analysis

The chlorophyll fluorescence was measured by a Dual Pulse Amplitude Modulated Fluorometer (Water-PAM Heinz Walz GmbH, Effeltrich, Germany). Dark adaption was carried out for 10 min before applying a saturating pulse (0.6 s, 1,400 $\mu mol \cdot m^{-2} \cdot s^{-1}$) to measure the maximal quantum yield of PS II (F_v/F_m), non-photochemical quenching (NPQ) and actual quantum yield of PS II (F/F_m') (Chi et al., 2016; Liu et al., 2018).

RNA-Seq and Differentially Expressed Gene Analysis

Total RNAs were, respectively, extracted from three biological replicates of *D. salina* cells cultivated with or without H_2O_2 supplementation using a Total RNA Extraction System (Takara, Japan) following the previous method (Liang et al., 2020). The RNA concentration and integrity were assessed using NanoDrop 2000 (Thermo) and an Agilent 2100 Bioanalyzer (Agilent Technologies, CA, USA). The mRNA was purified and fragmented to about 200 nt. These fragments were used as templates to synthesize cDNA. After purification, their sequencing was performed in Novogene Bioinformatics Technology Co. (Beijing, China).

RNA-seq data was analyzed by Novogene Bioinformatics Technology Co. (Beijing, China). Clean reads obtained from editing raw reads were mapped onto unigene sequences using Bowtie2-2.2.3. The expected number of Fragments Per Kilobase of transcript sequence per Millions base pairs sequenced (FPKM) was performed to quantify gene expression levels, and DESeq R package was used to analyze the differentially expressed genes (DEGs) in *D. salina* cells between control and H_2O_2-induced samples with a significantly differential expression at $p < 0.05$ and fold change ≥1. The Kyoto Encyclopedia of Genes and Genomes (KEGG) pathways for DEGs were annotated by KEGG automatic annotation server (Liang et al., 2020).

Statistical Analysis

All the experiments were carried out in three biological replicates, and the data were presented as the mean value ± standard division (SD). Correlation between ROS and β-carotene content was analyzed using Spearman correlation analysis and the statistical analyses were conducted using SPSS 19.0 (SPSS, Chicago, IL, USA).

RESULTS AND DISCUSSION

The β-Carotene Production Was Enhanced Under Stress Conditions in *D. salina*

To date, several studies have reported the effect of different culture conditions (e.g., HL, HS, and N-) on the β-carotene content in *D. salina*, respectively (Liu et al., 2012; Mirshekari et al., 2019; Zhao et al., 2019). However, it is difficult to directly compare the exact results of these studies, mainly due to various initial cell numbers inoculated and different illumination techniques applied. To study whether various stress conditions result in the same oxidative stress for carotenoid accumulation, we compared the effect of different stress conditions on β-carotene and biomass production in *D. salina*. We inoculated the cells with the same initial biomass density ($0.11 \ g \cdot L^{-1}$) and cultivated them in photobioreactors that enable well-defined light regimes and remain constant cultivation conditions throughout experiments. The lower biomass concentrations were observed under N- and HS stress conditions compared with optimal growth conditions (N+) (**Figure 1A**). For example, the biomass concentrations were, respectively, 0.31 and $0.33 \ g \cdot L^{-1}$ under the N– and HS conditions upon 96 h, which were significantly lower than that of the N+ condition ($0.42 \ g \cdot L^{-1}$). However, under HL conditions *D. salina* has a higher biomass concentration (e.g., $0.51 \ g \cdot L^{-1}$ upon 96 h) compared with the N+ condition (**Figure 1A**). Although the cell growth was arrested under N– and HS conditions, β-carotene accumulation was enhanced under

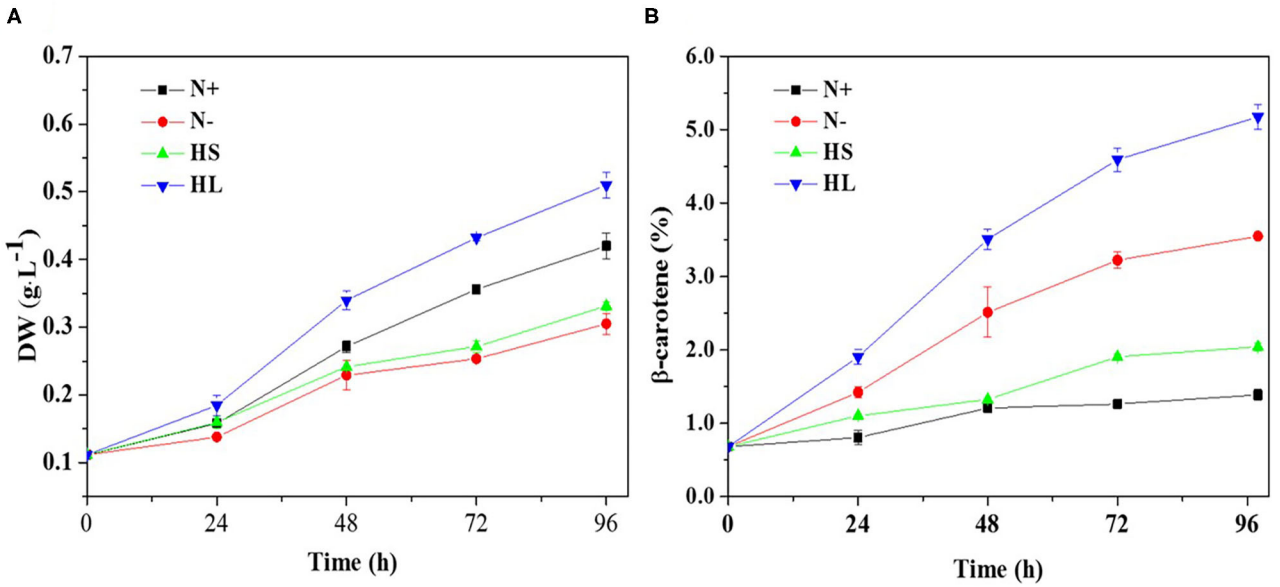

FIGURE 1 | Time profiles of the growth and β-carotene accumulation **(A,B)** of *D. salina* cells cultivated under different stress conditions. DW, dry weight; N+, optimal growth condition (control); N–, nitrogen starvation; HS, high salinity; HL, high light. Plotted data are the averages ± standard division (SD) of three biological replicates.

all the stress conditions tested. The maximal β-carotene content was observed under HL (5.18%), followed by 3.55 and 2.04% under N- and HS conditions, which are significantly higher than that under N+ conditions (1.38%) (**Figure 1B**). These results suggest that the slower growth rate or the higher light intensity can enhance the production level of β-carotene. The increased β-carotene levels might be due to the response to these stress conditions.

In *D. salina*, β-carotene is largely accumulated under N- conditions (Lamers et al., 2012). β-Carotene accumulation was also enhanced under HL or HS conditions (Lamers et al., 2008, 2010; Einali and Valizadeh, 2015). Indeed, we have also found that the production level of β-carotene is higher in those stress conditions tested (**Figure 1**). Moreover, our results suggested that the content of β-carotene is higher but the biomass is lower under N- and HS stress conditions (**Figure 1A**). This could be partially due to large amounts of carbon and ATP being channeled from synthesis of energy compounds for growth to the synthesis of metabolites (e.g., carotenoids) (Liu et al., 2018). Noticeably, the biomass and β-carotene accumulation are both higher in HL conditions compared with other cultivation conditions tested (**Figure 1**). This could be due to the fact that more energy was transferred to biomass production and β-carotene synthesis under HL conditions in *D. salina* (Wu et al., 2016; Habiby et al., 2018; Song et al., 2018). It is likely that HL is a more potent inducer of β-carotene overproduction than nitrogen depletion (**Figure 1B**). However, in terms of energy cost, β-carotene production through nitrogen depletion still appears more promising, since 20 times less light energy was applied than that in the HL condition (**Table 1**). In contrast to the other stress conditions tested, the intracellular β-carotene content was only increased to 2.04% upon 96 h after high-salinity treatment (**Figure 1B**). This result indicated that salinity-induced β-carotene accumulation was very limited in *D. salina*. Recently, it was also reported that high-salinity stress does not significantly promote the accumulation of β-carotene or even has adverse effects in an isolated *D. salina* strain (GY-H13) (Zhu et al., 2020), which is similar with reports in other microalgae, such as *Dunaliella parva* (Shang et al., 2018). Taken together, our results indicated that β-carotene production was enhanced under all the stress conditions tested, even though the increased levels of β-carotene and growth rate in response to stimuli derived from different stress are varied.

Correlation Between Photosynthesis Activity and β-Carotene Accumulation

Carotenoids are essential components of photosynthetic organisms including algae. We examined the relationship between photosynthesis activity and β-carotene accumulation. Although under stress conditions (i.e., HL, N–, and HS) the β-carotene content was increased (**Figure 1B**), the maximal quantum yield of PS II (F_v/F_m) was decreased significantly and the non-photochemical quenching (NPQ) was enhanced (**Figures 2A,B**).

Furthermore, Spearman correlation analysis was used to investigate the correlation between photosynthesis activity and β-carotene accumulation under stress conditions. The maximal Spearman correlation coefficient (-0.924, $p < 0.05$) was observed by plotting the F_v/F_m against the corresponding β-carotene content (%) (**Figure 2C**), while the coefficient of 0.895 ($p < 0.05$) was obtained when plotting NPQ (**Figure 2D**). These results show that F_v/F_m were negatively while NPQ were positively correlated with β-carotene accumulation under

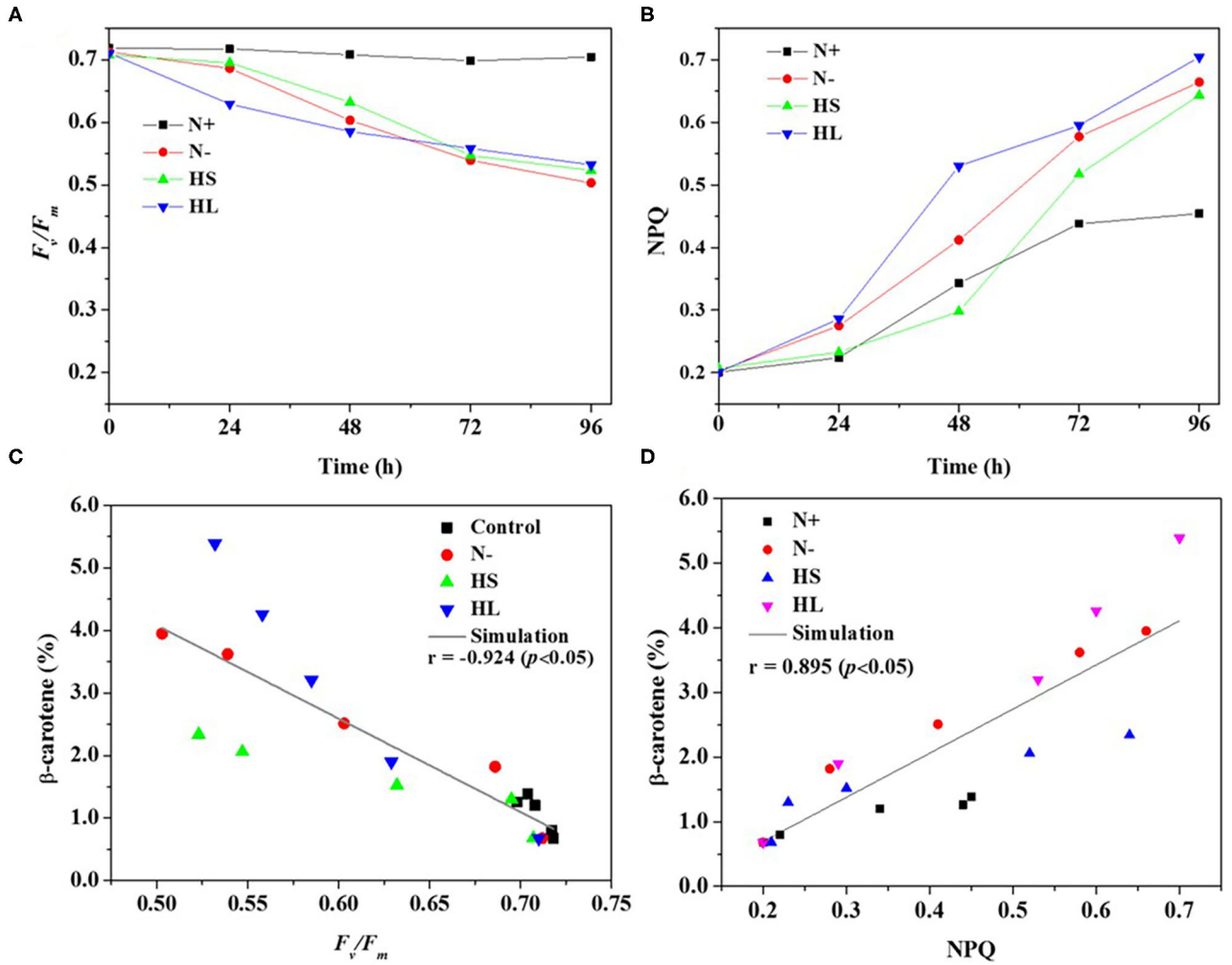

FIGURE 2 | The profiles of the F_v/F_m and NPQ **(A,B)** evaluated over time, and the correlation of the F_v/F_m and NPQ with corresponding carotene content **(C,D)** under different culture conditions, respectively. F_v/F_m, maximum quantum efficiency of PS II; NPQ, non-photochemical quenching; N+, optimal growth condition (control); N-, nitrogen starvation; HS, high salinity; HL, high light. Plotted data are the averages ± SD of three biological replicates.

different stress conditions. It is found that F_v/F_m can be regarded as a stress indicator (Cao et al., 2019); the decrease of F_v/F_m suggested that the photosynthesis activity was arrested under N starvation, HL, and HS stress conditions. NPQ is a protection process that thermally dissipates excessive light energy absorbed by photosynthesis pigment (Wang et al., 2016). It was reported that ROS produced under stress conditions can decrease photosynthetic activity through the peroxidation of lipids in the thylakoids, damage of PSII complex, and decrease in overall activity of the electron transport chain of PSII (Salguero et al., 2003; Zhang L. et al., 2019). Therefore, ROS generation may be one of the major factors accounting for the decrease of photosynthesis efficiency (the effective photochemical efficiency of PSII reaction centers) in *D. salina* under stresses conditions.

Correlation Between ROS Production and β-Carotene Accumulation

In the photosynthetic microorganisms, the imbalance between light harvesting and energy utilization during stress conditions will result in the production of ROS, due to overexcitation of chlorophyll molecules (Shi et al., 2017). Then, the contents of total ROS and representative ROS (e.g., H_2O_2) were investigated under the aforementioned stress conditions. We found that the contents of total ROS and H_2O_2 are significantly higher under all the stress conditions compared with normal condition (N+) (**Figures 3A,B**). However, the ROS and H_2O_2 levels are varied among all stress conditions tested with the highest level under the HL condition (**Figures 3A,B**). The plateau period of ROS and H_2O_2 contents appeared at 48 and 72 h, respectively (**Figures 3A,B**), which indicate that other ROS (e.g.,

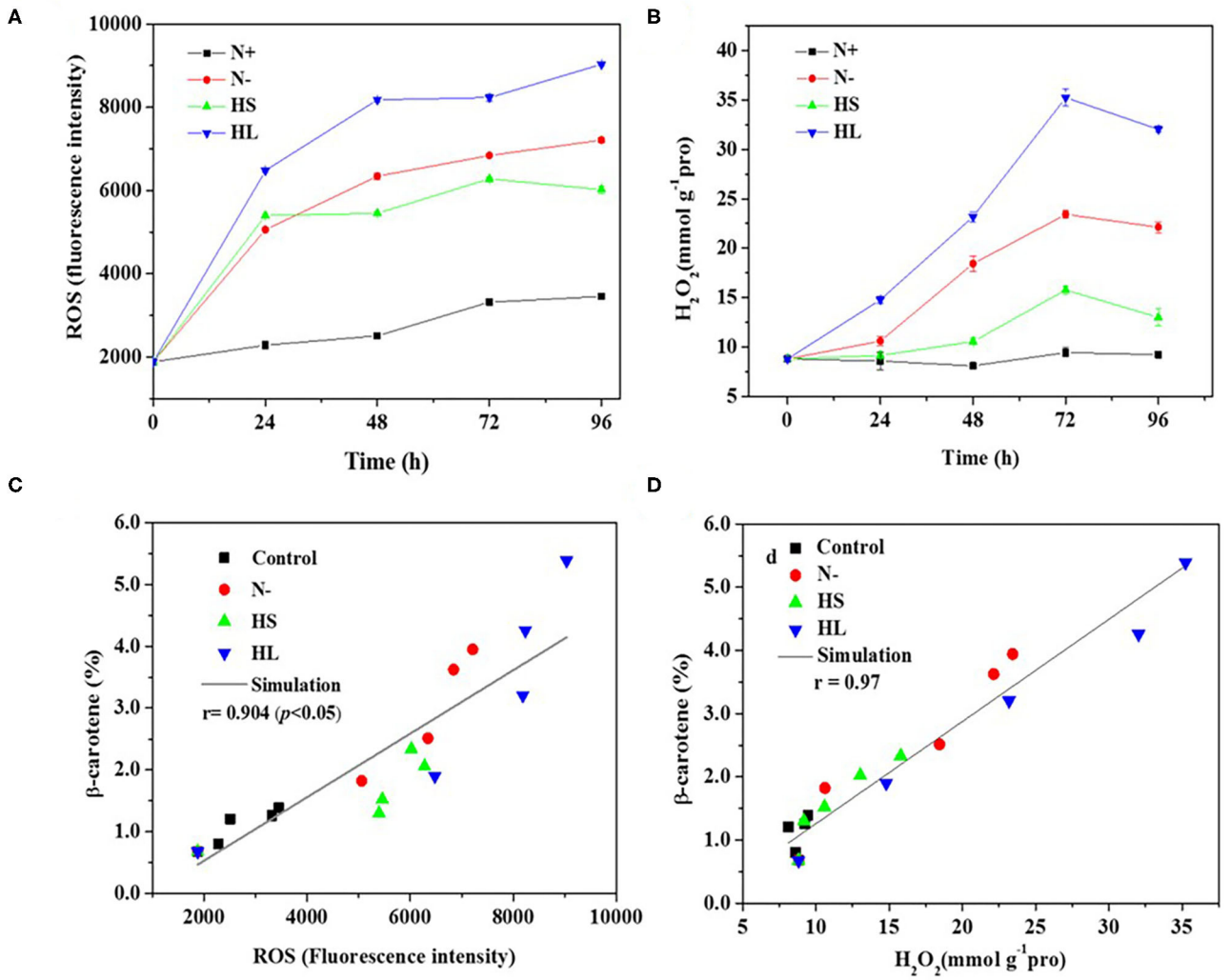

FIGURE 3 | The intracellular contents of ROS and H_2O_2 **(A,B)**, and relationship of total ROS and H_2O_2 with corresponding β-carotene content **(C,D)** under different stress conditions, respectively. N+, optimal growth condition (control); N–, nitrogen starvation; HS, high salinity; HL, high light. The experiments were carried out in triplicate and the data were presented as the mean value ± SD.

$O2^{\cdot}$- and $OH^{\cdot}$) are also promptly produced in the cells under stress conditions.

Although a simultaneous increase in ROS and β-carotene accumulation under stress conditions was observed in *D. salina*, the relationship between ROS production and β-carotene accumulation is currently still unclear. In this study, Spearman correlation analysis was used to investigate the correlation between the two events. Here, four stress conditions were evaluated together rather than examining a single condition to avoid false-positive correlations. The maximal Spearman correlation coefficient (0.90, $p < 0.01$) was observed by plotting the ROS concentration against the corresponding β-carotene content (%) (**Figure 3C**), while the coefficient of 0.97 ($p < 0.01$) was obtained when plotting H_2O_2 (**Figure 3D**). Generally, if the Spearman correlation coefficient is more than 0.8, it is assumed that there is a strong correlation between two events (Zhang L. et al., 2019). Thus, our results show that intracellular ROS and H_2O_2 levels were positively correlated with β-carotene accumulation under different stress conditions. The simultaneous increases of ROS and β-carotene contents under stress conditions were also found in other green microalgae such as *C. reinhardtii* (Sun et al., 2018). Moreover, it was reported that the upregulation of *de novo* carotenoid synthesis in *C. reinhardtii* cells under HL conditions is mediated through H_2O_2 (Chang et al., 2013).

Overall, our data indicated that the stress conditions are likely to cause the decrease of F_v/F_m accompanied with the high level of ROS generated. Subsequently, the ROS trigger the overaccumulation of β-carotene. The elevated β-carotene content under stress conditions might be due to the stimuli caused by ROS in *D. salina* under stress conditions.

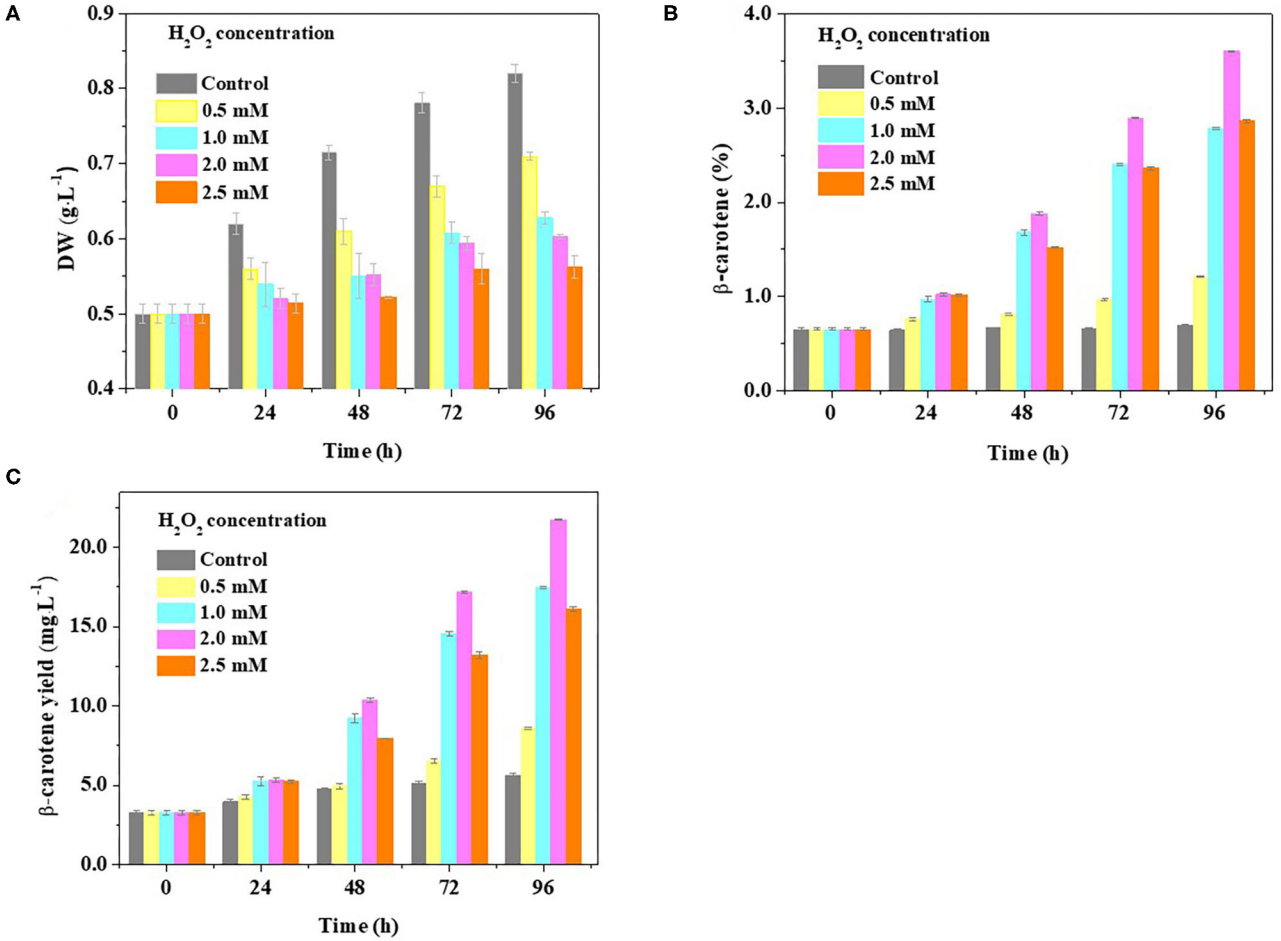

FIGURE 4 | Effect of H_2O_2 supplementation on biomass and β-carotene content in *D. salina*. Time-course analyses of the biomass **(A)** and β-carotene content and yield **(B,C)** when the cells were cultivated with H_2O_2 supplementation of different concentrations. DW, dry weight. Plotted data are the averages ± SD of three biological replicates.

H_2O_2 Supplementation Results in Lower Biomass and β-Carotene Overaccumulation

To further evaluate the idea that β-carotene overaccumulation observed in *D. salina* may result from an increased ROS, we determined the β-carotene contents in the cells cultivated with H_2O_2 supplementation. Considering the dual role of H_2O_2 on cell physiology and metabolism, the H_2O_2 concentration used was optimized in this work based on the ratio of H_2O_2 provided by previous reports (Yilancioglu et al., 2014; Zhang et al., 2016). We found that the biomass was reduced while the β-carotene content was increased when the amount of H_2O_2 concentration supplemented is increasing (**Figures 4A,B**). A significant increase in cellular β-carotene concentration ($p < 0.05$) was observed at 2.0 mM H_2O_2 upon 96 h (**Figure 4B**). The β-carotene content was increased to 6.7-fold, and the yield of β-carotene was 3.9-fold higher at 2.0 mM H_2O_2 than that under optimal growth conditions (**Figures 4B,C**). These results suggest that β-carotene accumulation can be enhanced by moderate H_2O_2 supplementation.

Transcriptomic Analysis Reveals Key Genes Involved in β-Carotene Overaccumulation Induced by ROS

To explore the transcriptional response induced by H_2O_2, the differentially expressed genes (DEGs) from *D. salina* grown with H_2O_2 supplementation (2.0 mM) were investigated by transcriptomic analysis. A high correlation coefficient was obtained within the same treatment condition, while a low correlation coefficient was observed between the different treatment conditions (**Figure 5A**). These results indicate that the transcriptome data were reliable. There are 2,252 genes with a change of at least 2-fold that we assumed as DEGs, of which 1,114 genes were upregulated, and 1,138 genes were downregulated (**Figure 5B**).

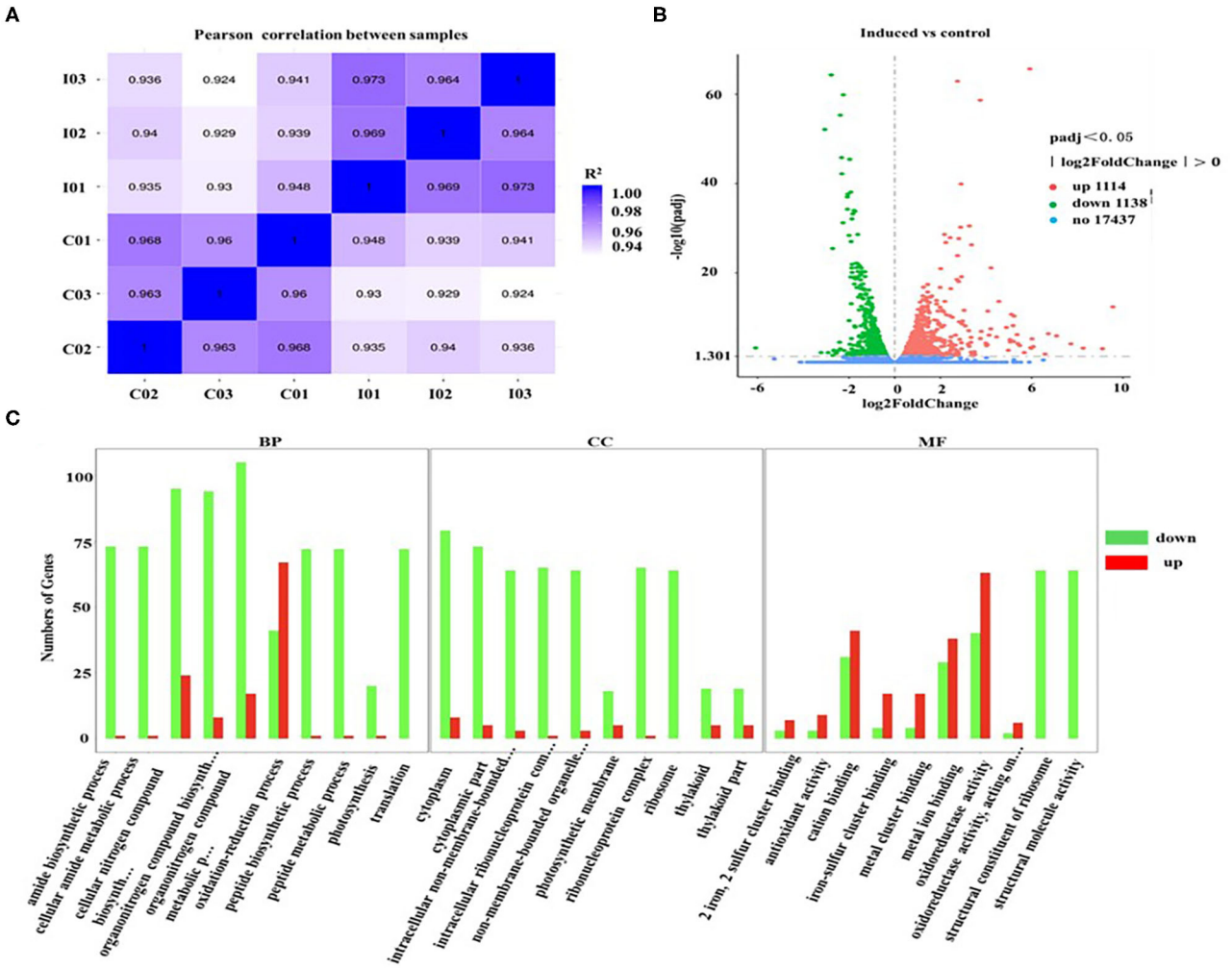

FIGURE 5 | Gene ontology classification analysis of unigenes that are involved in the overaccumulation of β-carotene induced by ROS. **(A)** The correlation plot between different samples. I01, I02, and I03 (2.0 mM H_2O_2); C01, C02, and C03 (Control, 0 mM H_2O_2). **(B)** MA plot of differentially expressed genes (DEGs). Significantly upregulated and downregulated genes are shown as red and green dots, respectively. Genes with no significant changes are shown as blue spots. **(C)** Gene ontology (GO) classification analysis of DEGs. The X-axis shows the GO function. The Y-axis shows the number of genes detected. Significantly upregulated and downregulated genes are shown as red and green rectangles. BP, biological processes; CC, cellular components; and MF, molecular functions.

Furthermore, the gene ontology (GO) classification was performed according to the gene annotations. Most of DEGs were distributed in three GO terms, among which 526, 197, and 679 of DEGs were assigned in the biological process category, cellular component category, and molecular function category, respectively (**Figure 5C**). In the biological processes, the most active subcategories were the clusters of the "metabolic process" and "cellular process." The main subcategories in molecular functions were the clusters of "binding" and "catalytic activity." In the cellular components, most of the detected DEGs were dominantly located in "cell" and "cell part." Moreover, the genes involved in the biological processes of "reproduction" and "reproductive processes" were significantly downregulated in *D. salina* (**Figure 5C**), which partially account for the reasons of the increased growth of the cells as shown in **Figure 1A**.

We found that the β-carotene and ROS contents were increased but photosynthesis activity was reduced during cultivation of *D. salina* (**Figures 1**, **2**) under stress conditions, and therefore, the genes involved in the photosynthesis and β-carotene biosynthesis were analyzed upon H_2O_2 supplementation. Most of DEGs involved in photosynthesis pathways (e.g., antenna proteins) were significantly downregulated when H_2O_2 was supplemented (**Supplementary Figures 1**, **2**). This result is consistent with a previous study that the major DEGs involved in photosynthesis pathways (e.g., PSII) exhibited a dramatic downregulation with ROS burst in *Dunaliella bardawil* under heat stress conditions (Liang et al., 2020). In other microalgae such as *Chromochloris zofingiensis*, it was also reported that most genes encoding components of PS I, PS II, light-harvesting complexes

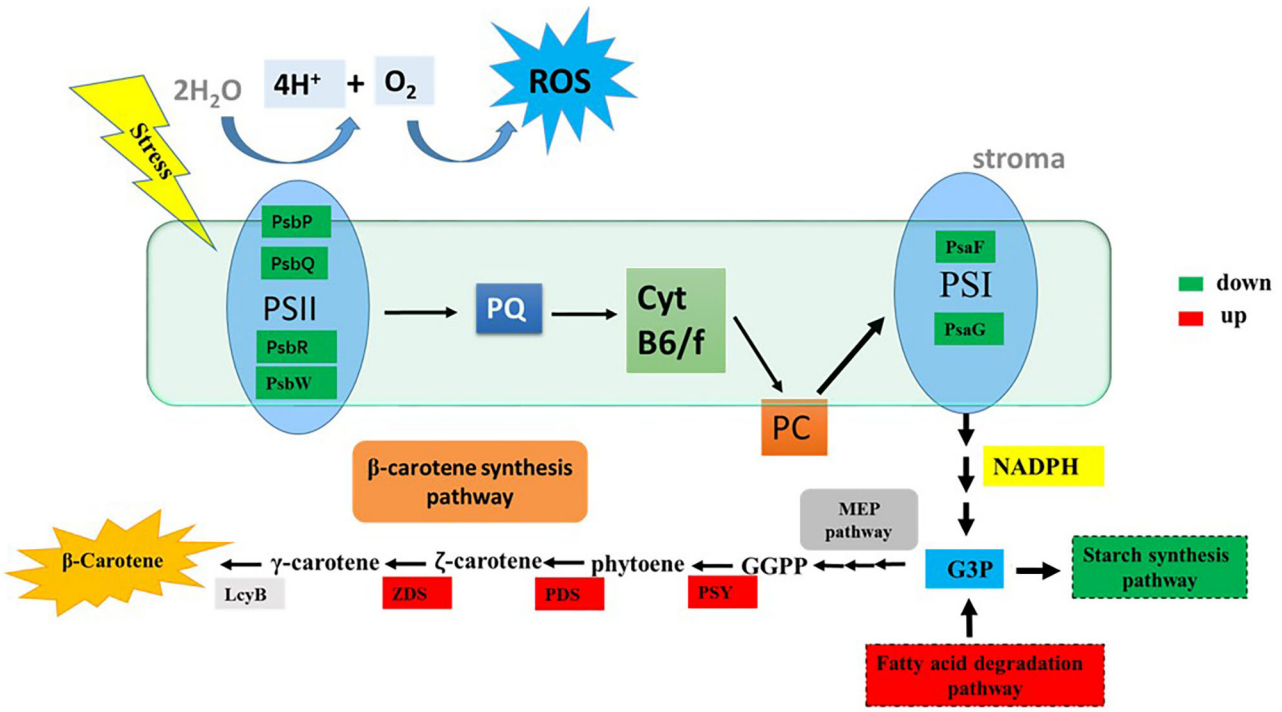

FIGURE 6 | The tentative model of the correlationship between ROS and β-carotene accumulation. G3P, glyceraldehyde-3-phosphate; GGPP, geranylgeranyl diphosphate; LcyB, lycopene β-cyclase; PDS, phytoene desaturase; PSY, phytoene synthase; ZDS, z-Carotene desaturase; PQ, plastoquinone; PC, plastocyanin; ROS, reactive oxygen species; PsbP, photosystem II oxygen-evolving enhancer protein; PsbQ, photosystem II oxygen-evolving enhancer protein; PsbR, photosystem II 10 kDa protein; PsbW, photosystem II reaction center W protein; PsaF, photosystem I reaction center subunit III; PsaG, photosystem I reaction center subunit V. Significantly upregulated and downregulated genes are shown as red and green rectangles.

(LHCs), and Cyt b_6/f exhibited dramatic downregulation in response to nitrogen deprivation (Zhang Y. et al., 2019). Furthermore, our results showed that the key genes involved in biosynthesis of carotenoids were upregulated upon H_2O_2 supplementation (**Supplementary Figure 3**). For example, phytoene synthase (PSY), phytoene desaturase (PDS), and zeta-carotene desaturase (ZDS), known as the rate-limiting enzymes during carotenoid biosynthesis (Shang et al., 2018; Zhu et al., 2020), were highly overexpressed upon H_2O_2 supplementation (**Supplementary Figure 3**). These results are consistent with the previous studies that the expressions of *PSY*, *PDS*, and *ZDS* were upregulated by quantitative RT-PCR validation in *D. salina* under stress conditions (e.g., high light, nutrient deprivation, high salinity), respectively (Coesel et al., 2008; Lv et al., 2016; Zhu et al., 2020). Similarly, in the H_2O_2-treated *C. reinhardtii* cells, the transcripts of both *PSY* and *PDS* were also dramatically increased (Chang et al., 2013). The increased expression of these key genes indicated that they might play an important role in the biosynthesis of β-carotene.

The genes involved in starch, sucrose, fatty acids, and amino acid metabolism were also examined. There are 9 genes that are involved in the synthesis of starch and sucrose which were downregulated in *D. salina* cells when cultivated with H_2O_2 supplementation (**Supplementary Table 1**). The expression of 28 genes which are involved in the biosynthesis of amino acids pathway was negatively correlated with H_2O_2 (**Supplementary Table 2**). A similar phenomenon was also found in the previous study that the DEGs responsible for the biosynthesis of amino acids was downregulated in *D. bardawil* under heat stress (Liang et al., 2020). Our transcriptomic data showed that genes such as *FabF*, *FabD*, *FabG*, *FabZ*, and *FabI* that are involved in the fatty acid biosynthesis pathway were downregulated (**Supplementary Table 3**), while the genes such as *FDH1*, *ATO1*, *ACAT*, and *ACSL* that are involved in the fatty acid degradation were highly expressed when H_2O_2 was supplemented (**Supplementary Table 4**). Most of the DEGs involved in fatty acid biosynthesis were also downregulated in *D. bardawil* under heat stress (Liang et al., 2020) and in *C. zofingiensis* upon nitrogen deprivation condition (Zhang Y. et al., 2019; Zhang et al., 2020). Overall, our results indicated that the increased expressions of genes involved in fatty acid degradation and the decreased expression of genes involved in the pathways of fatty acid, amino acid, and starch biosynthesis might facilitate β-carotene overaccumulation in *D. salina* after H_2O_2 was supplemented. Moreover, the transcriptome data show that the expressions of key genes involved in the synthesis of energy storage compounds (e.g., starch and lipids) and the photosynthesis activity were decreased, respectively, in *D. salina* cells cultivated with H_2O_2 supplementation, which might account for the changes of cellular photosynthetic efficiency and energy metabolism (Liska et al., 2004; Li et al., 2010; Zhao et al., 2019).

In this study, the potential relationship between ROS and β-carotene biosynthesis is proposed in *D. salina* under stress conditions (**Figure 6**). Our results suggested that the key genes involved in photosynthesis pathways were downregulated in the cells when H_2O_2 was supplemented (**Supplementary Figure 1**), which indicated that the photosynthetic activity was reduced. The excessive electrons from the photosynthesis system could lead to ROS generation and overaccumulation (Shaish et al., 1993), which will further result in decreased generation of NADPH and ATP. Therefore, NADPH and ATP might not be sufficient for the synthesis of glyceraldehyde-3-phosphate (G3P, which is the precursor and carbon skeleton for β-carotene biosynthesis) through the Calvin cycle. The downregulated genes for the synthesis of starch and upregulated genes for the fatty acid degradation pathway under H_2O_2 supplementation in this study indicate that more cellular energy and precursors might be recycled or shuttled for β-carotene biosynthesis. Overaccumulated ROS are proposed to trigger the high expressions of key genes (e.g., *PSY*, *PDS*, *ZDS*, and *LcyB*) that are involved in β-carotene synthesis (**Figure 6**) and thus lead to β-carotene overaccumulation in *D. salina* under stress conditions. Therefore, it is likely that ROS can also serve as mediators or second messengers and play important roles in the regulation of intracellular energy metabolism in response to environmental stress in microalgae *D. salina*. In this work, we found that β-carotene overaccumulation was induced by ROS through fine-tuning the genes involved in β-carotene biosynthesis. Based on these results, the relationship between ROS and β-carotene accumulation in *D. salina* under stress conditions was proposed. This study provided a better understanding of the regulatory mechanism involved in β-carotene accumulation in *D. salina*, which will be useful for overaccumulation of carotenoids and other valuable compounds in other microalgae.

CONCLUSIONS

In this study, a high positive Spearman correlation coefficient was observed between the cellular ROS level and β-carotene content in *D. salina* under stress conditions. Moreover, our transcriptome data indicate that most of the DEGs involved in biosynthesis of β-carotene were significantly upregulated, and those of which involved in photosynthesis activity were downregulated when the cells cultivated with H_2O_2 supplementation. Overall, our results indicated that ROS induce β-carotene biosynthesis caused by changes of photosynthesis efficiency and energy metabolism in *D. salina* under stress conditions.

DATA AVAILABILITY STATEMENT

The raw data supporting the conclusions of this article will be made available by the authors, without undue reservation.

AUTHOR CONTRIBUTIONS

YX, FK, and ZC conceived and designed the experiments. YX performed all the experiments. YX and FK analyzed the data and drafted the manuscript. All authors contributed to the article and approved the submitted version.

FUNDING

This work was supported by the National Natural Science Foundation of China (31900221), Natural Science Foundation of Liaoning Province of China (2020-MS-102), and Fundamental Research Funds for the Central Universities [DUT18RC(3)041].

ACKNOWLEDGMENTS

We thank Dr. Song Xue from Dalian University of Technology for the useful discussions and critical reading of the manuscript.

SUPPLEMENTARY MATERIAL

The Supplementary Material for this article can be found online at: https://www.frontiersin.org/articles/10.3389/fbioe.2020.613768/full#supplementary-material

REFERENCES

Cao, X., Xi, Y., Liu, J., Chu, Y., Wu, P., Yang, M., et al. (2019). New insights into the CO_2-steady and pH-steady cultivations of two microalgae based on continuous online parameter monitoring. *Algal Res.* 38, 1–6. doi: 10.1016/j.algal.2018.11.021

Chang, H., Kang, C., and Lee, T. (2013). Hydrogen peroxide production protects *Chlamydomonas reinhardtii* against light-induced cell death by preventing singlet oxygen accumulation through enhanced carotenoid synthesis. *J. Plant Physiol.* 170, 976–986. doi: 10.1016/j.jplph.2013.02.001

Chew, K., Yap, J., Show, P., Suan, N., Juan, J., Ling, T., et al. (2017). Microalgae biorefinery: high value products perspectives. *Bioresour. Technol.* 229, 53–62. doi: 10.1016/j.biortech.2017.01.006

Chi, L., Yao, C., Cao, X., and Xue, S. (2016). Coordinated regulation of nitrogen supply mode and initial cell density for energy storage compounds production with economized nitrogen utilization in a marine microalga *Isochrysis zhangjiangensis*. *Bioresour. Technol.* 200, 1–12. doi: 10.1016/j.biortech.2015.10.059

Coesel, S., Baumgartner, A., Teles, L., Ramos, A., Henriques, N., Cancela, L., et al. (2008). Nutrient limitation is the main regulatory factor for carotenoid accumulation and for Psy and Pds steady state transcript levels in *Dunaliella salina* (Chlorophyta) exposed to high light and salt stress. *Marine Biotechnol.* 10, 602–611. doi: 10.1007/s10126-008-9100-2

Combe, C., Hartmann, P., Rabouille, S., Talec, A., Bernard, O., and Sciandra, A. (2015). Long-term adaptive response to high-frequency light signals in the unicellular photosynthetic eukaryote *Dunaliella salina*. *Biotechnol. Bioeng.* 112, 1111–1121. doi: 10.1002/bit.25526

Cowan, A., and Rose, P. (1991). Abscisic-acid metabolism in salt-stressed cells of *Dunaliella salina*-possible interrelationship with beta-carotene accumulation. *Plant Physiol.* 97, 798–803. doi: 10.1104/pp.97.2.798

Cowan, A., Rose, P., and Horne, L. (1992). *Dunaliella-salina*-a model system for studying the response of plant-cells to stress. *J. Exp. Bot.* 43, 1535–1547. doi: 10.1093/jxb/43.12.1535

Doddaiah, K., Narayan, A., Aswathanarayana, R., and Ravi, S. (2013). Effect of metabolic inhibitors on growth and carotenoid production in *Dunaliella bardawil*. *J. Food Sci. Technol.* 50, 1130–1136. doi: 10.1007/s13197-011-0429-6

Einali, A., and Valizadeh, J. (2015). Propyl gallate promotes salt stress tolerance in green microalga *Dunaliella salina* by reducing free radical oxidants and enhancing beta-carotene production. *Acta Physiol. Plantarum* 37,1–10. doi: 10.1007/s11738-015-1832-9

Habiby, O., Nahor, O., Israel, A., Liberzon, A., and Golberg, A. (2018). Exergy efficiency of light conversion into biomass in the macroalga Ulva sp (Chlorophyta) cultivated under the pulsed light in a photobioreactor. *Biotechnol. Bioeng.* 115, 1–12. doi: 10.1002/bit.26588

Harvey, P., and Xu, Y. (2019). Carotenoid production by *Dunaliella salina* under red light. *Antioxidants* 8, 1–14. doi: 10.3390/antiox8050123

Henriquez, V., Escobar, C., Galarza, J., and Gimpel, J. (2016). Carotenoids in microalgae. *Subcell. Biochem.* 79, 219–237. doi: 10.1007/978-3-319-39126-7_8

Jin, E., and Melis, A. (2003). Microalgal biotechnology: carotenoid production by the green algae *Dunaliella salina*. *Biotechnol. Bioprocess Eng.* 8, 331–337. doi: 10.1007/BF02949276

Kamalanathan, M., Dao, L., Chaisutyakorna, P., Gleadow, R., and Beardall, J. (2017). Photosynthetic physiology of *Scenedesmus sp* (Chlorophyceae) under photoautotrophic and molasses-based heterotrophic and mixotrophic conditions. *Phycologia* 56, 666–674. doi: 10.2216/17-45.1

Kleinegris, D., Janssen, M., Brandenburg, W., and Wijffels, R. (2010). The selectivity of milking of *Dunaliella salina*. *Marine Biotechnol.* 12, 14–23. doi: 10.1007/s10126-009-9195-0

Kleinegris, D., van Es, M., Janssen, M., Brandenburg, W., and Wijffels, R. (2011). Phase toxicity of dodecane on the microalga *Dunaliella salina*. *J. Appl. Phycol.* 23, 949–958. doi: 10.1007/s10811-010-9615-6

Kong, F., Burlacot, A., Liang, Y., Légeret, B., Alseekh, S., Brotman, Y., et al. (2018). Interorganelle communication: peroxisomal malate dehydrogenase2 connects lipid catabolism to photosynthesis through redox coupling in *Chlamydomonas*. *Plant Cell* 30, 1824–1847. doi: 10.1105/tpc.18.00361

Lamers, P., Janssen, M., De Vos, R., Bino, R., and Wijffels, R. (2008). Exploring and exploiting carotenoid accumulation in *Dunaliella salina* for cell-factory applications. *Trends Biotechnol.* 26, 631–638. doi: 10.1016/j.tibtech.2008.07.002

Lamers, P., Janssen, M., De Vos, R., Bino, R., and Wijffels, R. (2012). Carotenoid and fatty acid metabolism in nitrogen-starved *Dunaliella salina*, a unicellular green microalga. *J. Biotechnol.* 162, 21–27. doi: 10.1016/j.jbiotec.2012.04.018

Lamers, P., van de Laak, C., Kaasenbrood, P., Lorier, J., Janssen, M., De Vos, R. C., et al. (2010). Carotenoid and fatty acid metabolism in light-stressed *Dunaliella salina*. *Biotechnol. Bioeng.* 106, 638–648. doi: 10.1002/bit.22725

Li, Y., Han, D., Hu, G., Sommerfeld, M., and Hu, Q. (2010). Inhibition of starch synthesis results in overproduction of lipids in *Chlamydomonas reinhardtii*. *Biotechnol. Bioeng.* 107, 258–268. doi: 10.1002/bit.22807

Liang, M., Jiang, J., Wang, L., and Zhu, J. (2020). Transcriptomic insights into the heat stress response of *Dunaliella bardawil*. *Enzyme Microb. Technol.* 132,1–13. doi: 10.1016/j.enzmictec.2019.109436

Liang, M., Wang, L., Wang, Q., Zhu, J., and Jiang, J. (2019). High-value bioproducts from microalgae: strategies and progress. *Crit. Rev. Food Sci. Nutr.* 59, 2423–2441. doi: 10.1080/10408398.2018.1455030

Liska, A., Shevchenko, A., Pick, U., and Katz, A. (2004). Enhanced photosynthesis and redox energy production contribute to salinity tolerance in *Dunaliella* as revealed by homology-based proteomics. *Plant Physiol.* 136, 2806–2817. doi: 10.1104/pp.104.039438

Liu, J., Yao, C., Meng, Y., Cao, X., Wu, P., and Xue, S. (2018). The Delta F/F-m '-guided supply of nitrogen in culture medium facilitates sustainable production of TAG in *Nannochloropsis oceanica* IMET1. *Biotechnol. Biofuels.* 11,1–8. doi: 10.1186/s13068-018-1168-y

Liu, W., Ming, Y., Li, P., and Huang, Z. (2012). Inhibitory effects of hypo-osmotic stress on extracellular carbonic anhydrase and photosynthetic efficiency of green alga *Dunaliella salina* possibly through reactive oxygen species formation. *Plant Physiol. Biochem.* 54, 43–48. doi: 10.1016/j.plaphy.2012.01.018

Lv, H., Cui, X., Wahid, F., Xia, F., Zhong, C., and Jia, S. (2016). Analysis of the physiological and molecular responses of *Dunaliella salina* to macronutrient deprivation. *PLoS ONE* 11:e0152226. doi: 10.1371/journal.pone.0152226

Mirshekari, M., and Einali, A., Valizadeh, J. (2019). Metabolic changes and activity pattern of antioxidant enzymes induced by salicylic acid treatment in green microalga *Dunaliella salina* under nitrogen deficiency. *J. Appl. Phycol.* 31, 1709–1719. doi: 10.1007/s10811-018-1715-8

Nethravathy, M., Mehar, J., Mudliar, S., and Shekh, A. (2019). Recent advances in microalgal bioactives for food, feed, and healthcare products: commercial potential, market space, and sustainability. *Comp. Rev. Food Sci. Food Safety* 18, 1882–1897. doi: 10.1111/1541-4337.12500

Salguero, A., de la Morena, B., Vigara, J., Vega, J., Vilchez, C., and Leon, R. (2003). Carotenoids as protective response against oxidative damage in *Dunaliella bardawil*. *Biomol. Eng.* 20, 249–253. doi: 10.1016/S1389-0344(03)00065-0

Shaish, A., Avron, M., Pick, U., and Ben-Amotz, A. (1993). Are active oxygen species involved in induction of beta-carotene in Dunaiella bardawil? *Planta* 190, 363–368. doi: 10.1007/BF00196965

Shang, C., Wang, W., Zhu, S., Wang, Z., Qin, L., Alam, M., et al. (2018). The responses of two genes encoding phytoene synthase (Psy) and phytoene desaturase (Pds) to nitrogen limitation and salinity up-shock with special emphasis on carotenogenesis in *Dunaliella parva*. *Algal Res.* 32, 1–10. doi: 10.1016/j.algal.2018.03.002

Shi, K., Gao, Z., Shi, T., Song, P., Ren, L., Huang, H., et al. (2017). Reactive oxygen species-mediated cellular stress response and lipid accumulation in oleaginous microorganisms: the state of the art and future perspectives. *Front. Microbiol.* 8:793. doi: 10.3389/fmicb.2017.00793

Song, H., Byeon, S., Chung, G., Jung, S., Choi, J., and Shin, H. (2018). A systematic correlation analysis of carotenoids, chlorophyll, non-pigmented cell mass, and cell number for the blueprint of *Dunaliella salina* culture in a photobioreactor. *Bioprocess Biosyst. Eng.* 41, 1295–1303. doi: 10.1007/s00449-018-1957-5

Sun, H., Mao, X., Wu, T., Ren, Y., Chen, F., and Liu, B. (2018). Novel insight of carotenoid and lipid biosynthesis and their roles in storage carbon metabolism in *Chlamydomonas reinhardtii*. *Bioresour. Technol.* 263, 450–457. doi: 10.1016/j.biortech.2018.05.035

Wang, J., Li, X., Lu, D., Du, Y., Ma, L., Li, W., et al. (2016). Photosynthetic effect in *Selenastrum capricornutum* progeny after carbon-ion irradiation. *PLoS ONE* 11:e0149381. doi: 10.1371/journal.pone.0149381

Wu, Z., Duangmanee, P., Zhao, P., Juntawong, N., and Ma, C. (2016). The effects of light, temperature, and nutrition on growth and pigment accumulation of three *Dunaliella salina* strains isolated from saline soil. *J. Microbiol.* 9, 1–10. doi: 10.5812/jjm.26732

Ye, Z., Jiang, J., and Wu, G. (2008). Biosynthesis and regulation of carotenoids in *Dunaliella*: Progresses and prospects. *Biotechnol. Adv.* 26, 352–360. doi: 10.1016/j.biotechadv.2008.03.004

Yilancioglu, K., Cokol, M., Pastirmaci, I., Erman, B., and Cetiner, S. (2014). Oxidative stress is a mediator for increased lipid accumulation in a newly isolated *Dunaliella salina* strain. *PLoS ONE* 9:e00911957. doi: 10.1371/journal.pone.0091957

Zhang, L., Liao, C., Yang, Y., Wang, Y., Ding, K., Huo, D., et al. (2019). Response of lipid biosynthesis in *Chlorella pyrenoidosa* to intracellular reactive oxygen species level under stress conditions. *Bioresour. Technol.* 287, 1–14. doi: 10.1016/j.biortech.2018.09.080

Zhang, Y., Ding, W., Mao, X., Li, Y., Gerken, H., and Liu, J. (2020). Astaxanthin is ketolated from zeaxanthin independent of fatty acid synthesis in *Chromochloris zofingiensis*. *Plant Physiol.* 183, 883–897. doi: 10.1104/pp.20.00325

Zhang, Y., Shi, M., Mao, X., Kou, Y., and Liu, J. (2019). Time-resolved carotenoid profiling and transcriptomic analysis reveal mechanism of carotenogenesis for astaxanthin synthesis in the oleaginous green alga *Chromochloris zofingiensis*. *Biotechnol. Biofuels* 12, 1–19. doi: 10.1186/s13068-019-1626-1

Zhang, Z., Sun, D., Mao, X., Liu, J., and Chen, F. (2016). The crosstalk between astaxanthin, fatty acids and reactive oxygen species in heterotrophic *Chlorella zofingiensis*. *Algal Res.*19, 178–183. doi: 10.1016/j.algal.2016.08.015

Zhao, Y., Wang H, Han, B., and Yu, X. (2019). Coupling of abiotic stresses and phytohormones for the production of lipids and high-value

by-products by microalgae: a review. *Bioresour. Technol.* 274, 549–556. doi: 10.1016/j.biortech.2018.12.030

Zhu, C., Zhai, X., Jia, J., Wang, J., Han, D., Li, Y., et al. (2018). Seawater desalination concentrate for cultivation of *Dunaliella salina* with floating photobioreactor to produce beta-carotene. *Algal Res.* 35, 319–324. doi: 10.1016/j.algal.2018.08.035

Zhu, Q., Zheng, J., and Liu, J. (2020). Transcription activation of beta-carotene biosynthetic genes at the initial stage of stresses as an indicator of the increased beta-carotene accumulation in isolated *Dunaliella salina* strain GY-H13. *Aquat. Toxicol.* 222, 1054–1072. doi: 10.1016/j.aquatox.2020.105472

Conflict of Interest: The authors declare that the research was conducted in the absence of any commercial or financial relationships that could be construed as a potential conflict of interest.

frontiers in Bioengineering and Biotechnology

ORIGINAL RESEARCH
published: 21 January 2021
doi: 10.3389/fbioe.2021.618969

Serine/threonine Kinases Play Important Roles in Regulating Polyunsaturated Fatty Acid Biosynthesis in *Synechocystis* sp. PCC6803

Gao Chen[1,2], Yuelei Cao[1,2], Huairong Zhong[2], Xiaodong Wang[2], Yanle Li[2], Xiaoyan Cui[1,2], Xiaoyuan Lu[1,2], Xiangdong Bi[3] and Meixue Dai[1]**

[1] School of Life Sciences, Shandong Normal University, Jinan, China, [2] Biotechnology Research Center, Shandong Academy of Agricultural Sciences, Shandong Provincial Key Laboratory of Genetic Improvement, Ecology and Physiology of Crops, Jinan, China, [3] Key Laboratory of Aquatic-Ecology and Aquaculture of Tianjin, College of Fishery, Tianjin Agricultural University, Tianjin, China

OPEN ACCESS

Edited by:
Chengwei Liang,
Qingdao University of Science and Technology, China

Reviewed by:
Corinne Cassier-Chauvat,
UMR9198 Institut de Biologie Intégrative de la Cellule (I2BC), France
Xiaojin Song,
Qingdao Institute of Bioenergy and Bioprocess Technology (CAS), China

***Correspondence:**
Xiangdong Bi
yl801123@aliyun.com
Meixue Dai
daimeixue@sdnu.edu.com

Specialty section:
This article was submitted to Bioprocess Engineering, a section of the journal Frontiers in Bioengineering and Biotechnology

Received: 19 October 2020
Accepted: 04 January 2021
Published: 21 January 2021

Citation:
Chen G, Cao Y, Zhong H, Wang X, Li Y, Cui X, Lu X, Bi X and Dai M (2021) Serine/threonine Kinases Play Important Roles in Regulating Polyunsaturated Fatty Acid Biosynthesis in Synechocystis sp. PCC6803. Front. Bioeng. Biotechnol. 9:618969. doi: 10.3389/fbioe.2021.618969

Serine/threonine kinases (STKs) play important roles in prokaryotic cellular functions such as growth, differentiation, and secondary metabolism. When the external environment changes, prokaryotes rely on signal transduction systems, including STKs that quickly sense these changes and alter gene expression to induce the appropriate metabolic changes. In this study, we examined the roles of the STK genes *spkD* and *spkG* in fatty acid biosynthesis in the unicellular cyanobacterium *Synechocystis* sp. PCC6803, using targeted gene knockout. The linoleic acid (C18: 2), γ-linolenic acid (C18: 3n6), α-linolenic acid (C18: 3n3), and stearidonic acid (C18: 4) levels were significantly lower in *spkD* and *spkG* gene knockout mutants than in the wild type at a culture temperature of 30°C and a light intensity of 40 $\mu mol \cdot m^{-2} \cdot s^{-1}$. The expression levels of fatty acid desaturases and STK genes differed between the *spkD* and *spkG* gene knockout mutants. These observations suggest that *spkD* and *spkG* may directly or indirectly affect the fatty acid composition in *Synechocystis* sp. PCC6803 by regulating the expression of fatty acid desaturases genes. Therefore, the STK genes *spkD* and *spkG* play important roles in polyunsaturated fatty acid biosynthesis in *Synechocystis* sp. PCC6803. These findings could facilitate the development of cyanobacteria germplasm resources that yield high levels of fatty acids. In addition, they provide a theoretical basis for the genetic engineering of cyanobacteria with improved yields of secondary metabolites and increased economic benefits.

Keywords: microalgae, serine/threonine kinase system, polyunsaturated fatty acids, biosynthesis, *Synechocystis* sp. PCC6803

INTRODUCTION

Polyunsaturated fatty acids (PUFAs) are fatty acids with multiple unsaturated bonds (any number of carbon atoms). Long chain PUFAs has multiple unsaturated bonds and more than 18 carbon atoms in the fatty acid chain. PUFAs are divided into multiple categories based on the position where the unsaturated bond starts relative to the methyl end of the fatty acid carbon chain, using

the ω (omega) numbering system. ω-3 and ω-6 PUFAs play important roles in various organisms (Mayra et al., 2020). In addition to having important physiological functions, these PUFAs, including linoleic acid (C18: 2), α-linolenic acid (C18: 3n3), γ-linolenic acid (C18: 3n6), stearidonic acid (C18: 4), arachidonic acid (C20: 4n6), eicosapentaenoic acid (C20: 5), and docosahexaenoic acid (C22: 6), have high nutritional and medicinal value. PUFAs are critical to the function and structure of the nervous system, especially in children. Thus, the demand for PUFAs is increasing. The large-scale industrialization of PUFAs would provide a solution to the PUFA supply and demand (Jan et al., 2010).

PUFAs have traditionally been derived from oils obtained from deep-sea fish and shellfish (Pauly et al., 2005; Hibbeln et al., 2006). However, factors such as seasonal restrictions, increased environmental pollution, overfishing, and residual fishy odor during the purification of PUFAs from fish oil have limited the production of PUFAs (Drexler et al., 2003). Cyanobacteria have been genetically engineered to produce PUFAs that do not have the shortcomings of traditional PUFAs sources (Gong and Miao, 2019; Somayeh et al., 2019). These prokaryotes use sunlight and carbon dioxide to produce a variety of valuable metabolites. Cyanobacteria have beneficial characteristics that make them ideal for large-scale cultivation, including a rapid growth rate and high metabolic yield (Jan et al., 2010). The single-cell cyanobacterium *Synechocystis* sp. PCC6803, a facultative autotrophic organism that uses light energy, is considered a model organism to study PUFA biosynthesis (Guedes et al., 2011; Sara et al., 2015).

Serine/threonine kinases (STKs) play important roles in the growth, differentiation, and secondary metabolism of prokaryotic cells (Rajagopal et al., 2003). When the external environment changes, prokaryotes such as cyanobacteria rely on signal transduction systems that include STKs to quickly perceive changes, and through the precise regulation of gene expression, alter their metabolic processes accordingly. The mechanism employed by STKs in cyanobacteria is similar to that in eukaryotes. After receiving the signal, STKs become activated through phosphorylation of their serine and threonine residues, and cooperate with other signal molecules. For example, when exposed to ultraviolet radiation, osmotic stress, heat stress, salt stress, or cold stress, STK proteins are activated and phosphorylate their downstream molecules, ultimately allowing these external signals to be transmitted to the nucleus (Zhang et al., 2007). The precise regulation of gene expression (Hasegawa et al., 2000) leads to changes in metabolite levels, allowing the cyanobacterium to withstand various types of adversity (Liu et al., 2015; Piyoosh et al., 2019).

Synechocystis is the first cyanobacterium whose entire genome has been sequenced. Based on its genome sequence, *Synechocystis* contains seven STK genes, including *spkA* (*sll1574*), *spkB* (*slr1697*), *spkC* (*slr0599*), *spkD* (*sll0776*), *spkE* (*slr1443*), *spkF* (*slr1225*), and *spkG* (*slr0152*) (Zhou et al., 2011). *spkA* and *spkB* of *Synechocystis* sp. PCC6803 contribute to cell movement, *spkE* encodes a protein lacking kinase activity, *spkC*, *spkF,* and *spkK* have been found to be involved in the phosphorylation of the small molecular chaperone protein GroES (Zorina et al., 2011) and *PknD* of *Anabaena* sp. PCC7120 is involved in regulating nitrogen metabolism (Zhang and Libs, 1998; Zhou et al., 2015). Therefore, we first constructed *spkD* and *spkG* knockout mutant strains, and identified a potential connection between these genes and PUFAs.

The main function of STKs is signal transduction. Several STK genes are involved in cell growth and cell survival, but their roles in unsaturated fatty acid biosynthesis is remaining unknown. We previously performed qRT-PCR of STK genes in *Synechocystis* sp. PCC6803 at 2, 4, and 6 days of culture, finding that *spkD* and *spkG* were expressed at significantly higher levels in strains with high levels of PUFAs compared to the wild type when grown at a temperature of 30°C and a light intensity of 40 $\mu mol \cdot m^{-2} \cdot s^{-1}$. In addition, there have been related reports showing that *spkG* plays an important role in STKs (Liang et al., 2011), and we obtained two knockout mutants, *spkG* and *spkD*. These findings suggest that *spkD* and *spkG* play important roles in unsaturated fatty acid biosynthesis in *Synechocystis* sp. PCC6803.

Most studies of the unsaturated fatty acid biosynthesis pathway conducted in *Synechocystis* to date have aimed to identify gene functions through analyses of mutants with metabolic deficiencies. However, our knowledge of the genes that function in *Synechocystis* fatty acid metabolism is incomplete. STKs have a variety of physiological functions in the cyanobacteria *Synechocystis* sp. PCC6803 and *Anabaena* sp. PCC7120, such as biological movement, osmotic pressure regulation, and cell survival. For example, the STK genes *spkA* and *spkB* are thought to function in cell movement (Kamei et al., 2001); *spkH* is thought to help maintain osmotic pressure in the cell (Kalyanee et al., 2004); and *spkD* affects cell survival (Laurent et al., 2008). However, the roles of other STK genes are still being explored, and the roles of STKs in PUFA biosynthesis in cyanobacteria are currently unknown.

Through the screening of STKs genes and the construction of plasmids, we obtained two mutants: *spkD* and *spkG*. Preliminary experimental results showed that PUFA accumulation in *spkD* and *spkG* deletion mutants was significantly lower than that in the wild type. Therefore, we carried out subsequent experiments using these mutants.

In this study, we further studied the role of *spkD* and *spkG* in PUFA biosynthesis in *Synechocystis* sp. PCC6803. We constructed *spkD* and *spkG* deletion mutant strains of *Synechocystis* sp. PCC6803 (*spkD*- and *spkG*-) and measured the expression levels of fatty acid desaturases and STK genes in the mutants at various points throughout the lifecycle. Fatty acid desaturases catalyze the dehydrogenation of carrier-bound fatty acids to form double bonds in the fatty acid chain. Fatty acid desaturases play an important role in the metabolism of fatty acids and in the maintenance of the correct structure and biological function of the membrane in the organism. Therefore, fatty acid desaturases were analyzed in our experiment. The contents of four unsaturated fatty acids were lower in the *spkD* and *spkG* deletion mutants than in the wild type, whereas the expression levels of fatty acid desaturases genes were higher in the mutants, indicating that *spkD* and *spkG* play important roles in PUFA biosynthesis in *Synechocystis* sp. PCC6803. This study lays the foundation for further investigating the effects of other STK genes on fatty acid biosynthesis.

RESULTS

Inactivation of *spkD* and *spkG* in *Synechocystis* sp. PCC6803

We constructed *spkD* and *spkG* deletion plasmids (**Figures 1A,B**) by replacing these genes with a kanamycin resistance cassette and *spkD* and *spkG* were separated into 0.9 and 1.0 kb fragments, respectively. These plasmids were used to transform into *Synechocystis* sp. PCC6803 to obtain the *spkD* Kan^r locus and *spkG* Kan^r locus mutants, here after referred to as *spkD*-and *spkG*-, respectively. To verify that *spkD*/*spkG* were successfully knocked out, we conducted PCR analysis using primer pair 1 (*spkD*-F and *spkD*-R) and primer pair 2 (*spkG*-F and *spkG*-R; **Table 1**). Whereas primer pairs 1 and 2 amplified 1.9 kb fragments from wild type genomic DNA, they amplified 3.3 kb fragments from the mutant genomic DNA. All amplification products were of the predicted size (**Figures 1C,D**). PCR is confirmed that all copies of *spkD*/*spkG* in the *Synechocystis* sp. 6,803 genome were replaced by the deletion cassette. Thus, we successfully knocked out the *spkD* and *spkG* genes in *Synechocystis*, and obtained two deletion mutant strains.

Growth Characteristics of Wild Type and Mutant Strains

To determine whether the knockout of *spkD* and *spkG* genes would affect the normal growth of *Synechocystis*, we incubated the cultures for 10 days under normal light intensity (40 $\mu mol \cdot m^{-2} \cdot s^{-1}$) and measured the OD_{730} value once daily. Based on these OD_{730} values, we generated growth curves of the wild type and two mutant strains. The growth patterns of all three *Synechocystis* strains were roughly similar (**Figure 2A**). The OD_{730} values of the knockout mutants were slightly higher than that of the wild type under the same conditions; the final OD_{730} value of the *spkG* knockout mutant was the highest. Nevertheless, the overall differences among the three strains were small, indicating that the algal cell density and growth rates were approximately the same.

We generated a standard curve of *Synechocystis* density and OD_{730} ($y = 32{,}798x + 6{,}249$, $R^2 = 0.9896$). Using this growth curve, the density of *Synechocystis* under different OD values could be determined. We conducted a statistical analysis of the growth rates of the two mutant strains and the wild type under normal light conditions (**Figure 2B**). The growth rates of all three

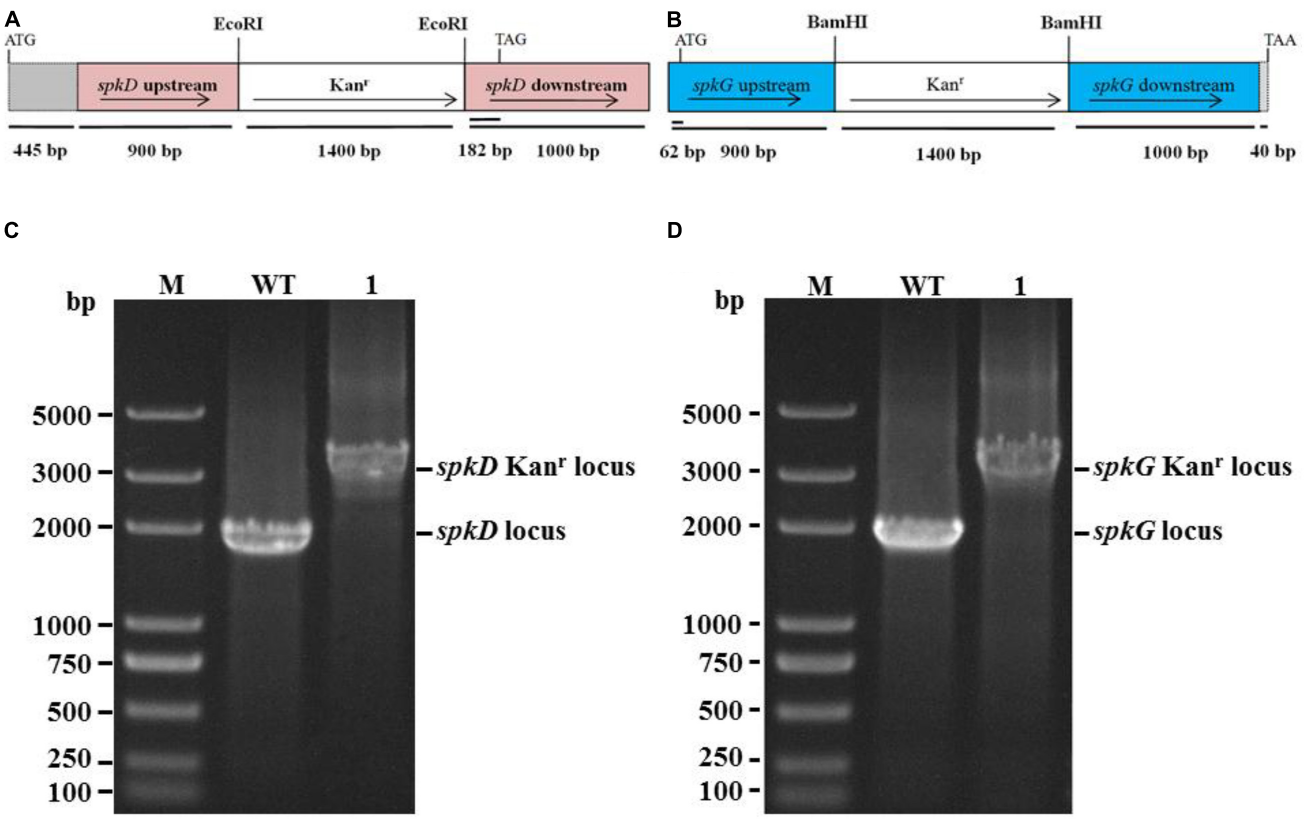

FIGURE 1 | Construction of Synechocystis spkD and spkG gene knockout vectors and PCR detection of mutant strains. **(A)** Diagram of the *spkD* gene-directed knockout vector. The gray region (445 bp) shows the unamplified area in the ORF of *spkD*; **(B)** Diagram of the *spkG* gene-directed knockout vector. The gray region (40 bp) shows the unamplified area in the ORF of *spkG*; **(C)** PCR detection of *spkD* gene-directed knockout, M: *Trans* 2K plus DNA Marker, WT: *spkD* gene in wild type *Synechocystis*, Lane 1: *spkD* gene knockout mutant; **(D)** PCR detection of *spkG* gene knockout, M: *Trans* 2K plus DNA Marker, WT: *spkG* gene in wild type *Synechocystis*; Lane 1: *spkG* gene knockout mutant.

TABLE 1 | Primer sequences used in this study.

Primer	Sequence (5′–3′)
spkD-F	ACTTACCCGTTCTGATTGA
spkD-R	TAACCATTGATAAGCAGAT
spkG-F	AGACTTTCTCTATTGCCTC
spkG-R	GGACCCAAATCCAGAAGAC
rnpB-F	GTGAGGACAGTGCCACAGAA
rnpB-R	GGCAGGAAAAAGACCAACCT
16S rRNA-F	AGCGTCCGTAGGTGGTTATG
16S rRNA-R	CTACGCATTTCACCGCTACA
spkD-RT-F	TGAGCCAGCACTTCCA
spkD-RT-R	CCACAATAATCCCAATAAGA
spkG-RT-F	CGACATTTATGCTGTGGGTA
spkG-RT-R	GGGCAAGTAAGGGAGGA
spkA-RT-F	TGTAGCGGATGCTGGAC
spkA-RT-R	ACTCAACACGGATATGGAA
spkB-RT-F	CAAATTGATTCGGTCCTCT
spkB-RT-R	TTCCCAGTCCATCTCCC
spkC-RT-F	GCCACCAAGGTTTACACTC
spkC-RT-R	CCGCCAATCACTAGCAGTA
spkF-RT-F	TCGCCATGACCAGATTC
spkF-RT-R	CACCCAACGCACTTCC
d15D-RT-F	TCGCCTCAAACAAAGC
d15D-RT-R	AATCGGATAGAAGAACCAG
d6D-RT-F	GCCATTGATGACGAGTG
d6D-RT-R	TAGCCAGCGATAGTTAGAG
d9D-RT-F	GGCATTGGCATTACTTT
d9D-RT-R	CCTTATTAGAATCGTGGG
d12D-RT-F	TGGACAGGGACAGCCTTAAC
d12D-RT-R	TTTTGTTGGTGTGGAGGTGA

cyanobacterial strains peaked on the second day of culture, began to increase slightly on the fourth day, and reached a second small peak on the sixth day. However, after this stage of culture, the growth rate began to decline until it reached the lowest value and became stable. Overall, there was no significant difference in growth rates between the mutant and wild type strains.

Effects of Knocking Out *spkD* and *spkG* Under Normal Light Conditions on STK Gene Expression in *Synechocystis*

To examine the effect of *spkD* and *spkG* gene knockout on the expression of other STK genes, we conducted follow-up experiments investigating differences in the expression levels of these related genes in wild type and mutant *Synechocystis* sp. PCC6803 under normal light conditions. The STK-related genes were generally expressed at lower levels in the *spkD* knockout mutant than in the wild type (**Figure 3**). Except for *spkA* transcript levels at 24 h of light treatment, the differences in gene expression patterns between the mutant and wild type strains were substantial, with a maximum difference in expression observed at approximately 6 h of light treatment, especially in the case of *spkE*. Knockout of *spkD* had the greatest effect on *spkE* expression, pointing to a possible association between these genes. In addition, the STK-related genes were expressed at higher levels in the mutant than in the wild type *Synechocystis* sp. PCC6803 before 6 h of light treatment, suggesting that *spkD* might be involved in regulating the expression of some inhibitors during the early stages of STK biosynthesis.

We also examined the expression of STK-related genes in the *spkG* knockout mutant under the same conditions. Under normal light conditions, the difference in *spkA* and *spkB* gene expression in the *spkG* knockout mutant vs. the wild type was greatest at 24 h, and the expression of *spkC*, *spkD*, *spkE,* and *spkF* increased overtime (**Figure 3**). The difference in gene expression also gradually increased over time. Since the knockout of *spkG* strongly affected

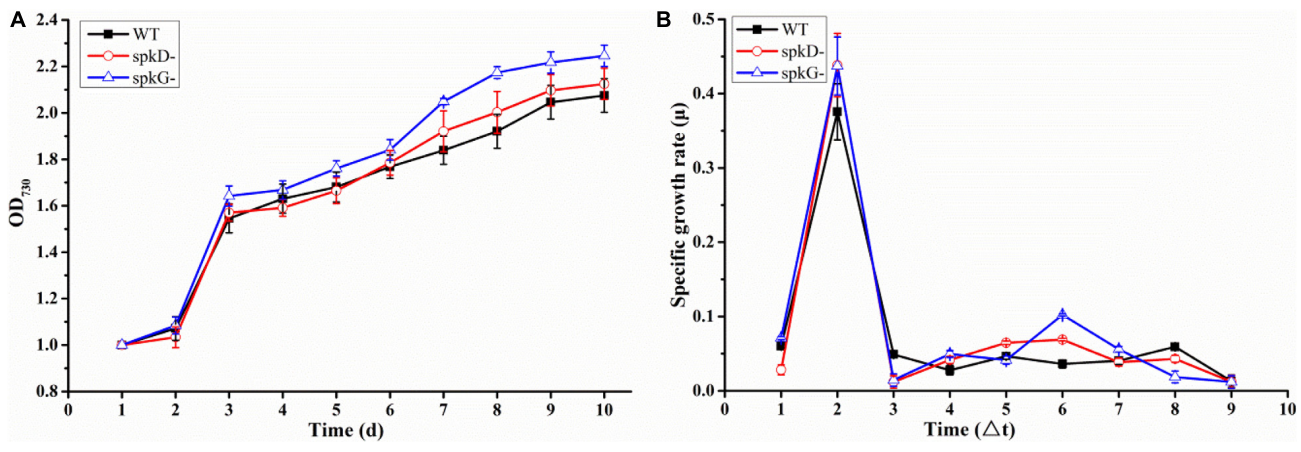

FIGURE 2 | Growth curves and specific growth rates of mutant and wild type cultures under normal light conditions **(A)** Growth curves of wild type *Synechocystis* sp. PCC6803 and two knockout mutants; **(B)** Specific growth rates of wild type *Synechocystis* sp. PCC6803 and two knockout mutants. WT represents wild type; *spkD* represents *spkD* knockout mutant; and *spkG* represents *spkG* knockout mutant. The experiment was carried out under a normal light intensity of 40 $\mu mol \cdot m^{-2} \cdot s^{-1}$. $\triangle t$ is the length of the time interval in days. Values are means ± SD (bars) of three independent experiments conducted on different days. The absence of a bar indicates that the SD falls within the symbol.

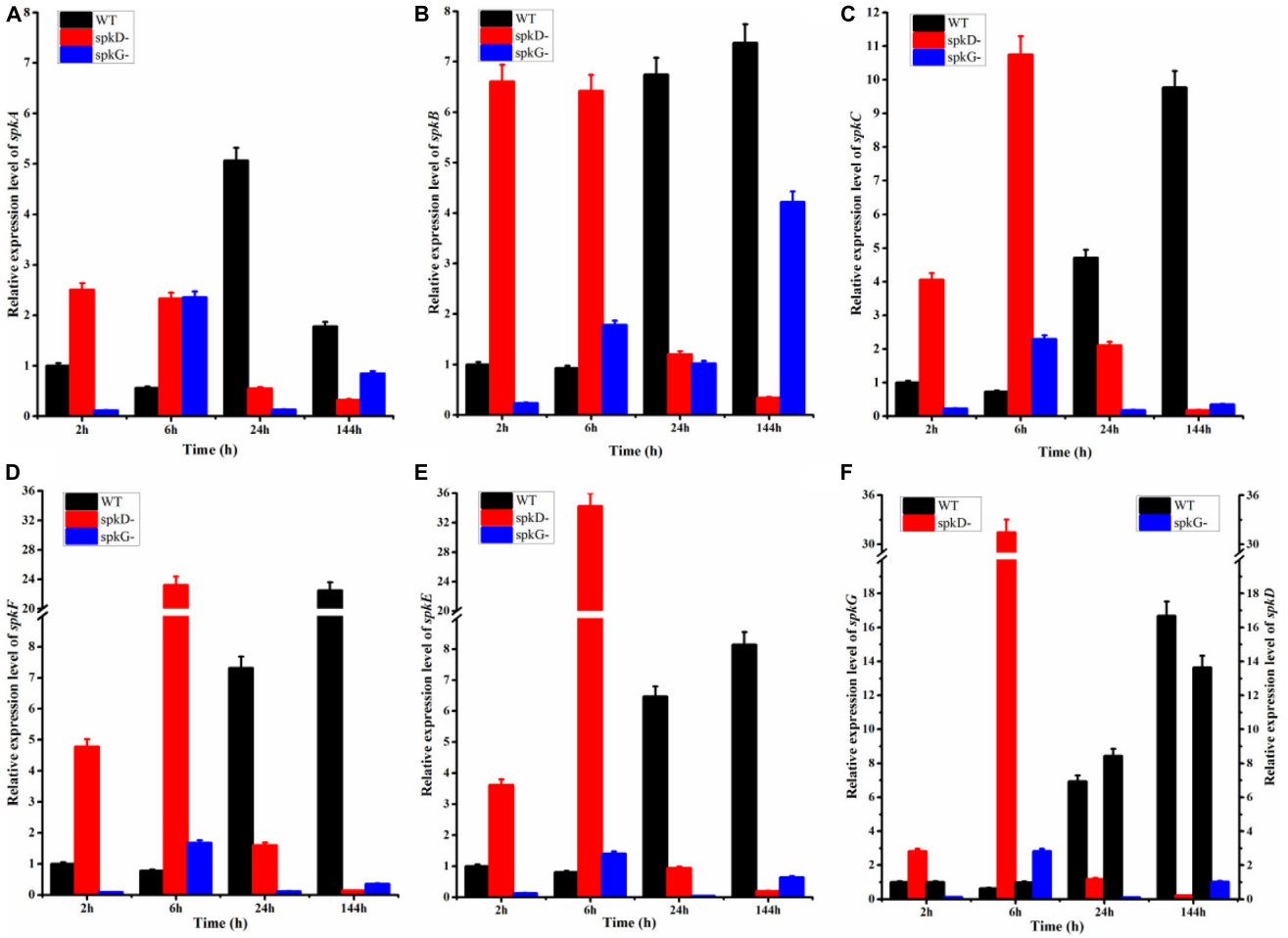

FIGURE 3 | Changes in serine/threonine kinase (STK) gene expression in wild type and mutant strains detected after different periods of exposure to normal light. WT represents wild type *Synechocystis* sp. PCC6803; *spkD*- represents the *spkD* knockout mutant; *spkG*- represents the *spkG* knockout mutant. The experiment was carried out under a normal light intensity of 40 $\mu mol \cdot m^{-2} \cdot s^{-1}$. **(A–E)** show the relative expression levels of *spkA*, *spkB*, *spkC*, *spkF,* and *spkE*, respectively, in the wild type and two mutant strains. **(F)** Relative expression levels of *spkG* in the wild type and *spkD*-. The data correspond to the left vertical axis. The black bars represent the wild type. *Synechocystis* sp. PCC6803, and the red bars represent the mutation that knocked out *spkD*. The right vertical axis shows the relative expression levels of *spkD* in the wild type and *spkG*-, and the black bar represents the wild type. The blue bar represents the mutation that knocked out *spkG*. Values are means ± SD (bars) of three independent experiments conducted on different days. The absence of a bar indicates that the SD falls within the symbol.

spkC, *spkD*, *spkE,* and *spkF* expression, we speculate that *spkG* is associated with the expression of these genes in *Synechocystis* sp. PCC6803.

Effects of Knocking Out *spkD* and *spkG* on the Expression of Fatty Acid Desaturases Genes in *Synechocystis*

Fatty acid desaturases is a key enzyme in the PUFA biosynthesis pathway, catalyzing the formation of double bonds at specific locations on the fatty acid chain. There are four types of fatty acid desaturasess in cyanobacteria: delta 6 fatty acid desaturases, delta 9 fatty acid desaturases, delta 12 fatty acid desaturases and delta 15 fatty acid desaturases. Referred to, respectively, as *d6D*, *d9D*, *d12D,* and *d15D*, these fatty acid desaturases differ depending on where they form double bonds in fatty acids.

Using qRT-PCR, we compared the expression patterns of the four fatty acid desaturases genes in the wild type and mutant strains at different time points under normal light conditions. The expression of the fatty acid desaturases related genes tended to decrease over time in both mutant strains, but to increase in the wild type. These genes were expressed at higher levels in the *spkD* knockout mutant than in the *spkG* knockout mutant. Under normal light conditions, desaturases are expressed at higher levels in the *spkD* deletion mutants than in the wild type during the early stages of growth, with peak expression at 6 h in the mutant. Because the expression level of the wild type was low in the early stages of culture, the difference between the expression level of the wild type and that of the two mutant strains reached a maximum at 6 h. However, this difference decreased over time, and the genes were ultimately expressed at higher levels in the wild type (**Figure 4**). These results indicate that *spkD* and *spkG* are strongly

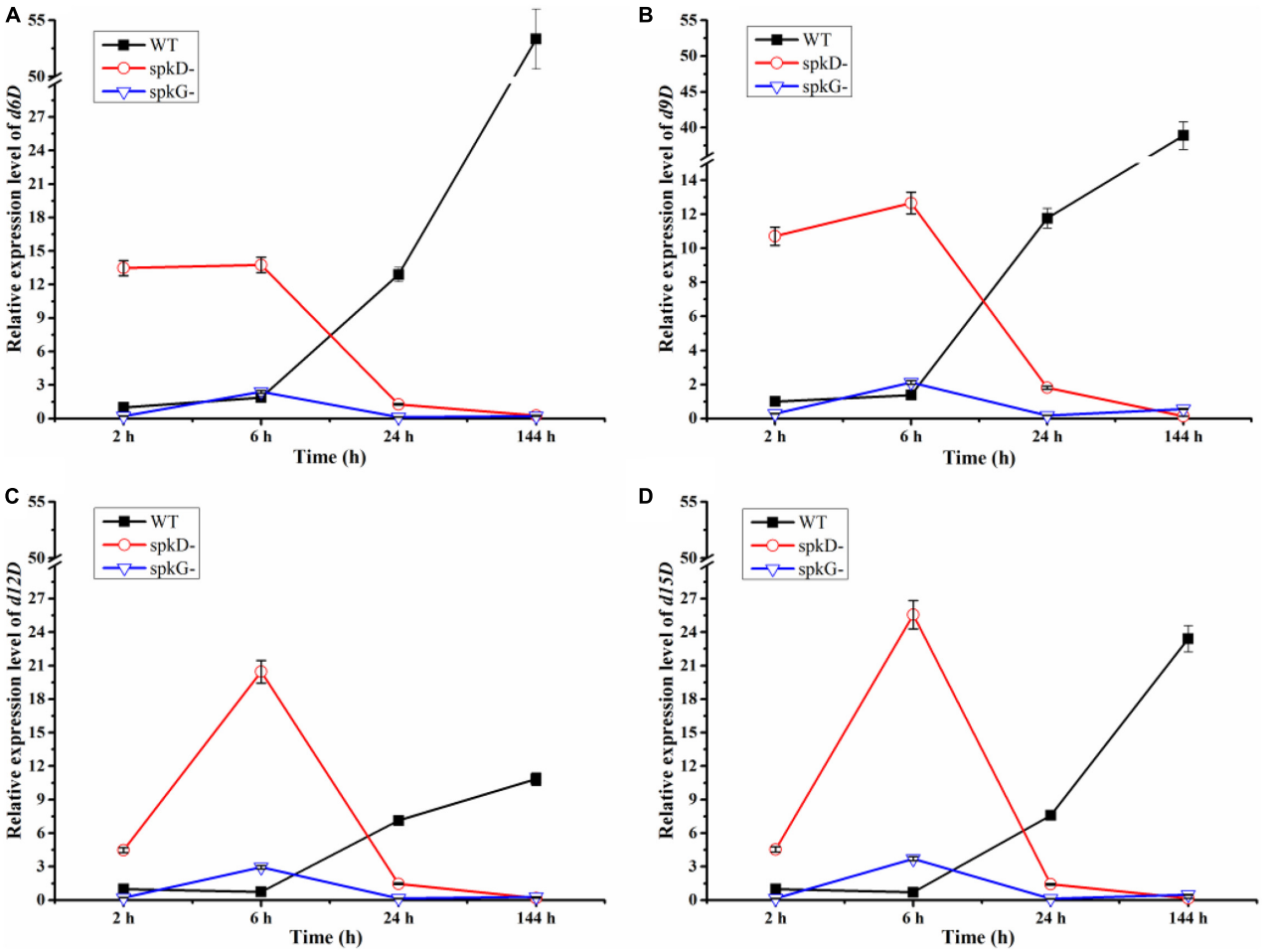

FIGURE 4 | Changes in fatty acid desaturases gene expression in the wild type, *spkD* and *spkG* knockout mutants under normal light conditions. WT represents wild type *Synechocystis* sp. PCC6803; *spkD-* represents the *spkD* knockout mutant; *spkG-* represents the *spkG* knockout mutant. The experiment was carried out under a normal light intensity of 40 $\mu mol \cdot m^{-2} \cdot s^{-1}$. (**A–D** show the relative expression levels of the *d6D, d9D, d12D, and d15D* fatty acid desaturases genes, respectively, in wild type *Synechocystis* sp. PCC6803 and the two knockout mutants) Values are means ± SD (bars) of three independent experiments conducted on different days. The absence of a bar indicates that the SD falls within the symbol.

associated with the expression of fatty acid desaturases genes in *Synechocystis* sp. PCC6803 (**Figure 4**).

In addition, we compared the expression levels of the four fatty acid desaturases genes in the two mutant strains. In the *spkG* knockout mutant, the expression of the four fatty acid desaturases genes was maintained at relatively low levels. The expression patterns of all four genes in the *spkD* knockout mutants were opposite to those of the wild type. These results indicate that knockout of *spkG* affects the expression of fatty acid desaturases genes and that this gene has a greater influence on fatty acid desaturases gene expression than *spkD*.

We speculate that, after 6 h of light exposure, the expression level of fatty acid enzymes of the mutant strains transiently increased compared with the wild type. After 24 h of light treatment, the expression level of these genes decreased in the mutants, to levels that were lower than in wild-type *Synechocystis* sp. PCC6803. After 144 h of light exposure, the knockout of *spkD* and *spkG* in the mutant strain further inhibited the expression of fatty acid enzyme genes, leading to further reductions in their expression in the mutants. Thus, deletion of *spkD* and *spkG* decreased the expression of the four genes (encoding *d6D*, *d9D*, *d12D,* and *d15D*).

Changes in Fatty Acid Contents in the *spkD* and *spkG* Knockout Mutants

To characterize differences in fatty acid content between the mutant and wild type, we analyzed the fatty acid contents of *Synechocystis* sp. PCC6803 cultured at 30°C and a light intensity of 40 $\mu mol \cdot m^{-2} \cdot s^{-1}$ by gas chromatography. There was little difference in total fatty acid content in the wild type and mutant strains (**Figure 5**). However, the contents of C18: 2, C18: 3n6, C18: 3n3, and C18: 4 were slightly lower in the mutants than in the wild type. The contents of other fatty acids were lower in the wild type than in the mutants, and the contents of these fatty acids in the two mutants were similar. The C18: 3n3 and C18: 4 contents were significantly lower in the *spkG* than in the *spkD* knockout mutant.

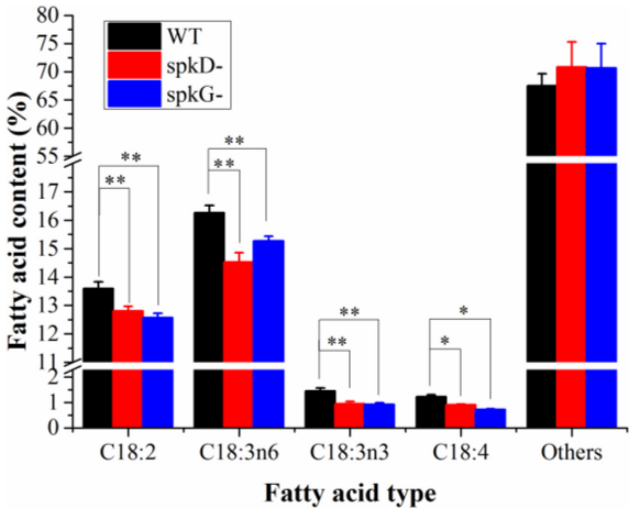

FIGURE 5 | Fatty acid composition and content in *spkD* and *spkG* knockout mutants. Data are the mean values of three experiments; the cultivation temperature was 30°C and the light intensity was 40 $\mu mol \cdot m^{-2} \cdot s^{-1}$; WT: *Synechocystis* sp. PCC6803; *spkD*-: *spkD* knockout mutant strain; *spkG*-: *spkG* knockout mutant strain. Values are means ± SD (bars) of three independent experiments conducted on different days. The absence of a bar indicates that the SD falls within the symbol. Asterisks mark statistically (*t*-test) significant differences from the WT value (**$p < 0.01$; *$p < 0.05$).

DISCUSSION

Genetic engineering to modify metabolic pathways represents an efficient, convenient method for increasing the yields and types of unsaturated fatty acids produced by an organism. The fatty acid biosynthetic pathways in plants and cyanobacteria have been well studied. *Synechocystis* sp. PCC6803 is a single-cell cyanobacterium, making it an ideal choice for studying fatty acid biosynthetic pathways whose potential as a tool for the commercial production of biofuels and fatty acids has been explored (Ruiz-López et al., 2012). For example, the delta 6 and delta 15 fatty acid desaturases genes were transferred into *Synechocystis* sp. PCC6803 to produce unsaturated fatty acids (Chen et al., 2014).

Cyanobacteria are the earliest photosynthetic autotrophic organisms. During the long evolutionary process, cyanobacteria developed an efficient adaptive system to cope with the constant changes in the external environment. For example, a complex signal transduction network system in *Synechocystis* sp. PCC6803 allows it to adapt to a variety of environments (Lei et al., 2014). The prokaryotic cyanobacteria are dominated by a binary signal transduction system. In 1991, eukaryotic protein kinases including STKs were also identified in the prokaryotic organism *Myxococcus* and shown to play major roles in prokaryotic cells (Zorina et al., 2014).

STKs contain multiple genes, and two mutant strains, *spkD* and *spkG*, were successfully obtained by knockout. The genes knocked out in the *spkD* and *spkG* strains have been well characterized, but the association between these genes and fatty acids remains to be explored. Based on this, we studied these two genes.

Here, to verify the roles of STKs in unsaturated fatty acid biosynthesis in *Synechocystis* sp. PCC6803, we knocked out these genes in this cyanobacterium and obtained gene knockout mutants. Gas chromatography analysis revealed that the contents of C18: 2, C18: 3n6, C18: 3n3, and C18: 4 were significantly lower in the two mutant strains than in the wild type. The C18: 3n3 and C18: 4 contents were significantly lower in the *spkG* than in the *spkD* knockout mutant, whereas the contents of other unsaturated fatty acids such as C18: 2 and C18: 3n6 in the two mutants were similar.

To verify this finding, we extracted RNA from the cultures and performed qRT-PCR to analyze fatty acid-related gene expression levels. Fatty acid desaturases genes were expressed at higher levels in the two mutant strains vs. the wild type, and the expression levels of these genes in the *spkD* and *spkG* knockout mutants significantly differed at different time points and under different light intensities. These findings suggest that *spkD* and *spkG* play different roles in unsaturated fatty acid biosynthesis.

We also analyzed the changes in fatty acid desaturases gene expression in the mutants and wild type at different time points under normal light intensity. The expression levels of these genes in the wild type and mutant strains were significantly different. Under normal light conditions (40 $\mu mol \cdot m^{-2} \cdot s^{-1}$), the fatty acid desaturases genes were expressed at higher levels in the *spkD*- mutant than in the *spkG*- mutant prior to 144 h of cultivation. Unlike the wild type, these genes were expressed at their highest levels in the mutants at 6 h of light treatment, with the most obvious differences detected in the *spkD* knockout mutant. After the 6 h time point, the expression levels of these genes in the wild type continued to increase. These results indicate that knockout of *spkD* and *spkG* indeed affects the relative fatty acid desaturases contents of *Synechocystis* sp. PCC6803, indirectly demonstrating that the two genes are closely related to fatty acid biosynthesis.

Subsequently, we detected the changes in expression levels of other STK genes and established that *spkD* and *spkG* influence the expression patterns of these genes as well, as the knockout of these genes significantly altered the expression levels of other STK genes. Our findings suggest that in *Synechocystis* sp. PCC6803, *spkD* is most closely associated with *spkE* expression and *spkG* is somewhat associated with *spkC*, *spkD*, *spkE,* and *spkF* expression.

In addition, with the extension of light time, in contrast to wild type *Synechocystis*, the expression of other STKs genes in the *spkD* knockout mutants initially increased, before decreasing. Perhaps *spkD* is related to the pre-expression phase of these genes, a process that might involve some inhibitory factors or other genes. Compared to the *spkD* knockout mutant, other STK genes were significantly down regulated in the *spkG* knockout mutant, indicating that *spkG* is more closely associated with the expression of other STK genes than is *spkD*. The expression levels of the STK genes of these two knockout mutants peaked after approximately 6 h of light exposure. The importance of this time point will be the subject of subsequent experiments.

As we had expected, in the subsequent determination of fatty acid content, we also noticed that several fatty acids were significantly higher in the wild type than in the two knockout mutant strains. This difference has to do with fatty acid desaturases and coincides with the results of STKs obtained previously, further illustrating that *spkD* and *spkG* are associated with fatty acid metabolism and are worth further examination.

A previous related study indicated that *sll0776* (*spkD*) is part of the gene cluster (*sll0775*, *sll0776*, *sll0777*, and *sll0778*). However, the intergenic region of this gene cluster could not be amplified by qRT-PCR, indicating that *sll0776* was not organized in an operon with the adjacent genes, and the protein sequences encoded by the other genes had low similarity with the corresponding proteins in the database. Therefore, we chose *spkD* gene as the research object. *spkD* is not thought to be an essential gene, but may be associated with the TCA cycle. Deletion of *spkD* maybe affects cyanobacterial growth, and the growth can be recovered by adding specific metabolites of HCO_3^- or TCA cycle as auxiliary elements (Laurent et al., 2008). In our research, the STK-related genes were expressed at higher levels in the *spkD* deletion mutant strains in the first 6 h, and gradually decreased in the later stages. We speculated that this may be due to a lack of a bit substances related to growth (**Figure 3**). Another study revealed that certain cyanobacterial genes are expressed soon after exposure to light, and their expression gradually decreases or even disappears at later stages (He et al., 2001). This may also explain why *spkA*, *spkB*, *spkC*, *spkF*, and *spkE* are expressed at relatively high levels suddenly after exposure to light, however, the specific mechanism remains to be elucidated.

Recent studies of *spkG* (*slr0152*) also identified a relationship between spkG kinase and fatty acids. The *slr0144–slr0152* gene cluster encodes a protein that was recently annotated as Ferredoxin 5 (Fd5), which appears to be a phosphoprotein. SpkG kinase is involved in the phosphorylation of Ferredoxin 5 (Fd5) (Angeleri et al., 2018). Our study confirms that *spkG* influences the contents of fatty acids. Furthermore, knockout of *spkG* (Δ*slr0152*) will not have an obvious effect on the expression of genes that function downstream of genes in the cluster. We are planning to study other genes in the gene cluster to further explore the connection between *spkG* and fatty acid metabolism. As *slr0151* and *spkG* have similar functions, we speculate that *spkG* kinase and *slr0151* protein may have complementary functions, which would result in the loss of *spkD* inhibiting cyanobacterial growth to a greater extent than the loss of *spkG*. This would also explain why other STKs and fatty acid desaturases are altered greater in *spkD* deletion mutants than in *spkG* deletion mutants (**Figures 3**, **4**).

In this study, we successfully constructed *spkD* and *spkG* gene knockout mutants in *Synechocystis* sp. PCC6803 via insertional inactivation to study the effects of these genes on fatty acid biosynthesis. Under normal light conditions, the expression levels of fatty acid desaturases genes were significantly higher in the wild type than in the two knockout mutants. Knockout of *spkD* and *spkG* also affected the expression of other STK-related genes to different extents, indicating that these genes play different roles in fatty acid biosynthesis. In addition, the contents of several major fatty acids were lower in the mutant strains than in the wild type. Our results indicate that STKs affect fatty acid biosynthesis, and *spkD* and *spkG* directly or indirectly participate in the regulation of STK gene expression. In addition, the knockout of these two genes affected fatty acid biosynthesis. However, how specific genes cooperate with each other to regulate fatty acid biosynthesis mechanisms remains to be determined. We plan to conduct more in-depth research to improve the biosynthesis of fatty acids in cyanobacteria. This study lays the foundation for further improving the fatty acid biosynthesis pathway in cyanobacteria and for the efficient production of PUFAs.

MATERIALS AND METHODS

Strains and Growth Conditions

The cyanobacterium *Synechocystis* sp. PCC6803 was obtained from the Freshwater Algae Culture Collection of the Institute of Hydrobiology, Chinese Academy of Sciences. *Synechocystis* sp. PCC6803 was cultivated in BG-11 medium at 30°C (Chen et al., 2014). For solid BG-11 medium, 1.5% (w/v) Difco Bacto-agar (Becton Dickinson, Sparks, MD, United States), 0.3% (w/v) sodium thiosulfate, and 10 mM TES 2- [(2-hydroxy-1, 1-bis (hydroxylmethyl) ethyl) amino] ethanesulfonic acid pH 8.2 were added to BG-11 medium. The culture was bubbled with air under a light intensity of 40 $\mu mol \cdot m^{-2} \cdot s^{-1}$ (Teruo and Kaplan, 2003). Transformed strains were selected by adding 50 μg/mL kanamycin (Dingguo Company, Beijing, China) to both liquid and solid BG-11 medium. The mutant and wild type in the logarithmic growth phase were added to the liquid medium without kanamycin. Under a light intensity of 40 $\mu mol \cdot m^{-2} \cdot s^{-1}$, 30°C, after waiting for a period of growth (about 3–5 days), the OD_{730} value was uniformly adjusted to 1.0. Samples were collected and measured at the same time each day. Cell density was determined by measuring the optical density (OD) of the suspension at 730 nm (OD_{730}) with a spectrophotometer (DU-70, Beckman Coulter, Brea, CA, United States).

Generation of the *spkD* and *spkG* Mutants

A 1.9 kb DNA fragment including the *spkD* coding region (*sll0776*, GenBank: AB046600) was amplified by PCR from genomic DNA of *Synechocystis* sp. PCC6803 using the primer pair *spkD*-F and *spkD*-R (**Table 1**). A 1.9 kb DNA fragment including the *spkG* (*slr0152*, GenBank: CP028094) coding region was amplified by PCR from genomic DNA of *Synechocystis* sp. PCC6803 using the primer pair *spkG*-F and *spkG*-R (**Table 1**). The amplified DNA fragments were cloned separately into the pClone007 simple vector (TSINGKE Biological Technology). In our experiments, the *Eco*RI restriction site was found at position 1,327 bp of the *spkD* gene, and the *Bam*HI restriction site was found at position 866 bp of the *spkG* gene. We designed primers for the two gene sequences and inserted Kan fragments using enzyme digestion. The mutant was constructed by inserting a 1.2 kb kanamycin resistance cassette into the restriction site of the amplified DNA fragment. The *Synechocystis* sp. PCC6803 strain was transformed as described (Kamei et al., 2001).

Transformants were selected on standard medium containing 50 μg/mL kanamycin. Complete segregation of the mutant was confirmed by PCR.

RNA Isolation and cDNA Synthesis

Wild type and transformant cell lines were cultured and harvested during the exponential growth phase, and total RNA was isolated from the samples using Trizol Reagent (Invitrogen, Carlsbad, CA, United States) following the manufacturer's instructions. First-strand cDNA was synthesized using M-MLV reverse transcriptase and modified oligo (dT) following the manufacturer's instructions (TaKaRa, Dalian, China).

Quantitative Reverse-Transcription PCR

Quantitative reverse-transcription PCR (qRT-PCR) of STK gene expression was carried out RNA Bio-Rad iQ5 real-time PCR system. The resulting cDNA molecules were amplified by PCR using the following gene-specific primers: *rnpB*-F and *rnpB*-R to amplify the *rnpB* gene and 16S rRNA-F and 16S rRNA-R to amplify the 16S rRNA gene, which was used as the loading control. Primers were also designed to amplify the following STK genes (**Table 1**): *spkA* (*spkB*, *spkC*, *spkD*, *spkG*, *spkF*) -RT-F and *spkA* (*spkB*, *spkC*, *spkD*, *spkG*, *spkF*) -RT-R to amplify *spkA* (*spkB*, *spkC*, *spkD*, *spkG*, *spkF*); *d6D* (*d9D*, *d12D*, *d15D*) -RT-F and *d6D* (*d9D*, *d12D*, *d15D*) -RT-R to amplify *d6D* (*d9D*, *d12D*, *d15D*). Reactions were prepared following the manufacturer's instructions, and qRT-PCR was performed using a Bio-Rad iQ5 system. Each PCR was repeated four times in a total volume of 20 μL containing 2 × SYBR Green I PCR Master Mix (TaKaRa), 100 nM of each primer, and 1 μL diluted (1:20) template cDNA. Reactions were carried out in 96-well optical-grade PCR plates and a matched optical-grade membrane (TaKaRa). The amplification program was as follows: an initial denaturation step of 1 min at 95°C; 42 cycles of 10 s at 95°C, 30 s at 60°C, and 30 s at 72°C; and then an additional cycle of 10 s at 95°C, 30 s at 58°C, and 5 min at 72°C, followed by 10 s at 95°C for melting curve analysis. The data were analyzed using Bio-Rad iQ5 software. The relative expression levels of STK genes at various developmental stages were calculated using the relative $2^{-\Delta\Delta Ct}$ method (Livak and Schmittgen, 2001); the error bars indicate SD (n = 3). Sterile water was used as negative control instead of template in each primer set.

Culture Conditions

Three *Synechocystis* strains (wild type and mutants) were cultured under normal light conditions (40 $\mu mol \cdot m^{-2} \cdot s^{-1}$) for 10 days at 30°C. After a brief centrifugation (6,000 × g, 10 min at room temperature), the cyanobacteria were added to BG-11 medium to a cell density of 4.578×10^9 ind./L (individual/liter) and cultured under a normal light intensity of 40 $\mu mol \cdot m^{-2} \cdot s^{-1}$ for 6 days. All treatments had four replicate flasks, and cyanobacteria cultured continuously under 40 $\mu mol \cdot m^{-2} \cdot s^{-1}$ served as controls. During the light culture stage, algal growth was estimated each day based on the OD_{730}, as measured with a spectrophotometer. A standard curve relating *Synechocystis* cell density to OD_{730} was established using serial dilutions of cyanobacterial culture. Total RNA for subsequent qRT-PCR analysis was isolated from the cyanobacteria at 0, 2, 4, 6, 24, and 144 h.

Calculation of Specific Growth Rate

The specific growth rate of the cyanobacteria was calculated using the following formula: $\mu = (\ln N_t - \ln N_0)/\Delta t$, where N_0 is the population cell density at the beginning of the time interval, N_t is the cell density at the end of the time interval, and Δt is the length of the time interval in days. The growth rate was calculated based on measurements taken from the first 2 days of the experiment onward. Data from the second day was compared with that from the first day, and the rate was calculated by comparison.

Extraction of Total Fatty Acids From *Synechocystis*

Synechocystis cells were collected in 1,000 mL autoclaved flasks, each containing 400 mL of sterile BG-11 medium, and grown for 10 days at a light intensity of 40 $\mu mol \cdot m^{-2} \cdot s^{-1}$ and a constant temperature of 30°C. When the culture reached OD_{730} = 2.2, the cyanobacterial fluid was collected by centrifugation (4,500 × g, 10 min at room temperature), and the pellet was washed with distilled water and centrifuged again (4,500 × g, 10 min at room temperature). The washing and centrifugation steps were performed three times (Chen et al., 2017). The cultured cyanobacterial cells were harvested by centrifugation (6,000 × g, 15 min at room temperature) and dried under a vacuum. Each 0.2 g sample of dried cyanobacterial powder was placed in a mortar, repeatedly ground in liquid nitrogen, extracted with 7.0 mL of methanol-chloroform (2:1, v: v), and sonicated for 10 min. After the sample was centrifuged at 6,000 × g for 15 min at room temperature, 1.5 mL of methanol-chloroform (2: 1, v: v) was added to the residue. The sample was centrifuged (6,000 × g, 10 min at room temperature) and the organic phase was retained; this step was repeated once. The organic phase extracts were combined in a separatory funnel. After adding 2.5 mL of chloroform and 3.0 mL of sodium chloride solution (1:100, v: v), the sample was mixed well and allowed to stand for layer separation. The lower layer was recovered, and 2.5 mL of chloroform was added to the original upper and middle layers and extracted again. The lower layers were combined; this step was repeated once. The combined lower layers were placed in a fat-lifting bottle, and the solvent was evaporated to constant weight with nitrogen at 50°C (Sheng et al., 2011; Ryckebosch et al., 2012). The total fatty acids and the total weight of the fat-lifting bottle were measured using an electronic scale.

Analysis of Fatty Acid Composition in *Synechocystis*

The extracted total fat was dissolved in 4 mL of chloroform in a 10 mL test tube with a stopper, combined with 5 mL of 0.04 M potassium hydroxide-methanol solution, and mixed well. The sample was incubated in a 60°C water bath for 60 min for saponification, with oscillation every 10 min during saponification. The saponified sample was removed from the

water bath, cooled, combined with 4.0 mL hydrochloric acid-methanol (1:9) solution, and mixed well. Then 20.0 μL of 1.5 mg/mL non-adecanoic acid (C19: 0) was added to the sample as an internal standard. The sample was methylated in a water bath at 60°C for 20 min with shaking every 10 min during the methylation process (Ichihara and Fukubayashi, 2010). After cooling, the methylated sample was combined with 3.0 mL of saturated saline, followed by 1.0 mL of n-hexane, and shaken thoroughly. After letting the sample stand (at room temperature for about 30 min), the n-hexane layer was subjected to chromatographic analysis. The extracted n-hexane was dehydrated with an appropriate amount of anhydrous sodium sulfate and centrifuged at high speed (13,000 × g, 3 min) at room temperature (about 30°C). The supernatant [*Synechocystis* sample fatty acid methyl ester (FAME) eluent] was subjected to gas chromatography (GC) using an Elite-wax column in an ASXL instrument (Perkin-Elmer, Waltham, MA, United States) (Kenichi and Yumeto, 2010). The flame ionization detection temperature was 250°C, and the operating temperature was maintained at 220°C. The samples used in the experiment are from the same batch. The value for each sample was averaged over three experiments.

Statistical Analysis

Data are expressed as means ± SD (n = 3). The data were subjected to a t-test to determine significant differences between treatments ($^{*}p < 0.05$; $^{**}p < 0.01$).

DATA AVAILABILITY STATEMENT

The original contributions presented in the study are included in the article/supplementary material, further inquiries can be directed to the corresponding author/s.

AUTHOR CONTRIBUTIONS

GC, XB, and MD conceived and designed the experiments. YC, HZ, XW, YL, and XC performed the experiments. GC contributed reagents, materials, and analysis tools. GC, YC, and XW wrote the manuscript. All authors have read and agreed to the published version of the manuscript.

FUNDING

This work was financially supported by the National Key Research and Development Program of Shandong (2019GSF107098 and 2018GSF121019), the National Key Research and Development Program of China (2018YFE0108600), the National Natural Science Foundation of China (31772857), the Science and Technology Plan Project of Tianjin (19YFZCSN00070), and the Key Laboratory of Algal Biology, Institute of Hydrobiology, Chinese Academy of Sciences (2018-006).

REFERENCES

Angeleri, M., Zorina, A., Aro, E. M., and Battchikova, N. (2018). Interplay of SpkG kinase and the Slr0151 protein in the phosphorylation of Ferredoxin 5 in *Synechocystis* sp. strain PCC 6803. *FEBS Lett.* 592, 411–421. doi: 10.1002/1873-3468.12970

Chen, G., Chen, J., He, Q. F., Zhang, Y., Peng, Z. Y., Fan, Z. X., et al. (2017). Functional expression of the *Arachis hypogaea* L. Acyl-ACP thioesterases *AhFatA* and *AhFatB* enhances fatty acid production in *Synechocystis* sp. PCC6803. *Energies* 10:2093. doi: 10.3390/en10122093

Chen, G., Qu, S. J., Wang, Q., Bian, F., Peng, Z. Y., Zhang, Y., et al. (2014). Transgenic expression of delta-6 and delta-15 fatty acid desaturases enhances omega-3 polyunsaturated fatty acid accumulation in *Synechocystis* sp. PCC6803. *Biotechnol. Biofuels* 7, 1–10. doi: 10.1186/1754-6834-7-32

Drexler, H., Spiekermann, P., Meyer, A., Domergue, F., Zank, T., Sperling, P., et al. (2003). Metabolic engineering of fatty acids for breeding of new oilseed crops, strategies, problems and first results. *J. Plant Physiol.* 16, 779–802. doi: 10.1078/0176-1617-01025

Gong, Y., and Miao, X. L. (2019). Short chain fatty acid biosynthesis in microalgae *Synechococcus* sp. PCC 7942. *Mar. Drugs* 17:255. doi: 10.3390/md17050255

Guedes, A., Amaro, H. M., Barbosa, C. R., Pereira, R. D., and Malcata, F. X. (2011). Fatty acid composition of several wild microalgae and cyanobacteria, with a focus on eicosapentaenoic, docosahexaenoic and α-linolenic acids for eventual dietary uses. *Food Res. Int.* 44, 2721–2729. doi: 10.1016/J.FOODRES.2011.05.020

Hasegawa, P. M., Bressan, R. A., Zhu, J. K., and Bohnert, H. J. (2000). Plant cellular and molecular responses to high salinity. *Annu. Rev. Plant Physiol. Plant Mol. Biol.* 51, 163–199. doi: 10.1146/ANNUREV.ARPLANT.51.1.463

He, Q. F., Dolganov, N., Bjrkman, O., and Grossman, A. R. (2001). The high light-inducible polypeptides in *Synechocystis* PCC6803. Expression and function in high light. *J. Korean Soc. Appl. Bi.* 276, 304–314. doi: 10.1074/jbc.M008686200

Hibbeln, J. R., Nieminen, L. R., Blasbalg, T. L., Riggs, J. A., and Lands, W. E. (2006). Healthy intakes of n-3 and n-6 fatty acids, estimations considering worldwide diversity. *Am. J. Clin. Nutr.* 83, 1483S–1493S. doi: 10.1186/1476-511X-5-14

Ichihara, K., and Fukubayashi, Y. (2010). Preparation of fatty acid methyl esters for gas-liquid chromatography. *J. Lipid Res.* 51, 635–640. doi: 10.1194/jlr.D001065

Jan, P. S., Michael, H., Manuela, S., and Andreas, H. (2010). Significance of long-chain polyunsaturated fatty acids (PUFAs) for the development and behaviour of children. *Eur. J. Pediatr.* 169, 149–164. doi: 10.1007/s00431-009-1035-8

Kalyanee, P., Maria, A. S., Yu, K., Satoh, S., Satoshi, T., Dmitry, A. L., et al. (2004). Five histidine kinases perceive osmotic stress and regulate distinct sets of genes in *Synechocystis*. *J. Biol. Chem.* 279, 53078–53086. doi: 10.1074/jbc.M410162200

Kamei, A., Yuasa, T., Orikawa, K., Geng, X. X., and Ikeuchi, M. (2001). A eukaryotic type protein kinase, *SpkA*, is required for normal motility of the unicellular Cyanobacterium *Synechocystis* sp. strain PCC6803. *J. Bacteriol.* 183, 1505–1510. doi: 10.1128/JB.183.5.1505-1510.2001

Kenichi, I., and Yumeto, F. (2010). Preparation of fatty acid methyl esters for gas-liquid chromatography. *J. Lipid Res.* 51, 635–640. doi: 10.1194/jlr.D001065

Laurent, S., Jang, J. C., Janicki, A., Zhang, C. C., and Be′du, S. (2008). Inactivation of *spkD*, encoding a Ser/Thr kinase, affects the pool of the TCA cycle metabolites in *Synechocystis* sp. strain PCC 6803. *Microbiology* 154, 2161–2167. doi: 10.1099/MIC.0.2007/016196-0

Lei, H. J., Chen, G., Wang, Y. L., Ding, Q. L., and Wei, D. (2014). *Sll0528*, a site-2-protease, is critically involved in cold, salt and hyperosmotic stress acclimation of Cyanobacterium *Synechocystis* sp. PCC6803. *Int. J. Mol. Sci.* 15, 22678–22693. doi: 10.3390/IJMS151222678

Liang, C. W., Zhang, X. W., Chi, X. Y., Guan, X. Y., Li, Y. X., Qin, S., et al. (2011). Serine/Threonine protein kinase *spkG* is a candidate for high salt resistance in the unicellular Cyanobacterium *Synechocystis* sp. PCC 6803. *PLoS One* 6:e18718. doi: 10.1371/journal.pone.0018718

Liu, Z. X., Li, H. C., Wei, Y. P., Chu, W. Y., Chong, Y. L., Long, X. H., et al. (2015). Signal transduction pathways in *Synechocystis* sp. PCC6803 and biotechnological implications under abiotic stress. *Crit. Rev. Biotechnol.* 35, 269–280. doi: 10.3109/07388551.2013.838662

Livak, K. J., and Schmittgen, T. D. (2001). Analysis of relative gene expression data using real-time quantitative PCR and the 2 (-Delta Delta C (T)) method. *Methods* 25, 402–408. doi: 10.1006/METH.2001.1262

Mayra, M. A., Belen, T. R., Zhen, T., Owen, M. V., Mario, M. M., Shaheen, A., et al. (2020). Importance of the role of ω-3 and ω-6 polyunsaturated fatty acids in the progression of brain cancer. *Brain Sci.* 10:381. doi: 10.3390/brainsci10060381

Pauly, D., Watsn, R., and Alder, J. (2005). Global trends in world fisheries, impacts on marine ecosystems and food security. *Philos. Trans. R. Soc. B* 360, 5–12. doi: 10.1098/rstb.2004.1574

Piyoosh, K. B., Kumar, J., and Venkatesh, C. (2019). Proteomic De-regulation in Cyanobacteria in response to abiotic stresses. *Front. Microbiol.* 10:1315. doi: 10.3389/fmicb.2019.01315

Rajagopal, L., Clancy, A., and Rubens, C. E. (2003). A eukaryotic type Serine/Threonine kinase and phosphatase in *Streptococcus agalactiae* reversibly phosphorylate an inorganic pyrophosphatase and affect growth, cell segregation, and virulence. *J. Biol. Chem.* 278, 14429–14441. doi: 10.1074/JBC.M212747200

Ruiz-López, N., Sayanova, O., Napier, J. A., and Haslam, R. P. (2012). Metabolic engineering of the omega-3 long chain polyunsaturated fatty acid biosynthetic pathway into transgenic plants. *J. Exp. Bot.* 63, 2397–2410. doi: 10.1093/JXB/ERR454

Ryckebosch, E., Muylaert, K., and Foubert, I. (2012). Optimization of an analytical procedure for extraction of lipids from microalgae. *J. Am. Oil Chem. Soc.* 89, 189–198. doi: 10.1007/S11746-011-1903-Z

Sara, P. C., Miguel, A. R., Raveender, V., Lai, Y. S., Bruce, E. R., and Roberto, P. (2015). Effects of light intensity and carbon dioxide on lipids and fatty acids produced by *Synechocystis* sp. PCC6803 during continuous flow. *Algal Res.* 12, 10–16. doi: 10.1016/J.ALGAL.2015.07.018

Sheng, J., Vannela, R., and Rittmann, B. E. (2011). Evaluation of methods to extract and quantify lipids from *Synechocystis* PCC 6803. *Bioresour. Technol.* 102, 1697–1703. doi: 10.1016/J.BIORTECH.2010.08.007

Somayeh, G. F., Anithachristy, S. A., Behnam, T., Chen, H., Lu, J., and Sitther, V. (2019). Augmenting Fremyella diplosiphon cellular lipid content and unsaturated fatty acid methyl esters via sterol desaturase gene overexpression. *Appl. Biochem. Biotech.* 189, 1127–1140. doi: 10.1007/s12010-019-03055-5

Teruo, O., and Kaplan, A. (2003). Inorganic carbon acquisition systems in cyanobacteria. *Photosynth. Res.* 77, 105–115. doi: 10.1023/A:1025865500026

Zhang, C. C., and Libs, L. (1998). Cloning and characterisation of the *pknD* gene encoding an eukaryotic-type protein kinase in the Cyanobacterium *Anabaena* sp. PCC7120. *Mol. Gen. Genet.* 258, 26–33. doi: 10.1007/s004380050703

Zhang, X. W., Zhao, F. Q., Guan, X. Y., Yang, Y., Liang, C. W., and Qin, S. (2007). Genome wide survey of putative Serine/Threonine protein kinases in cyanobacteria. *BMC Genom.* 8:395. doi: 10.1186/1471-2164-8-395

Zhou, P., Wong, D., Li, W., Xie, J., and Av-Gay, Y. (2015). Phosphorylation of Mycobacterium tuberculosis protein tyrosine kinase A *PtkA* by Ser/Thr protein kinases. *Biochem. Biophys. Res. Commun.* 467, 421–426. doi: 10.1016/j.bbrc.2015.09.124

Zhou, W. G., Li, Y., Min, M., Hu, B., Chen, P., and Ruan, R. (2011). Local bioprospecting for high-lipid producing microalgal strains to be grown on concentrated municipal wastewater for biofuel production. *Bioresour. Technol.* 102, 6909–6919. doi: 10.1016/j.biortech.2011.04.038

Zorina, A., Stepanchenko, N., Novikova, G. V., Sinetova, M., Panichkin, V. B., Moshkov, I. E., et al. (2011). Eukaryotic-like. Ser/Thr protein kinases SpkC/F/K are involved in phosphorylation of GroES in the Cyanobacterium *Synechocystis*. *DNA Res.* 18, 137–151. doi: 10.1093/dnares/dsr006

Zorina, A. A., Bedbenov, V. S., Novikova, G. V., Panichkin, V. B., and Los, D. A. (2014). Involvement of serine/threonine protein kinases in the cold stress response in the Cyanobacterium *Synechocystis* sp. PCC6803: functional characterization of *SpkE* protein kinase. *Mol. Biol.* 48, 390–398. doi: 10.1134/S0026893314030212

Conflict of Interest: The authors declare that the research was conducted in the absence of any commercial or financial relationships that could be construed as a potential conflict of interest.

frontiers in Bioengineering and Biotechnology

ORIGINAL RESEARCH
published: 31 March 2021
doi: 10.3389/fbioe.2021.652021

Global Metabolomics Reveals That *Vibrio natriegens* Enhances the Growth and Paramylon Synthesis of *Euglena gracilis*

Ying Ouyang[1,2], Shuyu Chen[2], Liqing Zhao[2], Yiting Song[3], Anping Lei[1], Jiayi He[1,4] and Jiangxin Wang[1,4]*

[1] Shenzhen Key Laboratory of Marine Bioresources and Eco-Environmental Science, Shenzhen Engineering Laboratory for Marine Algal Biotechnology, Guangdong Provincial Key Laboratory for Plant Epigenetics, College of Life Sciences and Oceanography, Shenzhen University, Shenzhen, China, [2] College of Chemistry and Environmental Engineering, Shenzhen University, Shenzhen, China, [3] Department of Microbiology, University of Illinois Urbana-Champaign, Champaign, IL, United States, [4] Key Laboratory of Optoelectronic Devices and Systems of Ministry of Education and Guangdong Provinces, College of Physics and Optoelectronic Engineering, Shenzhen University, Shenzhen, China

The microalga *Euglena gracilis* is utilized in the food, medicinal, and supplement industries. However, its mass production is currently limited by its low production efficiency and high risk of microbial contamination. In this study, physiological and biochemical parameters of *E. gracilis* co-cultivated with the bacteria *Vibrio natriegens* were investigated. A previous study reports the benefits of *E. gracilis* and *V. natriegens* co-cultivation; however, no bacterium growth and molecular mechanisms were further investigated. Our results show that this co-cultivation positively increased total chlorophyll, microalgal growth, dry weight, and storage sugar paramylon content of *E. gracilis* compared to the pure culture without *V. natriegens*. This analysis represents the first comprehensive metabolomic study of microalgae-bacterial co-cultivation, with 339 metabolites identified. This co-cultivation system was shown to have synergistic metabolic interactions between microalgal and bacterial cells, with a significant increase in methyl carbamate, ectoine, choline, methyl N-methylanthranilate, gentiatibetine, 4R-aminopentanoic acid, and glu-val compared to the cultivation of *E. gracilis* alone. Taken together, these results fill significant gaps in the current understanding of microalgae-bacteria co-cultivation systems and provide novel insights into potential improvements for mass production and industrial applications of *E. gracilis*.

Keywords: ***Euglena gracilis, Vibrio natriegens,*** **co-cultivation, metabolomics, paramylon**

OPEN ACCESS

Edited by:
Wei Xiong,
National Renewable Energy Laboratory (DOE), United States

Reviewed by:
Chun Wan,
University of Colorado Boulder, United States
Pau Loke Show,
University of Nottingham Malaysia Campus, Malaysia

****Correspondence:***
Jiayi He
jiayihe@szu.edu.cn

Specialty section:
This article was submitted to Bioprocess Engineering, a section of the journal Frontiers in Bioengineering and Biotechnology

Received: *11 January 2021*
Accepted: *10 March 2021*
Published: *31 March 2021*

Citation:
Ouyang Y, Chen S, Zhao L, Song Y, Lei A, He J and Wang J (2021) Global Metabolomics Reveals That Vibrio natriegens Enhances the Growth and Paramylon Synthesis of Euglena gracilis. Front. Bioeng. Biotechnol. 9:652021. doi: 10.3389/fbioe.2021.652021

INTRODUCTION

Euglena gracilis is a single-celled flagellate alga with characteristics typical of both plants and animals, including the lack of a cell wall. Additionally, *E. gracilis* possesses two flagella for cell mobility (Zakryś et al., 2017). *E. gracilis* cells are rich in minerals, amino acids, unsaturated fatty acids, lutein, chlorophyll, zeaxanthin and 59 other essential nutrients for human health.

Abbreviations: IAA, indole-3-acetic acid; KEGG, Kyoto Encyclopedia of Genes and Genomes; OPLS-DA, orthogonal projections to latent structures discriminant analysis; PCA, principal component analysis; VIP, variable importance in projection.

Furthermore, it can be used to produce many valuable products, such as α-tocopherol, wax esters and paramylon (Kottuparambil et al., 2019). However, the low production efficiency in the large-scale cultivation of *E. gracilis* limits its further development. We therefore sought to determine whether the novel approach of utilizing co-cultivation would improve the efficacy of *E. gracilis* production.

There are several ecological mechanisms, such as quorum sensing, which occur among microbial communities to facilitate cell-cell communication (Zhou et al., 2016). The microalgae-bacteria co-cultivation system involves a mixture of microalgae and bacteria at specific ratios with the intent to increase the production of microalgae or specific substances by microalgae (Taniguchi and Tanaka, 2004). Such co-cultivation systems have been studied extensively. For instance, it has been found that the microbial interaction between the bacterium *Azospirillum brasilense* and the microalga *Chlorella vulgaris* has a significant effect on fatty acid and lipid accumulation in the microalga (Leyva et al., 2014). Additionally enhancement of microalgal growth, lipid and protein content of *Chlorella variabilis* was shown when the green microalga was co-cultivated with the siderophore-producing bacterium, *Idiomarina loihiensis* RS14, in an optimized ratio under iron-deficient conditions (Rajapitamahuni et al., 2019). When microalga *Chlorella* was co-cultured with bacteria *Bacillus firmus* and *Beijerinckia fluminensis* to treat wastewater in vinegar production, though algal biomass was slightly decreased, a higher rate of nutrients removal was achieved (Huo et al., 2020). Earlier work in *E. gracilis* reported that *Vibrio natriegens* can increase its biomass accumulation (Kim et al., 2019). Previous reports have also indicated that the biomass and paramylon production of *E. gracilis* is increased when it is co-cultivated with the bacterium *Pseudoalteromonas* under optimal conditions, the extracellular polymeric substances (EPS) of the bacterium contributed to the results (Jeon et al., 2019, 2020). When co-cultivated with the microalga growth-promoting bacterium *Emticicia*, *E. gracilis* was found to have higher biomass and produce more lipids (Toyama et al., 2019). Despite all of the beneficial effects found in these co-cultivation systems, the underlying mechanisms have not been sufficiently studied.

Metabolomics is the study of the physiology of organisms by profiling the changes in metabolites under different conditions. As downstream products biosynthesized after complex transcriptional, translational and regulatory processes, the types and amounts of metabolites vary significantly depending on different conditions (Nicholson et al., 1999). Thus, metabolomics has been applied to obtain a general understanding of the regulatory networks involved in microalgal metabolism. A metabolic profiling technique was developed for the model green microalga, *Chlamydomonas reinhardtii*, under stress conditions such as nitrogen-, phosphorus-, sulfur- and iron-depletion (Bölling and Fiehn, 2005). A method to assess the metabolism of freshwater microalga *C. vulgaris* and *Scenedesmus obliquus* after being exposed to the flame retardant triphenyl phosphate was also recently established (Wang et al., 2019). Furthermore, potential biomarkers of *C. reinhardtii* grown in photobioreactors in the context of nitrogen starvation were found using metabolomics (Courant et al., 2013).

In this study, we reproduced the previous finding that *V. natriegens* enhances both growth and paramylon production of *E. gracilis* (Kim et al., 2019). What's more, we employed metabolomics in culture medium to gain a better understanding of the underlying causes of the improvements observed in the co-cultivation experiment, which revealed several interesting interactions between the two species since, and the results will be easily applied to large-scale exploitation for *E. gracilis* in the future. This is the first report utilizing culture medium metabolomics to understand this co-cultivation system, and therefore, fills a gap in the current understanding of microalgae-bacteria symbiosis on a metabolomic level.

MATERIALS AND METHODS

Strains and Culture Conditions

Euglena gracilis CCAP 1224/5Z was purchased from the Culture Collection of Algae and Protozoa[1]. The microalgal cells were grown under a continuous light at a light intensity of approximately 100 $\mu mol/m^2/s$ in an illuminating incubator at 26°C in EM medium [1.8 g/L NH_4Cl, 0.6 g/L KH_2PO_4, 0.6 g/L $MgSO_4$, 60 mg/L Urea, 0.02g/L $CaCl_2$, 0.48 mg/L Na_2EDTA, 2 mg/L $Fe_2(SO_4)_3$, 60 μL HCl, 0.01 mg/L Vb_1, 0.0005 mg/L Vb_{12}, 20 mg/L $CuSO_4{\cdot}5H_2O$, 0.4 g/L $ZnSO_4{\cdot}7H_2O$, 1.3 g/L Co $(NH_3){\cdot}H_2O$, and 1.6 g/L $MnCl_2{\cdot}4H_2O$] until reaching stationary phase. Subcultures of alga were done every 6 days at a ratio of 10% (Afiukwa and Ogbonna, 2007).

Vibrio natriegens 1H00025 was purchased from the Third Institute of Oceanography, MNR (Xiamen, China). The bacterial cells were grown in sterilized 2216E (CM0471) medium and incubated at 26°C with rotational shaking (120 r/min) in the dark. Subcultures of alga were done every 3 days at a ratio of 1% (Weinstock et al., 2016).

Co-cultivation of *E. gracilis* and *V. natriegens*

Euglena gracilis cells were harvested during the stationary phase when the OD_{750} reached 3.0. The OD_{750} of each initial inoculum was adjusted to 3.0 after being washed three times in EG medium (Afiukwa and Ogbonna, 2007). *V. natriegens* cells were harvested during the exponential phase when OD_{600} reached 1.0. The OD_{600} of the initial inoculums were adjusted to 1.0 after being washed three times in EG medium. The inoculation volume ratio of *E. gracilis* to *V. natriegens* was 10:1 (200 mL: 20 mL). After mixing the two inoculums, additional medium was added to reach a final volume of 1.5 L. After dilution, co-cultivation of *E. gracilis* and *V. natriegens* was performed in an illuminating incubator at 26°C in EG medium under a continuous light at a light intensity of approximately 100 $\mu mol/m^2/s$, no shaking or aeration was used during experiment.

[1]https://www.ccap.ac.uk/

Growth (Cell Number, Chlorophyll Content, Dry Weight) and Paramylon Content of *E. gracilis*

The growth of *E. gracilis* was calculated by measuring its cell number, total chlorophyll content, and dry weight. Paramylon content was also calculated. Cell growth was measured by counting cell number with a microscope in a 0.1 mL counting chamber. The total chlorophyll of a 1 mL sample was extracted with 80% acetone and the chlorophyll content was determined using the Arnon method (Arnon, 1949). The dry weight of the 100 mL sample was measured using the oven-drying method (Edmunds, 1966). Paramylon extraction and measurement was carried out as reported previously (Takenaka et al., 1997). Cell number and total chlorophyll were measured daily over the course of 9 days. Dry weight and paramylon content were measured every two days. Three biological replicates were used for each experiment.

The Cell Number of *V. natriegens*

The cell number of *V. natriegens* was measured manually with a microscope in a 0.1 mL counting chamber. Samples were first stained with crystal violet (Kannan et al., 2019) at a 9:1 ratio of sample to crystal violet for 15 minutes. Next, 100 μL of the stained sample was added into the counting chamber and completely fixed on the chamber surface after being dried in an oven.

Preparation of Samples for LC-MS/MS Analysis

For LC-MS/MS analysis, samples taken after six days of incubation were first centrifuged at 5,000 g for 5 min at 4°C (Thermo Heraeus Fresco17, United States) to obtain supernatant. After centrifugation, 300 μL aqueous methanol (1 μg/mL of the inner label) was plunged into 100 μL of each supernatant sample, followed by vortexing for 30 s, then 10 min on ice in an ultrasonic disruptor. Samples were then incubated at −40°C for 1 h, followed by centrifugation at 12,000 rpm for 15 min at 4°C. The resulting supernatant was then utilized for LC-MS/MS measurements (Doppler et al., 2016).

LC-MS/MS Analysis

LC-MS/MS analyses were performed using a UHPLC system (1290, Agilent Technologies) with a UPLC HSS T3 column (2.1 mm × 100 mm, 1.8 μm) coupled to a Q Exactive mass spectrometer (Orbitrap MS, Thermo). The mobile phase A consisted of 0.1% formic acid in water at the positive mode and 5 mmol/L ammonium acetate in water for the negative mode, and the mobile phase B was acetonitrile. The elution gradient was set as follows: 0–1 min, 1% B; 1–8 min, 1%–99% B; 8–10 min, 99% B; 10–10.1 min, 99%–1% B; 10.1–12 min, 1% B. The flow rate was set to 0.5 mL/min, while the injection volume was set to 2 μL. A QE mass spectrometer was utilized to acquire MS/MS spectra, with the collective mode set to information-dependent acquisition (IDA) in the acquisition software (Xcalibur 4.0.27, Thermo). In this mode, the acquisition software continuously evaluates the full scan MS spectrum. The ESI source conditions were set as follows: sheath gas flow rate as 45 Arb, aux gas flow rate as 15 Arb, capillary temperature 400°C, full MS resolution as 70000, MS/MS resolution as 17500, collision energy as 20/40/60 eV in NCE mode, spray Voltage as 4.0 kV (positive) or −3.6 kV (negative), respectively (Periannan, 2003).

Statistical Analyses

The cell number, chlorophyll content, dry weight, and paramylon content of *E. gracilis* were analyzed using a parametric two-way analysis of variance (ANOVA) with treatment (co-cultivated and axenic) as the source of variations. All data fulfilled the assumptions of the parametric test and no data transformation was needed. The statistical analysis was carried out by SPSS 17.0 for Windows.

For the metabolomic study, after the raw data profiles were preprocessed, Student's *t*-tests were utilized for univariate analysis, while principal component analysis (PCA) and orthogonal projections to latent structures discriminant analysis (OPLS-DA) were used for multivariate analysis. Variable importance in projection (VIP) score was combined with P-value to screen significant differential metabolites. In-house database and online databases (HMDB and Metlin) were applied in metabolite identification. Metabolites which were found to be statistically significantly different in different samples were then qualitatively analyzed based on relevant KEGG pathway and literature information (Mangalam et al., 2013).

RESULTS

Effects of Co-cultivation on the Growth (Cell Number, Chlorophyll Content, Dry Weight) and Paramylon Content of *E. gracilis*

When compared to the *E. gracilis* control, the co-cultivation group had significantly higher biomass and produced more paramylon. As shown in **Figure 1A**, the average growth rate of *E. gracilis* was faster when co-cultivated with *V. natriegens*, and the co-cultivation group not only entered the exponential phase approximately 24 h earlier than the control but also entered the stationary phase 24 h later. The average division speed of *E. gracilis* under the co-cultivation system was also much faster than that of the control. When the control entered the stationary phase after 6 days and the cell division slowed, the co-cultivation group continued to divide rapidly. After 9 days of cultivation, the cell number of the co-cultivation group was 23% higher than that of the control group. Interestingly, as shown in **Figure 1B**, the chlorophyll content of the co-cultivation group (47.73 μg/mL) in the late culture period (D9) increased by 23.75% compared with that of the control (38.57 μg/mL).

Changes in the number of *V. natriegens* cells in the co-cultivation system are shown in **Figure 1A**. *V. natriegens* grew slowly during D1–D3 of co-cultivation, and the number of bacteria began to increase sharply from D3 onward. On D5, the growth of *V. natriegens* entered into a stationary phase (7.23 x 10^5 cells/mL), while the number of *V. natriegens* was 15.38 times

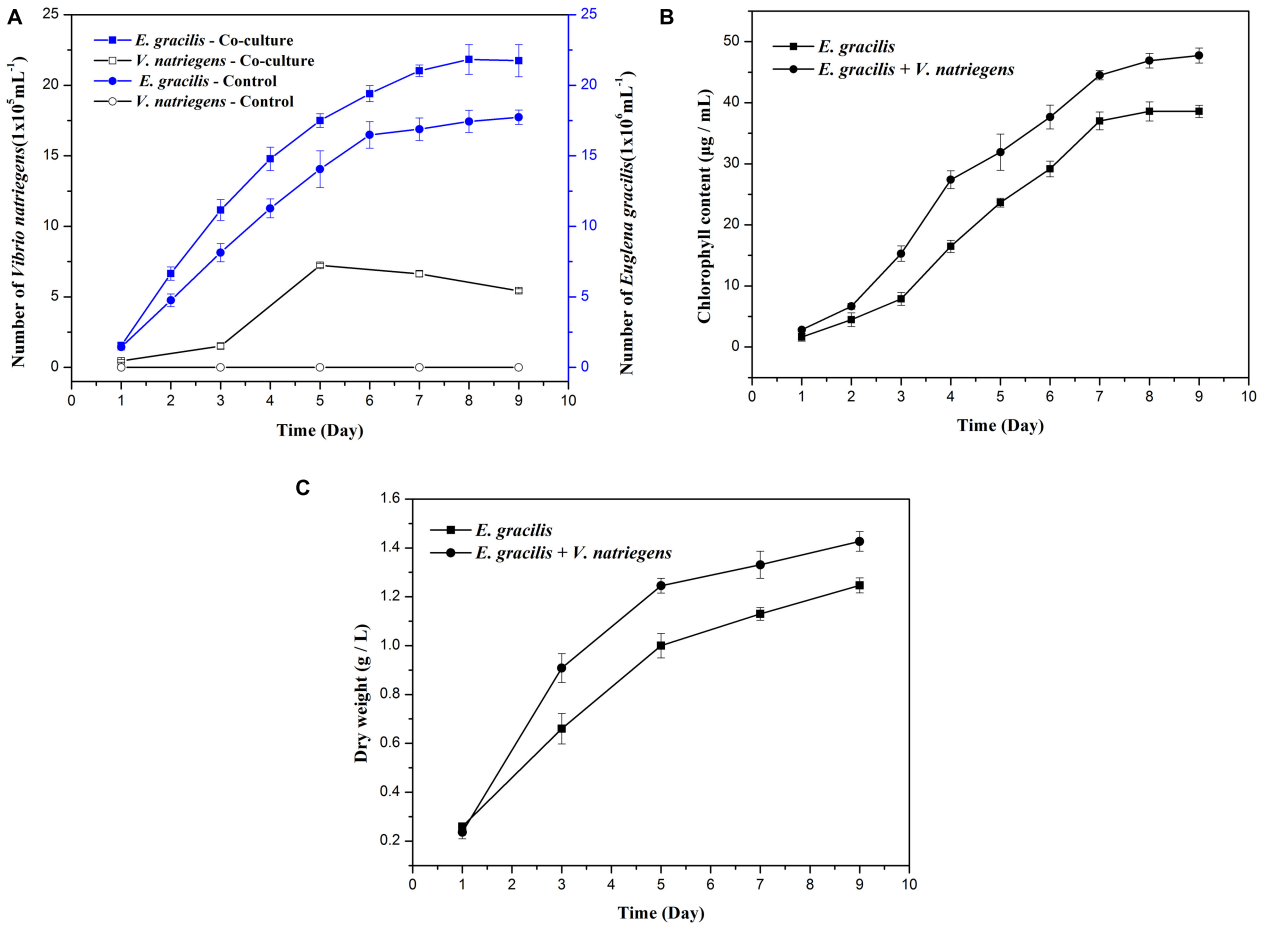

FIGURE 1 | Effects of the co-cultivation system on the growth of *E. gracilis*. **(A)** Cell number of *E. gracilis* and *V. natriegens*. **(B)** Chlorophyll content. **(C)** Dry weight. There was an extremely significant effect of the treatment (co-cultivated and axenic) according to ANOVA test at the $p < 0.0001$ level for the three conditions (*F*-values are 229.557, 381.066, and 120.642, respectively).

and 1.33 times higher than that on D1 (0.47 x 10^5 cells/mL) and D9 (5.43 x 10^5 cells/mL), respectively. The *V. natriegens* cell count then began to decline, indicating that this species can exist symbiotically with *E. gracilis*, and its presence is correlated with higher *E. gracilis* growth rates.

As shown in **Figures 1C**, **2**, both the dry weight and paramylon content increased in the two groups over time, but the dry weight and paramylon content in the co-cultivation group were significantly higher than that of the control group. On D9, dry weight and paramylon content of the co-cultivation group reached their maximum values, 1.42 and 0.76 g/L, respectively, which were approximately 15 and 12% higher than the control (1.24 and 0.68 g/L).

Comparison of the Metabolic Changes in the Co-cultivation Group and Axenic *E. gracilis* Group

General Analysis of Metabolites

A total of 5165 metabolites were detected in the samples (**Table 1**), and 100 metabolites were identified and shown in **Supplementary Data**. Metabolites with *p*-values < 0.05 and VIP > 1 were considered differential metabolites between the two groups, and 339 metabolites were identified as passing these criteria. Among these significantly differentially expressed metabolites, 172 were upregulated and 167 were downregulated when comparing the co-cultivation group to the control group.

Multivariate Data Analysis

Principal component analysis plots of the metabolomic profiles after 6 days of cultivation between the co-cultivation group and the control were generated, as shown in **Figure 3A**. All the samples were within the 95% confidence ellipses. **Figure 3A** indicates that a suitable distance was found between dispersion and aggregation samples when comparing the control and co-cultivation groups, suggesting that the two groups of samples have significant differences in the chemical composition of metabolites. OPLS-DA scatter plots are shown in **Figure 3B**. The two groups of samples were distinguished significantly and were both within the 95% confidence ellipses. The control and the co-cultivation group were distributed along the first principal component t [1] axis, with no crossover or overlap, indicating

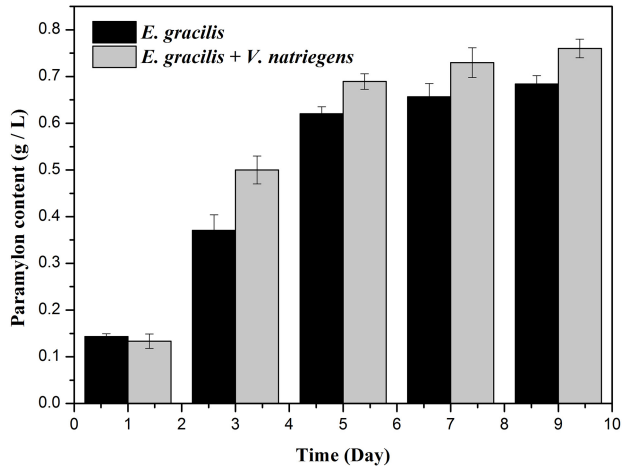

FIGURE 2 | Effects of the co-cultivation system on active substance (paramylon content) accumulation of *E. gracilis*. There was an extremely significant effect of the treatment (co-cultivated and axenic) according to ANOVA test at the $p < 0.0001$ level for dry weight (F-value = 63.938).

TABLE 1 | The general and differential ion numbers in metabolomic results.

Mode	Total ion number	VIP > 1 ion number	*p*-value < 0.05 ion number	Up	Down
Pos	5165	1838	339	172	167
Neg	5259	1968	317	213	104

that the composition of the metabolites in the two groups was significantly different, and the extracellular metabolites of *E. gracilis* were affected by *V. natriegens*. The OPLS-DA permutation plots are shown in **Figure 3C**. R^2Y was used to estimate the matching degree between the structured model and the Y data, and Q^2 was utilized to judge the predictive ability of the structured model. The values of R^2Y and Q^2 were both higher than 0.05, indicating that the original model had a high degree of fit and high explanatory and predictive capabilities. After visualizing the differential metabolites in the form of volcano plots in **Figure 3D** (VIP > 1 and p-value < 0.05), it can be found that the differences between the control group and the co-cultivation group were significant.

Significant Differential Metabolites

Metabolites with p-value < 0.05 were considered significant differential metabolites, and were the driving force of the separation shown in the models constructed previously (**Table 2**). When compared to the control, the co-cultivation group had significantly higher levels of methyl carbamate, ectoine, choline, methyl N-methylanthranilate, gentiatibetine, 4R-aminopentanoic acid and glu-val, while the levels of 3-butylpyridine, proline, sn-glycero-3-phosphocholine, N-butyl-1H-pyrazolo[3,4-d]pyrimidin-4-amine, and myosmine were lower.

Correlation Analysis of Significant Differential Metabolites

To investigate the correlation of significantly differential metabolites, heat maps were generated (**Figure 4**) using the Pearson's correlation coefficient. Positive R values denote positive correlation while negative R values denote negative correlation. The metabolite 4R-aminopentanoic acid, for example, was positively correlated with methyl carbamate, methyl N-methylanthranilate, ectoine, glu-val, and gentiatibetine, with glu-val and gentiatibetine showing the highest R values. At the same time, this metabolite was negatively correlated with 3-butylpyridine, proline, sn-glycero-3-phosphocholine, N-butyl-1H-pyrazolo[3,4-d]pyrimidin-4-amine and myosmine, with proline and sn-glycero-3-phosphocholine showing the lowest R values.

GO KEGG Analyses

In addition to multivariable analysis, metabolites were mapped to KEGG metabolic pathways for enrichment analysis (**Table 3**). Pathway enrichment analysis showed that "Glycine, serine and threonine metabolism," "Glycerophospholipid metabolism," and "ABC transporters" were statistically significantly enriched.

DISCUSSION

Growth (Cell Number, Chlorophyll, Dry Weight) and Paramylon Content Under Co-cultivation

Under the optimal microalgae-bacteria ratio and co-cultivation conditions, the growth of *E. gracilis* can be improved significantly by *V. natriegens*. In the co-cultivation group, *E. gracilis* entered its exponential phase earlier and the exponential phase lasted longer compared to the control. The co-cultivation group also had values of cell number, chlorophyll content, dry weight and paramylon content which were 123, 124, 115, and 112% of the control, respectively.

Taken together, these results indicate that *V. natriegens* had a positive influence on *E. gracilis* under optimum growth conditions, resulting in higher reproductive efficiency, increased biomass and higher production of bioactive materials accumulation in *E. gracilis*. When the diatom *Thalassiosira pseudonana* was co-cultivated with the bacteria *Dinoroseobacter shibae* at a 1:1 ratio, the metabolism of *T. pseudonana* was altered, but its overall growth rate was unchanged (Paul et al., 2013). When cyanobacteria *Microcystis aeruginosa* PCC 7806 and microalga *Desmodesmus subspicatus* were co-cultivated in a designated dialysis tubing, the presence of *M. aeruginosa* did not influence the growth of the microalga at the early logarithmic growth phase, while the microalga started to out-compete the co-cultivated bacteria during the exponential phase of growth (Omidi et al., 2019). These findings indicate that species, cultivation conditions and co-cultivation ratio can all influence the results of co-cultivation. There're other ways to optimize the biomass and bioactive materials accumulation in microalgae, different approaches were reported

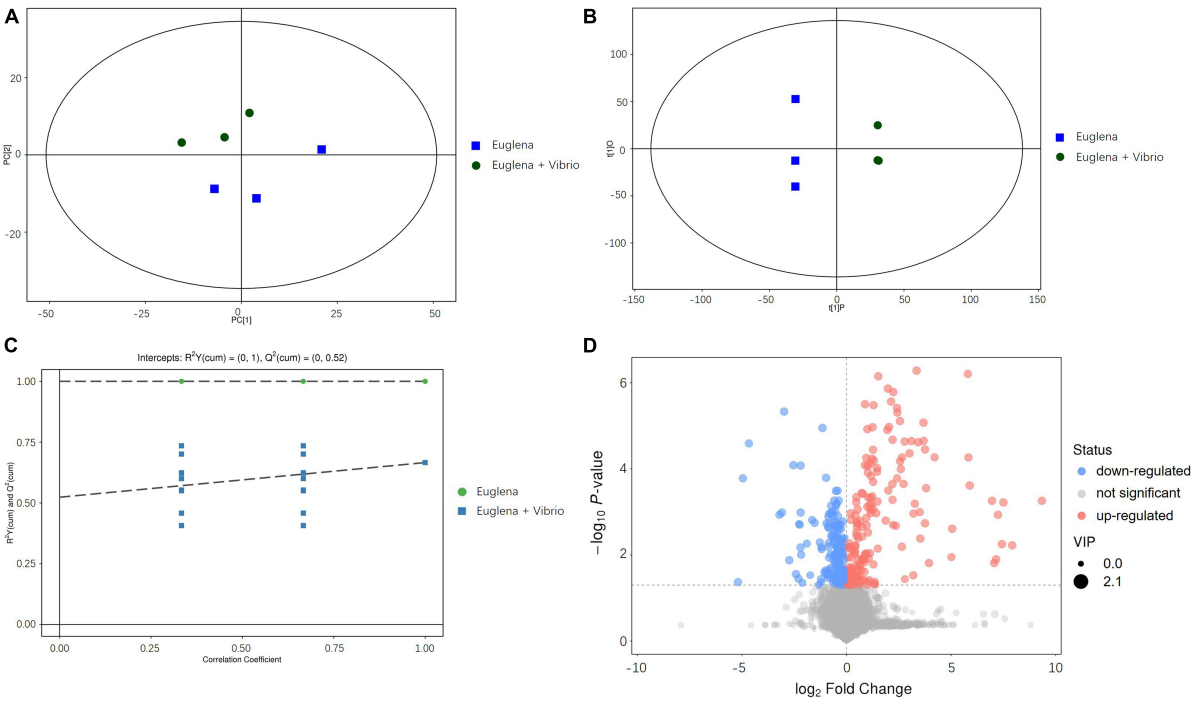

FIGURE 3 | (A) PCA analysis of metabolomic profiles. **(B)** OPLS-DA scattered plots of metabolomic profiles. **(C)** OPLS-DA permutation plots of metabolomic profiles. **(D)** Volcano plots of metabolomic profiles.

depend on the different purposes (Chew et al., 2017). For instance, optimizing the algal photobioreactor (Cheah et al., 2020) or modifying algal particles (Cheng et al., 2019) for wastewater treatment, many researches were also done to explore sustainable ways to utilize algae in bioenergy production (Chia et al., 2018).

Previous studies have also shown that when *E. gracilis* was heterotrophically co-cultivated with *V. natriegens*, significant increases in biomass and paramylon content were found (Kim et al., 2019). Although this previous study found positive results from co-cultivation, it did not explore the possible mechanisms or effects on the metabolites present in the system. In the current study, we not only analyzed the metabolites of the co-cultivation culture system, but also confirmed that bacteria can live in an algae-dominant environment, which may work to exclude the presence of other unwanted bacteria.

V. natriegens in the Co-cultivation System

Under the optimal microalgae-bacteria ratio and cultivation conditions of this study, a balance of oxygen, carbon dioxide and nutrient substances was established between *V. natriegens* and *E. gracilis*. Meanwhile, the cell density of *V. natriegens* increased as *E. gracilis*' cell density increased, indicating that the dead cells of *V. natriegens* (which could have been providing nutrients) were not the main reason why the production of *E. gracilis* was increased. It is plausible that *V. natriegens* produced metabolites that positively influenced the growth of *E. gracilis.* Moreover, *V. natriegens* entered both the stationary and decline phases earlier than *E. gracilis*, indicating that *V. natriegens* had a shorter life cycle than *E. gracilis,* Therefore, subsequent addition of more bacteria could be considered if this strategy was applied in the actual production process.

Metabolomics of the Co-cultivation Group

General Metabolomic Analysis

Principal component analysis and OPLS-DA plots both revealed that the control and co-cultivation samples broke out into two

TABLE 2 | The differential metabolites and their indexes.

Metabolite	*p*-value	Fold change
Gentiatibetine	0.0005	1.39
4R-aminopentanoic acid	0.0006	124.23
sn-Glycero-3-phosphocholine	0.0010	0.12
Glu-Val	0.0012	151.38
Methyl N-methylanthranilate	0.0062	1.32
Proline	0.0065	0.55
Choline	0.0079	1.33
3-Butylpyridine	0.0101	0.67
Ectoine	0.0202	1.49
Methyl carbamate	0.0270	1.11
N-Butyl-1H-pyrazolo[3,4-d]pyrimidin-4-amine	0.0458	0.71
Myosmine	0.0493	0.40

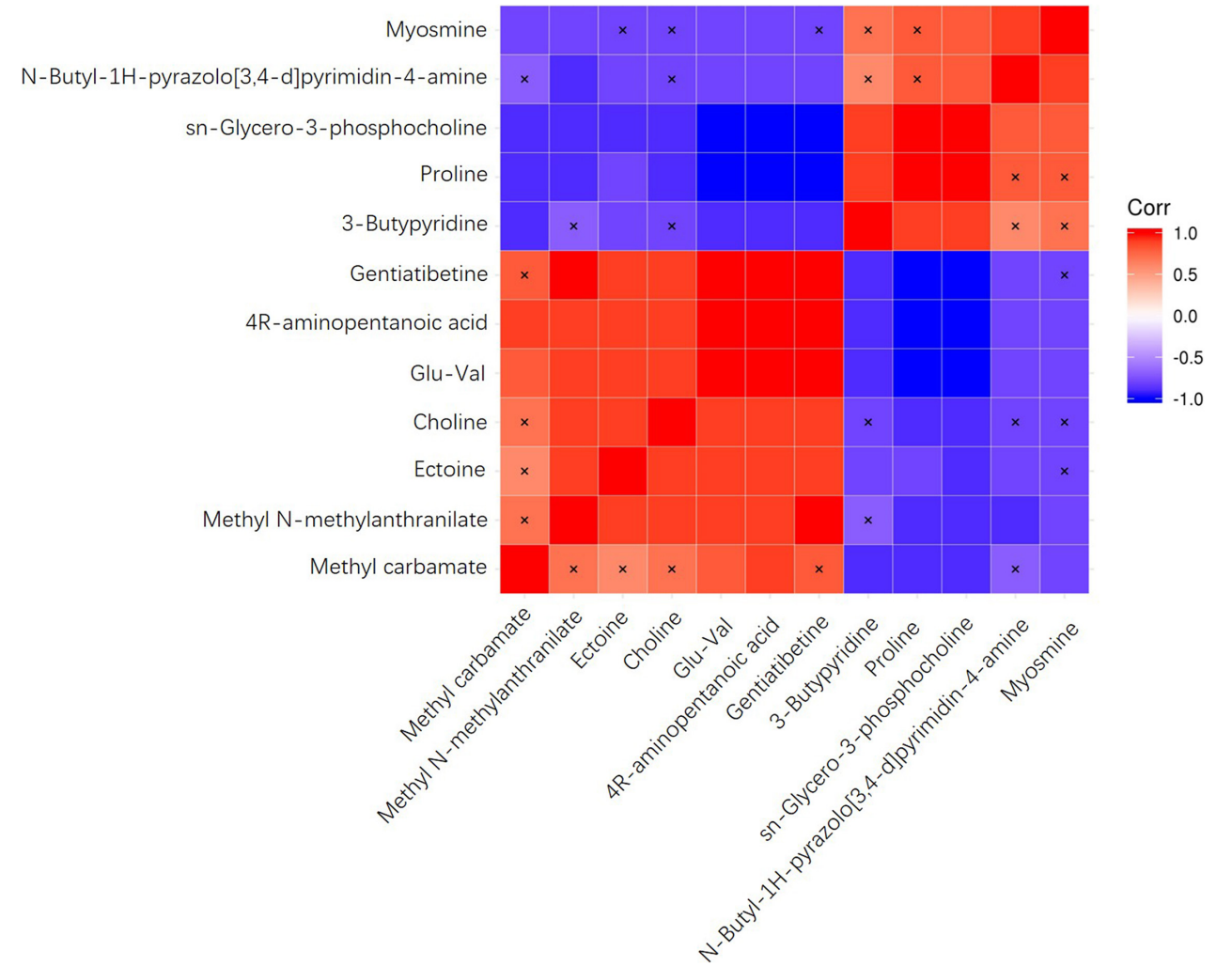

FIGURE 4 | Heatmaps of correlation analysis plots of differential metabolites.

distinct groups, indicating the two groups had significantly different metabolite profiles. Despite these significant differences, similarities were also found. The main metabolites identified from both groups were of similar types and quantities, including phosphoric acid, 2,5-xylidine, dimethylimidazole and 2-Aminopyridine. Although the existence of *V. natriegens* changed the composition of metabolites to some extent, the two groups were still cultured in the same medium and laboratory conditions, which led to the existence of similarities between metabolite profiles.

TABLE 3 | The variation trends of differential metabolites in each enriched pathway.

Metabolites	Metabolic pathways		
	Glycine, serine and threonine metabolism	Glycerophospholipid metabolism	ABC transporters
Choline	↑	↑	↑
Ectoine	↑	–	↑
sn-Glycero-3-phosphocholine	–	↓	–
Proline	–	–	↓

Many active substances were found at high levels in both the control and co-cultivation samples. 2-aminopyridine is an inhibitor of the beta-secretase enzyme and is useful in the treatment of conditions such as Alzheimer's disease (Coburn et al., 2011). 1-butylamine and 2,5-xylidine are mainly utilized for organic synthesis and are important intermediates for the synthesis of some pesticides and medicines (Cao et al., 2011; Kricka and Vernon, 2011), while 2,5-xylidine can also be used for the synthesis of disazo acid dyes (Dombchik, 1977). Dimethicone is widely used in skincare and hair products (Pellicoro et al., 2013) and is also swallowed prior to upper endoscopy procedures due to its ability to reduce the foam and bubbles in both the stomach and the duodenum to increase visibility. The discovery of these

active substances indicates a significant potential for *E. gracilis* production (Bertoni et al., 1992).

Metabolites Which Are Related to the Proliferation of *E. gracilis*

The metabolite with the highest fold change (151) was glu-val. Glu-val belongs to the class of organic compounds known as peptides (Maehashi et al., 1999), and it is usually generated from proteolysis, which may be related to the downregulation of sn-glycero-3-phosphocholine and upregulation of choline. Choline is an important substrate involved in the synthesis of phosphatidylcholine (Li and Vance, 2008), which is necessary for the biosynthesis of the eukaryotic cell membrane (Chen et al., 2014). Since *V. natriegens* is a prokaryotic organism, the upregulation of phosphatidylcholine directly indicates the increase of *E. gracilis* membrane and further indicates an increase of *E. gracilis* biomass, which is in keeping with our analysis of biomass during co-cultivation. A higher quantity of *E. gracilis* cells would result in a higher rate of proteolysis, which may explain the increased level of glu-val in the co-cultivation group, as well as the downregulation of proline content. Interestingly, the mean value of glu-val in the co-cultivation group (0.0593) was much higher than that in the control (0.0004), even though both values were relatively small. This may be due to the generation of excess glu-val directly by *V. natriegens* or indirectly by *E. gracilis* under the influence of *V. natriegens*.

In the co-cultivation group, *V. natriegens* likely produced a significant amount of ectoine to adapt to the osmotic stress change in the medium (Teixidó et al., 2005). Ectoine is a solute that is accumulated by the halophilic or halotolerant microorganisms to prevent osmotic stress, which can also protect non-halophilic cells (Fallet et al., 2010). Meanwhile, studies have shown that ectoine causes an increase in the expression level of the ABC transporter substrate-binding protein EhuB (Richter et al., 2019). It therefore seems likely that uptake of ectoine by *E. gracilis* caused the upregulation of metabolites which are imported by ABC transporters.

Ectoine is widely used in the plant industry, due to its ability to accelerate the enzymatic conversion of triglycerides in biodiesel synthesis (Wang and Zhang, 2010). Ectoine can also increase cellular tolerance to high salt concentration, which can block chlorophyll synthesis in plants and microalgae (Pinheiro et al., 2008). The mean value of ectoine in the co-cultivation group (0.0104) was slightly higher than that in the control group (0.0070), likely because ectoine was either generated by *V. natriegens* or *E. gracilis* under the influence of *V. natriegens.*

Metabolites Related to the Value of Large-Scale Exploitation of *E. gracilis*

4R-aminopentanoic acid content in the co-cultivation group was higher than that in the control group (124-fold). This study represents the first time that 4R-aminopentanoic acid has been found in microalgae. In pharmacology, derivatives of this compound can be used as GABA transaminase and NEP inhibitors, which act as anticonvulsants (Callery et al., 1982). The synthesis of 4-aminopentanoic acid mainly depends on artificial means (Silverman and Levy, 2002), but with the discovery of the ability of *E. gracilis* to produce 4-aminopentanoic acid opens up new possibilities for producing this important compound. Similar to glu-val, the mean value of 4R-aminopentanoic acid in the co-cultivation group (6.6746) was much higher than that in the control group (0.0537), likely because this metabolite was produced by *V. natriegens* or *E. gracilis* under the influence of *V. natriegens.*

Some of the metabolites identified in this study are of commercial finterest, potentially increasing the value of *E. gracilis* cultivation. For example, methyl N-methylanthranilate and methyl carbamate were both upregulated in the co-cultivation group. Methyl N-methylanthranilate is a natural fragrance that can be found in flowers and fruit (Mookherjee et al., 1990), which is also added to wine as an aroma constituent (Nelson et al., 1977). Additionally, it appears in several essential oils, such as neroli and bergamot (Taupp et al., 2005). Myosmine is a minor tobacco alkaloid which is downregulated during co-cultivation (Zwickenpflug and Tyroller, 2006). This compound has been shown to be a potential risk factor for the development of esophageal adenocarcinoma (Vogt et al., 2006), and its downregulation could improve the safety of *E. gracilis* consumption.

In a previous study, it was proposed that *V. natriegens* increased the production of *E. gracilis* through the impact of indole-3-acetic acid (IAA) (Kim et al., 2019), but we were unable to confirm this result. This previous study also noted that the IAA produced by *V. natriegens* played a significant role in the positive growth regulation of *E. gracilis*, but the IAA concentration in our study was too low to be detected in the differential metabolite analysis.

Pathway Enrichment and KEGG Analyses

Choline and ectoine are known to participate in glycine, serine and threonine metabolism. Choline is a downstream product of serine, which is derived from 3P-D-glycerate, while 3P-D-glycerate is a derivative of glycolysis, and glycine is derived from serine. Threonine can only be synthesized by bacteria and plants, but not by animals (Shaul and Galili, 1993). Threonine is derived from aspartic acid (Szczesiul and Wampler, 2002).

Two metabolites of sn-glycero-3-phosphocholine and choline participate in glycerophospholipid metabolism (Tocher, 1995). These two metabolites are the downstream products of phosphatidylcholine (Li and Vance, 2008), and choline is a precursor for the synthesis of phosphatidylcholine (Vance and Adeli, 2008). Since phosphatidylcholine generally does not exist in prokaryotes (Fagone and Jackowski, 2013), it can be inferred that the change in this pathway is originated in *E. gracilis.* It is worth noting that, similar to the differential metabolite ectoine, the metabolomic results show that the mean values of choline in the co-cultivation group (0.4197) and in the control group (0.0316) are both low. Therefore, it seems likely that this metabolite was produced by either microalgal or bacterial cells under the influence of *V. natriegens,* and may have played a role in the increased growth rate of *E. gracilis*.

ABC transporter activity influences the levels of proline, osmo-protectants and histidine compounds (Boncompagni et al., 2000). These transporters are membrane integral proteins that use the energy generated by hydrolyzing ATP to actively transport carbohydrates, amino acids, peptides, proteins and various cellular metabolites (Rees et al., 2009). They can be found in the cell membranes of both eukaryotes and prokaryotes (Pohl et al., 2005), and the changes to their expression significantly impact the transport capacity of microbial membranes in the co-cultivation system.

CONCLUSION

Effects of *E. gracilis* and *V. natriegens* co-cultivation on microalgal physiological characteristics, cellular metabolites and metabolic networks revealed that the biomass and paramylon content of *E. gracilis* was enhanced by *V. natriegens*. A total of 339 differential metabolites were found, including economically important metabolites such as choline, ectoine, 4R-aminopentanoic acid, methyl N-methylanthranilate and methyl carbamate. This study represents the first comprehensive metabolomic study of culture medium involving a microalgae-bacteria co-cultivation system. Overall, this study significantly increases the understanding of microalgae-bacteria co-cultivation systems and provides a number of new avenues to explore for improving the mass production of *E. gracilis*.

DATA AVAILABILITY STATEMENT

The original contributions presented in the study are included in the article/**Supplementary Material**, further inquiries can be directed to the corresponding author/s.

AUTHOR CONTRIBUTIONS

JH and JW contributed to the conceptualization, methodology, writing (review and editing), formal analysis, and investigation. YO and SC contributed to the investigation, data curation, writing (original draft), and formal analysis. LZ contributed to the writing (review and editing). YS contributed to the investigation. AL contributed to the data curation and writing (review and editing). All authors contributed to the article and approved the submitted version.

FUNDING

This work was supported by the National Key R&D Program of China (2018YFA0902500), National Natural Science Foundation of China (No. 31670116), the Natural Science Foundation of Guangdong Province, China (2014A030313562), and Shenzhen Basic Research Projects (JCYJ20180507182405562).

ACKNOWLEDGMENTS

The authors gratefully acknowledge the support from the Instrumental Analysis Center of Shenzhen University (LiHu Campus). They would also like to thank TopEdit (www.topeditsci.com) for English language editing of this manuscript.

SUPPLEMENTARY MATERIAL

The Supplementary Material for this article can be found online at: https://www.frontiersin.org/articles/10.3389/fbioe.2021.652021/full#supplementary-material

REFERENCES

Afiukwa, C. A., and Ogbonna, J. C. (2007). Effects of mixed substrates on growth and vitamin production by *Euglena gracilis*. *Afr. J. Biotechnol.* 6:2613. doi: 10.4314/ajb.v6i22.58156

Arnon, D. I. (1949). Copper enzymes in isolated chloroplasts. Polyphenoloxidase in *Beta vulgaris*. *Plant Physiol.* 24, 1–15.

Bertoni, G., Gumina, C., Conigliaro, R., Ricci, E., Staffetti, J., Mortilla, M. G., et al. (1992). Randomized placebo-controlled trial of oral liquid simethicone prior to upper gastrointestinal endoscopy. *Endoscopy* 24, 268–270. doi: 10.1055/s-2007-1010479

Bölling, C., and Fiehn, O. (2005). Metabolite profiling of *Chlamydomonas reinhardtii* under nutrient deprivation. *Plant Physiol.* 139, 1995–2005. doi: 10.1104/pp.105.071589

Boncompagni, E., Dupont, L., Mignot, T., Østerås, M., Lambert, A., Poggi, M.-C., et al. (2000). Characterization of a Snorhizobium meliloti ATP-binding cassette histidine transporter also involved in betaine and proline uptake. *J. Bacteriol.* 182, 3717–3725. doi: 10.1128/JB.182.13.3717-3725.2000

Callery, P. S., Geelhaar, L. A., Nayar, M. S. B., Stogniew, M., and Rao, K. G. (1982). Pyrrolines as prodrugs of γ-aminobutyric acid analogues. *J. Neurochem.* 38, 1063–1067. doi: 10.1111/j.1471-4159.1982.tb05348.x

Cao, Z., Liu, B., Liu, W., Yao, G., Li, H., and Zou, T. (2011). Synthesis of 4-[4-(3-pyridinyl)imidazol-1-Yl]-1-butylamine. *J. Chem. Res.* 35, 600–601. doi: 10.3184/174751911X13176543106368

Cheah, W. Y., Show, P. L., Yap, Y. J., Zaid, H. F. M., Lam, M. K., Lim, J. W., et al. (2020). Enhancing microalga *Chlorella sorokiniana* CY-1 biomass and lipid production in palm oil mill effluent (POME) using novel-designed photobioreactor. *Bioengineered* 11, 61–69. doi: 10.1080/21655979.2019.1704536

Chen, X., Chen, T., Lin, Z., Li, X., Wu, W., and Li, J. (2014). Choline phosphate functionalized surface: protein-resistant but cell-adhesive zwitterionic surface potential for tissue engineering. *Chem. Commun.* 51, 487–490. doi: 10.1039/C4CC08681C

Cheng, S. Y., Show, P.-L., Lau, B. F., Chang, J.-S., and Ling, T. C. (2019). New prospects for modified algae in heavy metal adsorption. *Trends Biotechnol.* 37, 1255–1268. doi: 10.1016/j.tibtech.2019.04.007

Chew, K. W., Yap, J. Y., Show, P. L., Suan, N. H., Juan, J. C., Ling, T. C., et al. (2017). Microalgae biorefinery: high value products perspectives. *Bioresour. Technol.* 229, 53–62. doi: 10.1016/j.biortech.2017.01.006

Chia, S. R., Ong, H. C., Chew, K. W., Show, P. L., Phang, S.-M., Ling, T. C., et al. (2018). Sustainable approaches for algae utilisation in bioenergy production. *Renew. Energy* 129, 838–852. doi: 10.1016/j.renene.2017.04.001

Coburn, C. A., Holloway, M. K., and Stachel, S. J. (2011). *2-aminopyridine Compounds Useful as β-Secretase Inhibitors for the Treatment of Alzheimer's Disease. U.S. Patent No. 7,932,275*. Washington, DC: Patent and Trademark Office.

Courant, F., Martzolff, A., Rabin, G., Antignac, J.-P., Le Bizec, B., Giraudeau, P., et al. (2013). How metabolomics can contribute to bio-processes: a proof of concept study for biomarkers discovery in the context of nitrogen-starved

microalgae grown in photobioreactors. *Metabolomics* 9, 1286–1300. doi: 10.1007/s11306-013-0532-y

Dombchik, S. A. (1977). *Sulfophenyl-azo-Phenyl-azo-(4-Hydroxyalkoxyphenyl) Compounds. U.S. Patent No. 4,055,560*. Washington, DC: Patent and Trademark Office.

Doppler, M., Kluger, B., Bueschl, C., Schneider, C., Krska, R., Delcambre, S., et al. (2016). Stable isotope-assisted evaluation of different extraction solvents for untargeted metabolomics of plants. *Int. J. Mol. Sci.* 17:1017. doi: 10.3390/ijms17071017

Edmunds, L. N. (1966). Studies on synchronously dividing cultures of *Euglena gracilis* Klebs (strain Z). III. Circadian components of cell division. *J. Cell. Physiol.* 67, 35–43. doi: 10.1002/jcp.1040670105

Fagone, P., and Jackowski, S. (2013). Phosphatidylcholine and the CDP-choline cycle. *Biochim. Biophys. Acta* 1831, 523–532. doi: 10.1016/j.bbalip.2012.09.009

Fallet, C., Rohe, P., and Franco-Lara, E. (2010). Process optimization of the integrated synthesis and secretion of ectoine and hydroxyectoine under hyper/hypo-osmotic stress. *Biotechnol. Bioeng.* 107, 124–133. doi: 10.1002/bit.22750

Huo, S., Kong, M., Zhu, F., Qian, J., Huang, D., Chen, P., et al. (2020). Co-culture of *Chlorella* and wastewater-borne bacteria in vinegar production wastewater: enhancement of nutrients removal and influence of algal biomass generation. *Algal Res.* 45:101744. doi: 10.1016/j.algal.2019.101744

Jeon, M. S., Han, S.-I., Kim, J. Y., and Choi, Y.-E. (2020). Co-cultivation of *Euglena gracilis* and *Pseudoalteromonas* sp. MEBiC 03607 for paramylon production. *J. Appl. Phycol.* 32, 3679–3686. doi: 10.1007/s10811-020-02215-z

Jeon, M. S., Oh, J.-J., Kim, J. Y., Han, S.-I., Sim, S. J., and Choi, Y.-E. (2019). Enhancement of growth and paramylon production of *Euglena gracilis* by co-cultivation with *Pseudoalteromonas* sp. MEBiC 03485. *Bioresour. Technol.* 288:121513. doi: 10.1016/j.biortech.2019.121513

Kannan, S., Krishnamoorthy, G., Kulanthaiyesu, A., and Marudhamuthu, M. (2019). Effect of biosurfactant derived from *Vibrio natriegens* MK3 against *Vibrio harveyi* biofilm and virulence. *J. Basic Microbiol.* 59, 936–949. doi: 10.1002/jobm.201800706

Kim, J. Y., Oh, J.-J., Jeon, M. S., Kim, G.-H., and Choi, Y.-E. (2019). Improvement of *Euglena gracilis* paramylon production through a cocultivation strategy with the indole-3-acetic acid-producing bacterium *Vibrio natriegens*. *Appl. Environ. Microbiol.* 85:e1548–19. doi: 10.1128/AEM.01548-19

Kottuparambil, S., Thankamony, R. L., and Agusti, S. (2019). *Euglena* as a potential natural source of value-added metabolites. A review. *Algal Res.* 37, 154–159. doi: 10.1016/j.algal.2018.11.024

Kricka, L. J., and Vernon, J. M. (2011). Some derivatives of 2,5-Xylidine and their cyclization to Indoles. *Can. J. Chem.* 52, 299–302. doi: 10.1139/v74-048

Leyva, L. A., Bashan, Y., Mendoza, A., and de-Bashan, L. E. (2014). Accumulation fatty acids of in *Chlorella vulgaris* under heterotrophic conditions in relation to activity of acetyl-CoA carboxylase, temperature, and co-immobilization with *Azospirillum brasilense*. *Naturwissenschaften* 101, 819–830. doi: 10.1007/s00114-014-1223-x

Li, Z., and Vance, D. E. (2008). *Thematic review series: Glycerolipids*. Phosphatidylcholine and choline homeostasis. *J. Lipid Res.* 49, 1187–1194. doi: 10.1194/jlr.R700019-JLR200

Maehashi, K., Matsuzaki, M., Yamamoto, Y., and Udaka, S. (1999). Isolation of peptides from an enzymatic hydrolysate of food proteins and characterization of their taste properties. *Biosci. Biotechnol. Biochem.* 63, 555–559. doi: 10.1271/bbb.63.555

Mangalam, A., Poisson, L., Nemutlu, E., Datta, I., Denic, A., Dzeja, P., et al. (2013). Profile of circulatory metabolites in a relapsing-remitting animal model of multiple sclerosis using global metabolomics. *J. Clin. Cell. Immunol.* 4, 3–6. doi: 10.4172/2155-9899.1000150

Mookherjee, B. D., Trenkle, R. W., and Wilson, R. A. (1990). The chemistry of flowers, fruits and spices: live vs. dead, a new dimension in fragrance research. *Pure Appl. Chem.* 62, 1357–1364.

Nelson, R. R., Acree, T. E., Lee, C. Y., and Butts, R. M. (1977). Methyl anthranilate as an aroma constituent of American wine. *J. Food Sci.* 42, 57–59. doi: 10.1111/j.1365-2621.1977.tb01217.x

Nicholson, J. K., Lindon, J. C., and Holmes, E. (1999). "Metabonomics": understanding the metabolic responses of living systems to pathophysiological stimuli via multivariate statistical analysis of biological NMR spectroscopic data. *Xenobiotica* 29, 1181–1189. doi: 10.1080/004982599238047

Omidi, A., Esterhuizen-Londt, M., and Pflugmacher, S. (2019). Interspecies interactions between *Microcystis aeruginosa* PCC 7806 and *Desmodesmus subspicatus* SAG 86.81 in a co-cultivation system at various growth phases. *Environ. Int.* 131:105052. doi: 10.1016/j.envint.2019.105052

Paul, C., Mausz, M. A., and Pohnert, G. (2013). A co-culturing/metabolomics approach to investigate chemically mediated interactions of planktonic organisms reveals influence of bacteria on diatom metabolism. *Metabolomics* 9, 349–359. doi: 10.1007/s11306-012-0453-1

Pellicoro, C., Marsella, R., and Ahrens, K. (2013). Pilot study to evaluate the effect of topical dimethicone on clinical signs and skin barrier function in dogs with naturally occurring atopic dermatitis. *Vet. Med. Int.* 2013:e239186. doi: 10.1155/2013/239186

Periannan, A. (2003). Quantitative estimation of ebastine in formulations by HPTLC,jol. Planar chromatography. *JPC J. Planar Chromatogr. Mod. TLC* 2:16.

Pinheiro, H. A., Silva, J. V., Endres, L., Ferreira, V. M., Câmara, C., de, A., et al. (2008). Leaf gas exchange, chloroplastic pigments and dry matter accumulation in castor bean (*Ricinus communis L*) seedlings subjected to salt stress conditions. *Ind. Crops Prod.* 27, 385–392. doi: 10.1016/j.indcrop.2007.10.003

Pohl, A., Devaux, P. F., and Herrmann, A. (2005). Function of prokaryotic and eukaryotic ABC proteins in lipid transport. *Biochim. Biophys. Acta BBA Mol. Cell Biol. Lipids* 1733, 29–52. doi: 10.1016/j.bbalip.2004.12.007

Rajapitamahuni, S., Bachani, P., Sardar, R. K., and Mishra, S. (2019). Co-cultivation of siderophore-producing bacteria *Idiomarina loihiensis* RS14 with *Chlorella variabilis* ATCC 12198, evaluation of micro-algal growth, lipid, and protein content under iron starvation. *J. Appl. Phycol.* 31, 29–39. doi: 10.1007/s10811-018-1591-2

Rees, D. C., Johnson, E., and Lewinson, O. (2009). ABC transporters: the power to change. *Nat. Rev. Mol. Cell Biol.* 10, 218–227. doi: 10.1038/nrm2646

Richter, A. A., Mais, C.-N., Czech, L., Geyer, K., Hoeppner, A., Smits, S. H. J., et al. (2019). Biosynthesis of the stress-protectant and chemical chaperon ectoine: biochemistry of the transaminase EctB. *Front. Microbiol.* 10:2811. doi: 10.3389/fmicb.2019.02811

Shaul, O., and Galili, G. (1993). Concerted regulation of lysine and threonine synthesis in tobacco plants expressing bacterial feedback-insensitive aspartate kinase and dihydrodipicolinate synthase. *Plant Mol. Biol.* 23, 759–768. doi: 10.1007/BF00021531

Silverman, R. B., and Levy, M. A. (2002). Syntheses of (S)-5-substituted 4-aminopentanoic acids: a new class of gamma-aminobutyric acid transaminase inactivators. *J. Org. Chem.* 45, 815–818. doi: 10.1021/jo01293a011

Szczesiul, M., and Wampler, D. E. (2002). Regulation of a metabolic system *in vitro*: synthesis of threonine from aspartic acid. *Biochemistry* 15, 2236–2244. doi: 10.1021/bi00655a033

Takenaka, S., Kondo, T., Nazeri, S., Tamura, Y., Tokunaga, M., Tsuyama, S., et al. (1997). Accumulation of trehalose as a compatible solute under osmotic stress in *Euglena gracilis* Z. *J. Eukaryot. Microbiol.* 44, 609–613. doi: 10.1111/j.1550-7408.1997.tb05967.x

Taniguchi, M., and Tanaka, T. (2004). "Clarification of interactions among cicroorganisms and development of co-culture system for production of useful substances," in *Recent Progress of Biochemical and Biomedical Engineering in Japan I, Advances in Biochemical Engineering*, ed. T. Kobayashi (Berlin: Springer), 35–62. doi: 10.1007/b94191

Taupp, M., Harmsen, D., Heckel, F., and Schreier, P. (2005). Production of natural methyl anthranilate by microbial N-demethylation of N-methyl methyl anthranilate by the topsoil-isolated bacterium *Bacillus megaterium*. *J. Agric. Food Chem.* 53, 9586–9589. doi: 10.1021/jf0521395

Teixidó, N., Cañamás, T. P., Usall, J., Torres, R., Magan, N., and Viñas, I. (2005). Accumulation of the compatible solutes, glycine–betaine and ectoine, in osmotic stress adaptation and heat shock cross-protection in the biocontrol agent *Pantoea agglomerans* CPA-2. *Lett. Appl. Microbiol.* 41, 248–252. doi: 10.1111/j.1472-765X.2005.01757.x

Tocher, D. R. (1995). "Chapter 6 Glycerophospholipid metabolism," in *Biochemistry and Molecular Biology of Fishes* Metabolic Biochemistry, eds P. W. Hochachka and T. P. Mommsen (Amsterdam: Elsevier), 119–157. doi: 10.1016/S1873-0140(06)80009-3

Toyama, T., Hanaoka, T., Yamada, K., Suzuki, K., Tanaka, Y., Morikawa, M., et al. (2019). Enhanced production of biomass and lipids by *Euglena gracilis* via co-culturing with a microalga growth-promoting bacterium, *Emticicia* sp. EG3. *Biotechnol. Biofuels* 12:205. doi: 10.1186/s13068-019-1544-2

Vance, J. E., and Adeli, K. (2008). "Chapter 18 - Assembly and secretion of triacylglycerol-rich lipoproteins," in *Biochemistry of Lipids, Lipoproteins and Membranes*, Fifth Edn, eds D. E. Vance and J. E. Vance (San Diego: Elsevier), 507–531. doi: 10.1016/B978-044453219-0.50020-9

Vogt, S., Fuchs, K., and Richter, E. (2006). Genotoxic effects of myosmine in a human esophageal adenocarcinoma cell line. *Toxicology* 222, 71–79. doi: 10.1016/j.tox.2006.01.025

Wang, L., Huang, X., Lim, D. J., Laserna, A. K. C., and Li, S. F. Y. (2019). *Uptake and Toxic Effects of Triphenyl Phosphate on Freshwater Microalgae Chlorella Vulgaris* and *Scenedesmus Obliquus*: *Insights from untargeted metabolomics*. Available online at: https://pubag.nal.usda.gov/catalog/6131343 (accessed November 18, 2020).

Wang, Y., and Zhang, L. (2010). Ectoine improves yield of biodiesel catalyzed by immobilized lipase. *J. Mol. Catal. B Enzym.* 62, 90–95. doi: 10.1016/j.molcatb.2009.09.014

Weinstock, M. T., Hesek, E. D., Wilson, C. M., and Gibson, D. G. (2016). *Vibrio natriegens* as a fast-growing host for molecular biology. *Nat. Methods* 13, 849–851. doi: 10.1038/nmeth.3970

Zakryś, B., Milanowski, R., and Karnkowska, A. (2017). "Evolutionary origin of *Euglena*," in *Euglena: Biochemistry, Cell and Molecular Biology* Advances in Experimental Medicine and Biology, eds S. D. Schwartzbach and S. Shigeoka (Cham: Springer International Publishing), 3–17. doi: 10.1007/978-3-319-54910-1_1

Zhou, J., Lyu, Y., Richlen, M. L., Anderson, D. M., and Cai, Z. (2016). *Vibrio natriegens* as a fast-growing host for molecular biology. *Crit. Rev. Plant Sci.* 35, 81–105. doi: 10.1080/07352689.2016.1172461

Zwickenpflug, W., and Tyroller, S. (2006). Reaction of the tobacco alkaloid myosmine with hydrogen peroxide. *Chem. Res. Toxicol.* 19, 150–155. doi: 10.1021/tx0502802

Conflict of Interest: The authors declare that the research was conducted in the absence of any commercial or financial relationships that could be construed as a potential conflict of interest.

frontiers in Bioengineering and Biotechnology

ORIGINAL RESEARCH
published: 10 May 2021
doi: 10.3389/fbioe.2021.673402

Reciprocal Effect of Copper and Iron Regulation on the Proteome of *Synechocystis* sp. PCC 6803

*Zhang-He Zhen[1,2], Song Qin[1,3], Qing-Min Ren[1,2], Yu Wang[1], Yu-Ying Ma[1] and Yin-Chu Wang[1,3]**

[1] Yantai Institute of Coastal Zone Research, Chinese Academy of Sciences, Yantai, China, [2] University of Chinese Academy of Sciences, Beijing, China, [3] Center for Ocean Mega-Science, Chinese Academy of Sciences, Qingdao, China

Cyanobacteria can acclimate to changing copper and iron concentrations in the environment via metal homeostasis, but a general mechanism for interpreting their dynamic relationships is sparse. In this study, we assessed growth and chlorophyll fluorescence of *Synechocystis* sp. PCC 6803 and investigated proteomic responses to copper and iron deductions. Results showed that copper and iron exerted reciprocal effect on the growth and photosynthesis of *Synechocystis* sp. PCC 6803 at combinations of different concentrations. And some proteins involved in the uptake of copper and iron and the photosynthetic electron transport system exhibit Cu–Fe proteomic association. The protein abundance under copper and iron deduction affected the photosynthetic electronic activity of *Synechocystis* sp. PCC 6803 and eventually affected the growth and photosynthesis. Based on these results, we hypothesize that the Cu–Fe proteomic association of *Synechocystis* sp. PCC 6803 can be elucidated via the uptake system of outer membrane-periplasmic space-inner plasma membrane-thylakoid membrane, and this association is mainly required to maintain electron transfer. This study provides a broader view regarding the proteomic association between Cu and Fe in cyanobacteria, which will shed light on the role of these two metal elements in cyanobacterial energy metabolism and biomass accumulation.

Keywords: cyanobacteria, copper, iron, proteome, deduction

OPEN ACCESS

Edited by:
Changhong Yao,
Sichuan University, China

Reviewed by:
Jianfeng Yu,
Shenzhen University, China
Shengxi Shao,
Imperial College London, United Kingdom
Fudan Gao,
Shanghai Normal University, China

***Correspondence:**
Yin-Chu Wang
ycwang@yic.ac.cn

Specialty section:
This article was submitted to Bioprocess Engineering, a section of the journal Frontiers in Bioengineering and Biotechnology

Received: *27 February 2021*
Accepted: *14 April 2021*
Published: *10 May 2021*

Citation:
Zhen Z-H, Qin S, Ren Q-M, Wang Y, Ma Y-Y and Wang Y-C (2021) Reciprocal Effect of Copper and Iron Regulation on the Proteome of Synechocystis sp. PCC 6803. Front. Bioeng. Biotechnol. 9:673402. doi: 10.3389/fbioe.2021.673402

INTRODUCTION

Cyanobacterial metal homeostasis is important for the metal ion-driven photosynthetic machinery, rendering metals the limiting factors for cyanobacteria growth (Huertas et al., 2014; Chandra and Kang, 2016). Both copper and iron are essential metal elements for cyanobacteria. Iron, important trace metal element in the cyanobacterial thylakoid membrane (TM), has been shown to be involved in photosynthetic electron transfer, respiratory electron transfer, light-harvesting pigment synthesis, and various other important metabolic processes (Öquist, 1974; Sedwick et al., 1999). Copper is also an essential micronutrient that plays crucial roles in metal homeostasis and normal plant metabolism during photosynthesis and respiration (Yruela et al., 2000; Bernal et al., 2004).

The mechanism via which copper and iron functioned together has undergone environmental changes during the evolution of cyanobacteria. Notably after the Great Oxidation Event 2.35 billion years ago, the soluble copper content increased significantly, whereas the bioavailability of iron became limited in aquatic environments (Holland, 2002; Anbar et al., 2007). Therefore, cyanobacteria are believed to have gradually evolved different metal-binding proteins to acclimate to the changing environment, and some copper-containing proteins have functionally replaced iron-related proteins, reducing the effect of iron restriction on cell growth (De la Cerda et al., 2007). The appearance of plastocyanin in cyanobacteria probably conferred a selective advantage in iron-limited ecosystems, such as in more oxidizing environments, by releasing O_2 via oxygenic photosynthesis (Molina-Heredia et al., 2002; Peers and Price, 2006). These imply an evolutionary association between copper and iron in cyanobacteria.

Cyanobacteria have also developed physiological regulatory mechanisms to acclimate to environmental changes in copper and iron levels. Intracellular copper and iron content must be balanced via mechanisms depending on their aquatic bioavailability. These two essential metal elements work together in some processes. Copper metalloenzymes and iron metalloenzymes can participate in diverse cellular processes, such as energy transduction and oxidative stress response (Huertas et al., 2014), and sometimes Cu-binding and Fe-binding proteins can function interchangeably. For instance, it is well known that the iron-binding cytochrome c_6 (Cyt c_6) replaces the copper-binding plastocyanin in the absence of copper (Molina-Heredia et al., 2002). In addition, iron and copper act synergistically have unraveled the relationship between iron and copper homeostasis in cyanobacteria (Nicolaisen et al., 2010). On one hand, a cuproenzyme is involved in iron mobilization (Rensing and Grass, 2003; Rademacher and Masepohl, 2012; Huertas et al., 2014). On the other hand, the periplasmic iron-binding protein, FutA2, is related to copper import in *Synechocystis* sp. PCC 6803 (hereinafter *Synechocystis* 6803) (Waldron et al., 2007); a TonB-dependent iron transporter (*iacT*, All4026), located at the outer membrane (OM), affected the rate of copper transport (Nicolaisen et al., 2010). Overall, several studies have elucidated that copper and iron function together and compensate for each other's levels in cyanobacteria.

Currently, reports regarding Cu–Fe association and its association mechanism are scarce. In mutant strains of *Anabaena* sp. PCC 7120, Nicolaisen et al. (2010) observed that the iron and copper content is affected by the TonB-dependent iron transporter, which revealed the intracellular homeostasis of copper and iron, although the specific mechanism via which homeostasis is maintained has not been reported. In addition, using proteomics, Castielli et al. (2009) analyzed the protein associations during copper and iron deduction in *Synechocystis* 6803 and confirmed the substitution reaction of Plastocyanin and Cytochrome *c* on the electron transfer chain; however, they did not comprehensively analyze other copper-related and iron-related proteins. Therefore, a general mechanism for interpreting their dynamic relationships is sparse, especially when one or both are limited or lacking. Fortunately, many detailed reports regarding the effects of individual iron or copper deduction stress on cyanobacteria are now available. On one hand, many studies regarding cyanobacterial iron deduction stress have showed that iron deficiency can induce remodulation of photosystem complexes (Michel and Pistorius, 2004; Latifi et al., 2005; Allen et al., 2008), and that the expression of iron stress-induced chlorophyll binding protein A (IsiA) (Burnap et al., 1993), iron transporters (Shcolnick et al., 2009), and alternative redox vectors were up-regulated (Wood, 1978; Sandmann, 1985). On the other hand, copper deduction has been shown to reduce synthesis of plastoquinone and disintegration of thylakoid membranes (Hutber et al., 1977; Guikema and Sherman, 1983; Ivanov et al., 2000; Sandström et al., 2002), and upregulate proteins involved in the main metabolic pathways, such as C and N fixation and carbohydrate metabolism (Angeleri et al., 2019). Based on the extensive influence of iron and copper on cell metabolism (Meisch and Bielig, 1975; Verma and Singh, 1990; Shavyrina et al., 2001; Pehlivan, 2018), we speculated that the association of Cu–Fe-related proteins may not only be limited to the electron transport chain, but may have a broader physiological impact to cyanobacteria.

In this study, the growth pattern of *Synechocystis* 6803 in response to the given copper-iron combination was examined, then followed by comparative proteomic analyses to reveal the proteins associated with copper and iron stress. We anticipate that our study would provide a theoretical basis for understanding the relationship between copper and iron in cyanobacteria at the protein level and shed light on the role of these two metal elements in energy metabolism and biomass accumulation of cyanobacteria.

MATERIALS AND METHODS

Metal-Deduction Treatments and Growth Curve Measurements

To deplete the stored copper and iron in the cells to meet the set concentration gradients, the *Synechocystis* 6803 were cultured in BG11 medium (with copper sulfate and ferric ammonium citrate removed from the normal recipe) lacking Fe and Cu for 5 days under normal conditions as mentioned below: light intensity = 50 μmol photons m^{-2} s^{-1}, light/dark period = 12 h/12 h, and supply of filtered air bubbled at 30°C (Rippka et al., 1979; Singh et al., 2003; Georg et al., 2017). The method of determining the abundance of copper and iron refers to other reports (Varga et al., 1999; Li et al., 2011).

To determine the optimum iron and copper concentrations for the growth of *Synechocystis* 6803, the strain was transferred to normal BG11 medium supplemented with 25 different combinations of copper and iron concentrations for acclimatation and maintained in exponential growth phase for 3 days in advance. Copper and iron concentrations were set to form a 5 × 5 matrix: copper C1−C5 (0, 112.5, 225, 337.5, and 450 nM) and iron F1−F5 (0, 6.25, 12.5, 18.75, and 25 μM). The matrix covers the optimal Cu/Fe concentration combination for *Synechocystis* growth via beforehand repeated exploratory experiments. The copper concentrations were set

below the copper toxic concentration (0.5 μM) to *Synechocystis* 6803 (Cheloni et al., 2019). And the iron concentrations were set to coordinate with the copper conditions to balance the coverage and precision. The Cu/Fe concentrations of the 25 cultures and their designations were based on the combinations of the two series. For instance, group C2F4 contained 112.5 nM copper (C2) and 18.75 μM iron (F4). Then, cultures were diluted to equal cell densities [OD_{730} = 0.04 in a 96-well plate (200 μL) using a microplate reader] and were transferred to new medium (with no change in Cu/Fe concentrations and incubation conditions). Finally, the cell densities were measured after every 24 h in a 96-well plate (200 μl) using a microplate reader (Shanpu SuPerMax 3100, Shanghai, China) (the standard curve of optical densities measured with the microplate reader and normal spectrophotometer at 730 nm of *Synechocystis* 6803 was shown in **Supplementary Figure 1**). Three replicates were performed for each group.

Chlorophyll Fluorescence Measurements

Chlorophyll fluorescence of the 25 cultures (each group with three replicates) were measured using Diving-PAM (WALZ, Germany) to analyze how Cu/Fe concentrations affected photosynthesis in the strain. During logarithmic growth phase (120 h), cultures were acclimated in dark for at least 15 min, and F_o, F_m, F_m parameters were measured under actinic light (50 μmol photons m^{-2} s^{-1}) after applying a saturating pulse (3,577 μmol photons m^{-2} s^{-1}, 800 ms) (Xu et al., 2012). The maximum quantum yield of PSII (F_v/F_m), the actual effective quantum yield of PSII [Y(II)], and the relative electron transfer rate (rETR) were calculated according to Maxwell (Maxwell and Johnson, 2000).

Protein Extraction and TMT Tagging

With the fastest growing cultures (the F4C4 group, see section "Physiological response to copper and iron deduction" in Result) set as the control group, the Fe-deduction group (i.e., F1C4), Cu-deduction group (i.e., F4C1), and Cu–Fe dual deduction group (i.e., F1C1) were set as the experimental groups. Three replicates were performed for each group. These cultures have the same culture conditions and growth status as the cultures used for growth curve measurement and were investigated using TMT quantitative proteomics to determine the effect of Cu/Fe deductions on *Synechocystis* 6803 protein levels. Cells in logarithmic growth phase were collected for proteomic determination after 120 h of metal-deduction.

Proteins were extracted from cyanobacteria using the SDT [4% w/v sodium dodecul sulfate (SDS), 100 mM Tris/HCl pH 7.6, 0.1 M dithiothreitol (DTT)] cleavage method (Wiśniewski et al., 2009), and total protein levels were quantified using the bicinchoninic acid assay (BCA) method. Each sample was trypsinized using the filter-aided proteome preparation (FASP) method and the peptides were quantified (OD_{280}) (Wiśniewski et al., 2009). The peptides (100 μg) of each sample were labeled according to the instructions of the TMT labeling kit (Thermo, United States).

LC MS/MS Data Collection and Analysis

The TMT-labeled peptides of each group were mixed in equal amounts and fractionated using the high pH reverse phase peptide fractionation kit (Thermo, United States). Each fractionated sample was separated using high performance liquid chromatography (HPLC) (Thermo scientific, United States). Buffer A consisted of 0.1% formic acid solution and buffer B contained 0.1% formic acid-84% acetonitrile solution. The column was equilibrated with 95% buffer A. Samples were separated using a loading column (nanoViper C18, Thermo Scientific Acclaim PepMap100, 100 μm × 2 cm) and an analytical column (Thermo Scientific EASY column, 10 cm, ID75 μm, 3 μm, C18-A2). The flow rate was set to 300 nL/min.

The separated samples were analyzed using Q-Exactive MS under positive ion mode. The scanning range of the precursor ion was 300−1800 *m/z*, AGC (automatic gain control) target was 1×10^{-6}, maximum IT was 50 ms, and dynamic exclusion time was 60.0 s. Several 20 fragment maps (MS2 scan, MS2 activation type: HCD) were collected after each full scan. The isolation window was set to 2 *m/z*. Normalized collision energy was 30 eV and underfill was 0.1%.

The MS data was identified and quantitatively analyzed using Mascot ver. 2.2 (Matrix Science) and Proteome Discoverer 1.4 (Thermo, United States). The maximum missed cleavage was set to 2; peptide mass tolerance and fragment mass tolerance was set to ±20 ppm and 0.1 Da, respectively. Peptide false discovery rate (FDR) was set at < 0.01. Protein quantification was performed based on the median of only the unique peptides of the protein. The mass spectrometry proteomics data have been deposited to the ProteomeXchange Consortium via the PRIDE (Perez-Riverol et al., 2019) partner repository with the dataset identifier PXD024873."

Data Analysis

SPSS ver. 19.0 was used to perform parametric one-way analysis of variance (ANOVA) for analyzing the differences in the growth rate, F_v/F_m, Y(II), and rETR values of the cultures among different groups.

Differentially expressed proteins were filtered using a fold change ≥ 1.2 and ≤ 0.83, and P-value < 0.05 (paired t-test or one-way ANOVA) (Cox and Mann, 2008). Blast2GO ver. 5.2 (BioBam, Spain) was used to annotate Gene Ontology (GO) function entries for all identified proteins, and Kyoto Encyclopedia of Genes and Genomes (KEGG) Automatic Annotation Server (KAAS) was used to allocate the differentially expressed proteins to the biological pathways. GO function and each KEGG pathway protein were analyzed for the significance of enrichment using Fisher's exact test.

The paired t-tests were performed on the corrected ratios (the intensity of the fragmented tag in a sample to the intensity of the fragmented tag in the control sample) to identify the proteins and their proteomic associations after Fe or Cu deductions. The Cochran–Mantel–Haenszel tests for repeated 2 × 2 tests of independence were performed to identify the proteins under the conditional association of copper and iron (Rayner and Rippon, 2018). All tests were performed and verified using SPSS ver. 19.0.

RESULTS

Physiological Response to Copper and Iron Deduction

The growth rates of 25 groups of *Synechocystis* 6803 under different culture conditions in terms of combinations of copper and iron concentrations were continuously monitored for 7 days (**Figure 1**). As shown in **Figure 1**, the increase of iron concentration from F1 to F5 tends to promote cell growth (**Figures 1A–E**), and the growth rates of F1 groups were significantly lower ($P < 0.05$). The change of copper concentrations has little effect on cell growth rate in the F1–F5 series, but the change of copper concentration affected the optimal iron concentration for growth. The fastest growth rate was observed in the F4C4 group (OD_{730} = 0.404), followed by that in the F5C3 group (OD_{730} = 0.393) (**Figure 1F**).

As shown in **Figure 2**, three parameters related to chlorophyll fluorescence were measured: F_v/F_m (the maximum quantum yield of PSII), Y(II) (the actual effective quantum yield of PSII) and rETR (the relative electron transfer rate). In the C1−C3 series, the fluorescence parameters increased with Fe concentrations (from F1 to F5 series) and peaked in the F5 group. However, for C4 and C5 series, the highest value was not observed in the F5 group. The maximum values of rETR and Y(II) were observed in the F4C4 group, while the maximum value of F_v/F_m was observed in the F5C3 group.

General Proteomic Analyses

The effects of copper deduction, iron deduction, and copper-iron deduction on the protein profile of *Synechocystis* 6803 were investigated using TMT quantitative proteomics technology. In total, 1,555 proteins were identified based on 8350 peptides and 8197 unique peptides identified in *Synechocystis* 6803; proteins with expression ≥ 1.2 times or ≤0.83 times that of the control and p-value < 0.05 were considered significant.

Venn diagrams show (**Figures 3A,B**) that the number of differentially expressed proteins induced by dual deduction of copper and iron was the largest (up, 329; down, 367), followed by those induced by iron deduction (up, 262; down, 324), while copper deduction induced the least number of differentially expressed proteins (up, 143; down 204).

The GO functional analysis of all the differentially expressed proteins yielded 139 GO functional annotation entries ($P < 0.05$) in the Fe-deduction group, 52 GO functional annotation entries ($P < 0.05$) in the Cu-deduction group and 87 GO functional annotation entries ($P < 0.05$) in the Cu, Fe dual deduction group. These proteins were further categorized into three groups: biological processes, cellular components, and molecular functions based on functional differences. **Table 1** lists the first eight groups of most significant annotations. Some photosynthesis-related and non-photosynthesis-related differentially expressed proteins present in these annotations have been listed in **Supplementary Tables 1**, **2**, respectively.

In all three deduction groups, various cellular components of the thylakoid and photosynthetic membrane changed significantly. For example, the significantly down-regulated proteins ($P < 0.05$) included the chloroplast import-associated channel IAP75, membrane protein PilM and membrane-associated protein Slr1513, while the significantly up-regulated proteins included cyanobacterial orthologs of chloroplast proteins Ycf35 and Ycf23 ($P < 0.05$) (**Supplementary Table 2**); Photosynthesis was the most predominant biological process (BP) under all three conditions (**Table 1**), and various proteins involved in photosynthesis were significantly down-regulated, including photosynthesis assembly proteins (Slr0147, Slr0149, and Slr0151) and proteins related to phycobilisomes, PSII, PSI, Cytochrome b_6/f complex, photosynthetic electron transporter, and ATP synthase (**Supplementary Table 1**).

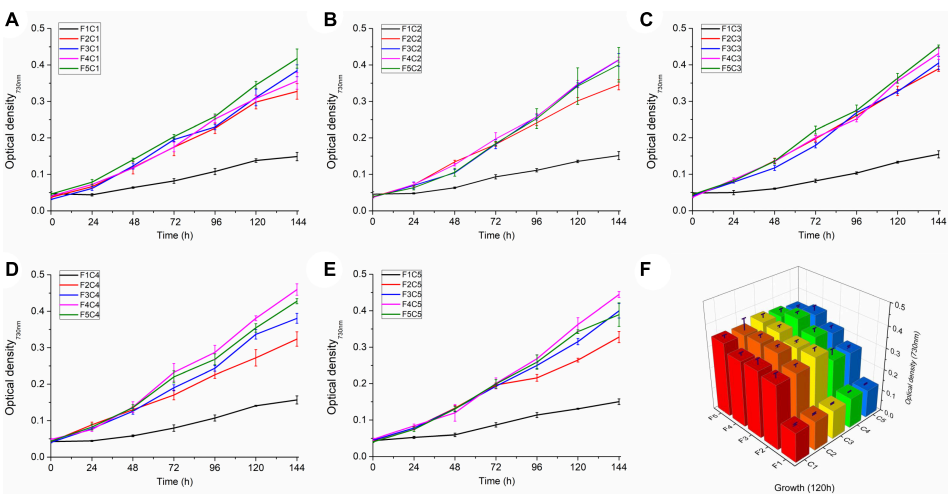

FIGURE 1 | Growth of *Synechocystis* sp. PCC 6803 under different Cu and Fe concentrations. **(A–E)** The growth curve of *Synechocystis* sp. PCC 6803 in the presence of different combinations of copper and iron concentrations; **(F)** Growth of *Synechocystis* sp. PCC 6803 at 120 h. C1∼C5 indicate Cu concentrations of 0, 112.5, 225, 337.5, and 450 nM, respectively; F1∼F5 indicate Fe concentrations of 0, 6.25, 12.5, 18.75, and 25 μM, respectively.

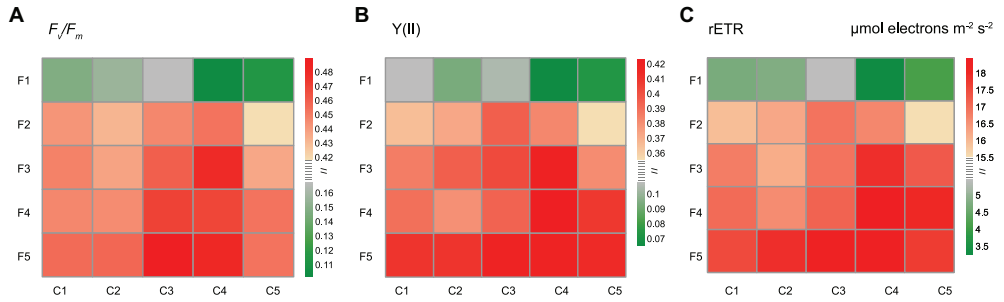

FIGURE 2 | Effects of different copper and iron concentrations on the chlorophyll fluorescence of *Synechocystis* sp. PCC 6803. **(A)** F_v/F_m (the maximum quantum yield of PSII); **(B)** Y(II) (the actual effective quantum yield of PSII); **(C)** rETR (the relative electron transfer rate).

However, individual proteins were up-regulated in response to certain conditions. For example, Cytochrome c_6 (18.06-fold) and Plastocyanin (1.44-fold) were significantly up-regulated in the Cu-deduction and Fe-deduction groups, respectively. Psb28 (Fe-deduction group: 1.54-fold; Cu–Fe dual deduction group: 2.51-fold) and IsiA (Fe-deduction group: 4.41-fold; Cu-Fe dual deduction group: 4.52-fold) were only up-regulated in response to iron deduction, but did not respond significantly to copper deduction. In addition, protein metabolism was one of the significantly enriched biological processes in the Fe-deduction group (**Supplementary Table 1**). Various ribosome-related proteins participated in this process (**Supplementary Table 2**), most of which were significantly down-regulated and few were significantly up-regulated. In the Cu-deduction group carbohydrate transport, lipid catabolic process, and organic substance transport ($P < 0.05$) were the significantly affected biological processes, which affected the expression of several metabolic enzymes, such as carbohydrate metabolizing enzymes, including ATP-dependent 6-phosphofructokinase (2.27-fold), Alpha-1,4 glucan phosphorylase (1.32-fold), and Aconitate hydratase B (1.59-fold), and various other carbon or nitrogen metabolism-associated proteins, including Biotin carboxylase (2.07-fold), Nitrate reductase (2.01-fold), Aminopeptidase (1.69-fold), Ribose phosphate isomerase B (1.46-fold), Glucose-6-phosphate 1-dehydrogenase (1.31-fold), and Glutamine synthetase (1.24-fold) (**Supplementary Table 2**). The molecular functions differed significantly in these three experimental groups (**Table 1**). Iron deduction and copper deduction alone affected electron transfer activity; however, in the group of Cu, Fe dual-deduction, the main molecular functions affected included structural molecule activity and structural constituent of ribosome (**Table 1**).

KEGG analysis of differentially expressed proteins showed that these proteins were mainly concentrated in the four signaling pathways of photosynthesis, photosynthetic-antenna proteins, ribosomes, and the cell cycle under the three deduction conditions (**Figure 3C**). Photosynthesis and photosynthetic-antenna proteins were highly enriched ($P < 0.01$) in the Cu-deduction and Fe-deduction groups ($P < 0.01$), while ribosomal proteins were highly enriched ($P < 0.01$) in the Cu, Fe dual deduction group, in addition to photosynthetic proteins. Furthermore, the cell cycle signaling pathway was also significantly enriched in the Fe-deduction group ($P < 0.05$) (**Figure 3C**).

Cu–Fe Proteomic Associations

Cochran–Mantel–Haenszel tests were performed to analyze whether protein expression was affected by the copper-iron reciprocal effect. We observed that the expression of ten proteins showed significant copper-iron proteomic association ($P < 0.05$) (**Table 2**), among which five were porins, two were iron transporters, and the remaining three were photosynthetic electron transport-related proteins.

The expression of five putative porins, namely, Slr1841, Slr1908, Slr0042, Sll1550, and Sll1271, mainly involved in ion transport (Qiu et al., 2018), showed significant copper-iron proteomic associations ($P < 0.05$) (**Table 2**). Among them, Slr1841, Slr1908, and Slr0042 were significantly down-regulated under copper as well as iron deduction conditions (**Supplementary Table 2**). However, Sll1550 was only significantly down-regulated under copper deduction (Cu-deduction group: 0.75-fold; Cu, Fe-dual deduction group: 0.68-fold), whereas Sll1271 was not significantly down-regulated under copper deduction and iron deduction conditions (**Supplementary Table 2**).

The expression of iron uptake-related proteins, ferrichrome-iron receptor (FhuA) and iron uptake protein A2 (FutA2) showed significant Cu–Fe proteomic association ($P < 0.05$) (**Table 2**). FhuA is a TonB-dependent OM transporter for iron that can incorporate iron from the extracellular environment and transport them to the periplasmic space (PP). The expression of FhuA in the was significantly up-regulated by 5.86-fold, 1.9-fold, and 6.8-fold in the Fe-deduction group, Cu-deduction group, and Cu, Fe-dual deduction group, respectively (**Supplementary Table 2**). FutA2 is a periplasmic water-soluble iron importer, which was significantly up-regulated under iron deduction or copper deduction conditions (3.81-fold up-regulation upon Fe deduction, 1.69-fold upon Cu deduction, and 4.18-fold upon Cu, Fe-dual deduction; **Supplementary Table 2**).

In addition, the expression of proteins related to photosynthetic electron transport, namely, PsbU (Photosystem II 12 kDa extrinsic protein), PsbQ, and Flavodoxin, also showed copper-iron correlation ($P < 0.05$) (**Table 2**). Among them, only PsbU was differentially expressed under iron deduction

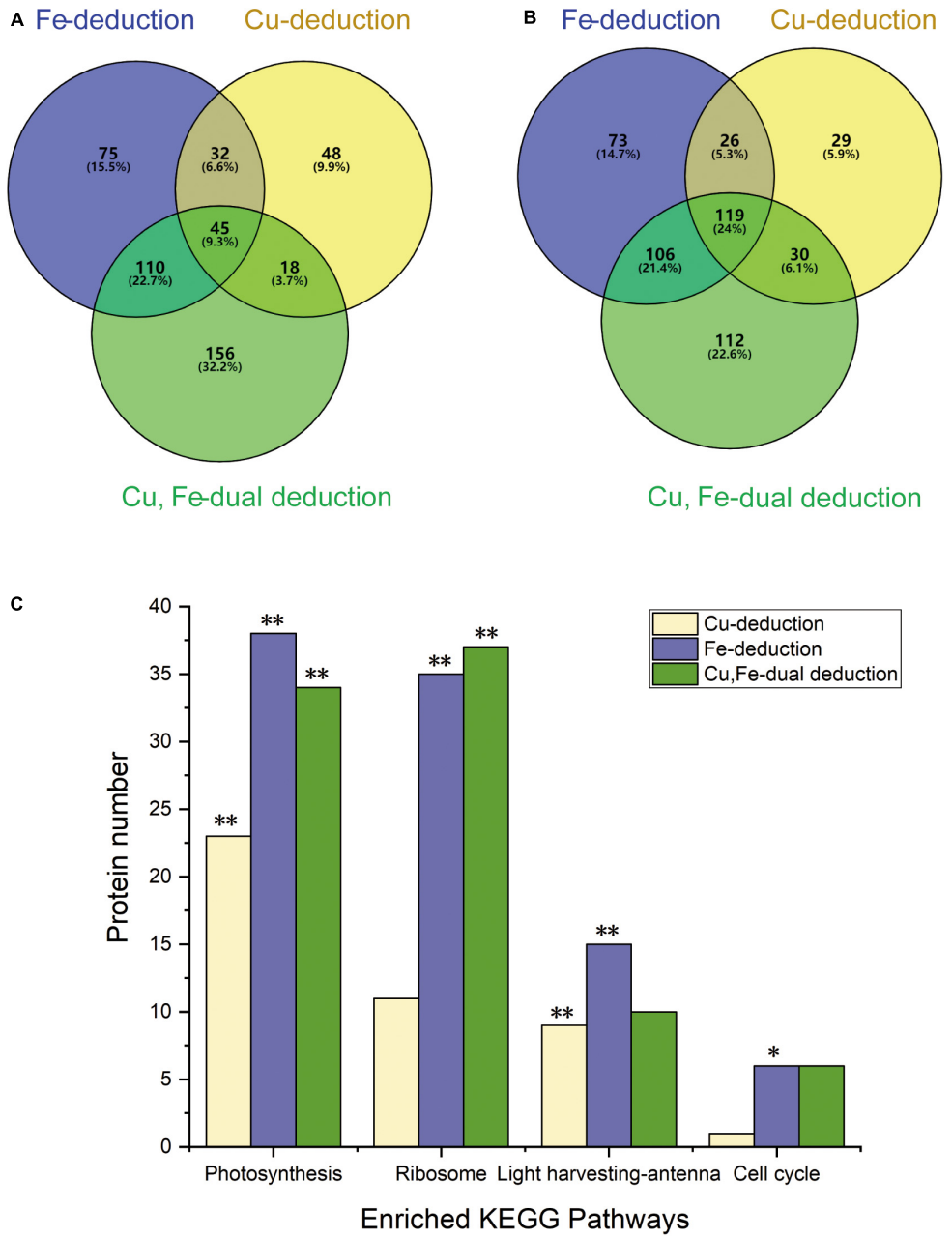

FIGURE 3 | Venn diagrams showing differential protein abundances and enriched KEGG pathways. **(A)** Up-regulated proteins (≥1.2-fold); **(B)** down-regulated proteins (≤0.83-fold); **(C)** $^{**}P < 0.01$, $^{*}P < 0.05$.

(Fe-deduction group: 0.53-fold; Cu–Fe dual deduction group: 0.4-fold), while no significant differential expression was observed under copper deduction (**Supplementary Table 1**). PsbQ was significantly down-regulated under these three deduction conditions; it was down-regulated by 0.41-fold in the Fe-deduction group, by 0.81-fold in the Cu-deduction group, and by 0.71-fold in the Cu-Fe dual deduction group (**Supplementary Table 1**). The expression of the electron carrier, Flavodoxin, was significantly up-regulated in response to copper deduction or iron deduction (Fe-deduction group: 4.29-fold; Cu-deduction group: 2.14-fold; Cu, Fe-dual deduction group: 7.51-fold) ($P < 0.05$) (**Supplementary Table 2**).

DISCUSSION

Growth, Photosynthesis, and Cu–Fe Association

The copper or iron deduction affects growth of *Synechocystis* 6803. As shown in **Figure 1**, iron played a crucial role in

TABLE 1 | Enriched Gene Ontology (GO) term.

Condition	Go Term	Protein number	*P*-value	Category
Fe-deduction	Photosynthetic membrane	72	2.57E-13	CC
	Thylakoid part	74	3.43E-13	CC
	Thylakoid	75	3.91E-13	CC
	Thylakoid membrane	67	3.88E-12	CC
	Protein-containing complex	111	6.01E-12	CC
	Organelle part	55	4.3E-11	CC
	Membrane protein complex	57	1.5E-10	CC
	Light-harvesting complex	19	9.56E-09	CC
	Photosynthesis	58	1.85E-09	BP
	Protein-chromophore linkage	15	4.99E-06	BP
	Cellular protein metabolic process	72	0.000443	BP
	Protein metabolic process	78	0.000815	BP
	Electron transport chain	16	0.000999	BP
	Establishment of protein localization	18	0.001214	BP
	Protein localization	18	0.001214	BP
	Macromolecule localization	18	0.001214	BP
	Electron transfer activity	25	3.95E-06	MF
	Tetrapyrrole binding	18	9.64E-05	MF
	Structural constituent of ribosome	35	0.000153	MF
	Structural molecule activity	36	0.000249	MF
	Heme binding	11	0.000797	MF
	rRNA binding	24	0.000804	MF
	ATP-dependent peptidase activity	8	0.008742	MF
	Chlorophyll binding	6	0.014444	MF
Cu-deduction	Cell envelope	38	3.37E-09	CC
	Envelope	38	4.26E-08	CC
	Periplasmic space	35	5.6E-08	CC
	Outer membrane-bounded periplasmic space	33	2.1E-07	CC
	Thylakoid	45	8.89E-07	CC
	Thylakoid part	43	3.76E-06	CC
	Membrane	101	8.04E-06	CC
	Photosynthetic membrane	40	2.19E-05	CC
	Protein-chromophore linkage	11	9.73E-05	BP
	Photosynthesis	33	0.000223	BP
	Carbohydrate transport	5	0.007985	BP
	Lipid catabolic process	3	0.011425	BP
	Organic substance transport	14	0.014585	BP
	Localization	25	0.018939	BP
	Transport	24	0.021303	BP
	Establishment of localization	24	0.021303	BP
	Electron transfer activity	14	0.005798	MF
	Siderophore transmembrane transporter activity	3	0.011425	MF
	Siderophore uptake transmembrane transporter activity	3	0.011425	MF
	Cofactor transmembrane transporter activity	3	0.011425	MF
	Wide pore channel activity	5	0.017382	MF
	Porin activity	5	0.017382	MF
	Tetrapyrrole binding	10	0.020033	MF
	Iron ion binding	10	0.020033	MF
Cu, Fe-dual deduction	Cell envelope	56	1.34E-09	CC
	Envelope	59	1.61E-09	CC

(Continued)

TABLE 1 | Continued

Condition	Go Term	Protein number	*P*-value	Category
	Periplasmic space	53	8.23E-09	CC
	Outer membrane-bounded periplasmic space	51	1.01E-08	CC
	Protein-containing complex	112	6.48E-07	CC
	Thylakoid membrane	63	3.37E-06	CC
	Photosynthetic membrane	66	4.8E-06	CC
	Thylakoid	69	6.53E-06	CC
	Photosynthesis	55	6.47E-05	BP
	Protein metabolic process	91	0.000299	BP
	Cellular protein metabolic process	81	0.00092	BP
	Peptide metabolic process	59	0.001128	BP
	Translation	56	0.001475	BP
	Peptide biosynthetic process	56	0.001475	BP
	Carbohydrate transport	7	0.003874	BP
	Homeostatic process	18	0.00607	BP
	Structural molecule activity	40	0.000329	MF
	Structural constituent of ribosome	38	0.000453	MF
	Porin activity	8	0.001747	MF
	Wide pore channel activity	8	0.001747	MF
	ATP-dependent peptidase activity	9	0.004681	MF
	Iron ion binding	17	0.004966	MF
	Electron transfer activity	22	0.00597	MF
	Enzyme binding	6	0.008584	MF

BP, biological process; MF, molecular function; CC, cellular component.

the growth of *Synechocystis* 6803, which has been confirmed previously (Odom et al., 1993). This might be due to iron which is an important cofactor in photosynthesis, such as cytochrome *c6* in the electron transport chain and Fe/S cluster proteins in PSI (Geider and La Roche, 1994). Therefore, severe iron deficiency affected photosynthesis. Copper also plays an important role in the growth of cyanobacteria, and studies have found that severe copper deficiency affects the growth of cyanobacteria (Manahan and Smith, 1973; Sandmann and Böger, 1980). In this study, strict copper starvation was not pursued and different levels of copper deduction were used to testify the effect of small-amount changes of copper on *Synechocystis* physiology. Result indicated that the effect was weak in the presence of increased iron. One of the most remarkable roles of copper affecting on cyanobacterial growth is as the binding metal element of plastocyanin participating in electron transfer. When copper is deficient, the iron-binding protein cytochrome *c6* can be functionally replaced with plastocyanin, which alleviates the impact of copper deprivation on cells (Peers and Price, 2006).

In the measurement of the growth curve, the most important finding is that the growth of Synechocystis 6803 shows Cu-Fe association, for example, among F4 condition (iron concentration: 18.75 μM), cells have the best growth rate among C4 condition (copper concentration: 337.5 nM); while among F5 condition (iron concentration: 25 μM), cells have the best growth rate among C3 condition (copper concentration: 225 nM) (**Figure 1**). The effect of copper and iron on cyanobacterial growth is consistent with previous reports (Sandmann and Malkin, 1983; Ivanov et al., 2000).

The copper or iron deduction affects the photosynthesis of *Synechocystis* 6803. Y(II) reflects the actual photosynthetic efficiency of PSII, and rETR reflects the relative electron transfer rate of PSII, both of which are related to the activity of linear electron transfer (Genty et al., 1989; Krause and Weis, 1991; Maxwell and Johnson, 2000), thereby showing the Cu–Fe reciprocal effect. For example, when the copper concentration was increased from C3 to C4, the optimal iron concentration of the two parameters decreased from F5 to F4 (**Figures 2B,C**). However, the maximum value of F_v/F_m, reflecting the potential photosynthetic activity of the five copper concentrations, was observed in the F5 series, indicating that F_v/F_m of these Synechocystis 6803 is mainly affected by the iron concentration owing to the wide-ranging influence of iron on the photosynthetic system (**Figure 2A**; Hopkinson et al., 2007). These results are consistent with previous reports (Abdel-Ghany and Pilon, 2008; Fraser et al., 2013; Georg et al., 2017).

The effect of copper and iron deduction on the growth of Synechocystis 6803 will directly affect the biomass accumulation, and the effect on photosynthesis will affect a series of metabolic processes including carbohydrate metabolism, lipid catabolic process and protein metabolism (detailed description in "General proteomic analyses").

Electron Transport Chain-Related Proteins and Cu–Fe Proteomic Association

Analyzing the Cu–Fe proteome association will help explain the physiologically Cu–Fe association of *Synechocystis* 6803. The

results of proteomic analysis (**Table 2**) showed that the expression of Flavodoxin, PsbU, and PsbQ, proteins related to the electron transport chain, showed significant Cu–Fe proteomic association. This may be due to the fact that electron transport in the electron transport chain is performed by Plastocyanin and/or Cytochrome *c* which containing essential Cu or Fe element respectively (Wood, 1978; Ullmann and Kostic, 1995; Cao et al., 2020), hence, some related proteins and physiological reactions (detailed discussion in section "Growth, photosynthesis, and Cu-Fe association"), such as PsbU and PsbQ, showed Cu–Fe proteome association. PsbU and PsbQ, located upstream of the electron transport chain, can protect the electron-donating Mn_4CaO_5 cluster (Mummadisetti et al., 2014; Kim and Debus, 2019). Flavodoxins, as electron transfer proteins located downstream of the electron transport chain (Sancho, 2006), can be induced by iron or copper deduction and also showed a significant Cu–Fe proteomic association (**Table 1**; Inda and Peleato, 2002). This may be a feedback regulation of cells to metal deduction.

The influence of copper or iron deduction on the electron transport chain will further affect the expression of a series of proteins involved in photosynthetic electron transport. On one hand, all proteins related to the photosynthetic system show differential expression, including various subunits of PSII, PSI, and the Cytochrome b_6f complex (**Supplementary Table 1**). On the other hand, changes in PSII leads to down-regulation of phycobilisome-related protein expression (**Supplementary Table 1**). These changes are consistent with previous reports (Allen et al., 2008; Rochaix, 2011; Georg et al., 2017; Angeleri et al., 2019). In addition, the influence of copper or iron limitation on electron transfer will affect the formation of electrochemical gradients of protons inside and outside the TM, which in turn affects the synthesis of ATP by ATP synthase (Ferguson and Sorgato, 1982; Van Walraven et al., 1985; Narayan et al., 2011). The lack of ATP synthesis will trigger a series of differential expression of ATP-dependent proteins and related metabolic changes, including those of ribosomal proteins, various tRNA enzymes, and many other proteins, which are in agreements with the results of protein differential expression identified in this study (**Supplementary Table 2**) and other reports (Allen et al., 2008; Georg et al., 2017; Angeleri et al., 2019).

Copper and Iron Uptake System and Cu–Fe Proteomic Association

Seven proteins related to copper and iron uptake, distributed in OM, PP, and TM, also showed significant Cu–Fe proteomic association (**Table 2**), except for the three TM proteins in the electron transport chain. Therefore, significant Cu–Fe proteomic association may also exist during the uptake of copper and iron from OM to PP and that this association was maintained during the transport of copper and iron through IM and TM.

Copper and iron were supposed mainly carried out from OM to PP in two ways. On the one hand, the OM porins of cyanobacteria promote the passive uptake of iron (Nikaido, 2003; Qiu et al., 2018) and may also be related to copper transfer (Speer et al., 2013; Stewart et al., 2019). On the other hand, copper and iron can also be actively transported to the PP via some transporters on the OM, including the TonB-dependence transporter (TBDT) and ABC transporter (Schöffler and Braum, 1989; Köster, 2001; Yue et al., 2003).

TABLE 2 | Reciprocal effect of copper and iron on protein expression.

Protein	Gene	*P*-value
Slr1908	*slr1908*	0.00005
Slr1841	*slr1841*	0.00011
Flavodoxin	*isiB*	0.00017
Photosystem II 12 kDa extrinsic protein	*psbU*	0.00613
Slr0042	*slr0042*	0.01004
Sll1271	*sll1271*	0.01076
Iron uptake protein A2	*futA2*	0.01795
Sll1638	*psbQ*	0.01902
Sll1550	*sll1550*	0.03325
Ferrichrome-iron receptor	*fhuA*	0.03342

We observed that porins Slr1841, Slr1908, and Slr0042 were significantly down-regulated under copper deduction and iron deduction conditions; Sll1550 was only significantly down-regulated under copper deduction conditions, while Sll1271 was not significantly down-regulated under copper deduction and iron deduction conditions (**Supplementary Table 2**). This is consistent with previous results regarding copper- or iron-related stress (Kowata et al., 2017; Angeleri et al., 2019; Kojima and Okumura, 2020). Studies have shown that the deletion of Sll0772, Sll1271, Sll1550, and Slr0042 retarded the growth of Synechocystis 6803 in iron-deficient media (Qiu et al., 2018), suggesting that these porins are associated with iron uptake. Based on this and combined with the Cu–Fe proteomic association results of this study (**Table 1**), we speculated that the porins, Slr1841, Slr1908, and Slr0042, may be involved in the uptake of copper and iron from the extracellular environment and their transport to the periplasm, while Sll1550 is only related to copper uptake. Reports show that expression of Sll1550 is induced in the knock outs of its homologs, Slr1908 or Slr1841 (Kowata et al., 2017; Kojima and Okumura, 2020). This suggests that these porins coordinate with each other during copper or iron uptake and possibly maintain the normal transport of iron or the dynamic balance between copper and iron uptake. A significant Cu–Fe reciprocal effect on the expression of Sll1271 was observed (**Table 1**), although it was not significantly down-regulated under copper or iron deduction conditions. Currently, reports regarding the function of Sll1271 are limited.

In addition to porins, iron or copper can also be actively transported to the periplasm via certain transporters. At present, reports regarding copper OM transfer proteins are limited; however, several iron OM transporters have been discovered, such as iron ABC transporter-FutA1, TonB-dependence transporter-FhuA1, and iron uptake transporter-IutA (Hantke and Braun, 1975; Moeck et al., 1997; Ferguson et al., 1998; Pawelek et al., 2006). Although whether FhuA can directly transport copper is not known, we observed that FhuA1 can respond to copper deduction (up 1.9-fold) or iron deduction (up 5.86-fold) via differential expression

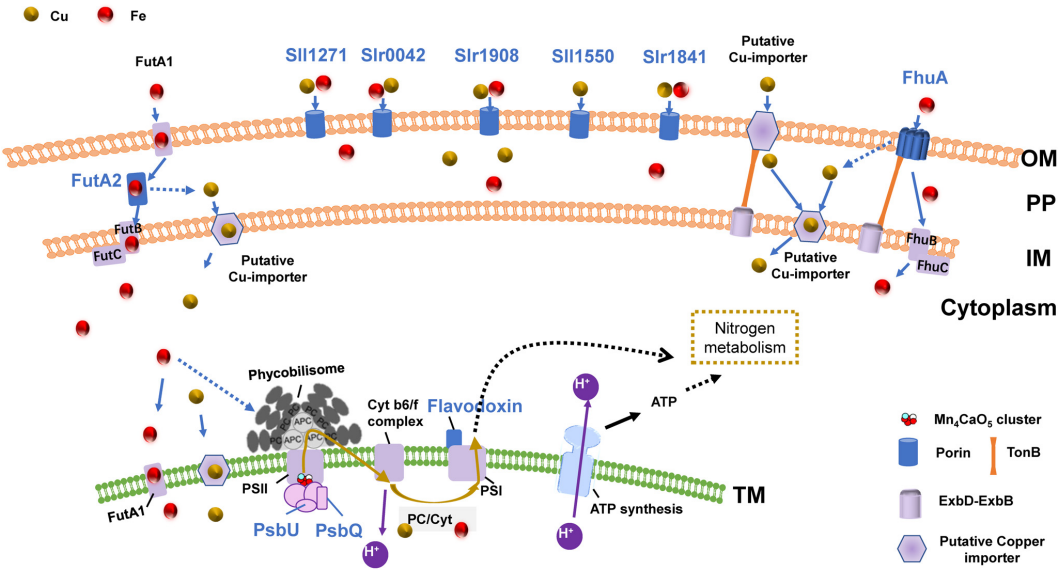

FIGURE 4 | The OM-PP-IM-TM Cu–Fe uptake system and photosynthetic electron transport chain. Proteins shown in blue: the protein expression shows significant Cu–Fe proteomic association; Solid arrow: direct influence; Dashed arrow: indirect influence.

(**Supplementary Table 2**) and significantly responds to the Cu–Fe reciprocal effect (**Table 1**). Similarly, the TonB-dependent iron transporter, -IacT, in *Anabaena* can also be significantly up-regulated in response to copper deduction (Nicolaisen et al., 2010). We speculated that the up-regulation of these two TonB-dependent iron transporters under copper deduction conditions may be related to TonB (Nicolaisen et al., 2010), as well as other related periplasmic proteins.

Recent studies have shown that after copper and iron are incorporated from the extracellular environment to the periplasmic space, some periplasmic transporters play important roles in maintaining the balance of copper and iron uptake. For example, the periplasmic protein FutA2 can not only participate in the uptake of Fe^{3+}, but also plays a vital role in copper uptake (Badarau et al., 2008). Absence of FutA2 will lead to insufficient copper supply in the thylakoid cavity, as FutA2 can restrict the abnormal binding of Fe^{3+} to important binding sites of copper by isolating Fe^{3+}, thereby indirectly assisting in passage of copper from the periplasm through the inner plasma membrane (IM) and TM to the thylakoid cavity. This explains our observation that FutA2 can be significantly up-regulated in response to copper or iron deduction and shows a Cu-Fe proteomic association (**Table 1** and **Supplementary Table 2**), which is reflected in the connection between the TM and OM-PP-IM.

In summary, these Cu–Fe associated proteins play important role in the process of copper and iron uptake from OM to PP and then through IM and TM. Previous studies have only reported Cu–Fe association of individual proteins, and have not been linked to other Cu–Fe associated uptake proteins (Hantke and Braun, 1975; Moeck et al., 1997; Ferguson et al., 1998; Pawelek et al., 2006; Badarau et al., 2008; Speer et al., 2013; Stewart et al., 2019). However, we conducted a systematic analysis of these Cu–Fe associated proteins. And we think that there is a Cu–Fe proteomic association in the process of Synechocystis 6803 uptake of copper and iron from the extracellular environment to the thylakoid cavity via the OM-PP-IM-TM uptake system.

Cu–Fe Proteomic Association With a Hypothetical Uptake System

Based on the above results regarding growth, chlorophyll fluorescence, and expression of certain proteins, as well as the important roles of copper and iron in the photosynthetic electron transport chain, we proposed a hypothesis (**Figure 4**): during copper or iron deduction, Synechocystis 6803 responds to and regulates intracellular copper and iron content via an OM-PP-IM-TM Cu-Fe uptake system to maintain copper and iron homeostasis. The response of this Cu–Fe uptake system continues to affect the photosynthetic electron transport chain, which ultimately affects photosynthesis and inhibits cell growth. This feedback regulation mechanism involves association within the Cu–Fe proteome, which is mainly affected by the Cu–Fe supply of the electron transport chain.

The proposed role of the OM-PP-IM-TM uptake system is supported by numerous evidences regarding membrane connectivity. For example, structural biology evidences have identified a thylakoid convergence region inside the cytoplasmic membrane, which proves that there may be a certain degree of membrane structural continuity between the thylakoid cavity, periplasmic and extracellular environment (Liu and Zhang, 2019; Rast et al., 2019). Studies have also shown that the absence of OM porins such as Slr0042, Slr1841, and Slr1908 induces the release of functional proteins in the thylakoid cavity, including Plastocyanin, Cytochrome *c*, PsbU, and other photosynthetic electron transport-related proteins (Kojima and Okumura, 2020).

This may be related to the connectivity of the membrane system, which will affect the electron transport chain.

The connectivity of the OM-PP-IM-TM membrane system suggests that the copper–iron transport is not limited to a single protein, but is possibly a consequence of the coordination of the entire copper–iron uptake system and the photosynthetic electron transport chain; for example, the synergy between active absorption and diffusion absorption in the OM (Qiu et al., 2018), and the functions of periplasmic proteins during the transfer of copper and iron from the periplasm into the membrane might be coordinated.

However, only few reports on copper uptake and copper-iron homeostasis are currently available, hence, the following questions have not been resolved: (1) what is the specific mechanism underlying the differential expression of several porins in response to copper and iron deduction? (2) can porins directly transport copper or iron? (3) how does the iron TonB-dependent transporter affect copper uptake? We look forward to verification of the hypothesis to address these questions, which needs a lot of future work.

CONCLUSION

Our research shows that the growth of Synechocystis 6803 was restricted during copper or iron deduction and was exhibited a Cu–Fe reciprocal effect under different copper and iron culture concentrations. Similarly, the data of chlorophyll fluorescence parameter Y(II) and rETR related to linear electron transfer activity also showed a Cu–Fe reciprocal effect. The proteomics results revealed that the three proteins (Flavodoxin, PsbU, and PsbQ) related to the electron transport chain showed significant Cu–Fe proteomic association. And many proteins involved in photosynthetic electron transport are also significantly differentially expressed, which will affect the photosynthetic metabolism and in turn affect other energy metabolism, such as carbohydrate metabolism, lipid catabolic process, and protein metabolism. In addition, the Cu–Fe proteomic association of Synechocystis 6803 is also manifested in the process of copper and iron uptake, which involves five porins (Slr1841, Slr1908, Slr0042, Sll1550, and Sll1271) and two iron transporters (FhuA and FutA2).

The above results reveal that in order to meet the intracellular requirements of copper or iron under deduction conditions, especially for the electron transport chain, these metals can be transferred into the cell via the uptake system (the OM-PP-IM-TM uptake system). Due to the functional substitution of copper-binding protein and iron-binding protein in the electron transport chain, some proteins involved in electron transport showed significant Cu-Fe proteomic association. In addition, the effect of copper and/or iron deduction on the photosynthetic electron transport chain will further affect the growth of *Synechocystis* 6803, and show a significant Cu-Fe association. Our research provides a theoretical basis for the regulatory link between copper and iron homeostasis in cyanobacteria, which will clarify the role of these two metal elements in cyanobacterial energy metabolism and biomass accumulation.

DATA AVAILABILITY STATEMENT

The data presented in the study are deposited in the ProteomeXchange repository, accession number PXD024873.

AUTHOR CONTRIBUTIONS

Y-CW and SQ had completed the experimental design and financial support. Q-MR, YW, and Y-YM had completed the data analysis. Z-HZ had completed the all experiments and thesis writing. All the authors read and approved the final manuscript.

FUNDING

This work was supported by the National Key Research and Development Program (2018YFA0903000) and the National Natural Science Foundation of China (42006111).

ACKNOWLEDGMENTS

We thank Prof. Yulin Cui, Wenjun Li, and Jialin Li from Yantai Institute of Coastal Zone Research, Chinese Academy of Sciences for their suggestions on experimental technique. We also thank Dr. Haonan Wang from Ocean University of China for his comments on writing.

SUPPLEMENTARY MATERIAL

The Supplementary Material for this article can be found online at: https://www.frontiersin.org/articles/10.3389/fbioe.2021.673402/full#supplementary-material

REFERENCES

Abdel-Ghany, S. E., and Pilon, M. (2008). MicroRna-mediated systemic down-regulation of copper protein expression in response to low copper availability in *Arabidopsis*. *J. Biol. Chem.* 283, 15932–15945. doi: 10.1074/jbc.M801406200

Allen, A. E., LaRoche, J., Maheswari, U., Lommer, M., Schauer, N., Lopez, P. J., et al. (2008). Whole-cell response of the pennate diatom *Phaeodactylum tricornutum* to iron starvation. *Proc. Natl. Acad. Sci. U S A.* 105, 10438–10443. doi: 10.1073/pnas.0711370105

Anbar, A. D., Duan, Y., Lyons, T. W., Arnold, G. L., Kendall, B., Creaser, R. A., et al. (2007). A whiff of oxygen before the great oxidation event? *Science* 317, 1903–1906. doi: 10.1126/science.1140325

Angeleri, M., Muth-Pawlak, D., Wilde, A., Aro, E. M., and Battchikova, N. (2019). Global proteome response of synechocystis 6803 to extreme copper

environments applied to control the activity of the inducible petJ promoter. *J. Appl. Microbiol.* 126, 826–841. doi: 10.1111/jam.14182

Badarau, A., Firbank, S. J., Waldron, K. J., Yanagisawa, S., Robinson, N. J., Banfield, M. J., et al. (2008). FutA2 is a ferric binding protein from synechocystis PCC 6803. *J. Biol. Chem.* 283, 12520–12527. doi: 10.1074/jbc.M709907200

Bernal, M., Roncel, M., Ortega, J. M., Picorel, R., and Yruela, I. (2004). Copper effect on cytochrome b559 of photosystem II under photoinhibitory conditions. *Physiol. Plant.* 120, 686–694. doi: 10.1111/j.1399-3054.2004.0286.x

Burnap, R. L., Troyan, T., and Sherman, L. A. (1993). The highly abundant chlorophyll-protein complex of iron-deficient *Synechococcus sp*. PCC7942 (CP43 [prime]) is encoded by the isiA gene. *Plant Physiol.* 103, 893–902. doi: 10.1104/pp.103.3.893

Cao, P., Cao, D., Si, L., Su, X., Tian, L., Chang, W., et al. (2020). Structural basis for energy and electron transfer of the photosystem I–IsiA–flavodoxin supercomplex. *Nat. Plants* 6, 167–176. doi: 10.1038/s41477-020-0593-7

Castielli, O., De la Cerda, B., Navarro, J. A., Hervás, M., and De la Rosa, M. A. (2009). Proteomic analyses of the response of cyanobacteria to different stress conditions. *FEBS Lett.* 583, 1753–1758. doi: 10.1016/j.febslet.2009.03.069

Chandra, R., and Kang, H. (2016). Mixed heavy metal stress on photosynthesis, transpiration rate, and chlorophyll content in poplar hybrids. *Forest Sci. Technol.* 12, 55–61. doi: 10.1080/21580103.2015.1044024

Cheloni, G., Gagnaux, V., and Slaveykova, V. I. (2019). Species-species interactions modulate copper toxicity under different visible light conditions. *Ecotox. Environ. Safe* 170, 771–777. doi: 10.1016/j.ecoenv.2018.12.039

Cox, J., and Mann, M. (2008). MaxQuant enables high peptide identification rates, individualized ppb-range mass accuracies and proteome-wide protein quantification. *Nat. Biotechnol.* 26, 1367–1372. doi: 10.1038/nbt.1511

De la Cerda, B., Castielli, O., Durán, R. V., Navarro, J. A., Hervás, M., and De la Rosa, M. A. (2007). A proteomic approach to iron and copper homeostasis in cyanobacteria. *Brief. Funct. Genom. Proteom.* 6, 322–329. doi: 10.1093/bfgp/elm030

Ferguson, A. D., Hofmann, E., Coulton, J. W., Diederichs, K., and Welte, W. (1998). Siderophore-Mediated iron transport: crystal structure of FhuA with bound lipopolysaccharide. *Science* 282, 2215–2220. doi: 10.1126/science.282.5397.2215

Ferguson, S. J., and Sorgato, M. C. (1982). Proton electrochemical gradients and energy-transduction processes. *Annu. Rev. Biochem.* 51, 185–217. doi: 10.1146/annurev.bi.51.070182.001153

Fraser, J. M., Tulk, S. E., Jeans, J. A., Campbell, D. A., Bibby, T. S., and Cockshutt, A. M. (2013). Photophysiological and photosynthetic complex changes during iron starvation in *Synechocystis sp*. PCC 6803 and *Synechococcus elongatus* PCC 7942. *PLoS One* 8:e59861. doi: 10.1371/journal.pone.0059861

Geider, R. J., and La Roche, J. (1994). The role of iron in phytoplankton photosynthesis, and the potential for iron-limitation of primary productivity in the sea. *Photosynth Res.* 39, 275–301. doi: 10.1007/BF00014588

Genty, B., Briantais, J.-M., and Baker, N. R. (1989). The relationship between the quantum yield of photosynthetic electron transport and quenching of chlorophyll fluorescence. *Biochimica et Biophysica Acta (BBA)-General Subjects* 990, 87–92. doi: 10.1016/S0304-4165(89)80016-9

Georg, J., Kostova, G., Vuorijoki, L., Schön, V., Kadowaki, T., Huokko, T., et al. (2017). Acclimation of oxygenic photosynthesis to iron starvation is controlled by the sRNA IsaR1. *Curr. Biol.* 27, 1425–1436. doi: 10.1016/j.cub.2017.04.010

Guikema, J. A., and Sherman, L. A. (1983). Organization and function of chlorophyll in membranes of cyanobacteria during iron starvation. *Plant Physiol.* 73, 250–256. doi: 10.1104/pp.73.2.250

Hantke, K., and Braun, V. (1975). Membrane receptor dependent iron transport in *Escherichia coli*. *FEBS Lett.* 49, 301–305. doi: 10.1016/0014-5793(75)80771-X

Holland, H. D. (2002). Volcanic gases, black smokers, and the great oxidation event. *Geochimica et Cosmochimica Acta* 66, 3811–3826. doi: 10.1016/S0016-7037(02)00950-X

Hopkinson, B. M., Mitchell, B. G., Reynolds, R. A., Wang, H., Selph, K. E., Measures, C. I., et al. (2007). Iron limitation across chlorophyll gradients in the southern drake passage: phytoplankton responses to iron addition and photosynthetic indicators of iron stress. *Limnol. Oceanography* 52, 2540–2554. doi: 10.4319/lo.2007.52.6.2540

Huertas, M. J., Lopez-Maury, L., Giner-Lamia, J., Sanchez-Riego, A. M., and Florencio, F. J. (2014). Metals in cyanobacteria: analysis of the copper, nickel, cobalt and arsenic homeostasis mechanisms. *Life (Basel)* 4, 865–886. doi: 10.3390/life4040865

Hutber, G., Hutson, K., and Rogers, L. (1977). Effect of iron dificiency on levels of two ferredoxins and flavodoxin in a cyanobacterium. *FEMS Microbiol. Lett.* 1, 193–196. doi: 10.1111/j.1574-6968.1977.tb00612.x

Inda, L. A., and Peleato, M. L. (2002). Immunoquantification of flavodoxin and ferredoxin from *Scenedesmus vacuolatus* (Chlorophyta) as iron-stress molecular markers. *Eur. J. Phycol.* 37, 579–586. doi: 10.1017/S0967026202003864

Ivanov, A., Park, Y.-I., Miskiewicz, E., Raven, J., Huner, N., and Öquist, G. (2000). Iron stress restricts photosynthetic intersystem electron transport in *Synechococcus sp*. PCC 7942. *FEBS Lett.* 485, 173–177. doi: 10.1016/S0014-5793(00)02211-0

Kim, C. J., and Debus, R. J. (2019). One of the substrate waters for O2 formation in photosystem II is provided by the water-splitting Mn4CaO5 cluster's Ca2+ Ion. *Biochemistry* 58, 3185–3192. doi: 10.1021/acs.biochem.9b00418

Kojima, S., and Okumura, Y. (2020). Outer membrane-deprived cyanobacteria liberate periplasmic and thylakoid luminal components that support the growth of heterotrophs. *bioRxiv [preprint]* doi: 10.1101/2020.03.24.006684

Köster, W. (2001). ABC transporter-mediated uptake of iron, siderophores, heme and vitamin B12. *Res. Microbiol.* 152, 291–301. doi: 10.1016/S0923-2508(01)01200-1

Kowata, H., Tochigi, S., Takahashi, H., and Kojima, S. (2017). Outer membrane permeability of cyanobacterium *Synechocystis sp*. strain PCC 6803: studies of passive diffusion of small organic nutrients reveal the absence of classical porins and intrinsically low permeability. *J. Bacteriol.* 199:e00371-17. doi: 10.1128/JB.00371-17

Krause, G., and Weis, E. (1991). Chlorophyll fluorescence and photosynthesis: the basics. *Annu. Rev. Plant Biol.* 42, 313–349. doi: 10.1146/annurev.pp.42.060191.001525

Latifi, A., Jeanjean, R., Lemeille, S., Havaux, M., and Zhang, C.-C. (2005). Iron starvation leads to oxidative stress in *Anabaena sp*. strain PCC 7120. *J. Bacteriol.* 187, 6596–6598. doi: 10.1128/JB.187.18.6596-6598.2005

Li, S.-X., Lin, L.-X., Zheng, F.-Y., and Wang, Q.-X. (2011). Metal bioavailability and risk assessment from edible brown alga *Laminaria japonica*, using biomimetic digestion and absorption system and determination by ICP-MS. *J. Agric. Food Chem.* 59, 822–828. doi: 10.1021/jf103480y

Liu, L.-N., and Zhang, Y.-Z. (2019). Cryoelectron microscopy delineates the in situ structure of the thylakoid network. *Mol. Plant* 12, 1176–1178. doi: 10.1016/j.molp.2019.07.005

Manahan, S. E., and Smith, M. J. (1973). Copper micronutrient requirement for algae. *Environ. Sci. Technol.* 7, 829–833. doi: 10.1021/es60081a013

Maxwell, K., and Johnson, G. N. (2000). Chlorophyll fluorescence—a practical guide. *J. Exp. Bot.* 51, 659–668. doi: 10.1093/jexbot/51.345.659

Meisch, H.-U., and Bielig, H.-J. (1975). Effect of vanadium on growth, chlorophyll formation and iron metabolism in unicellular green algae. *Arch. Microbiol.* 105, 77–82. doi: 10.1007/BF00447117

Michel, K. P., and Pistorius, E. K. (2004). Adaptation of the photosynthetic electron transport chain in cyanobacteria to iron deficiency: the function of IdiA and IsiA. *Physiol. Plant.* 120, 36–50. doi: 10.1111/j.0031-9317.2004.0229.x

Moeck, G. S., Coulton, J. W., and Postle, K. (1997). Cell envelope signaling in *Escherichia coli* ligand binding to the ferrichrome-iron receptor FhuA promotes interaction with the energy-transducing protein TonB. *J. Biol. Chem.* 272, 28391–28397. doi: 10.1074/jbc.272.45.28391

Molina-Heredia, F. P., Balme, A., Hervás, M., Navarro, J. A., and De la Rosa, M. A. (2002). A comparative structural and functional analysis of cytochrome c M, cytochrome c 6 and plastocyanin from the cyanobacterium *Synechocystis sp*. PCC 6803. *FEBS Lett.* 517, 50–54. doi: 10.1016/S0014-5793(02)02576-0

Mummadisetti, M. P., Frankel, L. K., Bellamy, H. D., Sallans, L., Goettert, J. S., Brylinski, M., et al. (2014). Use of protein cross-linking and radiolytic footprinting to elucidate PsbP and PsbQ interactions within higher plant Photosystem II. *Proc. Natl. Acad. Sci. U S A.* 111, 16178–16183. doi: 10.1073/pnas.1415165111

Narayan, O. P., Kumari, N., and Rai, L. C. (2011). Iron starvation-induced proteomic changes in *Anabaena (Nostoc) sp*. PCC 7120: exploring survival strategy. *J. Microbiol. Biotechnol.* 21, 136–146. doi: 10.4014/jmb.1009.09021

Nicolaisen, K., Hahn, A., Valdebenito, M., Moslavac, S., Samborski, A., Maldener, I., et al. (2010). The interplay between siderophore secretion and coupled iron and copper transport in the heterocyst-forming cyanobacterium *Anabaena sp*. PCC

7120. *Biochimica et Biophysica Acta (BBA)-Biomembranes* 1798, 2131–2140. doi: 10.1016/j.bbamem.2010.07.008

Nikaido, H. (2003). Molecular basis of bacterial outer membrane permeability revisited. *Microbiol. Mol. Biol. Rev.* 67, 593–656. doi: 10.1128/MMBR.67.4.593-656.2003

Odom, W. R., Hodges, R., Chitnis, P. R., and Guikema, J. A. (1993). Characterization of *Synechocystis sp*. PCC 6803 in iron-supplied and iron-deficient media. *Plant Mol. Biol.* 23, 1255–1264. doi: 10.1007/BF00042358

Öquist, G. (1974). Iron deficiency in the blue-green alga *Anacystis nidulans*: changes in pigmentation and photosynthesis. *Physiol. Plant.* 30, 30–37. doi: 10.1111/j.1399-3054.1974.tb04987.x

Pawelek, P. D., Croteau, N., Ng-Thow-Hing, C., Khursigara, C. M., Moiseeva, N., Allaire, M., et al. (2006). Structure of TonB in complex with FhuA. *E. coli* outer membrane receptor. *Science* 312, 1399–1402. doi: 10.1126/science.1128057

Peers, G., and Price, N. M. (2006). Copper-containing plastocyanin used for electron transport by an oceanic diatom. *Nature* 441, 341–344. doi: 10.1038/nature04630

Pehlivan, A. (2018). *Iron Acquisition in Cynobacteria Synechococcus sp. PCC 7002 Culture*. Høgskoleringen: NTNU.

Perez-Riverol, Y., Csordas, A., Bai, J., Bernal-Llinares, M., Hewapathirana, S., Kundu, D. J., et al. (2019). The PRIDE database and related tools and resources in 2019: improving support for quantification data. *Nucleic Acids Res.* 47, D442–D450. doi: 10.1093/nar/gky1106

Qiu, G.-W., Lou, W.-J., Sun, C.-Y., Yang, N., Li, Z.-K., Li, D.-L., et al. (2018). Outer membrane iron uptake pathways in the model cyanobacterium *Synechocystis sp*. strain PCC 6803. *Appl. Environ. Microbiol.* 84, e1512–e1518. doi: 10.1128/AEM.01512-18

Rademacher, C., and Masepohl, B. (2012). Copper-responsive gene regulation in bacteria. *Microbiology* 158, 2451–2464. doi: 10.1099/mic.0.058487-0

Rast, A., Schaffer, M., Albert, S., Wan, W., Pfeffer, S., Beck, F., et al. (2019). Biogenic regions of cyanobacterial thylakoids form contact sites with the plasma membrane. *Nat. Plants* 5, 436–446. doi: 10.1038/s41477-019-0399-7

Rayner, J., and Rippon, P. (2018). Recent extensions to the cochran–mantel–haenszel tests. *Stats* 1, 98–111. doi: 10.3390/stats1010008

Rensing, C., and Grass, G. (2003). *Escherichia coli* mechanisms of copper homeostasis in a changing environment. *FEMS Microbiol. Rev.* 27, 197–213. doi: 10.1016/S0168-6445(03)00049-4

Rippka, R., Deruelles, J., Waterbury, J. B., Herdman, M., and Stanier, R. Y. (1979). Generic assignments, strain histories and properties of pure cultures of cyanobacteria. *Microbiology* 111, 1–61. doi: 10.1099/00221287-111-1-1

Rochaix, J.-D. (2011). Assembly of the photosynthetic apparatus. *Plant Physiol.* 155, 1493–1500. doi: 10.1104/pp.110.169839

Sancho, J. (2006). Flavodoxins: sequence, folding, binding, function and beyond. *Cell. Mol. Life Sci. CMLS* 63, 855–864. doi: 10.1007/s00018-005-5514-4

Sandmann, G. (1985). Consequences of iron deficiency on photosynthetic and respiratory electron transport in blue-green algae. *Photosynthesis Res.* 6, 261–271. doi: 10.1007/BF00049282

Sandmann, G., and Böger, P. (1980). Copper deficiency and toxicity in scenedesmus. *Zeitschrift Für Pflanzenphysiologie* 98, 53–59. doi: 10.1016/S0044-328X(80)80219-4

Sandmann, G., and Malkin, R. (1983). Iron-sulfur centers and activities of the photosynthetic electron transport chain in iron-deficient cultures of the blue-green alga *Aphanocapsa*. *Plant Physiol.* 73, 724–728. doi: 10.1104/pp.73.3.724

Sandström, S., Ivanov, A. G., Park, Y. I., Öquist, G., and Gustafsson, P. (2002). Iron stress responses in the cyanobacterium *Synechococcus sp*. PCC7942. *Physiol. Plantarum* 116, 255–263. doi: 10.1034/j.1399-3054.2002.1160216.x

Schöffler, H., and Braum, V. (1989). Transport across the outer membrane of *Escherichia coli* K12 via the FhuA receptor is regulated by the TonB protein of the cytoplasmic membrane. *Mol. General Genet. MGG* 217, 378–383. doi: 10.1007/BF02464907

Sedwick, P. N., DiTullio, G. R., Hutchins, D. A., Boyd, P. W., Griffiths, F. B., Crossley, A. C., et al. (1999). Limitation of algal growth by iron deficiency in the Australian subantarctic region. *Geophys. Res. Lett.* 26, 2865–2868. doi: 10.1029/1998GL002284

Shavyrina, O., Gapochka, L., and Azovskii, A. (2001). Development of tolerance for copper in cyanobacteria repeatedly exposed to its toxic effect. *Biol. Bull. Russ. Acad. Sci.* 28, 183–187. doi: 10.1023/A:1009423201364

Shcolnick, S., Summerfield, T. C., Reytman, L., Sherman, L. A., and Keren, N. (2009). The mechanism of iron homeostasis in the unicellular cyanobacterium *Synechocystis sp*. PCC 6803 and its relationship to oxidative stress. *Plant Physiol.* 150, 2045–2056. doi: 10.1104/pp.109.141853

Singh, A. K., McIntyre, L. M., and Sherman, L. A. (2003). Microarray analysis of the genome-wide response to iron deficiency and iron reconstitution in the cyanobacterium *Synechocystis sp*. PCC 6803. *Plant Physiol.* 132, 1825–1839. doi: 10.1104/pp.103.024018

Speer, A., Rowland, J. L., Haeili, M., Niederweis, M., and Wolschendorf, F. (2013). Porins increase copper susceptibility of *Mycobacterium tuberculosis*. *J. Bacteriol.* 195, 5133–5140. doi: 10.1128/JB.00763-13

Stewart, L. J., Thaqi, D., Kobe, B., McEwan, A. G., Waldron, K. J., and Djoko, K. Y. (2019). Handling of nutrient copper in the bacterial envelope. *Metallomics : Integrated Biometal Sci.* 11, 50–63. doi: 10.1039/c8mt00218e

Ullmann, G. M., and Kostic, N. M. (1995). Electron-tunneling paths in various electrostatic complexes between cytochrome c and plastocyanin. anisotropy of the copper-ligand interactions and dependence of the iron-copper electronic coupling on the metalloprotein orientation. *J. Am. Chem. Soc.* 117, 4766–4774. doi: 10.1021/ja00122a005

Van Walraven, H., Hagendoorn, M., Krab, K., Haak, N., and Kraayenhof, R. (1985). ATP synthesis by ATPase proteoliposomes from the thermophilic cyanobacterium *Synechococcus* 6716 by ionophore-induced electric potentials and proton gradients. *Biochimica et Biophysica Acta (BBA)-Bioenergetics* 809, 236–244. doi: 10.1016/0005-2728(85)90067-2

Varga, I., Rierpl, E., and Tusai, A. (1999). Comparison of slurry preparation and microwave digestion of freshwater algae for multi-element analysis by total reflection X-ray fluorescence spectrometry. *J. Anal. Atomic Spectrometry* 14, 881–883. doi: 10.1039/a809028i

Verma, S., and Singh, S. (1990). Factors regulating copper uptake in a cyanobacterium. *Curr. Microbiol.* 21, 33–37. doi: 10.1007/BF02090097

Waldron, K. J., Tottey, S., Yanagisawa, S., Dennison, C., and Robinson, N. J. (2007). A periplasmic iron-binding protein contributes toward inward copper supply. *J. Biol. Chem.* 282, 3837–3846. doi: 10.1074/jbc.M609916200

Wiśniewski, J. R., Zougman, A., Nagaraj, N., and Mann, M. (2009). Universal sample preparation method for proteome analysis. *Nat. Methods* 6, 359–362. doi: 10.1038/nmeth.1322

Wood, P. M. (1978). Interchangeable copper and iron proteins in algal photosynthesis: studies on plastocyanin and cytochrome c-552 in chlamydomonas. *Eur. J. Biochem.* 87, 9–19. doi: 10.1111/j.1432-1033.1978.tb12346.x

Xu, K., Jiang, H., Juneau, P., and Qiu, B. (2012). Comparative studies on the photosynthetic responses of three freshwater phytoplankton species to temperature and light regimes. *J. Appl. Phycol.* 24, 1113–1122. doi: 10.1007/s10811-011-9741-9

Yruela, I., Alfonso, M., Barón, M., and Picorel, R. (2000). Copper effect on the protein composition of photosystem II. *Physiol. Plant.* 110, 551–557. doi: 10.1111/j.1399-3054.2000.1100419.x

Yue, W. W., Grizot, S., and Buchanan, S. K. (2003). Structural evidence for iron-free citrate and ferric citrate binding to the TonB-dependent outer membrane transporter FecA. *J. Mol. Biol.* 332, 353–368. doi: 10.1016/S0022-2836(03)00855-6

Conflict of Interest: The authors declare that the research was conducted in the absence of any commercial or financial relationships that could be construed as a potential conflict of interest.

frontiers in Bioengineering and Biotechnology

ORIGINAL RESEARCH
published: 21 May 2021
doi: 10.3389/fbioe.2021.638726

Trophic Transition Enhanced Biomass and Lipid Production of the Unicellular Green Alga *Scenedesmus acuminatus*

Hu Zhang[1,2], Liang Zhao[1], Yi Chen[1,2], Mianmian Zhu[1,2], Quan Xu[1,2], Mingcan Wu[1], Danxiang Han[1,3,4] and Qiang Hu[1,3,5,6]**

[1] Center for Microalgal Biotechnology and Biofuels, Institute of Hydrobiology, Chinese Academy of Sciences, Wuhan, China, [2] College of Life Sciences, University of Chinese Academy of Sciences, Beijing, China, [3] Key Laboratory for Algal Biology, Institute of Hydrobiology, Chinese Academy of Sciences, Wuhan, China, [4] The Innovative Academy of Seed Design, Chinese Academy of Sciences, Beijing, China, [5] Institute for Advanced Study, Shenzhen University, Shenzhen, China, [6] State Key Laboratory of Freshwater Ecology and Biotechnology, Institute of Hydrobiology, Chinese Academy of Sciences, Wuhan, China

OPEN ACCESS

Edited by:
Wei Xiong,
National Renewable Energy Laboratory (DOE), United States

Reviewed by:
Ankush Karemore,
Georgia Institute of Technology, United States
Jin Liu,
Peking University, China
Changhong Yao,
Sichuan University, China

***Correspondence:**
Danxiang Han
danxianghan@ihb.ac.cn
Qiang Hu
huqiang@szu.edu.cn

Specialty section:
This article was submitted to Bioprocess Engineering, a section of the journal Frontiers in Bioengineering and Biotechnology

Received: 07 December 2020
Accepted: 08 April 2021
Published: 21 May 2021

Citation:
Zhang H, Zhao L, Chen Y, Zhu M, Xu Q, Wu M, Han D and Hu Q (2021) Trophic Transition Enhanced Biomass and Lipid Production of the Unicellular Green Alga Scenedesmus acuminatus. Front. Bioeng. Biotechnol. 9:638726. doi: 10.3389/fbioe.2021.638726

Microalgal heterotrophic cultivation is an emerging technology that can enable producing high cell-density algal cell cultures, which can be coupled with photoautotrophic cultivation for valuable chemicals such as lipids manufacturing. However, how the heterotrophically grown algal cells respond to the lipid-inducing conditions has not been fully elucidated so far. In this study, when the heterotrophically grown *Scenedesmus acuminatus* cells were subjected to the high light (HL) and nitrogen-limited (NL) conditions, both the biomass and lipid productivity were enhanced as compared to that of the photoautotrophically grown counterparts. The chlorophyll *a* fluorometry analysis showed that the Fv/Fm and Y(II) of the heterotrophically grown cells subjected to the HL and NL conditions was recovered to the maximum value of 0.75 and 0.43, respectively, much higher than those of the photoautotrophically grown cells under the same stress conditions. Transcriptomic analysis revealed that heterotrophically grown cells fully expressed the genes coding for the photosystems proteins, including the key photoprotective proteins D1, PsbS, light-harvesting-complex (LHC) I and LHC II. Meanwhile, downregulation of the carotenoid biosynthesis and upregulation of the glycolysis/gluconeogenesis, tricarboxylic acid (TCA) cycle and oxidative phosphorylation pathways were observed when the heterotrophically grown cells were subjected to the HL and N-limited conditions for lipid production. It was deduced that regulation of these pathways not only enhanced the light utilization but also provided the reducing power and ATP by which the biomass accumulation was significantly elevated. Besides, upregulation of the acetyl-CoA carboxylase/biotin carboxylase, digalactosyl diacylglycerol synthase and diacylglycerol acyltransferase 2 encoding genes may be attributable to the enhanced lipid production. Understanding the cellular responses during the trophic transition process could guide improvement of the strength of trophic transition enhancing microalgal biomass and lipid production.

Keywords: *Scenedesmus acuminatus*, heterotrophically grown cells, lipid production, transcriptomic analysis, stress responses

INTRODUCTION

Microalgae are promising feedstocks for liquid biofuels production because of their high photosynthetic efficiencies, fast growth rates, high lipid contents and no competition with food production for arable land during cultivation (Yin et al., 2020). Production of biofuels from photoautotrophically grown microalgal biomass has already proved to be technically feasible at both lab and pilot-scales (Sajjadi et al., 2018; Yang et al., 2018; Tang et al., 2020). However, commercialization of microalgae-derived biofuels has been limited by the high costs, largely associated with biomass production (Su et al., 2017; Aziz et al., 2020). In the past decades, various cultivation strategies besides photoautotrophic cultivation have been emerging to enhance microalgal lipid production so as to balance the costs, which include heterotrophic cultivation, photoautotrophy-to-heterotrophy cultivation and heterotrophy-to-photoautotrophy cultivation (Xiong et al., 2010; Han et al., 2012; Zheng et al., 2013).

Among these cultivation modes, the heterotrophic cultivation mode offers many advantages that can enable fast growth and high biomass productivity for microalgae (Chen et al., 2020), while photoautotrophic cultivation is essential for producing many compounds of which the synthesis are highly dependent on photosynthesis, such as lipids requiring large amounts of photosynthetically produced reducing equivalent and fatty acids (Li-Beisson et al., 2015). Accordingly, heterotrophy-to-photoautotrophy cultivation takes advantages of both the cultivation modes, which are producing high-quality biomass via heterotrophy and inducing biosynthesis of particular end-products under photoautotrophic conditions. Currently, such a cultivation mode has been adopted for many algal strains for the manufacturing of a wide spectrum of chemicals, which included, but are not restricted to, *Chlorella* spp. and *Scenedesmus acuminatus* for lipid production (Han et al., 2012; Jin et al., 2020), *Haematococcus pluvialis* and *Chromochloris zofingiensis* for astaxanthin production (Wan et al., 2015; Sun et al., 2019), and *Botryococcus braunii* for hydrocarbons production (Wan et al., 2019). It is noteworthy that when the coupled cultivation mode was utilized for *Chlorella* spp. and *S. acuminatus*, the biomass yield and lipid productivity were significantly enhanced as compared with traditional photoautotrophic cultivation (Han et al., 2012; Jin et al., 2020).

Due to the above-mentioned merits of the heterotrophy-to-photoautotrophy cultivation mode, several studies have already been conducted to dissect the physiological and biochemical changes during the trophic transition of *Chlorella pyrenoidosa* and *Chromochloris zofingiensis* (Fan et al., 2015; Roth et al., 2019). However, the biological mechanisms underlying the enhanced microalgal biomass and lipid production under the heterotrophy-to-photoautotrophy cultivation mode has not been fully elucidated so far, especially for how heterotrophically grown algal cells adapt to the lipid-inducing conditions.

Scenedesmus acuminatus is a freshwater green alga capable of accumulating lipids as high as up to 50% of the dry wight under high light (HL) and nitrogen-limited (NL) conditions in photoautotrophic cultivation (Zhang et al., 2018). The alga is also able to grow robustly under heterotrophic conditions, reaching an ultrahigh-cell-density of 286 g L^{-1} (Jin et al., 2020). Interestingly, both the biomass concentration and lipid content of *S. acuminatus* cells were much higher under the heterotrophy-to-photoautotrophy cultivation conditions than those under the traditional photoautotrophic cultivation conditions (Jin et al., 2020). Thus, this alga is an ideal model to investigate the impact of the trophic transition from heterotrophy to photoautotrophy on algal cells. In this study, the heterotrophically grown cells (HC) of *S. acuminatus* and photoautotrophically grown ones (PC) were both subjected to the HL and NL conditions, and the cellular growth, lipid content and photosynthetic efficiency was compared between them, respectively. The responses of the genes involved in photosynthesis, central carbon metabolism, carotenoid biosynthesis and fatty acids biosynthesis were also surveyed by RNA-seq analysis in order to advance our understanding about mechanisms underlying the enhanced biomass and lipid production of *S. acuminatus* during trophic transition.

MATERIALS AND METHODS

Algal Strains and Culturing Conditions

The green alga *S. acuminatus* was isolated from South Lake of Guangzhou, China (Jin et al., 2020). For heterotrophic cultivation, algae cells were maintained in the modified Endo growth medium, containing glucose 30 g L^{-1}, KNO_3 3 g L^{-1}, KH_2PO_4 1.2 g L^{-1}, $MgSO_4{\cdot}7H_2O$ 1.2 g L^{-1}, trisodium citrate 0.2 g L^{-1}, $FeSO_4{\cdot}7H_2O$ 0.016 g L^{-1}, EDTA-Na_2 2.1 mg L^{-1}, $CaCl_2{\cdot}2H_2O$ 0.03 g L^{-1}, H_3BO_3 2.86 mg L^{-1}, $ZnSO_4{\cdot}7H_2O$ 0.222 mg L^{-1}, $MnCl_2{\cdot}4H_2O$ 1.81 mg L^{-1}, Na_2MoO_4 0.021 mg L^{-1}, $CuSO_4{\cdot}2H_2O$ 0.07 mg L^{-1}. Heterotrophic cultivation was performed as described in the previous study (Jin et al., 2020). Briefly, the algal cells cultured in 1 L Erlenmeyer flask containing 300 mL medium on a rotary shaker at 180 rpm in dark was used as inoculum for the heterotrophic cultivation in the 7.5-L fermenter (BIOFLO and CELLIGEN 310, New Brunswick, United States). The initial culture volume of fermenter was 2.8 L, and the airflow rate was 2.8 L min^{-1}. Dissolved oxygen was controlled automatically above 40% (*v*/*v*) via being coupled with the stirring speed. The initial glucose and urea concentration were 5 and 0.337 g L^{-1}, respectively, corresponding to the C/N ratio of 12. The feeding medium used during fermentation process was the 25-fold concentrated growth medium used for batch culturing, containing 750 g L^{-1} of glucose. Stepwise constant feeding strategy was adopted to control the glucose concentration below 5 g L^{-1} during the cultivation. Besides, the temperature and pH was set at 30°C and 6.0, respectively. Heterotrophically grown algae cells were used as inoculum for lipid induction when cell biomass reached *ca.* 200 g L^{-1} after 144 h of fermentation.

The BG-11 growth medium was used for photoautotrophic cultivation of *S. acuminatus* cells (Rippka et al., 1979). The algal cells were cultured in 800 mL column photobioreactors (PBRs) (i.d. 5 cm) containing 750 mL of BG-11 growth medium, and grown to exponential phase (4–5 days) under continuous light intensity of 90 μmol m^{-2} s^{-1} at 25 ± 2.5°C. Mixing and aeration

were provided by bubbling air containing 2.0% (*v/v*) CO_2 with a flow rate of 0.2 vvm.

The HC and PC were harvested by centrifugation (3000 *g*, 5 min) and resuspended in the NL BG-11 growth medium with 0.09375 g L^{-1} $NaNO_3$, corresponding to 1/16 of the original nitrate concentration of BG-11. The initial chlorophyll concentrations of above two cultures were adjusted to *ca.* 6.0 mg L^{-1}. The cell cultures were subjected to the continuously HL intensity of 400 μmol m^{-2} s^{-1} at 25 ± 2.5°C to induce lipid production.

Growth and Lipid Contents Determination

Cell growth was estimated by measuring the cellular dry weight (DW), cell number and chlorophyll concentration of the algal cell cultures. DW was measured according to the method described by Wen et al. (2016). Cell numbers were counted by using a hemacytometer (Improved Neubauer, United States) under the microscope (BX51, Olympus, Japan). Chlorophyll and carotenoids contents were determined by using the previously described method (Ma et al., 2017). Briefly, an aliquot (10 mL) of culture suspension was centrifuged (4000 × *g*, 10 min, 4°C) to collect the cell pellets. After discarding the supernatants, the cell pellets were kept at −80°C for 24 h. Methanol (10 mL) was added to the centrifuge tube, which was then placed in a water-bath at 75°C for 20 min in dark, followed by centrifugation (4000 × *g*, 10 min, 4°C). The supernatants were transferred to a cuvette for measurement of optical density at 653 nm (OD_{653}), 666 nm (OD_{666}) and 470 nm (OD_{470}).

$$C_a : \text{Chlorophyll a concentration} = (15.65 \times OD_{666} - 7.34 \times OD_{653}) \times V_{MeOH}/V_{algae}$$

$$C_b : \text{Chlorophyll b concentration} = (27.05 \times OD_{653} - 11.21 \times OD_{666}) \times V_{MeOH}/V_{algae}$$

$$\text{Chlorophyll concentration} = \text{Chlorophyll a concentration} + \text{Chlorophyll b concentration}$$

$$\text{Carotenoidsconcentration} = (1000 \times A_{470} - 2.86 \times C_a - 129.2 \times C_b)/221$$

where V_{MeOH} is the volume of methanol and V_{algae} is the volume of microalgae suspension used for the extraction of pigments.

The contents of fatty acid methyl esters (FAMEs) were determined according to the method described in our previous study (Jia et al., 2015). Briefly, 25 μL of the 10 mg mL^{-1} methyl tridecanoate, 200 μL of the chloroform:methanol (2:1, v/v) and 300 μL of the 5% (v/v) HCl:methanol were added to 10 mg sample and was transesterified in tightly sealed vials at 85°C for 1 h. FAMEs were extracted with 1 mL of hexane at room temperature for 1 h. Then the extracted FAMEs with pentadecane as internal standard was analyzed directly by a gas chromatography flame ionization detector (GC-FID) (Agilent, United States). FAMEs were quantified by using a FAME mixture standard (Sigma-Aldrich, United States) with C17:0 as the internal standard. Lipid bodies were observed by using the Olympus BX53 fluorescence microscopy (Olympus, Japan). The algal cells were diluted to a density of 1 × 10^7 cells mL^{-1} and then treated with 10% DMSO and stained for 10 min with 50 μM BODIPY 493/503 (Molecular Probes, Invitrogen Corporation, United States). Images were acquired by using the software cellSens DP6000 (Olympus, Japan). The BODIPY 493/503 fluorescence was detected using a 525/50 band-pass filter and the micrograph was taken using 488 nm excitation wavelength.

Chlorophyll *a* Fluorometry Analysis

Photosynthetic activities were measured by using a pulse amplitude modulated (PAM) fluorometer (Dual-PAM 100, Walz, Effeltrich, Germany). Algal cells were dark-adapted for 15 min to measure the minimum fluorescence (F_0). For the measurement of maximal fluorescence (Fm), a saturated pulse light (10,000 mmol photons m^{-2} s^{-1}, lasting for 0.8 s) was applied to fully close the PSII reaction centers (Genty et al., 1989). Saturating flashes at intervals of 35 s were applied under the different actinic light intensities (0–2004 $mmolm^{-2}$ s^{-1}). The maximum fluorescence in the light (Fm') and steady-state value of fluorescence (F) were recorded with saturation pulse analysis. The maximum photochemical efficiency of PSII (Fv/Fm) was calculated as (Fm-F_0)/Fm. The quantum yield of PSII [Y(II)] and non-photochemical quenching (NPQ) were calculated as follows: Y(II) = (Fm'-F_0)/Fm', NPQ = (Fm-Fm')/Fm' (Maxwell and Johnson, 2000).

RNA Extraction, Library Construction and Sequencing

Algal cells were collected at 6, 12, and 24 hours (h) of cultivation for the heterotrophically grown *S. acuminatus* cultivated under photoautotrophic lipid-inducing conditions (HL and NL) and heterotrophic conditions. For heterotrophic cultivation, 2 g L^{-1} of glucose was added into the N-limited BG-11 medium and the cells were grown under darkness. Mixing and aeration were provided by bubbling sterilized air at a flow rate of 0.2 vvm. For each time point, 3 biological replicates were prepared. Total RNA was extracted using TransZol Plant RNA Kit (TransGen, Beijing, China). For mRNA-Seq, the poly(A)-containing mRNA molecules were purified using NEBNext Poly(A) mRNA Magnetic Isolation Module (New England Biolabs). Directional transcriptome libraries were prepared using NEBNext Ultra Directional RNA Library Prep Kit for Illumina (New England Biolabs). Following the manufacturer's instructions, RNA dissolved in the first strand synthesis reaction buffer and random primer mix were fragmented into 250- to 400-bp fragments by incubating the sample at 94°C for 10 min.

The purified, fragmented and primed mRNA was converted into double-stranded cDNA. Then, adaptor ligation, purification of ligation reaction, PCR enrichment and purification of the PCR reaction were conducted, the final library was sequenced for 2 × 150-bp runs (paired-end) using Illumina Hiseq 2500 platform (Novogene Bioinformatics Technology Co., Ltd., Beijing, China).

Transcriptome Assembly and Functional Annotation

To get high-quality clean reads, the raw data containing adaptor sequences, reads with low-quality sequences, and unknown nucleotides were filtered by using Trimmomatic (version 0.35). Transcriptome *de novo* assembly and quality assessment were performed firstly using Trinity (Grabherr et al., 2011), and the longest assembled transcript of given gene was taken as a unigene. Then the unigenes were used for CDS (Coding Sequence) prediction and functional annotation in the databases including: NR (NCBI non-redundant protein sequences), COG (Clusters of Orthologous Groups of proteins), GO (Gene Ontology) and KEGG (Kyoto Encyclopedia of Genes and Genomes) (Chen et al., 2017). Finally, the gene expression quantitation was estimated by RSEM (Li and Dewey, 2011) and each unigene was then calculated and normalized to the number of Fragments Per Kilobase Million (FPKM). Based on the expression, the differentially expressed genes (DEGs) were analyzed using the DEGseq R package (Huang et al., 2019). The significant DEGs were identified by two calculated parameters, false discovery rate (FDR) and Log_2 fold change (Log_2FC). If FDR was less than 0.05 and the absolute value of Log_2FC was not less than 1, the gene was considered as significantly expressed one (Li X. et al., 2018).

Statistical Analyses

All data were obtained by using at least three biological samples to ensure the reproducibility of the results. Experimental results were expressed as mean ± standard deviation. The data were analyzed by using one-way ANOVA in SPSS (version 19.0). Statistically significant difference was considered at $p < 0.05$.

RESULTS AND DISCUSSION

Growth and FAMEs Contents of the HC and PC of *S. acuminatus* Subjected to the HL and NL Conditions

When the HC and PC of *S. acuminatus* were subjected to the HL and NL conditions at the same initial chlorophyll concentration (ca. 6 mg L^{-1}), the volumetric chlorophyll concentration of the HC culture increased more drastically than that of the PC culture within 24 h (**Figure 1A**). After 24 h, when the nitrate was completely consumed, the chlorophyll concentrations of both the cultures decreased. The chlorophyll concentration of the PC culture decreased more rapidly than that of the HC culture from 24 through 72 h under stresses (**Figure 1A**). Similarly, the volumetric carotenoid concentration of the HC culture doubled within 24 h and was much higher than that of the PC culture. After 24 h, the carotenoid concentrations of both the cultures decreased (**Figure 1B**).

When the two types of cells were inoculated at the same chlorophylls and carotenoids concentrations, the initial cell concentration was 2.1×10^6 and 3.1×10^6 cells mL^{-1}, respectively, for the HC and PC culture (**Figure 1C**). The cell number of the HC culture reached 3.15×10^7 cell mL^{-1} after 48 h under HL and NL stresses, which was about twice as many as that of the PC culture (1.49×10^7 cell mL^{-1}, $p < 0.05$, **Figure 1C**). The initial biomass concentration of the HC was twice as high as that of the PC (**Figure 1D**). Under the stress conditions, biomass yield of the HC culture was consistently higher than that of the PC culture during the 144 h under stresses ($p < 0.05$, **Figure 1D**). These results taken together indicated the HC can adapt to the HL and NL conditions in a more effective manner as compared to the PC.

To compare the capabilities in producing lipids of the two types of cells, the FAMEs contents and fatty acid profiles under HL and NL conditions were analyzed. As shown in **Figure 1E**, the initial FAMEs content of the HC was only 7.2% of DW, which was significantly lower than that of the PC (13.3% of DW) ($p < 0.05$). However, the FAMEs content of the HC increased sharply and reached 42.56% of DW by the end of cultivation, which was only a little lower than that of the PC (45.37% of DW). As a function of the biomass yield and the contents of FAMEs, the maximum FAMEs productivity of HC was significantly higher than that of PC under HL and NL conditions ($p < 0.05$, **Figure 1F**). Considering the total lipids of microalgae can be directly converted to the fatty acid methyl/ethyl esters for biofuels production (Nascimento et al., 2013; Sajjadi et al., 2018), the fatty acid profiles were compared between HC and PC. As shown in **Supplementary Table 1**, though the composition of PUFA was significantly higher in HC than that in PC, which was not suitable for biofuels manufacturing (Talebi et al., 2013), no significant difference in terms of the fatty acids profile was observed between them when HC and PC were subjected to HL and NL stresses over 144 h, indicating the coupled heterotrophy-and-photoautotrophy cultivation mode is an ideal technical route for biofuels production.

The cellular contents of chlorophylls and carotenoids were significantly higher in the HC than that in the PC ($p < 0.05$, **Figures 2A,B**). The weight of the individual HC was 2 times higher than that of the PC (**Figure 2C**). These results were consistent with the microscopic observation that showed the size of HC (length 20.1 ± 3.0 μm, width 14.3 ± 2.5 μm) was significantly larger than that of PC (length 9.4 ± 2.1 μm, width 3.1 ± 0.4 μm) (**Figure 2D**). When subjected to the HL and NL conditions, the cellular contents of chlorophylls and carotenoids both decreased immediately within the 24 h under the stresses (**Figures 2A,B**). After 96 h, the chlorophyll content per cell and carotenoids content per cell of the HC were much lower than those of the PC, respectively ($p < 0.05$, **Figures 2A,B**). Upon the onset of the stresses, the weight per HC decreased from 0.23 to 0.06 ng $cell^{-1}$ during the 24 h, while that of the PC slightly decreased (**Figure 2C**). After that, the weight of the two types of cells continuously increased and no significant difference was observed between them ($p > 0.05$,

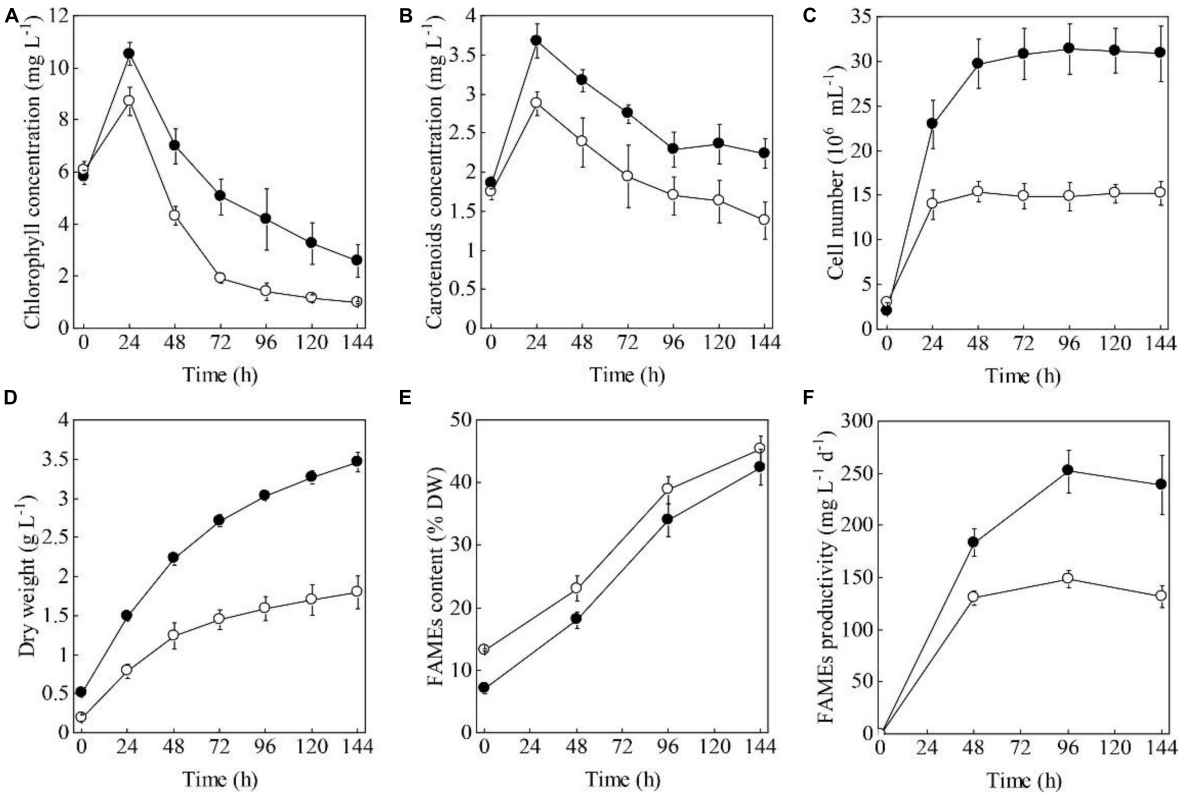

FIGURE 1 | Time evolution of the volumetric chlorophyll concentrations **(A)**, carotenoid concentrations **(B)**, cell numbers **(C)**, dry weights **(D)**, FAMEs contents **(E)**, and FAMEs productivities **(F)** of the heterotrophically (filled cycle)- and photoautotrophically (empty cycle)-grown *S. acuminatus* cells subjected to the high-light and N-limited conditions. The values represent mean ± S.D. (n = 3).

Figure 2C). Decreases in the weight per HC were consistent with the changes in cell morphology as shown in **Figure 2D**. Besides, the number and size of lipid bodies in the two types of cells were almost the same (**Figure 2D**). In addition, the calculated contents of chlorophylls and carotenoids based on cell dry weight were shown in **Supplementary Table 2**. The results showed that the chlorophyll content of HC and PC decreased to a comparable level under HL and NL stress conditions, though it was originally two times higher in PC than that in HC. By contrast, the carotenoid content per cell dry weight of PC was 98.6% higher than that of HC. When subjected to the stresses, the carotenoid content of PC decreased by 42.3% within 24 h, while that of HC decreased by 29.6%. Over 144 h under HL and NL stresses, the carotenoid contents of PC were constantly higher than that of HC.

Those results taken together indicated HC had the more or less same ability in accumulating lipids with the PC but much higher growth rate under HL and NL conditions. Different from many previous studies, which investigated the microalgal biomass and lipid yields during the trophic transition process (i.e., from heterotrophy to photoautotrophy) (Han et al., 2012; Wu et al., 2019), this study uncovered the changes in the morphology and biochemical compositions at the single cell level. Firstly, it was observed that both the HC and PC of *S. acuminatus* started to divide vigorously upon being subjected to the high light conditions, and the HC divided to more extent than PC did. After 24 h, when the nitrate in the growth media was completely consumed up, the division of PC immediately stopped but the division of HC continued until 48 h, albeit at a slightly lower rate than that of the first 24 h under HL stress. Though the original weight of HC was much heavier than that of PC, it decreased to a comparable level with that of PC over 144 h under HL and NL stresses. In the previous study, the enhanced growth rate of HC under HL and NL conditions was attributable to its remarkably reduced chlorophyll content (Jin et al., 2020). It was suggested that HC may possess truncated light-harvesting antennae, which can permit higher light penetration in high-cell-density-culture, less likelihood photoinhibition, and reduced energy loss as heat (Melis, 2009; Cazzaniga et al., 2014). However, it was found in this study that the chlorophyll contents of the PC and HC were reduced to a similar level under stresses (**Figure 2** and **Supplementary Table 1**). By contrast, it was observed that the cellular content of carotenoids of PC was higher than that of HC. Enhancement of the carotenoid biosynthesis is a strategy adopted by microalgae to cope with the excess light (Li L. et al., 2018). Thus, we assumed the relatively lower cell concentration of the PC culture led to the exposure of the single cells to excess illumination and therefore the retarded cell growth of PC under HL and NL stresses. Thus, understanding the physiological and biochemical changes that occurred in HC during the first 48 h

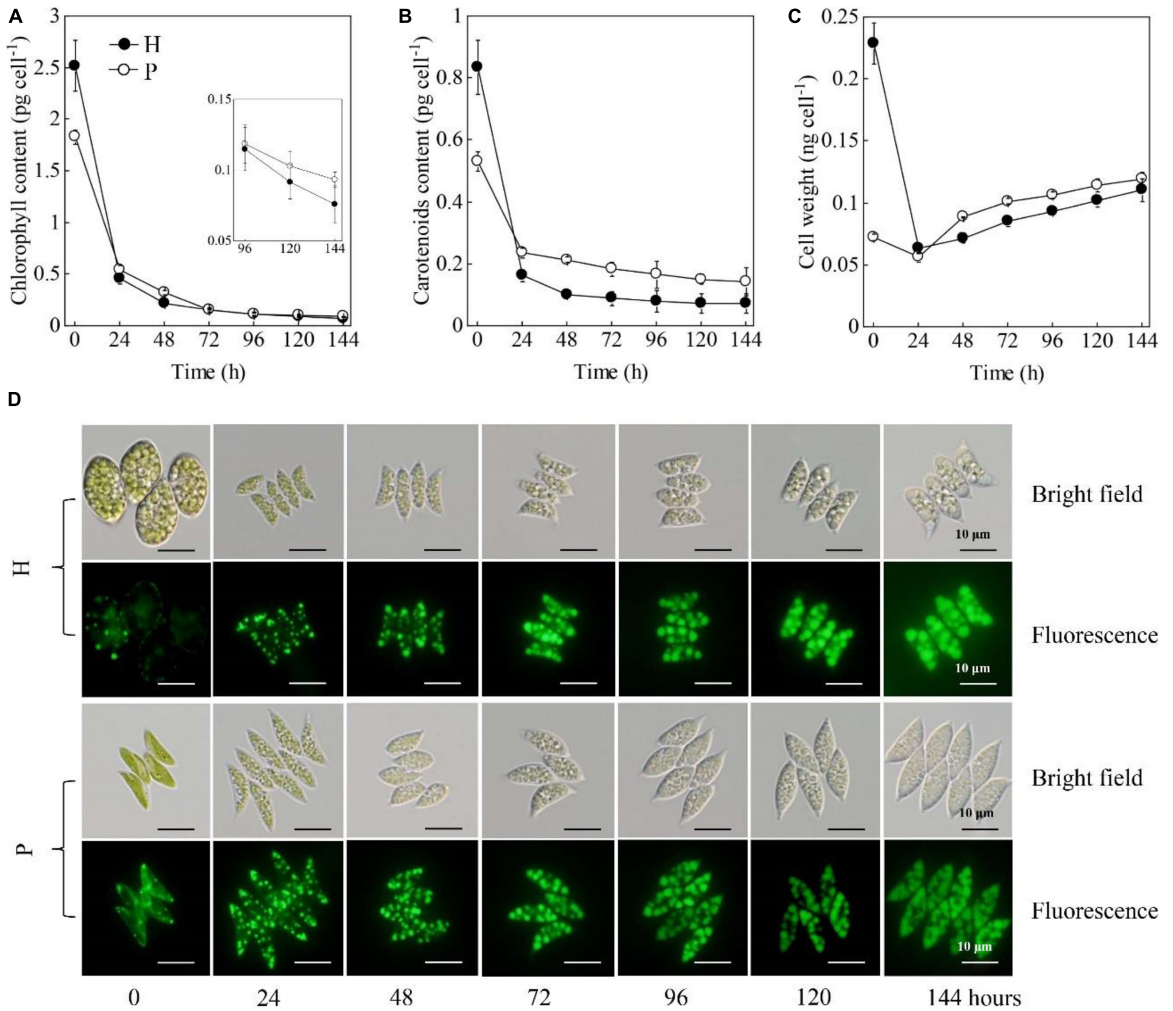

FIGURE 2 | Changes in chlorophyll contents **(A)**, carotenoids contents **(B)**, cell weights **(C)**, cell morphologies and lipid bodies **(D)** of the heterotrophically (H)- and photoautotrophically (P)-grown *S. acuminatus* cells subjected to the high-light and N-limited conditions. Intracellular lipid bodies were stained using BODIPY (green). Scale bar = 10 μm.

under stresses, which caused rapid cell division, is crucial for elucidating the mechanisms underlying the enhanced growth rate of HC. On the other hand, no significant difference was observed in the lipid contents between PC and HC. Previous studies on *Chlorella* spp. suggested that the lipid contents of the HC subjected to HL stress was significantly lower than that of PC under the same conditions (Han et al., 2012). Thus, the distinct capabilities in accumulating lipids between HC and PC subjected to the same stresses may vary among microalgal species.

Photosynthetic Efficiencies of the HC and PC Subjected to HL and NL Conditions

The impacts of the HL and NL stresses on the photosynthetic efficiencies of the two types of *S. acuminatus* cells were investigated by using the chlorophyll *a* fluorometry (**Figure 3**). The initial Fv/Fm of the PC was 0.78 (**Figure 3A**). However, the Fv/Fm of the PC decreased sharply after 24 h of cultivation under HL and NL conditions. On the contrary, although the initial Fv/Fm of the HC was only 0.31, which suggested that the photosynthetic complexes were not well developed or impaired in HC, it increased sharply during the first 12 h of cultivation and reached the maximum value of 0.75 at 24 h. Afterward, Fv/Fm of the HC showed a slight decrease during cultivation and it was much higher than that of the PC under the same conditions ($p < 0.05$, **Figure 3A**). Similar results were obtained in effective PSII quantum yield [Y(II)] (**Figure 3C**).

On the other hand, non-photochemical quenching (NPQ) of the PC subjected to HL and NL was greatly induced, and was significantly higher than that of the HC from 24 through 96 h of stresses ($p < 0.05$, **Figure 3B**), which was consistent with the results of the yield for dissipation by downregulation [Y(NPQ)] (**Figure 3E**). Although enhanced NPQ is a useful strategy for microalgal cells to cope with the excess light (Peers et al., 2009; Bailleul et al., 2010), more light energy dissipates as heat may

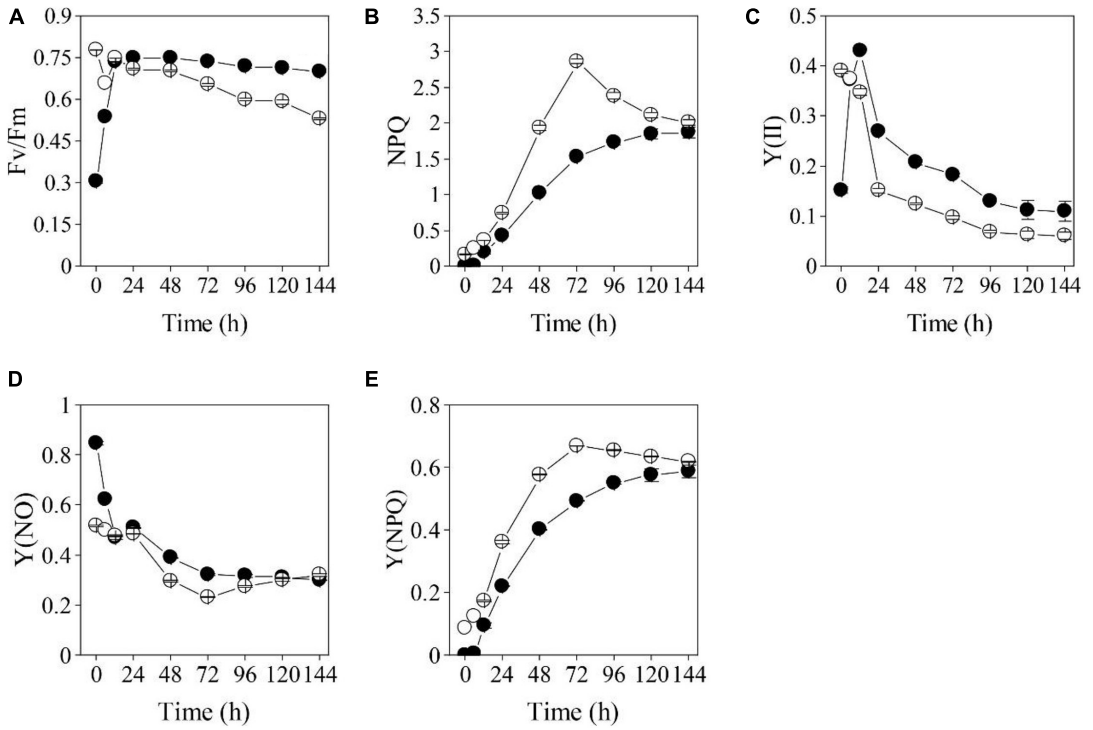

FIGURE 3 | Changes in chlorophyll fluorometry parameters [**(A):** Fv/Fm, **(B):** NPQ, **(C):** Y(II), **(D):** Y(NO), **(E):** Y(NPQ)] for the heterotrophically (filled cycle)- and photoautotrophically (empty cycle)-grown *S. acuminatus* cells subjected to the high-light and N-limited conditions. The values represent mean ± S.D. (n = 3).

cause less quantum yield. Thus, much lower NPQ of the HC than that of PC may lead to higher light energy utilization by the former one, which results in its higher growth rate and biomass yield under stresses. The yield of other non-photochemical losses [Y(NO)] of the cells in the two cultures were almost the same after 24 h of cultivation (**Figure 3D**).

To better understand the differences in photosynthetic physiology between the two types of cells, light-response curves were determined for them. The PC exhibited higher electron transport rate (ETR) and Y(II) than HC under the actinic light in the range of 34–2004 μmol photons m^{-2} s^{-1} (**Figures 4A,B**). However, those two parameters of the HC were much higher than that of the PC under the actinic light in the range of 34–1279 μmol photons m^{-2} s^{-1} after 12 h (**Figures 4E,F,I,J,M,N**). Moreover, Y(NPQ) of the PC subjected to HL and NL was higher than that of HC under the same stress conditions (**Figures 4D,H,L,P**), while Y(NO) of the two types of cell subjected to the stresses for 12 h had little disparity under the actinic light in the range of 65–2004 μmol photons m^{-2} s^{-1} (**Figures 4C,G,K,O**).

The heterotrophically grown algal cells are usually featured by the underdeveloped or impaired photosystems, indicated by the relatively low Fv/Fm value (Zhang et al., 2016; Roth et al., 2019). The Fv/Fm of *Haematococcus pluvialis* cells grown under heterotrophic conditions is found to be as low as 0.6. When *Chlorella protothecoides* was grown under heterotrophic conditions, many photosynthetic proteins were found to be degraded, reflecting changes in photosynthetic efficiencies (Gao et al., 2014). Different from photosynthetic cells of many microalgae, whose photosynthetic efficiencies dramatically declined when they are subjected to the HL stresses (Parkhill et al., 2010; Xia et al., 2014; He et al., 2015), the Fv/Fm and Y(II) and of HC immediately recovered during the trophic transition of *S. acuminatus* (**Figure 3**). Underlying mechanism for the rapid regeneration and reactivation of photosynthesis may be involved in removal of glucose that can suppress photosynthesis in HC (Roth et al., 2019). In addition, both the light and nitrate were found to be capable of inducing reconstruction of photosynthetic machine of heterotrophic algal cells (Zhang et al., 2016). The results of chlorophyll a fluorometry underlined the significance of changes during the first 24 h, which may confer the HC of *S. acuminatus* capabilities in adapting to the HL and NL conditions. The results also suggested that more light energy can be converted into photochemical energy and less light energy dissipated as heat in the HC than those in the PC, which could lead to the enhanced biomass production of HC under the HL and NL conditions.

Overview of the RNA-Seq Data

To dissect the mechanisms underlying the enhanced biomass and lipid production of heterotrophically grown *S. acuminatus* cells under stress conditions, transcriptomics analysis was performed for the HC subjected to photoautotrophic lipid-induing conditions (HL and NL) and the cells were kept under the heterotrophic conditions were used as control. After assembling the *de novo* sequenced transcripts and eliminating

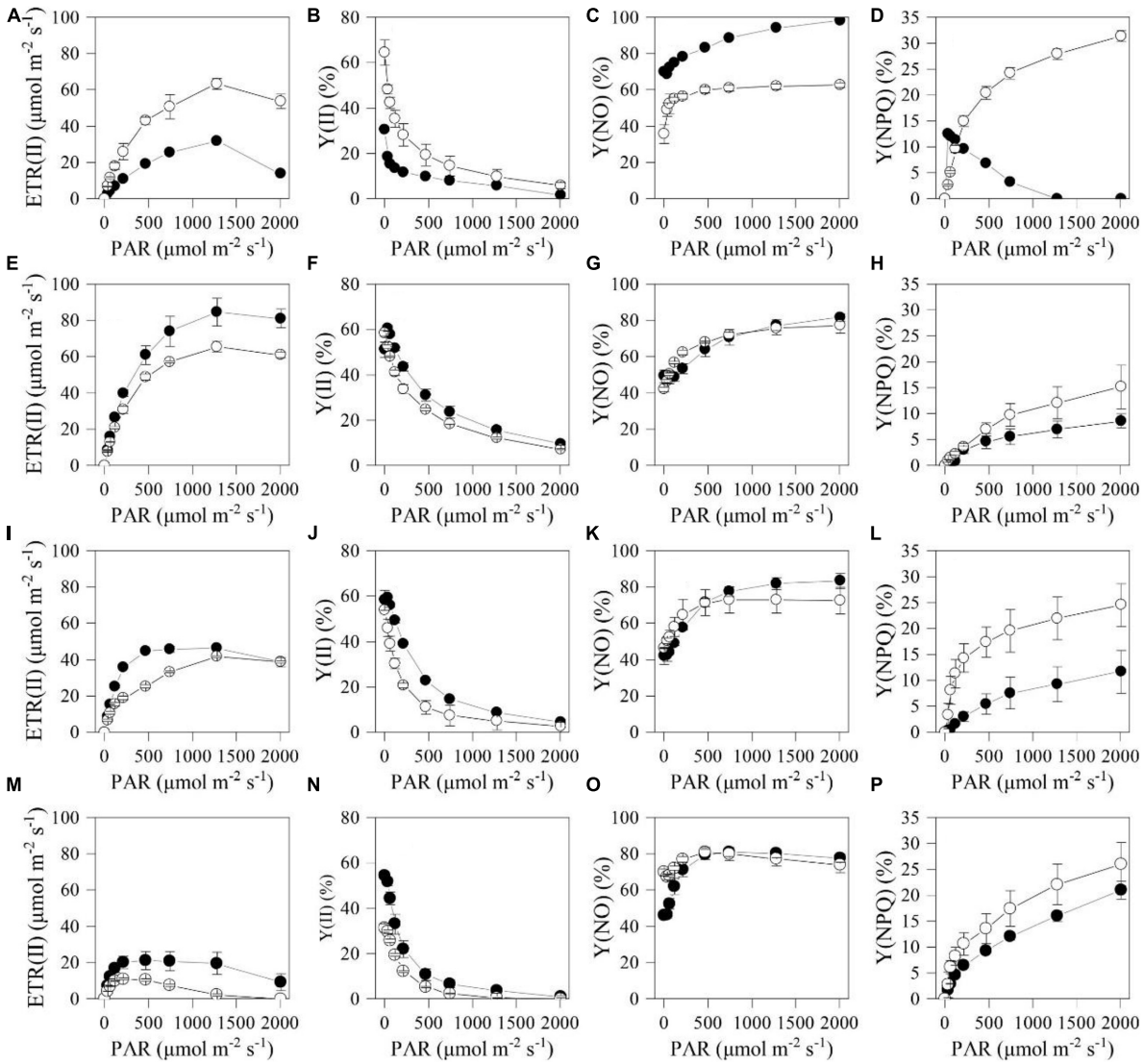

FIGURE 4 | Light response curves of the chlorophyll fluorometry parameters for the heterotrophically (filled cycle)- and photoautotrophically (empty cycle)-grown *S. acuminatus* cells subjected to the high-light and N-limited conditions. Chlorophyll fluorescence were obtained with a series of photosynthetically active radiances (0, 34, 65, 122, 218, 467, 746, 1279, 2004 μmol photons m^{-2} s^{-1}) to calculate ETR(II), Y(II), Y(NO) and Y(NPQ). **(A–D)**, **(E–H)**, **(I–L)**, and **(M–P)** were measured in 0, 12, 24, and 144 h of cultivation, respectively. The values represent mean ± S.D. (n = 3).

redundancy, 15,899 unigenes with an N50 length of 1,193 bp and GC content of 55.6% were obtained (**Supplementary Table 3**). To evaluate the accuracy and completeness of assembled unigenes, the transcripts were compared with single-copy gene sets of several large evolutionary branches in OrthoDB database[1] by BUSCO 3.0 (Simao et al., 2015), based on conservation of single-copy benchmarking universal single-copy orthologs (BUSCOs). The results showed a high degree of completeness with a BUSCO score of 76.5%, of which 1,659 genes were complete, 525 were complete duplicated, 230 were fragmented, and 279 were missing BUSCO orthologs out of the 2,168 groups searched (**Supplementary Table 3**). These results indicated high-quality transcriptomes were obtained in this study and can be further used for annotation and analysis.

There were 274 shared genes identified in both the treated (HC subjected to the HL and NL conditions) and control groups at three time points (**Figure 5A**). Besides, there were 5,351 DEGs in the heterotrophically grown *S. acuminatus* cells subjected to HL and NL as compared to the control. Among them, 923, 695, and 767 up-regulated and 828, 822, and 1,316 down-regulated DEGs were identified at 6, 12, and 24 h under the HL and NL conditions (**Figure 5B**). However, much more DEGs were observed when heterotrophically grown *C. pyrenoidosa* and *C. zofinginesis* were transferred to photoautotrophic conditions (Fan et al., 2015; Roth et al., 2019).

[1]http://cegg.unige.ch/orthodb6

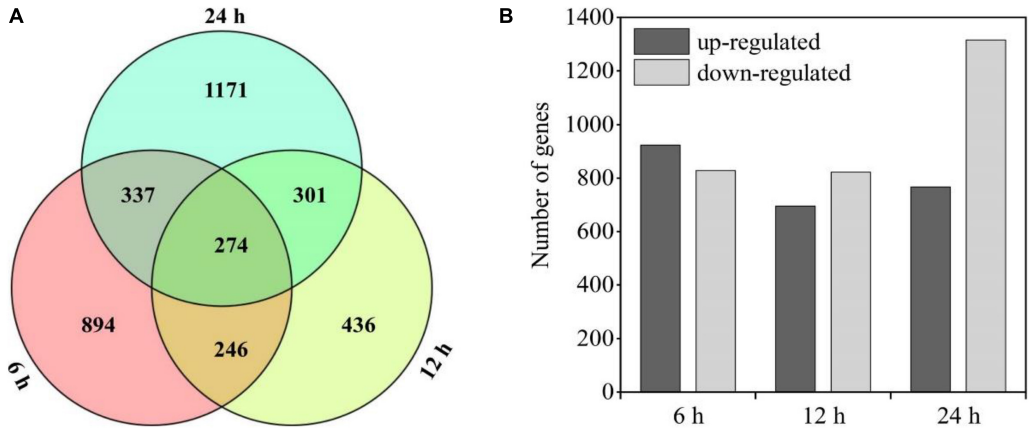

FIGURE 5 | Statistical chart of heterotrophically grown *S. acuminatus* cells subjected to the high-light and N-limited conditions. Venn diagram representation of shared/unique genes **(A)** and number of differently expressed genes (DEGs) **(B)** compared to heterotrophically grown cells at 6, 12, and 24 h of cultivation, respectively.

The unigenes were further classified by GO enrichment analysis and KEGG enrichment pathway analysis (**Supplementary Figures 1–3**). Notably, in the early stage of trophic transition (6 h), the transcript levels of the genes related to membrane and membrane part, which involved in chloroplast biosynthesis, were fluctuated remarkably (**Supplementary Table 4**). These findings suggested a large number of biological processes were reprogrammed in the HC of *S. acuminatus* during the trophic transition, which was also observed during the trophic transition processes in *C. pyrenoidosa* and *C. zofinginesis* (Fan et al., 2015; Roth et al., 2019).

Changes in the Key Biological Processes at Transcriptional Level During the Trophic Transition

Previous studies have revealed that a large number of pathways including photosynthesis, carbon fixation, central carbon metabolism, oxidative phosphorylation, lipid biosynthesis, and other metabolism pathways were regulated at the transcriptional level during the trophic transition process in many microalgae, which enabled microalgal cells coping with the changing environmental conditions (Fan et al., 2015; Roth et al., 2019). Photosynthesis produce the main energy sources (i.e., ATP and NADPH) for the growth and metabolism of algal cells (Huang et al., 2019). When dark-grown algal cells were subjected to HL condition, photosynthesis may be recovered immediately to provide energy for sustaining the algal cell growth. Four multi-subunit membrane-protein complexes in the thylakoid membranes including two photosystems (PSI and PSII), cytochrome b6f and ATPase were the basic elements for photoreaction (Nelson and Ben-Shem, 2004). The results showed that 37 genes coding for the above four photosynthetic apparatus were differently expressed at 6 h (**Table 1**). D1 protein turnover is an important defense strategy for plants and algae to cope with HL stresses (Wu et al., 2011; Li L. et al., 2018). The transcriptome data showed that although the D1 protein encoding gene psbA (c11222_c0_g1) was downregulated by 1.38-fold at 6 h, it was upregulated by 95 and 38% at 12 and 24 h, respectively (**Table 1**). This result suggested that D1 protein of the heterotrophically grown cells subjected to HL and NL can be repaired so as to enhance the function of PSII, which was consistent with the increase of Fv/Fm and Y(II) of algal cells during the same period of cultivation time (**Figures 3A,C**). Non-photochemical quenching of excess excitation energy is another photoprotective strategy in photosynthetic organisms (Correa-Galvis et al., 2016). Several studies have already confirmed that high quenching capacity depending on PsbS (Gerotto et al., 2015; Ware et al., 2015; Correa-Galvis et al., 2016). The gene (c19487_c0_g1) encoding PsbS was downregulated by 31% and 1.19 times at 6 and 12 h, respectively (**Table 1**). However, it was upregulated by 63% at 24 h. This result indicated NPQ was enhanced with extended culturing time under HL and NL stresses, which was consistent with changes in the NPQ during the same period of time (**Figures 3B,E**). LHCII is the primary site of photoprotection and its recovery is also useful for algal cells to eliminate photodamage caused by HL (Ruban et al., 2012). D1 protein turnover and PsbS upregulation indicated that some key proteins in LHCII were repaired under stresses, and it may provide protection for the core of PSII to some extent. Thus, downregulation of the expression of the genes involved in photosynthesis indicated that the low concentration of glucose (i.e., 0–5 g L^{-1}) adopted in this study may stimulate expression of many photosynthetic genes in the *S. acuminatus* cells grown under the heterotrophic conditions.

The genes involved in carotenoid biosynthesis were also surveyed. As shown in **Table 2**, the gene encoding phytoene synthase (PSY), which catalyzes the conversion of geranylgeranyl diphosphate to phytoene, was downregulated significantly at all three time points (**Table 2**). The major carotenoids of *S. acuminatus* are lutein, zeaxanthin, violaxanthin, and neoxanthin (Zhang et al., 2019). The expressions of corresponding genes were all downregulated, including beta-ring hydroxylase (CYP97A3) and carotenoid epsilon

TABLE 1 | Comparative transcriptomic analysis of photosynthesis for the heterotrophically grown *S. acuminatus* cells subjected to the high light and N-limited conditions.

Category	Gene_ID	KO_ID	Enzyme	Gene_name	6 h		12 h		24 h	
					Log_2FC	FDR	Log_2FC	FDR	Log_2FC	FDR
PSI	c11348_c0_g1	K02689	Photosystem I P700 chlorophyll a apoprotein A1	PsaA	−1.763	3.78E-16	−1.107	2.32E-04	−0.373	2.71E-01
	c2811_c0_g1	K02692	Photosystem I subunit II	PsaD	0.138	2.43E-03	−0.513	1.58E-14	−2.950	7.93E-272
	c16988_c0_g1	K08905	Photosystem I subunit V	PsaG	0.208	4.28E-04	0.094	2.74E-01	−2.539	4.22E-139
	c13333_c0_g1	K02696	Photosystem I subunit VIII	PsaI	0.217	1.94E-07	−0.442	2.46E-09	−3.678	4.01E-209
	c7310_c0_g1	K02699	Photosystem I subunit XI	PsaL	0.194	3.85E-06	−0.177	3.48E-02	−3.780	1.22E-272
	c6347_c0_g1	K02701	Photosystem I subunit PsaN	PsaN	0.947	2.67E-80	0.513	5.83E-12	−4.628	7.28E-306
	c15041_c0_g1	K02639	Ferredoxin	PetF	−0.622	7.13E-18	−1.825	6.23E-73	−2.927	3.64E-88
	c19224_c0_g3	K02638	Plastocyanin	PetE	−0.536	8.02E-51	−0.508	2.51E-11	−2.378	2.66E-131
	c16349_c0_g1	K02641	Ferredoxin-NADP + reductase	PetH	0.296	8.13E-13	0.027	7.58E-01	−1.821	9.11E-131
PSII	c11222_c0_g1	K02703	Photosystem II P680 reaction center D1 protein	PsbA	−1.383	2.23E-47	0.948	6.97E-07	0.375	2.69E-02
	c14164_c0_g1	K02704	Photosystem II CP47 chlorophyll apoprotein	PsbB	−2.446	1.49E-20	−2.224	4.76E-09	NA	NA
	c15153_c0_g1	K02705	Photosystem II CP43 chlorophyll apoprotein	PsbC	−1.006	1.30E-09	0.659	2.53E-03	−0.742	3.99E-04
	c2432_c0_g1	K02706	Photosystem II P680 reaction center D2 protein	PsbD	−2.088	5.01E-18	NA	NA	NA	NA
	c17184_c0_g1	K02716	Photosystem II oxygen-evolving enhancer protein 1	PsbO	0.471	2.62E-37	−0.236	5.32E-04	−3.520	0.00E + 00
	c17823_c0_g1	K02717	Photosystem II oxygen-evolving enhancer protein 2	PsbP	0.196	2.66E-07	−0.052	4.41E-01	−3.598	3.68E-291
	c16649_c0_g1	K08901	Photosystem II oxygen-evolving enhancer protein 3	PsbQ	0.587	6.94E-43	0.028	7.71E-01	−3.889	7.78E-247
	c18753_c1_g2	K03541	Photosystem II 10 kDa protein	PsbR	0.028	5.36E-01	−0.467	2.38E-09	−2.686	1.44E-233
	c19487_c0_g1	K03542	Photosystem II 22 kDa protein	PsbS	−0.310	9.70E-02	−1.194	6.65E-14	0.626	4.83E-03
	c18171_c0_g1	K02723	Photosystem II PsbY protein	PsbY	1.049	8.29E-108	−0.358	3.63E-06	−3.184	6.70E-154
	c15459_c0_g1	K08902	Photosystem II Psb27 protein	Psb27	0.436	2.85E-11	−0.365	6.61E-06	−2.292	9.67E-76
	c19359_c6_g1	K08903	Photosystem II 13 kDa protein	Psb28	−0.959	2.20E-05	−1.892	1.42E-20	−5.144	7.84E-56
LHC	c19400_c0_g1	K08907	Light-harvesting complex I chlorophyll a/b binding protein 1	LHCA1	−2.329	0.00E + 00	−1.931	1.70E-184	−2.795	0.00E + 00
	c13244_c1_g1	K08908	Light-harvesting complex I chlorophyll a/b binding protein 2	LHCA2	−0.024	5.98E-01	0.287	1.86E-04	−3.787	0.00E + 00
	c14924_c0_g1	K08909	Light-harvesting complex I chlorophyll a/b binding protein 3	LHCA3	−0.046	2.99E-01	0.156	2.54E-02	−4.177	0.00E + 00
	c12657_c0_g1	K08910	Light-harvesting complex I chlorophyll a/b binding protein 4	LHCA4	0.177	6.58E-06	−0.044	5.73E-01	−4.682	0.00E + 00
	c13616_c0_g1	K08911	Light-harvesting complex I chlorophyll a/b binding protein 5	LHCA5	0.211	3.72E-09	0.064	4.39E-01	−3.896	0.00E + 00
	c19523_c4_g1	K08912	Light-harvesting complex II chlorophyll a/b binding protein 1	LHCB1	0.368	9.03E-20	0.330	1.94E-06	−3.863	0.00E + 00
	c19022_c2_g6	K08915	Light-harvesting complex II chlorophyll a/b binding protein 4	LHCB4	0.354	1.75E-19	−0.194	1.25E-02	−3.417	3.08E-209
	c12740_c0_g1	K08916	Light-harvesting complex II chlorophyll a/b binding protein 5	LHCB5	−0.285	1.08E-10	−0.009	9.30E-01	−4.435	0.00E + 00
ATPase	c12514_c0_g1	K02109	F-type H + -transporting ATPase subunit b	ATPF0B	−0.216	1.69E-07	−0.523	9.20E-16	−3.084	0.00E + 00
	c19297_c1_g1	K02113	F-type H + -transporting ATPase subunit delta	ATPF1D	−0.295	1.91E-12	−0.329	4.95E-07	−3.131	0.00E + 00
	c19650_c0_g1	K02115	F-type H + -transporting ATPase subunit gamma	ATPF1G	0.111	1.51E-02	−0.493	2.05E-12	−2.715	4.64E-186
b6f	c19562_c6_g4	K08906	Cytochrome c6	PetJ	−0.689	1.45E-07	−1.521	2.04E-27	−3.483	8.69E-31
	c16278_c0_g2	K02636	Cytochrome b6-f complex iron-sulfur subunit	PetC	0.452	8.79E-27	−0.220	2.59E-03	−2.793	2.66E-231

TABLE 2 | Comparative transcriptomic analysis of carotenoid biosynthesis for the heterotrophically -grown *S. acuminatus* cells subjected to the high light and N-limited conditions.

Gene_ID	KO_ID	Enzyme	Gene_name	6 h		12 h		24 h	
				Log_2FC	FDR	Log_2FC	FDR	Log_2FC	FDR
c4751_c0_g1	K00514	Zeta-carotene desaturase	ZDS	−1.663	1.72E-59	−1.134	2.13E-32	−1.669	1.18E-42
c5887_c0_g1	K02291	Phytoene synthase	PSY	−1.985	3.22E-30	−3.587	4.94E-104	−4.356	2.92E-75
c6666_c0_g1	K09839	Violaxanthin de-epoxidase	VDE	0.239	5.88E-02	0.089	6.17E-01	−1.587	1.70E-06
c6677_c0_g1	K09838	Zeaxanthin epoxidase	ZEP	0.247	2.96E-04	−0.606	6.36E-13	0.021	8.49E-01
c7062_c5_g1	K06444	Lycopene epsilon-cyclase	LCYE	−1.518	4.14E-15	−2.820	3.13E-40	−3.642	3.45E-14
c7246_c6_g1	K06443	Lycopene beta-cyclase	LCYB	−1.736	4.89E-09	−0.407	4.41E-02	−1.213	1.74E-04
c7438_c7_g1	K09836	Beta-carotene/zeaxanthin 4-ketolase	BKT	−1.105	2.42E-22	−1.203	4.71E-16	−0.049	8.33E-01
c7533_c5_g3	K09843	(+)-abscisic acid 8′-hydroxylase	CYP707A	−0.075	7.97E-01	1.086	1.96E-04	2.393	3.11E-10
c7684_c6_g6	K09843	(+)-abscisic acid 8′-hydroxylase	CYP707A	−0.989	5.48E-50	−0.738	2.81E-17	−0.239	6.21E-02
c7728_c5_g5	K15747	Beta-ring hydroxylase	CYP97A3	−1.097	1.36E-04	−1.876	4.64E-15	−3.293	2.94E-19
c7760_c4_g2	K09837	Carotenoid epsilon hydroxylase	CYP97C1	−2.136	3.69E-24	−2.080	4.15E-15	NA	NA
c7813_c9_g1	K15745	Phytoene desaturase (3,4-didehydrolycopene-forming)	PDS	−1.884	2.28E-12	−1.884	5.20E-07	NA	NA
c8132_c5_g1	K15746	Beta-carotene 3-hydroxylase	CHYB	0.287	3.37E-01	−2.342	1.29E-24	−3.858	2.42E-22
c8212_c6_g1	K15744	Zeta-carotene isomerase	ZISO	−2.038	1.65E-28	−0.906	4.31E-05	NA	NA
c8551_c2_g1	K02293	Phytoene desaturase	PDS	−1.271	7.44E-84	−0.757	1.42E-24	−2.526	2.40E-181

Log_2FC is Log2 Fold Change. Positive value means upregulated and negative value means downregulated, NA means without detected gene.

hydroxylase (CYP97C1), beta-carotene 3-hydroxylase (CHYB) and violaxanthin de-epoxidase (VDE) (**Table 2**). These results indicated the carotenoid biosynthesis of *S. acuminatus* was downregulated at the gene expression level during the trophic transition process, which was consistent with the carotenoid quantification results shown in **Figure 2B**. Because lutein, zeaxanthin, violaxanthin and neoxanthin are four main carotenoids of the xanthophyll cycle (Janik et al., 2016), the down-regulation of corresponding genes may also decrease xanthophyll cycle and finally generate lower NPQ, which was confirmed by the results achieved in **Figure 3B**.

Photosynthetic carbon fixation can provide energy and carbon skeletons for biosynthesis of macromolecules. Ribulose-1,5-bisphosphate carboxylase/oxygenase (RuBsiCO) catalyzes the addition of gaseous carbon dioxide to ribulose-1,5-bisphosphate (RuBP), generating two molecules of 3-phosphoglyceric acid, is the key enzyme involved in photosynthetic carbon fixation. The transcriptomics analysis revealed that two transcripts encoding RuBsiCO were differently expressed during trophic transition. One transcript (c8501_c0_g1) encoding the large subunit (rbcL) of RuBsiCO was downregulated by 1.95 and 1.65 times at 6 and 24 h, respectively. The transcript (c13567_c0_g1) encoding the small subunit (rbcS) of RuBsiCO was downregulated by 2.94 times at 24 h (**Supplementary Table 5**). Though downregulation of RuBsiCO under HL and NL may reduce the efficiency of Calvin cycle, the carbon assimilation in *S. acuminatus* cells CO_2 fixation may be compensated by other processes. Despite that RuBisCO is the main primary CO_2-fixing enzyme in algae and C3 plants, these organisms also possess a second enzyme, phosphoenolpyruvate carboxylase (PEPC) that can efficiently fix carbon as it catalyzes the reaction of CO_2 and phosphoenolpyruvic acid to produce oxaloacetic acid (Chen et al., 2002; Durall and Lindblad, 2015). The results showed that the genes (c13707_c0_g1, c48143_c0_g1) encoding PEPC was up-regulated at 6 and 12 h (**Supplementary Table 5**). Moreover, another key enzyme belonging to C4 and Crassulacean Acid Metabolism (CAM) pathways for carbon fixation, pyruvate orthophosphate dikinase (PPDK), was up-regulated significantly at three time-points at the transcript level (**Supplementary Table 5**).

The glycolysis/gluconeogenesis pathway, pentose phosphate pathway (PPP) and the tricarboxylic acid (TCA) cycle were the central metabolic pathways of carbon metabolism in microalgae (Fan et al., 2015; Fan et al., 2016; Lv et al., 2019). In this study, the changes in the transcripts belonging to the central carbon metabolism are listed in **Supplementary Table 6**. Based on the data, the transcriptional regulation on glycolysis/gluconeogenesis and TCA cycle was constructed in **Figure 6**. The results showed that most genes involved in glycolysis/gluconeogenesis were remarkably upregulated at 6 and 12 h, including those encoding hexokinase (HK), 6-phosphofructokinase-1 (PFK-1), phosphoglucomutase (PGM), enolase (ENO), pyruvate kinase (PK) and pyruvate orthophosphate dikinase (PPDK). Besides, acetyl-CoA synthetase (ACS), which catalyzes production acetyl-CoA from acetate, was also significantly upregulated at 6 and 12 h (**Supplementary Table 6**). As acetyl-CoA is a precursor in the glyoxylate cycle, TCA cycle, and fatty acid biosynthesis,

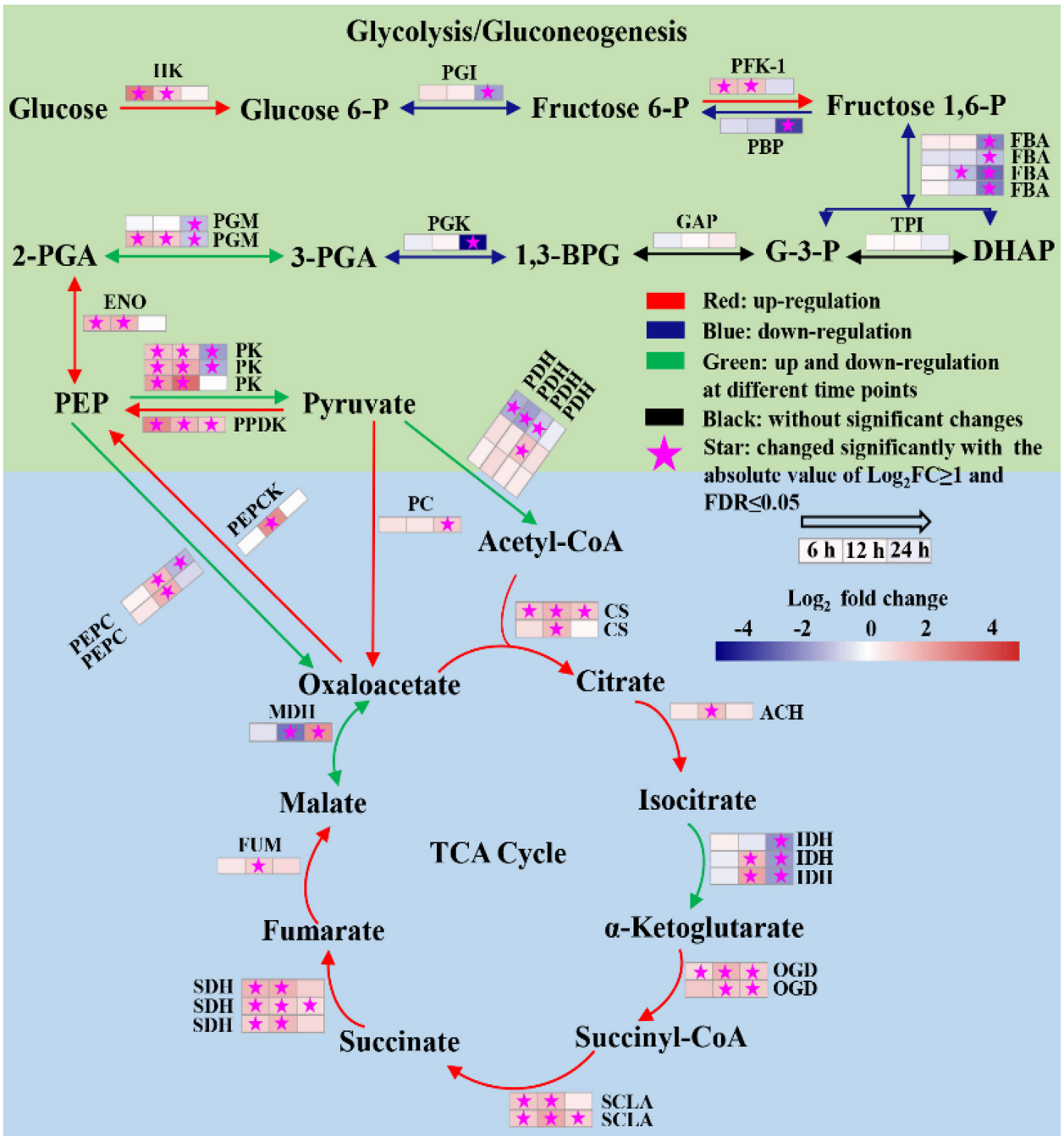

FIGURE 6 | Reconstructed glycolysis/gluconeogenesis and TCA cycle of heterotrophically grown *S. acuminatus* cells subjected to the high-light and N-limited conditions. Genes upregulated were indicated in red. Genes downregulated were indicated in blue. Genes upregulated and downregulated at different time points were indicated in green. No significant changes were indicated in black. The full names of the corresponding genes are given in **Supplementary Table 6**.

the upregulation of ACS may enhance the carbon flux in these pathways during the trophic transition process.

Tricarboxylic acid cycle produces NADH and FADH2 in aerobic organisms for carbon metabolism (Lv et al., 2019). As shown in **Figure 6**, most genes encoding key enzymes in TCA cycle were significantly upregulated at all three time points, including citrate synthase (CS), aconitate hydratase (ACH), 2-oxoglutarate dehydrogenase (OGDH), succinate dehydrogenase (SDHA), succinate dehydrogenase (SDH) and fumarate hydratase (FUM). It indicated that the TCA cycle was significantly enhanced of the heterotrophically grown *S. acuminatus* cells subjected to HL and NL. Besides, most

genes participated in electron transfer chains and oxidative phosphorylation were significantly upregulated at 6 and 12 h (**Supplementary Table 7**). Thus, NADH and FADH2 produced by TCA cycle could be used effectively through electron transfer chains and oxidative phosphorylation to form ATP. Therefore, enhanced TCA cycle and oxidative phosphorylation could be beneficial to produce reducing power and ATP for maintaining rapid growth of *S. acuminatus* cells during the trophic transition.

The elevated PPP activity was often induced by photooxidative stress and accompanied by the production of reactive oxygen species (ROS) (Zheng et al., 2017). Most enzymes in PPP were downregulated at the gene expression level at all three time points (**Supplementary Table 6**). In addition, it was observed that

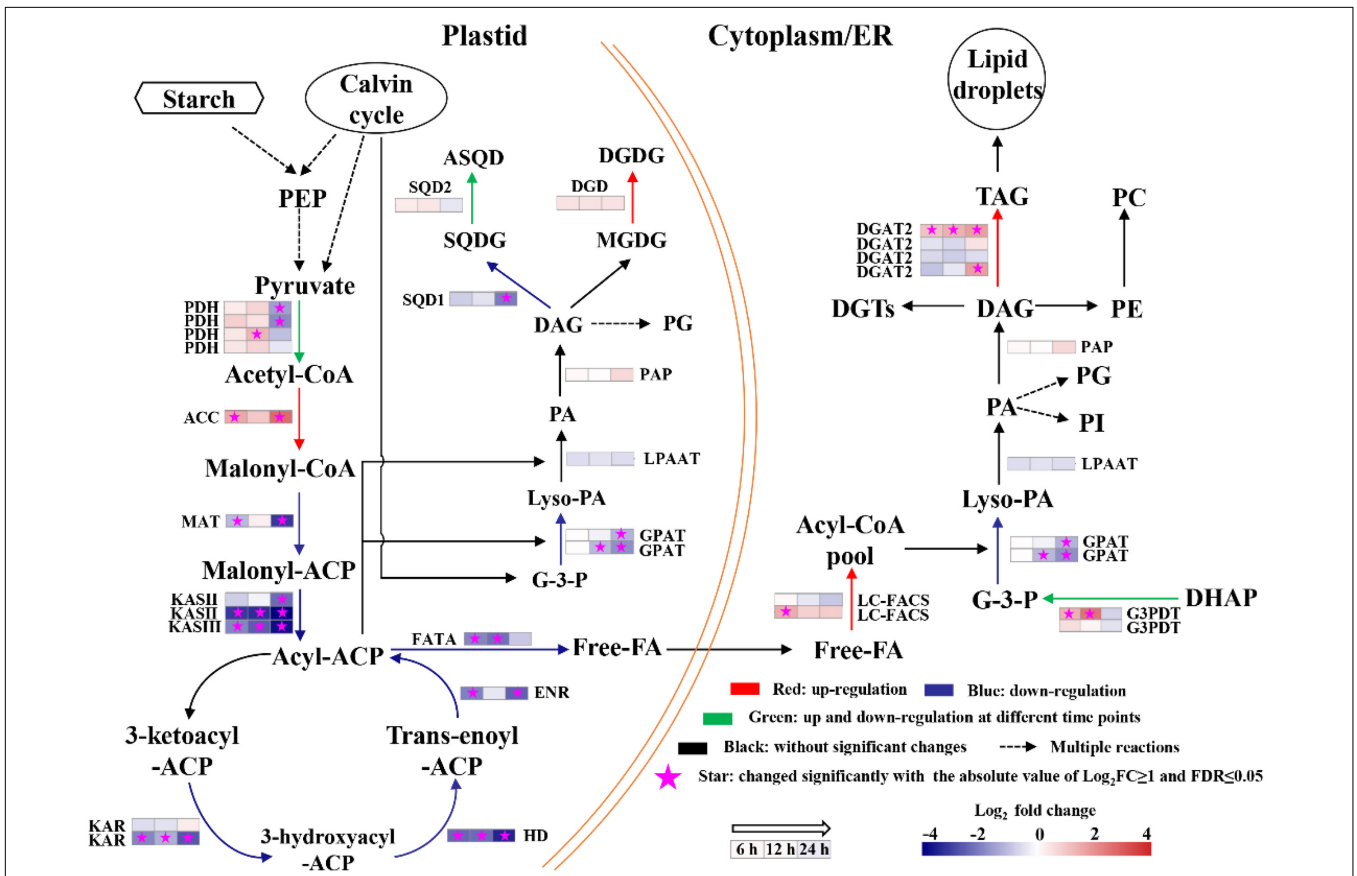

FIGURE 7 | Changes in transcript abundance of genes involved in fatty acids biosynthesis of heterotrophically grown *S. acuminatus* cells subjected to the high-light and N-limited conditions. Genes upregulated were indicated in red. Genes downregulated were indicated in blue. Genes upregulated and downregulated at different time points were indicated in green. No significant changes were indicated in black. The full names of the corresponding genes are given in **Supplementary Table 9**.

TABLE 3 | Changes in transcript expression of several genes related to very-long-chain fatty acids synthesis for the heterotrophically grown *S. acuminatus* cells subjected to the high-light and N-limited conditions.

Gene_ID	Enzyme	6 h		12 h		24 h	
		Log_2FC	FDR	Log_2FC	FDR	Log_2FC	FDR
c19395_c0_g1	3-ketoacyl-CoA synthase 6	2.670	0.00E + 00	−0.085	1.61E-01	0.901	5.74E-32
c19313_c4_g2	3-ketoacyl-CoA synthase 9	3.041	1.50E-119	0.114	1.76E-01	0.627	1.72E-06
c19313_c4_g12	3-ketoacyl-CoA synthase 1	2.602	2.17E-72	−0.197	1.99E-02	0.760	1.42E-06
c10824_c0_g1	3-ketoacyl-CoA synthase 11	2.226	3.94E-56	1.111	1.71E-39	1.774	1.10E-121
c37974_c0_g1	3-ketoacyl-CoA synthase 11	2.193	7.05E-32	1.064	4.83E-18	2.193	7.05E-32
c34341_c0_g1	3-ketoacyl-CoA synthase 19	2.088	2.59E-36	1.184	1.01E-32	2.015	3.74E-114
c19313_c4_g5	3-ketoacyl-CoA synthase 19	1.142	8.09E-07	2.145	2.58E-34	5.245	0.00E + 00
c11396_c1_g1	3-ketoacyl-CoA synthase 19	1.690	3.23E-06	2.423	8.14E-25	5.566	1.16E-267

Log_2FC is Log2 Fold Change. Positive value means upregulated and negative value means downregulated.

a number of antioxidant enzymes (i.e., glutathione peroxidase, catalase, iron-superoxide dismutase) encoding genes were downregulated during the trophic transition (**Supplementary Table 8**). Co-downregulation of the PPP and antioxidant enzymes suggested that no severe photodamage occurred in the algal cells during the trophic transition.

Fatty acid biosynthesis and glycerolipid biosynthesis pathways are responsible for converting the photosynthetically fixed carbon to triacylglycerols (TAGs) and membrane lipids. The transcriptomics data showed that although the gene encoding the acetyl-CoA carboxylase/biotin carboxylase (ACCase), which is the rate limiting enzyme of the fatty acid *de novo* biosynthesis pathway, was up-regulated at all three time points, whereas the other genes involved in fatty acid biosynthesis were significantly down-regulated (**Figure 7**). In addition, it was observed that the gene encoding digalactosyl diacylglycerol synthase (DGD), which catalyzes monogalactosyl diglyceride to digalactosyl diacylglycerol (DGDG), was up-regulated in the lipid biosynthesis pathway at 6, 12, and 24 h (**Supplementary Table 9**). DGDG is the main bilayer lipid of the thylakoid membranes of microalgae and plays an important role in maintaining the normal fluidity of thylakoid membrane (Sakurai et al., 2007). Therefore, the up-regulation of DGD may be beneficial to the reconstruction of photosynthetic membranes of *S. acuminatus* cells during the trophic transition. Besides, one copy of diacylglycerol acyltransferase 2 (DGAT2) was significantly upregulated at 6, 12, and 24 h (**Figure 7**). DGAT catalyzes the last step of triacylglycerol biosynthesis and its upregulation can enhance lipid production (Sharma and Chauhan, 2016). The identified DGAT encoding gene responsive to the trophic transition could be a target for genetic engineering to further increase the lipid production under the coupled heterotrophic and photoautotrophic cultivation mode. Such a limited number of DEGs were found to be involved in TAG assembly during the trophic transition process, reflecting unresponsive gene expression within the timeframe of this study. In addition, it is noteworthy that the expression patterns of most TAG assembly related genes are not correlated well with the TAG accumulation in microalgae, with the exception of a few copies of the DGAT genes (Blaby et al., 2013; Li et al., 2014). However, in *C. zofinginesis*, the expression of most genes responsible for TAG assembly, including those coding for glycerol-3-phosphate: acyl-CoA acyltransferase, lysophosphatidic acid: acyl-CoA acyltransferase, and phosphatidic acid phosphatase, are found to be congruent with TAG accumulation and degradation during the trophic transition process (Roth et al., 2019). Thus, responses of TAG biosynthesis during trophic transition remain to be an important area for future investigation. Moreover, TAG biosynthesis often accompanied by starch degradation in many microalgae (Wu et al., 2019). The transcriptomics data also showed that the genes encoding starch synthase were significantly downregulated at 24 h of cultivation (**Supplementary Table 10**), indicating the carbon fluxes were channeled to lipid synthesis. Besides, several genes involved in nitrogen metabolism were upregulated significantly at 24 h of cultivation, including nitrate/nitrite transporter, nitrate reductase [NAD(P)H], ferredoxin-nitrite reductase and glutamine synthetase (**Supplementary Table 11**), suggesting the nitrogen assimilation was enhanced in HC under stresses, which could provide precursors and energy for lipid biosynthesis.

Among the identified DEG, there were 8 very-long-chain fatty acid synthase encoding genes showing significant up-regulation at multiple time points from heterotrophy to photoautotrophy conditions (**Table 3**). Similar results were obtained from *C. zofinginesis*, of which 3 ketoacyl-CoA synthase encoding genes were significantly up-regulated when the algal cells were shifted from heterotrophy to photoautotrophy (Roth et al., 2019). Very-long-chain fatty acids are suggested to be the acyl groups of wax in many microalgae and land plants and to reduce the photodamage to cells under HL (Kondo et al., 2016; Rashidi and Trindade, 2018). However, it remains to be investigated whether *S. acuminatus* could synthesize wax under stress conditions in future studies.

CONCLUSION

In this study, we demonstrated that the heterotrophically grown *S. acuminatus* cells possessed the advantages over the photoautotrophically grown cells in terms of biomass and lipid production when subjected to HL and NL conditions. Under the stress conditions, the Fv/Fm and Y(II) of the heterotrophically grown cells were recovered to the maximum values after 24 h and were much higher than the photoautotrophically grown counterparts. Transcriptomic analysis revealed that heterotrophically grown cells fully expressed the photosystems encoding genes and the low concentration of glucose may stimulate the expression of a number of genes involved in photosynthesis. Moreover, regulation of a number of pathways involved in carbon metabolism was deduced to provide sufficient energy for sustaining vigorous growth of *S. acuminatus* cells under stresses. Enhanced lipid production may be attributable to the upregulation of ACCase and DGAT2 at the gene expression level. Our findings shed light on the mechanisms underlying the enhanced growth and lipid production in the algal cells during the trophic transition process.

DATA AVAILABILITY STATEMENT

The datasets presented in this study can be found in online repositories. The names of the repository/repositories and accession number(s) can be found below: https://www.ncbi.nlm.nih.gov/sra/PRJNA657679.

AUTHOR CONTRIBUTIONS

HZ performed most of the experiments, analyzed the data, and wrote the manuscript. LZ analyzed the transcriptomic data. YC, QX, and MW cultured heterotrophic seeds. MZ cultured

photoautotrophic seeds. DH and QH designed the experiments and wrote the manuscript. All authors contributed to the final approval of the article.

FUNDING

This work was supported by the State Development and Investment Corporation of China (IHB/CN/2014033), Natural Science Foundation of Hubei Province (Y53A 161Z01), and Chinese Academy of Sciences (ZDRW-ZS-2017).

ACKNOWLEDGMENTS

This project was supported by the Wuhan Branch, Supercomputing Center, Chinese Academy of Sciences, China.

SUPPLEMENTARY MATERIAL

The Supplementary Material for this article can be found online at: https://www.frontiersin.org/articles/10.3389/fbioe.2021.638726/full#supplementary-material

REFERENCES

Aziz, M. M. A., Kassim, K. A., Shokravi, Z., Jakarni, F. M., Liu, H. Y., Zaini, N., et al. (2020). Two-stage cultivation strategy for simultaneous increases in growth rate and lipid content of microalgae: a review. *Renew. Sust. Energ. Rev.* 119:109621. doi: 10.1016/j.rser.2019.109621

Bailleul, B., Rogato, A., de Martino, A., Coesel, S., Cardol, P., Bowler, C., et al. (2010). An atypical member of the light-harvesting complex stress-related protein family modulates diatom responses to light. *PNAS* 107, 18214–18219. doi: 10.1073/pnas.1007703107

Blaby, I. K., Glaesener, A. G., Mettler, T., Fitz-Gibbon, S. T., Gallaher, S. D., Liu, B., et al. (2013). Systems-level analysis of nitrogen starvation-induced modifications of carbon metabolism in a *Chlamydomonas reinhardtii* starchless mutant. *Plant Cell* 25, 4305–4323. doi: 10.1105/tpc.113.117580

Cazzaniga, S., Dall'Osto, L., Szaub, J., Scibilia, L., Ballottari, M., Purton, S., et al. (2014). Domestication of the green alga *Chlorella sorokiniana*: reduction of antenna size improves light-use efficiency in a photobioreactor. *Biotechnol. Biofuels* 7:157. doi: 10.1186/s13068-014-0157-z

Chen, C. Y., Lee, M. H., Dong, C. X., Leong, Y. K., and Chang, J. S. (2020). Enhanced production of microalgal lipids using a heterotrophic marine microalga *Thraustochytrium* sp. BM2. *Biochem. Eng. J.* 154:107429. doi: 10.1016/j.bej.2019.107429

Chen, J., Yang, X., Huang, X., Duan, S., Long, C., Chen, J., et al. (2017). Leaf transcriptome analysis of a subtropical evergreen broadleaf plant, wild oil-tea camellia (*Camellia oleifera*), revealing candidate genes for cold acclimation. *BMC Genom.* 18:211. doi: 10.1186/s12864-017-3570-4

Chen, L., Omiya, T., Hata, S., and Izui, K. (2002). Molecular characterization of a phosphoenolpyruvate carboxylase from a thermophilic cyanobacterium, *Synechococcus vulcanus* with unusual allosteric properties. *Plant Cell Physiol.* 43, 159–169. doi: 10.1093/pcp/pcf019

Correa-Galvis, V., Redekop, P., Guan, K., Griess, A., Truong, T. B., Wakao, S., et al. (2016). Photosystem II subunit PsbS is involved in the induction of LHCSR protein-dependent energy dissipation in *Chlamydomonas reinhardtii*. *J. Biol. Chem.* 291, 17478–17487. doi: 10.1074/jbc.M116.737312

Durall, C., and Lindblad, P. (2015). Mechanisms of carbon fixation and engineering for increased carbon fixation in cyanobacteria. *Algal Res.* 11, 263–270. doi: 10.1016/j.algal.2015.07.002

Fan, J., Ning, K., Zeng, X., Luo, Y., Wang, D., Hu, J., et al. (2015). Genomic foundation of starch-to-lipid switch in oleaginous *Chlorella* spp. *Plant Physiol.* 169, 2444–2461. doi: 10.1104/pp.15.01174

Fan, J., Xu, H., and Li, Y. (2016). Transcriptome-based global analysis of gene expression in response to carbon dioxide deprivation in the green algae *Chlorella pyrenoidosa*. *Algal Res.* 16, 12–19. doi: 10.1016/j.algal.2016.02.032

Gao, C., Wang, Y., Shen, Y., Yan, D., He, X., Dai, J., et al. (2014). Oil accumulation mechanisms of the oleaginous microalga *Chlorella protothecoides* revealed through its genome, transcriptomes, and proteomes. *BMC Genomics* 15:582. doi: 10.1186/1471-2164-15-582

Genty, B., Briantais, J. M., and Baker, N. R. (1989). The relationship between the quantum yield of photosynthetic electron transport and quenching of chlorophyll fluorescence. *BBA* 990, 87–92. doi: 10.1016/s0304-4165(89)80016-9

Gerotto, C., Franchin, C., Arrigoni, G., and Morosinotto, T. (2015). In vivo identification of photosystem II light harvesting complexes interacting with photosystem II subunits. *Plant Physiol.* 168, 1747–1761. doi: 10.1104/pp.15.00361

Grabherr, M. G., Haas, B. J., Moran, Y., Levin, J. Z., Thompson, D. A., Amit, I., et al. (2011). Full-length transcriptome assembly from RNA-Seq data without a reference genome. *Nat. Biotechnol.* 29, 644–652. doi: 10.1038/nbt.1883

Han, F., Huang, J., Li, Y., Wang, W., Wang, J., Fan, J., et al. (2012). Enhancement of microalgal biomass and lipid productivities by a model of photoautotrophic culture with heterotrophic cells as seed. *Bioresour. Technol.* 118, 431–437. doi: 10.1016/j.biortech.2012.05.066

He, Q., Yang, H., Wu, L., and Hu, C. (2015). Effect of light intensity on physiological changes, carbon allocation and neutral lipid accumulation in oleaginous microalgae. *Bioresour. Technol.* 191, 219–228. doi: 10.1016/j.biortech.2015.05.021

Huang, L., Gao, B., Wu, M., Wang, F., and Zhang, C. (2019). Comparative transcriptome analysis of a long-time span two-step culture process reveals a potential mechanism for astaxanthin and biomass hyper-accumulation in *Haematococcus pluvialis* JNU35. *Biotechnol. Biofuels* 12:18. doi: 10.1186/s13068-019-1355-5

Janik, E., Bednarska, J., Zubik, M., Sowinski, K., Luchowski, R., Grudzinski, W., et al. (2016). The xanthophyll cycle pigments, violaxanthin and zeaxanthin, modulate molecular organization of the photosynthetic antenna complex LHCII. *Arch. Biochem. Biophys.* 592, 1–9. doi: 10.1016/j.abb.2016.01.003

Jia, J., Han, D., Gerken, H. G., Li, Y., Sommerfeld, M., Hu, Q., et al. (2015). Molecular mechanisms for photosynthetic carbon partitioning into storage neutral lipids in *Nannochloropsis oceanica* under nitrogen-depletion conditions. *Algal Res.* 7, 66–77. doi: 10.1016/j.algal.2014.11.005

Jin, H., Zhang, H., Zhou, Z., Li, K., Hou, G., Xu, Q., et al. (2020). Ultrahigh-cell-density heterotrophic cultivation of the unicellular green microalga *Scenedesmus acuminatus* and application of the cells to photoautotrophic culture enhance biomass and lipid production. *Biotechnol. Bioeng.* 117, 96–108. doi: 10.1002/bit.27190

Kondo, S., Hori, K., Sasaki-sekimoto, Y., Kobayashi, A., Kato, T., Yuno-Ohta, N., et al. (2016). Primitive extracellular lipid components on the surface of the charophytic alga *Klebsormidium flaccidum* and their possible biosynthetic pathways as deduced from the genome sequence. *Front. Plant Sci.* 7:952. doi: 10.3389/fpls.2016.00952

Li, B., and Dewey, C. N. (2011). RSEM: accurate transcript quantification from RNA-Seq data with or without a reference genome. *BMC Bioinformatics* 12:323. doi: 10.1186/1471-2105-12-323

Li, J., Han, D., Wang, D., Ning, K., Jia, J., Wei, L., et al. (2014). Choreography of transcriptomes and lipidomes of *Nannochloropsis* reveals the mechanisms of oil synthesis in microalgae. *Plant Cell* 26, 1645–1665. doi: 10.1105/tpc.113.121418

Li, L., Aro, E. M., and Millar, A. H. (2018). Mechanisms of photodamage and protein turnover in photoinhibition. *Trends Plant Sci.* 23, 667–676. doi: 10.1016/j.tplants.2018.05.004

Li, X., Yuan, Y., Cheng, D., Gao, J., Kong, L., Zhao, Q., et al. (2018). Exploring stress tolerance mechanism of evolved freshwater strain *Chlorella* sp. S30

under 30g/L salt. *Bioresour. Technol.* 250, 495–504. doi: 10.1016/j.biortech.2017.11.072

Li-Beisson, Y., Beisson, F., and Riekhof, W. (2015). Metabolism of acyl-lipids in *Chlamydomonas reinhardtii*. *Plant J.* 82, 504–522. doi: 10.1111/tpj.12787

Lv, J., Zhao, F., Feng, J., Liu, Q., Nan, F., Liu, X., et al. (2019). Transcriptomic analysis reveals the mechanism on the response of *Chlorococcum* sp. GD to glucose concentration in mixotrophic cultivation. *Bioresour. Technol.* 288:121568. doi: 10.1016/j.biortech.2019.121568

Ma, M., Yuan, D., He, Y., Park, M., Gong, Y., and Hu, Q. (2017). Effective control of *Poterioochromonas malhamensis* in pilot-scale culture of *Chlorella sorokiniana* GT-1 by maintaining CO_2 -mediated low culture pH. *Algal Res.* 26, 436–444. doi: 10.1016/j.algal.2017.06.023

Maxwell, K., and Johnson, G. N. (2000). Chlorophyll fluorescence—a practical guide. *J. Exp. Bot.* 51, 659–668. doi: 10.1093/jexbot/51.345.659

Melis, A. (2009). Solar energy conversion efficiencies in photosynthesis: minimizing the chlorophyll antennae to maximize efficiency. *Plant Sci.* 177, 272–280. doi: 10.1016/j.plantsci.2009.06.005

Nascimento, I. A., Marques, S. S. I., Cabanelas, I. T. D., Pereira, S. A., Druzian, J. I., de Souza, C. O., et al. (2013). Screening microalgae strains for biodiesel production: lipid productivity and estimation of fuel quality based on fatty acids profiles as selective criteria. *Bioenerg. Res.* 6, 1–13. doi: 10.1007/s12155-012-9222-2

Nelson, N., and Ben-Shem, A. (2004). The complex architecture of oxygenic photosynthesis. *Nat. Rev. Mol. Cell Biol.* 5, 971–982. doi: 10.1038/nrm1525

Parkhill, J. P., Maillet, G., and Cullen, J. J. (2010). Fluorescence-based maximal quantum yield for PSII as a diagnostic of nutrient stress. *J. Phycol.* 37, 517–529. doi: 10.1046/j.1529-8817.2001.037004517.x

Peers, G., Truong, T. B., Ostendorf, E., Busch, A., Elrad, D., Grossman, A. R., et al. (2009). An ancient light-harvesting protein is critical for the regulation of algal photosynthesis. *Nature* 462, 518–521. doi: 10.1038/nature08587

Rashidi, B., and Trindade, L. M. (2018). Detailed biochemical and morphologic characteristics of the green microalga *Neochloris oleoabundans* cell wall. *Algal Res.* 35, 152–159. doi: 10.1016/j.algal.2018.08.033

Rippka, R., Deruelles, J., Waterbury, J. B., Herdman, M., and Stanier, R. Y. (1979). Generic assignments, strain histories and properties of pure cultures of cyanobacteria. *J. Microbiol.* 111, 1–61. doi: 10.1099/00221287-111-1-1

Roth, M. S., Gallaher, S. D., Westcott, D. J., Iwai, M., Louie, K. B., Mueller, M., et al. (2019). Regulation of oxygenic photosynthesis during trophic transitions in the green alga *Chromochloris zofingiensis*. *Plant Cell* 31, 579–601. doi: 10.1105/tpc.18.00742

Ruban, A. V., Johnson, M. P., and Duffy, C. D. P. (2012). The photoprotective molecular switch in the photosystem II antenna. *BBA* 1817, 167–181. doi: 10.1016/j.bbabio.2011.04.007

Sajjadi, B., Chen, W. Y., Raman, A. A. A., and Ibrahim, A. (2018). Microalgae lipid and biomass for biofuel production: a comprehensive review on lipid enhancement strategies and their effects on fatty acid composition. *Renew. Sust. Energ. Rev.* 97, 200–232. doi: 10.1016/j.rser.2018.07.050

Sakurai, I., Mizusawa, N., Wada, H., and Sato, N. (2007). Digalactosyldiacylglycerol is required for stabilization of the oxygen-evolving complex in photosystem II. *Plant Physiol.* 145, 1361–1370.doi: 10.1104/pp.107.106781

Sharma, T., and Chauhan, R. S. (2016). Comparative transcriptomics reveals molecular components associated with differential lipid accumulation between microalgal sp., *Scenedesmus dimorphus* and *Scenedesmus quadricauda*. *Algal Res.* 19, 109–122. doi: 10.1016/j.algal.2016.07.020

Simao, F. A., Waterhouse, R. M., Ioannidis, P., Kriventseva, E. V., and Zdobnov, E. M. (2015). BUSCO: assessing genome assembly and annotation completeness with single-copy orthologs. *Bioinformatics* 31, 3210–3212. doi: 10.1093/bioinformatics/btv351

Su, Y., Song, K., Zhang, P., Su, Y., Cheng, J., and Chen, X. (2017). Progress of microalgae biofuel's commercialization. *Renew. Sust. Energ. Rev.* 74, 402–411. doi: 10.1016/j.rser.2016.12.078

Sun, Z., Zhang, Y., Sun, L. P., and Liu, J. (2019). Light elicits astaxanthin biosynthesis and accumulation in the fermented ultrahigh-density *Chlorella zofinginesis*. *J. Agric. Food Chem.* 67, 5579–5586. doi: 10.1021/acs.jafc.9b01176

Talebi, A. F., Mohtashami, S. K., Tabatabaei, M., Tohidfar, M., Bagheri, A., Zeinalabedini, M., et al. (2013). Fatty acids profiling: a selective criterion for screening microalgae strains for biodiesel production. *Algal Res.* 2, 258–267. doi: 10.1016/j.algal.2013.04.003

Tang, D. Y. Y., Khoo, K. S., Chew, K. W., Tao, Y., Ho, S. H., and Show, P. L. (2020). Potential utilization of bioproducts from microalgae for the quality enhancement of natural products. *Bioresour. Technol.* 304:122997. doi: 10.1016/j.biortech.2020.122997

Wan, M., Zhang, Z., Wang, J., Huang, J., Fan, J., Yu, A., et al. (2015). Sequential Heterotrophy–Dilution–Photoinduction Cultivation of *Haematococcus pluvialis* for efficient production of astaxanthin. *Bioresour. Technol.* 198, 557–563. doi: 10.1016/j.biortech.2015.09.031

Wan, M., Zhang, Z., Wang, R., Bai, W., Huang, J., Wang, W., et al. (2019). High-yield cultivation of *Botryococcus braunii* for biomass and hydrocarbons. *Biomass Bioenerg.* 131:105399. doi: 10.1016/j.biombioe.2019.105399

Ware, M. A., Giovagnetti, V., Belgio, E., and Ruban, A. V. (2015). PsbS protein modulates non-photochemical chlorophyll fluorescence quenching in membranes depleted of photosystems. *J. Photoch. Photobio B* 152, 301–307. doi: 10.1016/j.jphotobiol.2015.07.016

Wen, X., Du, K., Wang, Z., Peng, X., Luo, L., Tao, H., et al. (2016). Effective cultivation of microalgae for biofuel production: a pilot-scale evaluation of a novel oleaginous microalga *Graesiella* sp. WBG-1. *Biotechnol. Biofuels* 9:123. doi: 10.1186/s13068-016-0541-y

Wu, H., Abasova, L., Cheregi, O., Deak, Z., Gao, K., and Vass, I. (2011). D1 protein turnover is involved in protection of Photosystem II against UV-B induced damage in the cyanobacterium *Arthrospira* (*Spirulina*) platensis. *J. Photochem. Photobiol. B* 104, 320–325. doi: 10.1016/j.jphotobiol.2011.01.004

Wu, M., Zhang, H., Sun, W., Li, Y., Hu, Q., Zhou, H., et al. (2019). Metabolic plasticity of the starchless mutant of *Chlorella sorokiniana* and mechanisms underlying its enhanced lipid production revealed by comparative metabolomics analysis. *Algal Res.* 42:101587. doi: 10.1016/j.algal.2019.101587

Xia, L., Yang, H., He, Q., and Hu, C. (2014). Physiological responses of freshwater oleaginous microalgae *Desmodesmus* sp. NMX451 under nitrogen deficiency and alkaline pH-induced lipid accumulation. *J. Appl. Phycol.* 27, 649–659. doi: 10.1007/s10811-014-0371-x

Xiong, W., Gao, C., Yan, D., Wu, C., and Wu, Q. (2010). Double CO_2 fixation in photosynthesis-fermentation model enhances algal lipid synthesis for biodiesel production. *Bioresour. Technol.* 101, 2287–2293. doi: 10.1016/j.biortech.2009.11.041

Yang, H., He, Q., and Hu, C. (2018). Feasibility of biodiesel production and CO_2 emission reduction by *Monoraphidium dybowskii* LB50 under semi-continuous culture with open raceway ponds in the desert area. *Biotechnol. Biofuels* 11:82. doi: 10.1186/s13068-018-1068-1

Yin, Z., Zhu, L., Li, S., Hu, T., Chu, R., Mo, F., et al. (2020). A comprehensive review on cultivation and harvesting of microalgae for biodiesel production: environmental pollution control and future directions. *Bioresour. Technol.* 301:122804. doi: 10.1016/j.biortech.2020.122804

Zhang, Y., Wu, H., Sun, M., Peng, Q., and Li, A. (2018). Photosynthetic physiological performance and proteomic profiling of the oleaginous algae *Scenedesmus acuminatus* reveal the mechanism of lipid accumulation under low and high nitrogen supplies. *Photosynth. Res.* 138, 73–102. doi: 10.1007/s11120-018-0549-1

Zhang, Y., Wu, H., Yuan, C., Li, T., and Li, A. (2019). Growth, biochemical composition, and photosynthetic performance of *Scenedesmus acuminatus* during nitrogen starvation and resupply. *J. Appl. Phycol.* 31, 2797–2809. doi: 10.1007/s10811-019-01783-z

Zhang, Z., Wang, B., Hu, Q., Sommerfeld, M., Li, Y., and Han, D. (2016). A new paradigm for producing astaxanthin from the unicellular green alga *Haematococcus pluvialis*. *Biotechnol. Bioeng.* 113, 2088–2099. doi: 10.1002/bit.25976

Zheng, Y., Li, T., Yu, X., Bates, P. D., Dong, T., and Chen, S. (2013). High-density fed-batch culture of a thermotolerant microalga *Chlorella sorokiniana* for biofuel production. *Appl. Energy* 108, 281–287. doi: 10.1016/j.apenergy.2013.02.059

Zheng, Z., Gao, S., He, Y., Li, Z., Li, Y., Cai, X., et al. (2017). The enhancement of the oxidative pentose phosphate pathway maybe

involved in resolving imbalance between photosystem I and II in *Dunaliella salina*. *Algal Res.* 26, 402–408. doi: 10.1016/j.algal.2017.07.024

Conflict of Interest: The authors declare that the research was conducted in the absence of any commercial or financial relationships that could be construed as a potential conflict of interest.

frontiers in Bioengineering and Biotechnology

ORIGINAL RESEARCH
published: 20 July 2021
doi: 10.3389/fbioe.2021.662655

Metabolic Responses of a Model Green Microalga *Euglena gracilis* to Different Environmental Stresses

Jiayi He[1,2], *ChenChen Liu*[1], *Mengzhe Du*[3], *Xiyi Zhou*[1], *Zhangli Hu*[1,2], *Anping Lei*[1] *and Jiangxin Wang*[1]*

[1] *Shenzhen Key Laboratory of Marine Bioresources and Eco-environmental Science, Shenzhen Engineering Laboratory for Marine Algal Biotechnology, Guangdong Provincial Key Laboratory for Plant Epigenetics, College of Life Sciences and Oceanography, Shenzhen University, Shenzhen, China,* [2] *Key Laboratory of Optoelectronic Devices and Systems of Ministry of Education and Guangdong Province, College of Physics and Optoelectronic Engineering, Shenzhen University, Shenzhen, China,* [3] *College of Chemistry and Environmental Engineering, Shenzhen University, Shenzhen, China*

Euglena gracilis, a green microalga known as a potential candidate for jet fuel producers and new functional food resources, is highly tolerant to antibiotics, heavy metals, and other environmental stresses. Its cells contain many high-value products, including vitamins, amino acids, pigments, unsaturated fatty acids, and carbohydrate paramylon as metabolites, which change contents in response to various extracellular environments. However, mechanism insights into the cellular metabolic response of *Euglena* to different toxic chemicals and adverse environmental stresses were very limited. We extensively investigated the changes of cell biomass, pigments, lipids, and paramylon of *E. gracilis* under several environmental stresses, such as heavy metal $CdCl_2$, antibiotics paromomycin, and nutrient deprivation. In addition, global metabolomics by Ultra-high-performance liquid chromatography tandem mass spectrometry (UHPLC–MS/MS) was applied to study other metabolites and potential regulatory mechanisms behind the differential accumulation of major high-valued metabolites. This study collects a comprehensive update on the biology of *E. gracilis* for various metabolic responses to stress conditions, and it will be of great value for *Euglena* cultivation and high-value metabolite production.

Keywords: *Euglena*, metabolomics, antibiotics, heavy metals, nutrient deprivation, environmental stresses

OPEN ACCESS

Edited by:
Wei Xiong,
National Renewable Energy Laboratory (DOE), United States

Reviewed by:
Changhong Yao,
Sichuan University, China
Koji Yamada,
Euglena Co Ltd., Japan

***Correspondence:**
Jiangxin Wang
jxwang@szu.edu.cn

Specialty section:
This article was submitted to Bioprocess Engineering, a section of the journal Frontiers in Bioengineering and Biotechnology

Received: *01 February 2021*
Accepted: *10 June 2021*
Published: *20 July 2021*

Citation:
He J, Liu C, Du M, Zhou X, Hu Z, Lei A and Wang J (2021) Metabolic Responses of a Model Green Microalga Euglena gracilis to Different Environmental Stresses. Front. Bioeng. Biotechnol. 9:662655. doi: 10.3389/fbioe.2021.662655

INTRODUCTION

Euglena gracilis, which began to appear 500 million years ago, is a species of unicellular organisms that live mostly in freshwater (Goto and Beneragama, 2010) and has no cell walls, giving it dual characteristics of plants and animals, which enable this microalga to adopt photosynthetic, heterotrophic, and mixotrophic conditions during long-term evolution (Edmunds, 1965; Zakryś et al., 2017). During this long evolution, *Euglena* became a highly adaptable microorganism that survived diverse and extreme conditions on the earth, such as high UV radiation, acid mine water, man-made antibiotics, heavy metal pollution, and nutrient deprivation (Ferreira et al., 2007; Moreno-Sánchez et al., 2017).

Among microalgae, *E. gracilis* is well-known as a producer of polyunsaturated fatty acids (PUFAs) (Schwarzhans et al., 2015), vitamin E (Takeyama et al., 2015), chlorophyll a and b, several types of carotenoid pigments (Tanno et al., 2020), and polysaccharose paramylon (β-1,3-glucan) (Ivusic and Santek, 2015). Nitrogen deficiency (as nitrogen deprivation, N–) is one of the most common environmental stresses to enhance lipid (biofuels) accumulation in microalgae (Peccia et al., 2013). An increase of total lipids in stationary growth phase cells in comparison to exponential growth phase cells in N deprived, mixotrophic *E. gracilis* cultures had been reported (Regnault et al., 1990). And a decrease in chlorophyll production by *E. gracilis* was observed during a short-term exposure to N– (García-Ferris et al., 1996). A long-term N limitation on lipid, protein, and pigment production of *E. gracilis* in photoheterotrophic cultures indicated that N– could increase total fatty acid production, with lower protein contents and pigment production (Tossavainen et al., 2019). The symptoms of N deficiency are well-documented, but the underlying molecular mechanisms are largely unknown in microalgae (Tossavainen et al., 2019).

Euglena gracilis is a highly promising group of microorganisms to be used in the bio-remediation of heavy metal-polluted aerobic and anaerobic acidic aquatic environments. Considering the current data and the fact that *E. gracilis* has an innate tolerance to relatively high concentrations of heavy metals, as demonstrated by the minimum inhibitory concentrations (MICs) obtained, that is, $CdCl_2$ (50 μM) induced diminution in cell growth (Castro-Guerrero et al., 2008) this organism has the potential for the management of particular heavy metal contamination of the environment (Khatiwada et al., 2020). In *E. gracilis*, $CdCl_2$ exposure can induce morphological alteration, linked to reactive oxygen stress (Watanabe and Suzuki, 2002). So far, the connection between Cd, paramylon, and lipid accumulation in *E. gracilis* is still unclear.

Euglena gracilis was reported to be highly tolerant to various antibiotics (Shao et al., 2018). When bacteria and other microalgal cells were significantly inhibited by antibiotics at the low concentration of 20–50 μg/ml (50 μg/ml Kanamycin *Chlamydomonas*; Bateman and Purton, 2000), *E. gracilis* cells still grew well. In *Euglena*, rapamycin induced the reduction of chlorophyll and the accumulation of neutral lipids without deterring its cell proliferation. In another green microalga of *Chlamydomonas*, however, rapamycin induced serious growth inhibition as reported elsewhere (Mukaida et al., 2016). Various antibiotics were used to bleach *Euglena* with concentrations as high as 200 μg/ml (Ebringer, 1964). Based on our preliminary experiments, paromomycin (PRM) could not inhibit *E. gracilis* cell growth at concentrations ranging from 10 to 50 μg/ml. Since streptomycin significantly bleached *Euglena* cells by deleting part of the chloroplast genome, we did not choose streptomycin for further investigation in this study. Currently, no report of PRM against *E. gracilis* has been listed, and the antibiotic resistance mechanism of *E. gracilis* is still unclear.

The research on different high-value metabolites and their potential control mechanisms under various environmental stresses are especially important and interesting. However, because of the absence of a high-dimension genome of *E. gracilis* (Ebenezer et al., 2017) and with limited previous OMICS studies, there is no definite conclusion on molecular mechanisms involved in responses to different environmental stresses.

With the advent of the post-genome era, various OMICS technologies, such as proteomics and metabolomics, appeared one after the other, in which metabolomics was the first to develop and the most widely applied technology (Johnson et al., 2016). Metabolomics has been an important branch of system biology in recent years. It can help to understand the biological process more directly and effectively, and the study of metabolites can also help to analyze complex sample traits (Johnson et al., 2016). We used the metabolomic approach to investigate the effects of different inoculum sizes on a green microalga *Chlorella* growth (Lu et al., 2012), salt stress in a model cyanobacterium (Wang et al., 2014), astaxanthin induction in *Haematococcus* (Su et al., 2014), antioxidant butylated hydroxyanisole on lipid accumulation in *Crypthecodinium cohnii* (Sui et al., 2014), and obtaining better understanding on the metabolic response mechanism of microalgae with different environments.

In this study, we explored global metabolomics to analyze metabolite changes under various conditions in *E. gracilis* for the first time, that is, heavy metals, antibiotics, and nutrient deficiency, to explore the mechanism of tolerance, acclimatization, and high-value product accumulations. The results show that pigments, lipids, and carbohydrates (paramylon) can be altered significantly under different stresses. Further, comparative metabolomics revealed some common and unique metabolic pathways and modules regulated by all selected stresses and individual stress, respectively.

MATERIALS AND METHODS

Strains and Culture Conditions

Euglena gracilis CCAP 224/5Z was obtained from the Culture Collection of Algae and Protozoa (https://www.ccap.ac.uk/). The microalgal cells were grown in the EM medium [1.8 g/L NH_4Cl, 0.6 g/L KH_2PO_4, 0.6 g/L $MgSO_4$, 60 mg/L urea, 0.02 g/L $CaCl_2$, 0.48 mg/L Na_2EDTA, 2 mg/L $Fe_2(SO_4)_3$, 60 μl HCl, 0.01 mg/L Vb_1, 0.0005 mg/L Vb_{12}, 20 mg/L $CuSO_4{\cdot}5H_2O$, 0.4 g/L $ZnSO_4{\cdot}7H_2O$, 1.3 g/L $Co(NH_3){\cdot}H_2O$, and 1.6 g/L $MnCl_2{\cdot}4H_2O$] in 6 ml culture volumes of a 6-well plate under a light intensity of ∼100 μmol/m^2/s in an illuminating incubator without shaking at 26°C until microalgal cells reached the stationary phase (Afiukwa and Ogbonna, 2007; Yanming et al., 2018).

Cultivation and Stress Treatments

Euglena gracilis cells were cultured for 6 days in the EM medium (10 ml EtOH in 100 ml EM medium), then 1×10^6 cells/ml were centrifuged at 5,000 × *g* for 3 min and transferred into an equal

Abbreviations: ARA, arachidonic acid; CAM, Crassulacean acid metabolism; CoA, coenzyme A; *E. gracilis*, *Eugleaa gracilis*; KEGG, Kyoto Encyclopedia of Genes and Genomes; OPLS-DA, orthogonal projections to latent structures discriminant analysis; PCA, principal component analysis; PE, phosphatidylethanolamine; PRM, paromomycin; PUFAs, polyunsaturated fatty acids; ROS, reactive oxygen species; VIP, variable importance in projection.

volume of the EM medium as the 1:10 dilution was applied to each treatment well in a 12-well plate. Treatments were applied, including supplementation with PRM (25 μg/ml), $CdCl_2$ (Cd) (0.5 mM), or nitrogen deprivation (N–) (without NH_4Cl nor urea). After 6 days, stationary phase cell samples were collected and used for future experiments.

Cell Growth, Chlorophyll, Paramylon, and Total Lipids

Cell growth was measured by counting cell numbers with a microscope in a 0.1-ml counting chamber. The total algal chlorophyll was extracted with 95% ethanol, and the content was spectrophotometrically assayed according to the method (Harris, 2009; Smith, 2009). The paramylon of 5×10^7-10^8 cells was extracted and measured as described previously (Sugiyama et al., 2009; Nakazawa et al., 2017; Guo et al., 2020). The total lipids of 10^7-10^8 cells were measured using the oven-drying method (Yang et al., 2018).

UHPLC–MS/MS Metabolite Analysis

For the LC–MS/MS analysis, samples took after 6 days of incubation were first centrifuged at 5,000 × *g* for 5 min at 4°C to harvest ∼10^6-10^7 cells. Metabolite extraction was followed as per previously reported protocol (Zhang et al., 2020). Cell pellets were then transported to a 1.5-ml Eppendorf microcentrifuge tube (Hamburg, Germany). After adding 1,000 μl extract solvent (acetonitrile:methanol:water, 2:2:1, containing internal standard), the samples were vortexed for 30 s using a XW-80A vortex mixer (Kylin-Bell Lab Instruments Co., Ltd., Haimen, China), homogenized at 45 Hz for 4 min using a tissue grinding machine (JXFSTPRP-24, Shanghai Jingxin Industrial Development Co., Ltd., Shanghai, China), and sonicated for 5 min in an ice-water bath using an ultrasonic cell-crushing device (Fangao Microelectronics Co., Ltd., Shenzhen, China). The homogenate and sonicate circle was repeated three times, followed by incubation at −20°C for 1 h and centrifugation at 12,000 rpm 4°C for 15 min. The LC–MS/MS analyses were performed using a ultra-high-performance liquid chromatography (UHPLC) system (1290, Agilent Technologies, Waldbronn, Germany) with a UPLC HSS T3 column (2.1 mm × 100 mm, 1.8 μm) coupled to Q Exactive mass spectrometer (Orbitrap MS, Thermo Fisher Scientific, San Jose, CA, USA). Mobile phase A was 0.1% formic acid in water for positive mode, and 5 mmol/L ammonium acetate in water for negative mode, and the mobile phase B was acetonitrile. The elution gradient was set as follows: 0–1.0 min, 1% B; 1.0–8.0 min, 1–99% B; 8.0–10.0 min, 99% B; 10.0–10.1 min, 99–1% B; 10.1–12 min, 1% B. The flow rate was 0.5 ml/min. The injected volume was 2 μl. QE mass spectrometer was used for its ability to acquire MS/MS spectra information-dependent acquisition (IDA) mode in the control of the acquisition software (Xcalibur 4.0.27, Thermo Fisher Scientific, San Jose, CA, USA). In this mode, the acquisition software continuously evaluates the full-scan MS spectrum. The electrospray ionization (ESI) source conditions were set as following: sheath gas flow rate as 45 arb, Aux gas flow rate as 15 arb, capillary temperature 400°C, full MS resolution as 70,000, MS/MS resolution as 17,500, collision energy as 20/40/60 eV in normalized collision energy (NCE) mode and spray voltage as 4.0 kV (positive) or −3.6 kV (negative), respectively (Periannan, 2003).

Compound identification from a non-targeted metabolite database were converted to the mzXML format using ProteoWizard and processed with an in-house program, which was developed using R and based on XCMS, for peak detection, extraction, alignment, and integration. Then an in-house MS2 database (BiotreeDB) was applied in metabolite annotation. The cutoff for annotation was set at 0.3. (Smith et al., 2006). Identified peaks were normalized to the peak intensity of ribitol. The pathway enrichment analysis on the metabolite dataset based on Kyoto Encyclopedia of Genes and Genomes (KEGG) was performed in Metaboanalyst 3.0[1] (Xia et al., 2015). Related assistance was performed at Shanghai Biotree Biotech Co., Ltd. (Shanghai, China).

Statistical Analysis

Significant differences in growth, chlorophyll content, biomass, and paramylon content were tested using the Dunnett's *t*-test. All data were obtained and averaged from at least three independent experiments, and standard errors were calculated and displayed as error bars. And after raw data profiles were processed, the Student's *t*-test was used for the univariate analysis. Principal component analysis (PCA) and orthogonal projections to latent structures discriminant analysis (OPLS-DA) were used for multivariate analysis. Variable importance in projection (VIP) score was combined with *p*-value to screen significant differential metabolites, and then the significant differential metabolites were qualitatively analyzed based on the relevant KEGG pathway and existing materials (Mangalam et al., 2013).

RESULTS

Cell Growth, Chlorophyll, Paramylon, and Lipids

Cell growth differed greatly under different environmental stresses (**Table 1**). The PRM treatment caused a slight decrease (7.17%, $p > 0.05$), whereas $CdCl_2$ (Cd) and nitrogen deprivation (N–) treatments significantly inhibited the growth of *E. gracilis* by 7.79% ($p < 0.05$) and 11.95% ($p < 0.05$), respectively.

Photosynthesis systems and chlorophyll in microalgae are sensitive to environmental stress. The addition of Cd, and N– decreased the chlorophyll content of *E. gracilis* significantly (**Table 1**), whereas PRM had no significant effect. Chlorophyll content decreased by 55% ($p < 0.05$) and 38% ($p < 0.001$) in cells treated with Cd and N–, respectively.

Similarly, there were obvious differences in the paramylon content of *E. gracilis* under different environmental treatments. PRM did not affect paramylon content; Cd caused a significant increase (171% of the control, $p < 0.05$), whereas N– showed an obvious reduction (66% of the control, $p < 0.05$) (**Table 1**).

[1]https://www.metaboanalyst.ca/MetaboAnalyst/home.xhtm.

TABLE 1 | Physiological parameter, cell density, chlorophyll contents, paramylon, and total lipids determined under different environmental stresses.

	Cell density (10^6 cell/ml)	Chlorophyll contents (mg/L)	Paramylon (μg/mg)	Total lipids (μg/mg)
EM	1.037 ±0.038	35.764 ±1.495	53.073 ±1.986	60.49 ±7.713
PRM	0.963 ±0.040	35.525 ±1.541	42.187 ±7.721	70.099 ±1.201
N–	0.913 ±0.044*	22.543 ±1.406**	35.133 ±0.590*	138.732 ±3.442**
Cd	0.956 ±0.025*	16.417 ±0.356*	84.310 ±4.560*	92.704 ±8.928*

*EM, control; PRM, paromomycin; N–, nitrogen deprivation; Cd, $CdCl_2$. All data were derived from at least three biological repeats. *$p < 0.05$, **$p < 0.01$.*

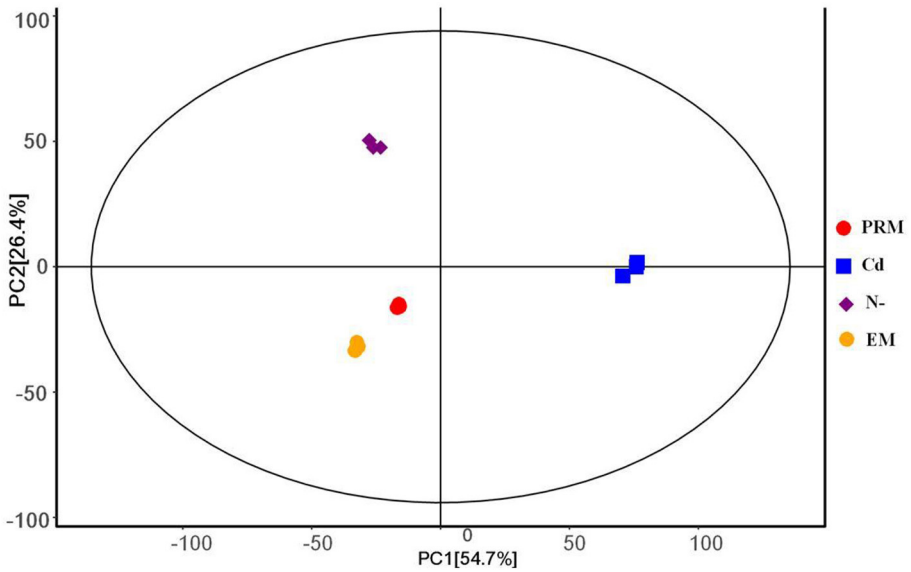

FIGURE 1 | PCA score plot under different treatment groups based on metabolites, each with 3 biological replicates. PRM, paromomycin; Cd, $CdCl_2$ addition; N–, nitrogen deprivation; EM, control.

Many environmental stresses could alter the metabolism, cellular membrane structure, and lipids. In this study, significant changes of total lipids were also detected in both Cd and N– treatments, with 53 and 129% increases compared to EM control, respectively. PRM caused no significant change in total lipid content in *E. gracilis*.

Comparative Metabolomics of *Euglena* Under Different Environmental Stresses

General Features of Metabolomics

In this study, the metabolic plasticity of *E. gracilis* under different stresses was elucidated using comparative metabolomic analysis. UHPLC–MS/MS revealed a total of 10,892 negative ion mode (NEG) and 11,003 positive ion mode (POS) peaks. Furthermore, 254 NEG and 583 POS metabolites, respectively, were annotated by the KEGG database (**Supplementary Table 1**).

The PCA analysis showed that all four groups, EM, PRM, N–, and Cd, of metabolites could be distinguished (**Figure 1**), indicating that the metabolic changes to stress were significantly different from each other. Among them, two groups of metabolites (EM and PRM) were relatively closer, indicating that smaller differences had occurred in the metabolic alterations of microalgae cells treated with PRM. Furthermore, the metabolites (N– and Cd) of two groups of microalgae cells were clearly distinguished between each other, and far from EM and PRM groups (**Figure 1**), suggesting that the metabolic pathways of the microalgae cells changed dramatically under N– and Cd.

According to the criteria of fold change (>2.0, or <0.5, and $p < 0.05$), 401 out of 426 (POS) and 170 of 196 (NEG) candidate metabolites were significantly changed under different treatments (**Figure 2**).

In total, numbers of significantly decreased metabolites were much more than increased ones in all stress treatment groups, for instance, 177 vs. 19 (PRM) and 313 vs. 21 (Cd) under the POS mode, whereas similar trends were also observed under the NEG mode, for instance, 52 vs. 8 (PRM) and 108 vs. 36 (Cd) (**Table 2**). These stresses inhibited *Euglena* cell growth by reducing the metabolism levels of cellular activity. Among stresses, Cd seems to cause more dramatic metabolic changes, with the most significantly changed metabolites as total 334 and 166 under POS and NEG mode, respectively, in contrast to N– group (179, 80) and PRM (196, 60) compared to the EM control.

TOP Changed Metabolites Under Stresses

Based on fold changes increased and decreased, TOP 10 metabolites under different stresses were analyzed (**Supplementary Table 2**). Interestingly, metabolites as organic oxygen compounds, organic acids, and derivatives

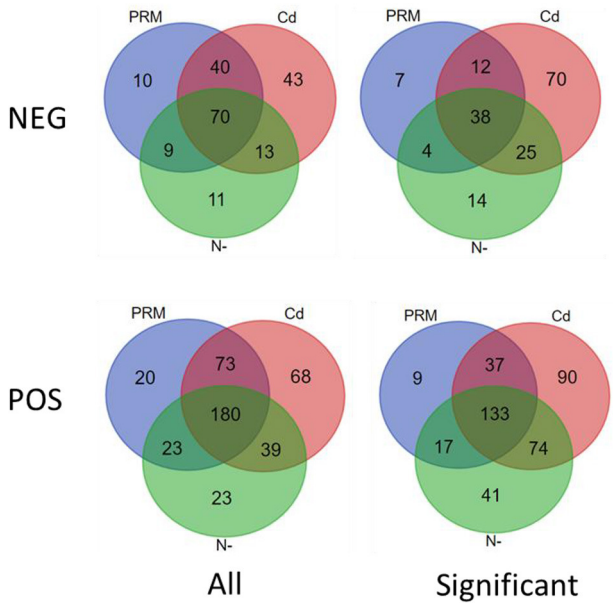

FIGURE 2 | Venn diagram of all (All) and significantly changed (significant) metabolites under stresses (PRM, paromomycin; Cd, $CdCl_2$; N–, nitrogen deprivation), under negative (NEG) and positive (POS) ion modes.

TABLE 2 | Summary of metabolomics: differential metabolites under different stresses (PRM, paromomycin; Cd, CdCl2; N–, nitrogen deprivation) and under negative (POS) and positive (NEG) ion modes.

Mode	POS				NEG			
	Down	Up	Sum	Total $p < 0.05$	Down	Up	Sum	Total $p < 0.05$
PRM	177	19	196	296	52	8	60	129
Cd	313	21	334	360	108	36	144	166
N–	160	19	179	265	72	8	80	103

(mostly amino acids) were deceased, and lipids and lipid-like molecules increased in PRM treatment. Under Cd, TOP changed metabolites include lipids and organoheterocyclic compounds and increased polyketides and benzenoids. While as expected, N– treatment induced significant lipids like PC (16:0/P-16:0; 24:0/14:0), PS (18:1/15:0; 15:0/16:1), DG (20:3), and reduced organic acids (mostly single amino acids as Tyr, Asp, and Arg, and two peptides like Arg-Ser, Thr-Arg, and Arg-Phe).

KEGG Pathway Enrichment

The KEGG-enriched metabolome bubble view showed all matched pathways according to the *p*-values from pathway enrichment analysis and the pathway impact values from pathway topology analysis (**Figure 3**). The candidate metabolites with $p < 0.05$ were enriched by one or several metabolic pathways under three stresses, such as Aminoacyl-tRNA biosynthesis, Purine metabolism, Nitrogen metabolism, "Taurine and hypotaurine metabolism," Butanoate metabolism, "Alanine, aspartate and glutamate metabolism," "Pantothenate and coenzyme A (CoA) biosynthesis," and Pyrimidine metabolism (**Figure 3**; for more details see **Supplementary Table 3** KEGG list only).

Under both POS and NEG modes, the aminoacyl-tRNA biosynthesis showed up under all stresses, which indicated that this metabolic pathway might be a key stress response of *Euglena* cells to different environmental stresses, such as nutrient deprivation, heavy metal, and antibiotics.

Overall, microalgae cell metabolic pathways under PRM conditions were primarily involved in the biosynthesis of Aminoacyl-tRNA, and Taurine and hypotaurine. With higher *p*-values ($p > 0.05$), some highly impacted pathways involved in amino acids, such as "Ala, Asp, and Glu metabolism," Phe metabolism, Tyrosine metabolism, "Glycine, Ser, and Thr metabolism," "Arginine and Proline metabolism," Isoquinoline alkaloid biosynthesis, and Riboflavin metabolism.

Relatively more significantly enriched metabolic pathways were enriched when cells were treated with Cd. In addition to the biosynthesis of aminoacyl-tRNA, 3 more pathways, Purine metabolism, "Ala, Asp, and Glu metabolism," and Butanoate metabolism, showed up in the Cd treatment. Similarly, all less significant pathways ($p > 0.05$) enriched in PRM were on the Cd pathway list (**Figure 3**), except for the Riboflavin metabolism.

Compared with PRM and Cd, N— treatment enriched the most significant metabolic pathways, including Aminoacyl-tRNA biosynthesis, "Taurine and hypotaurine metabolism," "Pantothenate and CoA biosynthesis," Nitrogen metabolism, and Pyrimidine metabolism. The late three pathways were N– group-specific, and nitrogen metabolism as the well-known pathways changed when nitrogen nutrient was absent.

Network Analyses of Metabolomics

Based on the metabolomic KEGG and network analyses, we also obtained groups of metabolic pathways and modules that play core roles in the metabolic networking (**Table 3** network plot). Several pathways and modules were plotted in all stress groups simultaneously, including Purine metabolism (module cvr00230), "Ala, Asp, and Glu metabolism" (cvr00250), Carbon fixation in photosynthetic organisms (cvr00710), Guanine ribonucleotide biosynthesis (M00050), Glycerophospholipid metabolism (cvr00564), and PRPP biosynthesis (M00005). M00005 is a module on KEGG, The KEGG MODULE database consists of KEGG modules identified by M numbers and KEGG reaction modules identified by RM numbers, which are manually defined functional units of gene sets and reaction sets, respectively. KEGG modules are further divided into pathway modules and signature modules as shown https://www.genome.jp/entry/M00005, and the PRPP: 5-Phosphoribosyl-1-Pyrophosphate.

On both PRM and Cd network lists, we found Crassulacean acid metabolism (CAM), dark (M00168) and light (M00169); C4-dicarboxylic acid cycle, nicotinamide adenine dinucleotide phosphate (NADP)-malic enzyme (M00172), Linoleic acid metabolism (cvr00591), and Phosphatidylethanolamine (PE) biosynthesis (M00092). However, on both Cd and N– lists, only two networks were detected as Guanine ribonucleotide biosynthesis (M00050) and Ornithine biosynthesis (M00028).

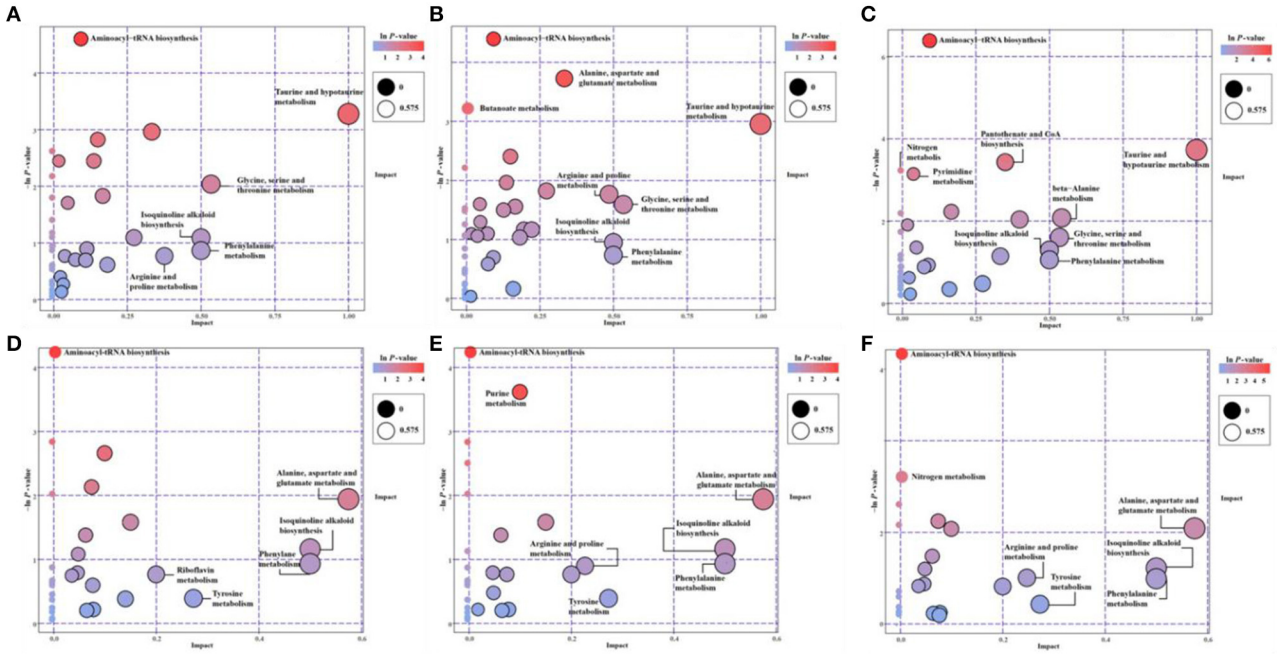

FIGURE 3 | The pathway enrichment and topology analysis of candidate metabolites from *E. gracilis* under different environmental stresses. **(A–C)** NEG modes; **(D–F)** POS modes. **(A,D)** PRM-NEG, PRM-POS; **(B,E)** Cd-NEG, Cd-POS; **(C,F)** N-NEG, N-POS. "Pathway Impact" on the *x*-axis represents the impact of these enriched pathways computed *via* topology analysis. "–log10(*p*)" on the *y*-axis refers to the negative natural logarithmic value of the original *p*-value from a statistical analysis of the pathway difference between the groups of stresses vs. the EM control. The redder the color, the higher the –log10(*p*) and pathway impact value, the more significant the enrichment degree.

Several specific networks were only detected in one individual stress. For examples, Ceramide biosynthesis (M00094) and Sphingosine biosynthesis (M00090) in the PRM group; Fatty acid degradation (cvr00071) and caffeine metabolism (cvr00232) in the Cd group; Plant hormone signal transduction (cvr04075), Arachidonic acid (ARA) metabolism (cvr00590), and Pyrimidine ribonucleotide biosynthesis (M00052) under N– group.

DISCUSSION

Euglena is highly adaptable to changing environments, some adverse stresses like UVB (Takahashi et al., 2006), heavy metals (Moreno-Sánchez et al., 2017), and antibiotics (Ebringer, 1964). In this study, microalgal cells showed tolerance to antibiotics, PRM, without significant cell growth inhibition, chlorophyll reduction, and paramylon and lipid alterations. The inhibition of chlorophyll formation in *Euglena* by antibiotics was reported previously (Linnane and Stewart, 1967). This may be caused by different antibiotics and different tolerant concentrations of *E. gracilis* cells. In the Cr(VI) treatments, a reduction of chlorophyll was observed, the ratio of proteins to paramylon content was augmented, and total lipid content was increased (Rocchetta et al., 2012). In contrast, the other two stresses, N– and Cd, showed obvious effects on above-mentioned physiological parameters and major macromolecules, such as polysaccharide (paramylon) and lipids.

This is the first time to apply global metabolomics to study the cellular response of *E. gracilis* to environmental stresses, such as antibiotics, heavy metals, and nutrient deprivation. Many metabolites and metabolic pathways, instead of standard physiological parameters, and macromolecules, were detected significantly altered by these stresses and shed light on the mechanisms of tolerance or toxic responses in *E. gracilis*. PRM did not cause much change of pigment, carbohydrates, and lipids in *E. gracilis* cells. However, based on metabolomics, hundreds of metabolites and several important metabolic pathways were detected significantly disturbed by PRM, indicating the sensitivity of metabolomics when studying the microalgal cellular response to changing environments. Metabolomics easily differentiates the groups of control, PRM, N–, and Cd treatments, even between control and PRM, by which cell growth, chlorophyll content, paramylon, and lipid changes could not distinguish significantly.

In this study, we detected paramylon degradation and lipids accumulation under N–. In most microalgae, lipids were induced to high accumulation under nitrogen starvation (Chen et al., 2017). There is a report showing induction of carbohydrates and no lipid accumulation with no nitrogen source in *Euglena* with NH_4Cl as the only nitrogen source (Coleman et al., 1988). However, there is a major difference compared to the reference above since we added urea and NH_4Cl as nitrogen sources. Thus, N– in this study means both NH_4Cl and urea depletion and may

TABLE 3 | Network plots of significantly enriched pathways and modules under stresses.

PRM	Cd	N–	Pathways and modules description
NEG			
cvr00230	cvr00230	cvr00230	Purine metabolism
cvr00250	cvr00250	cvr00250	Alanine, aspartate, and glutamate metabolism
cvr00710	cvr00710	cvr00710	Carbon fixation in photosynthetic organisms
M00050	M00050	M00050	Guanine ribonucleotide biosynthesis IMP
M00168	M00168		CAM (Crassulacean acid metabolism), dark
M00169	M00169		CAM (Crassulacean acid metabolism), light
M00172	M00172		C4-dicarboxylic acid cycle, NADP—malic enzyme
M00005			PRPP biosynthesis, ribose 5P => PRPP
	cvr00430		Taurine and hypotaurine metabolism
	M00028	M00028	Ornithine biosynthesis, glutamate => ornithin
		cvr04075	Plant hormone signal transduction
		cvr00590	Arachidonic acid metabolism
		M00052	Pyrimidine ribonucleotide biosynthesis
POS			
cvr00230	cvr00230	cvr00230	Purine metabolism
cvr00564	cvr00564	cvr00564	Glycerophospholipid metabolism
M00005	M00005	M00005	PRPP biosynthesis, ribose 5P => PRPP
	M00050	M00050	Guanine ribonucleotide biosynthesis IMP => GDP
cvr00591	cvr00591		Linoleic acid metabolism
M00092	M00092		Phosphatidylethanolamine (PE) biosynthesis
M00094			Ceramide biosynthesis
M00099			Sphingosine biosynthesis
	cvr00071		Fatty acid degradation
	cvr00232		Caffeine metabolism

cause differential accumulation (reduction) of carbohydrates and lipids in our study.

Based on hundreds of changed metabolites, significantly increased or decreased TOP 10 metabolites may suggest the major changes under different treatments. Even with no significantly changed lipids and paramylon under the PRM treatment, amino acids were found to decrease while lipids and lipid-like molecules increase. PRM is a broad-spectrum aminoglycoside antibiotic produced by *Streptomyces rimosus* var. *paromomycinus* (Davidson et al., 2009). The *in vitro* and *in vivo* antibacterial action of PRM closely parallels that of neomycin. PRM bind specifically to the RNA oligonucleotide at the A site of bacterial 30S ribosomes thereby causing misreading and premature termination of translation and leading to inhibition of protein synthesis followed by cell death (PubChem CID 165580). As reported, some antibiotics, such as chloramphenicol and other antibiotics that specifically inhibit the synthesis of proteins in mitochondria and bacteria, would also selectively inhibit protein synthesis by chloroplast (Linnane and Stewart, 1967). PRM did not reduce chlorophyll biosynthesis in *E. gracilis* cells at the concentration of 25 μg/ml, suggesting its inhibition pathways may not involve the synthesis of chloroplast proteins. Cd treatment in this study resulted in chlorophyll degradation, paramylon, and lipid accumulation. Under Cd treatment, metal-causing reactive oxygen species (ROS) changed the lipids and organoheterocyclic compounds, and N– increased lipids and decreased protein contents in *Euglena* cells. These TOP changed metabolites showed similar patterns as previous reports (Moreno-Sánchez et al., 2017; Tossavainen et al., 2019).

The KEGG enrichment provides metabolic pathways through which cells are regulated under specific treatments. The only common pathway enriched in all treatments is Aminoacyl-tRNA biosynthesis, suggesting this may be the common/universal stress responding pathway in *Euglena*. Aminoacyl-tRNA species are prevalent amino acid donors in the cell due to their critical role as substrates for ribosomal protein biosynthesis. It has become clear that aminoacyl-tRNAs are also utilized in an ever-growing number of other non-ribosomal biosynthetic pathways, particularly in bacteria, although some pathways also exist in eukaryotes (Shepherd and Ibba, 2013). Much has been uncovered in recent years about many novel functions, disease connection, and inter pathway connection of tRNA synthetases (Park et al., 2008; Zhou et al., 2020). PRM might inhibit protein synthesis by binding specifically to the RNA oligonucleotide at the site of bacterial, or microalgal mitochondrial and 30S ribosomes of chloroplast, and thus alter aminoacyl-tRNA biosynthesis. Nitrogen deprivation involves the degradation of carbohydrates, paramylon in *E. gracilis*, and constructive proteins, and accumulation of membrane lipids (Richter et al., 2015), and at the same time, specific enzymes/macromolecules have to be transformed or *de novo* synthesized *via* aminoacyl-tRNA biosynthesis pathway. Similarly, heavy metals are created ROS through lipid peroxidation and DNA damage (Rodriguez-Zavala et al., 2007; Khatiwada et al., 2020). Then the cells are induced to produce antioxidant chemicals and enzymes, such as superoxide dismutase and DNA repair proteins from protein biosynthesis with aminoacyl-tRNA biosynthesis pathway. However, whether the aminoacyl-tRNA biosynthesis pathway could be a novel biomarker for environmental stresses has yet to be worked out in the future with more investigations.

There are more pathways enriched under individual stresses according to our global metabolomics, reflecting different metabolic responses by different stresses.

In Cd treatment, "Purine metabolism," "Alanine, aspartate, and glutamate metabolism," and "Butanoate metabolism" pathways were detected significantly changed. Purine nucleotides are essential for many biochemical processes like energy transfer, metabolic regulation, and synthesis of DNA and RNA (Watanabe et al., 2014). Alanine, aspartate, and glutamate are derived from intermediates of central metabolism, mostly the citric acid cycle, in one or two steps. While the pathways are short, the importance and complexity of the functions of these amino acids befit their proximity to central metabolism (Limami et al., 2008). Butanoate metabolism describes the metabolic fate of several short-chain fatty acids or short-chain alcohols. Many of these molecules are eventually used in the production of ketone bodies, the

creation of short-chain lipids, or as precursors to the citrate cycle (pubchem.ncbi.nlm.nih.gov/pathway/PathBank:SMP0000073). Cd degraded chlorophyll and reduced the activity of photosynthesis of microalgal cells; however, short-term (6 days) Cd treatment also increased the contents of paramylon and lipids (Mendoza-Cozatl et al., 2002; Einicker-Lamas et al., 2003). Thus, we speculated that the mutual transformation of three major macromolecules, proteins, carbohydrates, and lipids may respond to heavy metals. In Cd treatment, decreasing amino acid contents and significantly enriched protein synthesis pathways with enhanced carbohydrates and lipid production were detected, indicating the mutual transformation of proteins into paramylon and lipids in *E. gracilis*.

When microalgal cells were treated with PRM, the "Taurine and hypotaurine metabolism" pathway was also enriched. Taurine, an active substance that regulates the normal physiological activities of cells, is associated with maintaining the osmotic pressure balance in cells, plus strengthening cell membranes and enhancing antioxidant capacity (Tevatia et al., 2015, 2019). Taurine is synthesized in large amounts by animals; however, plants, green microalgae, and fungi could only synthesize minute amounts (Tevatia et al., 2019). *E. gracilis* enriched this metabolic pathway where the metabolite was located under PRM treatment. Thus, our results indicated that the metabolic pathway played an important role in regulating antibiotics tolerance of *E. gracilis*, as it stabilized the cell membrane and maintained cellular functions.

Nitrogen deprivation also enriched the taurine and hypotaurine compounds, suggesting this pathway may also involve in nutrient deprivation stress perhaps just by using taurine and its relative amino acid compounds as alternative nitrogen resources for biosynthesis of new enzymes for maintaining basic cell survival. Under N– treatment, KEGG pathway enrichment also collected other pathways such as "Nitrogen metabolism," "Pantothenate and CoA biosynthesis," and "Pyrimidine metabolism."

Nitrogen makes up only a small fraction of plant and microalgal dry weight, but N compounds are extremely important physiologically. For instance, structural and storage proteins, enzymes, amino acids and amides, nucleic acids, and plant hormones, all contain N. The substituted purine and pyrimidine bases that constitute nucleic acids, nucleotides, and nicotinamide nucleotides also contain N (Pallardy, 2008). Transcriptome analysis revealed that genes involved in metabolism, plant hormone signal transduction (e.g., abscisic acid, auxin, and jasmonate), transporter activity, and oxidative stress responses were rapidly regulated by N– (based on our unpublished transcriptomic data in N– *Euglena*).

Pantothenate is vitamin B5 and is the key precursor for the biosynthesis of CoA, a universal and essential cofactor involved in a myriad of metabolic reactions, including the synthesis of phospholipids, the synthesis and degradation of fatty acids, and the operation of the tricarboxylic acid cycle (Leonardi and Jackowski, 2007). Pyrimidines metabolism pathway suggests the cells use the nitrogen from nucleic acids under N–. Although both pyrimidines and purines are components in nucleic acids, they are made in different ways. Likewise, products of pyrimidine degradation are more water-soluble than are the products of purine degradation (Wan et al., 2019).

In summary, the KEGG pathway enrichment showed that both common and specific metabolic pathways were employed to respond against different environmental stresses by *E. gracilis* cells.

Based on network plot analyses, we also targeted some specific metabolic pathways and modules under different stresses, especially on photosynthesis and carbon fixation, ROS, membrane lipids, and amino acid metabolisms.

Photosynthesis is a global sensor of environmental stress in green plants, microalgae, and cyanobacteria (Biswal et al., 2011). Photosynthesis and photosynthetic pigments in *E. gracilis* were reported as sensitive endpoints for the toxicity evaluation of liquid detergents (Azizullah et al., 2014). Carbon fixation is the process by which inorganic carbon is added to an organic molecule, and it occurs during the light-independent reaction of photosynthesis with the help of chlorophyll. This pathway is showed as a core responsive pathway in all three stresses in metabolic networking analyses, indicating photosynthesis and carbon fixation involves in the alternations caused by antibiotics, heavy metals, and N–. Cd and N– treatments significantly reduced chlorophyll contents with lower photosynthetic activity, whereas PRM did not decrease chlorophyll significantly. Further experiments with the photosynthetic activity will clarify this observation.

It is very interesting to locate the CAM pathway in PRM and Cd groups. CAM (also known as CAM photosynthesis) is a carbon fixation pathway that evolved in some plants as an adaptation to arid conditions. In CAM, the carboxylation (C3 + C1) occurs at night, and the (C4 – C3) decarboxylation occurs during the day (Libik-Konieczny et al., 2019; Gilman and Edwards, 2020). The C3 + C1 mechanism has been found in the green Ulvophyceae benthic macroalga *Udotea flabellum* and the planktonic diatom *Thalassiosira weissflogii* (Cheng et al., 2019). The photosynthetic metabolism (C3, C4, or CAM) seems to affect plant sensitivity to environmental stresses. CAM is a metabolic strategy allowing plants to maintain photosynthesis under stress conditions (Libik-Konieczny et al., 2019). Although N– also showed a significant reduction of chlorophyll contents as Cd treatment; however, only PRM and Cd triggered CAM metabolism changes. Heterotrophic CO_2 fixation by *E. gracilis* was reported in Levedahl (1966). A previous study indicated that *E. gracilis* can remove Cd under anaerobic conditions, which might be advantageous for heavy metal removal in sediment from polluted water bodies or bioreactors, where the O_2 concentration is particularly low (Geovanni Santiago-Martinez et al., 2015). Perhaps under PRM and Cd treatments, the damage of photosynthesis might be compensated partially by CAM metabolism, which needs further verification shortly.

Finally, *Euglena* appears to exemplify a strategy for survival and adaptation to various environmental conditions during the evolutionary process of euglenoids (Geovanni Santiago-Martinez et al., 2015; Ishikawa et al., 2017). Among various environmental stresses, heavy metal accumulation and resistance in *Euglena* are widely studied. Under Cd treatment, mitochondria and

chloroplasts were altered in shape, and thylakoid arrangement was changed, and osmiophilic plastoglobuli was increased (Duret et al., 1986). Cd causes cellular damage to *Euglena*, including DNA strand breaks and intracellular membrane damage, as a result of reactive oxygen stress (Watanabe and Suzuki, 2002). Enhanced alternative oxidase and antioxidant enzymes under Cd stress in *Euglena* were reported (Castro-Guerrero et al., 2008). The data suggested that Cd was compartmentalized into chloroplasts in a process that may involve the transport of free Cd and the participation of thiol-peptides in *E gracilis* (Mendoza-Cozatl et al., 2002). The chloroplasts appear to have a major role in the tolerance and accumulation of Cd in *E. gracilis* (Khatiwada et al., 2020). The variety of biochemical mechanisms evolved in *E. gracilis* to resist, accumulate, and remove heavy metals from the environment are summarized as follows: adsorption to the external cell pellicle, intracellular binding by glutathione and glutathione polymers, and their further compartmentalization as heavy metal complexes into chloroplasts and mitochondria, polyphosphate biosynthesis, and secretion of organic acids (Moreno-Sánchez et al., 2017).

Alternation of membrane lipids and PUFA pathways was also reported in all stresses. Lipid metabolism is crucial for the survival and propagation of the species since lipids are an essential cellular component for maintaining homeostasis in the presence of environmental stressors. Reactions in glycerolipid and glycerophospholipid metabolism occur at the membrane, which plays an important role in signaling and response to environmental stress. PE is one of the most abundant membrane phospholipids, in which metabolism was significantly changed under PRM and Cd. In both prokaryotes and eukaryotes, PE plays important role in various membrane functions. It is suggested that the synthesis of these membrane lipids was beneficial to increase the peristalsis and swimming ability of *E. gracilis*, which protected the integrity of the cell, improving the viability of the cell under these stresses.

Under the PRM treatment, ceramide biosynthesis and sphingosine metabolism were also disturbed. Ceramide biosynthesis begins in the endoplasmic reticulum with the condensation of palmitoyl-CoA and serine, catalyzed by the multimeric enzyme serine palmitoyltransferase to produce 3-ketosphinganine (Chaurasia and Summers, 2015). Sphingosine is a long-chain unsaturated amino alcohol C18H37O2N that is found especially in cell membranes and is a primary constituent of sphingolipids. Sphingosine itself increases the permeability of phospholipid membranes. With no cell walls in *E. gracilis* unlike other microalgae, the external cell pellicle and the cell membrane are the first front-line against the changing aquatic environment. Thus, distortions and alterations of membrane lipids of *Euglena* have to be sensitive and elastic in the environment.

As the major compound of membrane lipids, PUFAs are also very sensitive to environmental stresses at qualitative and quantitative levels. Halter et al. (2012) found that under adverse conditions, such as the presence of heavy metal arsenic, the content of unsaturated fatty acids in the cell membrane had significantly increased. In this study, linoleic acid (LA) metabolism was highlighted in groups of PRM and Cd (Halter et al., 2012). LA [18:2 ($n-6$)] is an omega-6 fatty acid and helps stimulate skin and hair growth, maintain bone health, regulate metabolism, and to maintain the reproductive system (Lee et al., 2018). Under abiotic stress by salt or ultraviolet light, the production of lutein and PUFAs were observed by the acidophilic eukaryotic microalga *Coccomyxa onubensis* (Bermejo et al., 2018). Thus, increasing the fluidity and hydrophobicity of the cell membrane by increasing PUFA allowed *E. gracilis* adaptability in the surrounding environments, such as PRM and Cd. Similar PUFA accumulation was also reported in freshwater microalgae *Chlamydomonas mexicana* and *Scenedesmus obliquus* grown under salt stress (Salama et al., 2013). Furthermore, it was determined that there is a relationship between the effects of Cd-induced oxidative stress on PUFAs and their degradation products and is also reflected on the increase in tolerance to Cd toxicity in plant cells (Pavlík et al., 2017). Specifically to N–, ARA metabolism reacted significantly. ARA is an integral constituent of the biological cell membrane, conferring it with fluidity and flexibility, so necessary for the function of all cells. Free ARA modulates the function of ion channels, several receptors, and enzymes *via* activation as well as inhibition (Tallima and El Ridi, 2018). Similarly, the green oleaginous microalga *Lobosphaera incisa* accumulates triacylglycerols enriched in the long-chain PUFA, such as ARA under nitrogen deprivation. This is consistent with the enhanced lipid accumulation under N– stress in *E. gracilis*.

CONCLUSIONS

This study demonstrated that metabolomics is sensitive and accurate enough to elucidate cellular responses of *E. gracilis* to different environmental stresses, even with no significantly changed physiological parameters, such as cell numbers, pigments, paramylon, and lipids under PRM treatment. Based on global metabolomics, a common metabolic pathway responding to multiple environmental stresses, aminoacyl-tRNA biosynthesis, was firstly targeted in *E. gracilis*. The other shared metabolic pathways and modules under selected stress include Purine metabolism, carbon fixation, Ala, Asp, and Glu metabolism, Glycerophospholipid metabolism, and PRPP biosynthesis. We observed the well-known changed metabolic pathways involved in stresses, like ROS in heavy metals, N metabolism during N deprivation, and protein biosynthesis inhibition with PRM. Some unique modules were individually detected under different stresses, like ceramide and sphingosine biosynthesis under PRM, ARA metabolism in N–, and fatty acid degradation and caffeine metabolism with Cd treatment. Under stresses, without cell walls, membrane lipids and PUFA in *E. gracilis* cells were altered to resist, acclimatize to, and remove the adverse factors like Cd and reactive oxidative species. All data suggest that the mutual interaction and transformation of macromolecular metabolites as proteins, pigments, lipids, and paramylon are regulated delicately to resist, tolerate, and/or remove these environmental stresses.

DATA AVAILABILITY STATEMENT

The data presented in the study were deposited in the MetaboLights repository, with the accession number MTBLS2878.

AUTHOR CONTRIBUTIONS

JW and ZH contributed to the conception and design of the study. JH, CL, MD, and XZ conducted the experiments. JH, CL, AL, and XZ involved in the statistical analysis. JW and JH wrote the first draft of the manuscript. AL and JW wrote the sections of the manuscript. JW and CL contributed to manuscript revision. All authors read and approved the submitted version.

FUNDING

This work was supported by the National Key R&D Program of China (2018YFA0902500), the Natural Science Foundation of Guangdong Province, China (2014A030313562), the Guangxi Innovation-Driven Development Special Fund (Gui Ke AA18242047), Shenzhen Basic Research Projects (JCYJ20180507182405562), and Grant Plan for Demonstration City Project for Marine Economic Development in Shenzhen (No. 86). They are used for the design of the study, data collection, data analysis, and writing the manuscript, respectively.

ACKNOWLEDGMENTS

The authors gratefully acknowledge support from the Instrumental Analysis Center of Shenzhen University (LiHu Campus). They are obliged to Biotechnology Co., Ltd. Shanghai, China for the suggestions of metabolomic analysis. They would like to thank TopEdit (http://www.topeditsci.com) for English language editing of this manuscript.

SUPPLEMENTARY MATERIAL

The Supplementary Material for this article can be found online at: https://www.frontiersin.org/articles/10.3389/fbioe.2021.662655/full#supplementary-material

REFERENCES

Afiukwa, C. A., and Ogbonna, J. C. (2007). Effects of mixed substrates on growth and vitamin production by *Euglena gracilis*. *Afr. J. Biotechnol.* 6:2417. doi: 10.5897/AJB2007.000-2417

Azizullah, A., Richter, P., and Hder, D. P. (2014). Photosynthesis and photosynthetic pigments in the flagellate *Euglena gracilis* - As sensitive endpoints for toxicity evaluation of liquid detergents. *J. Photochem. Photobiol. B. Biol.* 133, 18–26. doi: 10.1016/j.jphotobiol.2014.02.011

Bateman, J. M., and Purton, S. (2000). Tools for chloroplast transformation in Chlamydomonas: expression vectors and a new dominant selectable marker. *Mol. Gene. Genet. Mgg* 263, 404–410. doi: 10.1007/s004380051184

Bermejo, E., Ruiz-Domínguez, M. C., Cuaresma, M., Vaquero, I., Ramos-Merchante, A., Vega, J. M., et al. (2018). Production of lutein, and polyunsaturated fatty acids by the acidophilic eukaryotic microalga Coccomyxa onubensis under abiotic stress by salt or ultraviolet light - ScienceDirect. *J. Biosci. Bioeng.* 125, 669–675. doi: 10.1016/j.jbiosc.2017.12.025

Biswal, B., Joshi, P. N., Raval, M. K., and Biswal, U. C. (2011). Photosynthesis, a global sensor of environmental stress in green plants: Stress signalling and adaptation. *Curr. Sci.* 101, 47–56.

Castro-Guerrero, N. A., Rodríguez-Zavala, J. S., Marín-Hernández, A., Rodríguez-Enríquez, S., and Moreno-Sánchez, R. (2008). Enhanced alternative oxidase and antioxidant enzymes under Cd2+ stress in Euglena. *J. Bioenerget. Biomembr.* 40:227. doi: 10.1007/s10863-007-9098-6

Chaurasia, B., and Summers, S. A. (2015). Ceramides - lipotoxic inducers of metabolic disorders. *Trends Endocrinol. Metabo.* 26, 538–550. doi: 10.1016/j.tem.2015.07.006

Chen, B., Wan, C., Mehmood, M. A., Chang, J. S., Bai, F., and Zhao, X. (2017). Manipulating environmental stresses and stress tolerance of microalgae for enhanced production of lipid and value-added products-A review. *Bioresour. Technol.* 244, 1198–1206. doi: 10.1016/j.biortech.2017.05.170

Cheng, J., Zhu, Y., Zhang, Z., and Yang, W. (2019). Modification and improvement of microalgae strains for strengthening CO2 fixation from coal-fired flue gas in power plants. Bioresour. Technol. 291:121850. doi: 10.1016/j.biortech.2019.121850

Coleman, L. W., Barry, H. R., and Steven, D., Schwartzbach. (1988). Environmental control of carbohydrate and lipid synthesis in Euglena. *Plant Cell Physiol.* 29, 423–432

Davidson, R. N., Boer, M. D., and Ritmeijer, K. (2009). Paromomycin. *Transact. R. Soc. Trop. Med. Hygiene* 103, 653–660. doi: 10.1016/j.trstmh.2008.09.008

Duret, S., Bonaly, J., Bariaud, A., Vannereau, A., and Mestre, J. C. (1986). Cadmium-induced ultrastructural changes in Euglena cells. *Environ. Res.* 39, 96–103. doi: 10.1016/S0013-9351(86)80011-1

Ebenezer, T. G. E., Carrington, M., Lebert, M., Kelly, S., and Field, M. C. (2017). *Euglena gracilis Genome and Transcriptome: Organelles, Nuclear Genome Assembly Strategies and Initial Features*. London: Springer International Publishing. doi: 10.1007/978-3-319-54910-1_7

Ebringer, L. (1964). Bleaching of euglenas by antibiotics–a specific form of antagonism in actinomycetes. *Folia Microbiol.* 9, 249–255. doi: 10.1007/BF02875844

Edmunds, L. N. (1965). Studies on synchronously dividing cultures of *Euglena gracilis* Klebs (strain Z). II. Patterns of biosynthesis during the cell cycle. *J. Cell. Compar. Physiol.* 66, 159–181. doi: 10.1002/jcp.1030660205

Einicker-Lamas, M., Morales, M. M., Miranda, K., Garcia-Abreu, J., Oliveira, A. J. F., and Oliveira, F. L. S. S.M. (2003). P-glycoprotein-like protein contributes to cadmium resistance in *Euglena gracilis*. *J. Compar. Physiol. B* 173, 559–564. doi: 10.1007/s00360-003-0365-5

Ferreira, V. S., Rocchetta, I., Conforti, V., Bench, S., Feldman, R., and Levin, M. J. (2007). Gene expression patterns in *Euglena gracilis*: Insights into the cellular response to environmental stress. *Gene* 389, 136–145. doi: 10.1016/j.gene.2006.10.023

García-Ferris, C., Ríos, A. D. L., Ascaso, C., and Moreno, J. (1996). Correlated biochemical and ultrastructural changes in nitrogen-starved *Euglena gracilis*. *J. Phycol.* 32, 953–963. doi: 10.1111/j.0022-3646.1996.00953.x

Geovanni Santiago-Martinez, M., Lira-Silva, E., Encalada, R., Pineda, E., Carlos Gallardo-Perez, J., Zepeda-Rodriguez, A., et al. (2015). Cadmium removal by *Euglena gracilis* is enhanced under anaerobic growth conditions. *J. Hazard. Mater.* 288, 104–112. doi: 10.1016/j.jhazmat.2015.02.027

Gilman, I. S., and Edwards, E. J. (2020). Crassulacean acid metabolism. *Curr. Biol.* 30:R57–R62. doi: 10.1016/j.cub.2019.11.073

Goto, K., and Beneragama, C. K. (2010). Circadian clocks and antiaging: do non-aging microalgae like Euglena reveal anything? *Ageing Res. Rev.* 9, 91–100. doi: 10.1016/j.arr.2009.09.003

Guo, Q., Bi, D., Wu, M., Yu, B., Hu, L., Liu, C., et al. (2020). Immune activation of murine RAW264.7 macrophages by sonicated and alkalized paramylon

from *Euglena gracilis*. *BMC Microbiol.* 20:171. doi: 10.1186/s12866-020-01782-y

Halter, D., Casiot, C., Heipieper, H. J., Plewniak, F., Marchal, M., Simon, S., et al. (2012). Surface properties and intracellular speciation revealed an original adaptive mechanism to arsenic in the acid mine drainage bio-indicator Euglena mutabilis. *Appl. Microbiol. Biotechnol.* 93, 1735–1744. doi: 10.1007/s00253-011-3493-y

Harris, E. H. (2009). *The Chlamydomonas Sourcebook: Introduction to Chlamydomonas and Its Laboratory Use,* 2nd Edn. San Diego, CA: Academic Press, 119–158, 267–274

Ishikawa, T., Tamaki, S., Maruta, T., and Shigeoka, S. (2017). Biochemistry and physiology of reactive oxygen species in Euglena. *Adv. Experi. Med. Biol.* 979, 47–64. doi: 10.1007/978-3-319-54910-1_4

Ivusic, F., and Santek, B. (2015). Optimization of complex medium composition for heterotrophic cultivation of *Euglena gracilis* and paramylon production. *Bioprocess Biosyst. Eng.* 38, 1103–1112. doi: 10.1007/s00449-015-1353-3

Johnson, C. H., Ivanisevic, J., and Siuzdak, G. (2016). Metabolomics: beyond biomarkers and towards mechanisms. *Nat. Rev. Mol. Cell Biol.* 17:451. doi: 10.1038/nrm.2016.25

Khatiwada, B., Hasan, M. T., Sun, A., Kamath, K. S., Mirzaei, M., Sunna, A., et al. (2020). Probing the role of the chloroplasts in heavy metal tolerance and accumulation in *Euglena gracilis*. *Microorganisms* 8:115. doi: 10.3390/microorganisms8010115

Lee, M.-C., Park, J. C., and Lee, J.-S. (2018). Effects of environmental stressors on lipid metabolism in aquatic invertebrates. *Aquatic Toxicol.* 200, 83–92. doi: 10.1016/j.aquatox.2018.04.016

Leonardi, R., and Jackowski, S. (2007). Biosynthesis of pantothenic acid and coenzyme A. *Ecosal Plus* 2:4. doi: 10.1128/ecosal.3.6.3.4

Levedahl, B. H. (1966). Heterotrophic CO2 fixation by a bleached Euglena. *Exp. Cell Res.* 44, 393–402. doi: 10.1016/0014-4827(66)90445-9

Libik-Konieczny, M., Kuzniak, E., Surówka, E., Slesak, I., Nosek, M, and Miszalski, Z. (2019). Crassulacean acid metabolism and its role in plant acclimatization to abiotic stresses and defence against pathogens. *Prog. Botany* 81, 277–306. doi: 10.1007/124_2019_33

Limami, A. M., Glévarec, G., Ricoult, C., Cliquet, J. B., and Planchet, E. (2008). Concerted modulation of alanine and glutamate metabolism in young Medicago truncatula seedlings under hypoxic stress. *J. Exp. Bot.* 59, 2325–2335. doi: 10.1093/jxb/ern102

Linnane, A. W., and Stewart, P. R. (1967). The inhibition of chlorophyll formation in Euglena by antibiotics which inhibit bacterial and mitochondrial protein synthesis. *Biochem. Biophys. Res. Commun.* 27, 511–516. doi: 10.1016/S0006-291X(67)80016-0

Lu, S., Wang, J., Niu, Y., Yang, J., Zhou, J., and Yuan, Y. (2012). Metabolic profiling reveals growth related FAME productivity and quality of Chlorella sorokiniana with different inoculum sizes. *Biotechnol. Bioeng.* 109, 1651–1662. doi: 10.1002/bit.24447

Mangalam, A., Poisson, L., Nemutlu, E., Datta, I., and Giri, S. (2013). Profile of circulatory metabolites in a relapsing-remitting animal model of multiple sclerosis using global metabolomics. *J. Clin. Cell. Immunol.* 4, 1–12. doi: 10.4172/2155-9899.1000150

Mendoza-Cozatl, D., Devars, S., Loza-Tavera, H., and Moreno-Sánchez, R. (2002). Cadmium accumulation in the chloroplast of *Euglena gracilis*. *Physiol. Plant.* 115, 276–283. doi: 10.1034/j.1399-3054.2002.1150214.x

Moreno-Sánchez, R., Rodríguez-Enríquez, S., Jasso-Chávez, R., Saavedra, E., and García-García, J. D. (2017). Biochemistry and physiology of heavy metal resistance and accumulation in euglena. *Adv. Exp. Med. Biol.* 979, 91–121. doi: 10.1007/978-3-319-54910-1_6

Mukaida, S., Ogawa, T., Ohishi, K., Tanizawa, Y., Ohta, D., and Arita, M. (2016). The effect of rapamycin on biodiesel-producing protist *Euglena gracilis*. *Biosci. Biotechnol. Biochem.* 80, 1223–1229. doi: 10.1080/09168451.2016.1141040

Nakazawa, M., Hayashi, R., Takenaka, S., Inui, H., Ishikawa, T., Ueda, M., et al. (2017). Physiological functions of pyruvate:NADP+ oxidoreductase and 2-oxoglutarate decarboxylase in *Euglena gracilis* under aerobic and anaerobic conditions. *Biosci. Biotechnol. Biochem.* 81, 1386–1393. doi: 10.1080/09168451.2017.1318696

Pallardy, S. G. (2008). *Physiology of Woody Plants.* Academic Pr.

Park, S. G., Schimmel, P., and Kim, S. (2008). Aminoacyl tRNA synthetases and their connections to disease. *Proc. Nat. Acad. Sci. U.S.A.* 105, 11043–11049. doi: 10.1073/pnas.0802862105

Pavlík, M., Zemanová, V., Pavlíková, D., Kyjaková, P., and Hlavsa, T. (2017). Regulation of odd-numbered fatty acid content plays an important part in the metabolism of the hyperaccumulator *Noccaea* spp. adapted to oxidative stress. *J. Plant Physiol.* 208, 94–101. doi: 10.1016/j.jplph.2016.09.014

Peccia, J., Haznedaroglu, B., Gutierrez, J., and Zimmerman, J. B. (2013). Nitrogen supply is an important driver of sustainable microalgae biofuel production. *Trends Biotechnol.* 31, 134–138. doi: 10.1016/j.tibtech.2013.01.010

Periannan, A. (2003). Quantitative estimation of ebastine in formulations by HPTLC. Planar chromatography. *JPC* 2:16. doi: 10.1556/JPC.16.2003.2.16

Regnault, A., Piton, F., and Calvayrac, R. (1990). Growth, proteins and chlorophyll in Euglena adapted to various C/N balances. *Phytochemistry* 29, 3711–3715. doi: 10.1016/0031-9422(90)85318-A

Richter, P. R., Liu, Y., An, Y., Li, X., Nasir, A., Strauch, S. M., et al. (2015). Amino acids as possible alternative nitrogen source for growth of *Euglena gracilis* Z in life support systems. *Life Sci. Space Res.* 4:1. doi: 10.1016/j.lssr.2014.11.001

Rocchetta, I., Mazzuca, M., Conforti, V., Balzaretti, V., and Molina, M. D. C. R.D. (2012). Chromium induced stress conditions in heterotrophic and auxotrophic strains of *Euglena gracilis*. *Ecotoxicol. Environ. Saf.* 84, 147–154. doi: 10.1016/j.ecoenv.2012.07.020

Rodriguez-Zavala, J. S., Garcia-Garcia, J. D., Ortiz-Cruz, M. A., and Moreno-Sanchez, R. (2007). Molecular mechanisms of resistance to heavy metals in the protist *Euglena gracilis*. *J. Environ. Sci. Health Part A Toxic.* 42, 1365–1378. doi: 10.1080/10934520701480326

Salama, E. S., Kim, H. C., Abou-Shanab, R. A. I., Ji, M. K., Oh, Y. K., Kim, S. H., et al. (2013). Biomass, lipid content, and fatty acid composition of freshwater Chlamydomonas mexicana and Scenedesmus obliquus grown under salt stress. *Bioprocess Biosyst. Eng.* 36, 827–833. doi: 10.1007/s00449-013-0919-1

Schwarzhans, J. P., Cholewa, D., Grimm, P., Beshay, U., Risse, J. M., Friehs, K., et al. (2015). Dependency of the fatty acid composition of *Euglena gracilis* on growth phase and culture conditions. *J. Appl. Phycol.* 27, 1389–1399. doi: 10.1007/s10811-014-0458-4

Shao, Q., Jiang, Y., Lei, A., Hu, Z., and Wang, J. (2018). Advances in genetic transformation techniques of Euglena. *Acta Hydrobiol. Sinica.* 42, 207–214. doi: 10.7541/2018.081

Shepherd, J., and Ibba, M. (2013). Direction of aminoacylated transfer RNAs into antibiotic synthesis and peptidoglycan-mediated antibiotic resistance. *FEBS Lett.* 587, 2895–2904. doi: 10.1016/j.febslet.2013.07.036

Smith, C. A., Want, E. J., O'Maille, G., Abagyan, R., and Siuzdak, G. (2006). XCMS: processing mass spectrometry data for metabolite profiling using nonlinear peak alignment, matching, and identification. *Anal. Chem.* 78, 779–787. doi: 10.1021/ac051437y

Smith, E. F. (2009). *Physiology of Woody Plants*. San Diego, CA: Academic Press. doi: 10.1016/B978-0-12-370873-1.00044-7

Su, Y., Wang, J., Shi, M., Niu, X., and Zhang, W. (2014). Metabolomic and network analysis of astaxanthin-producing Haematococcus pluvialis under various stress conditions. *Bioresour. Technol.* 170, 522–529. doi: 10.1016/j.biortech.2014.08.018

Sugiyama, A., Suzuki, K., Mitra, S., Arashida, R., Yoshida, E., Nakano, R., et al. (2009). Hepatoprotective effects of paramylon, a β-1, 3-D-glucan isolated from *Euglena gracilis* Z, on acute liver injury induced by carbon tetrachloride in rats. *J. Vet. Med. Sci.* 71, 885–890. doi: 10.1292/jvms.71.885

Sui, X., Niu, X., Shi, M., Pei, G., Li, J., Chen, L., et al. (2014). Metabolomic analysis reveals mechanism of antioxidant butylated hydroxyanisole on lipid accumulation in *Crypthecodinium cohnii*. *J. Agricult. Food Chem.* 62, 12477–12484. doi: 10.1021/jf503671m

Takahashi, A., Shibata, N., Nishikawa, S., Ohnishi, K., Ishioka, N., and Ohnishi, T. (2006). UV-B light induces an adaptive response to UV-C exposure via photoreactivation activity in *Euglena gracilis*. *Photochem. Photobiol. Sci. Offi. J. Eur. Photochem. Assoc.* 5, 467–471. doi: 10.1039/b601971d

Takeyama, H., Kanamaru, A., Yoshino, Y., Kakuta, H., and Matsunaga, T. (2015). Production of antioxidant vitamins, beta-carotene, vitamin C, and vitamin E, by two-step culture of *Euglena gracilis* Z. *Biotechnol. Bioeng.* 53:185–190. doi: 10.1002/(SICI)1097-0290(19970120)53:2<185::AID-BIT8>3.0.CO;2-K

Tallima, H., and El Ridi, R. (2018). Arachidonic acid: physiological roles and potential health benefits - A review. *J. Adv. Res.* 11, 33–41. doi: 10.1016/j.jare.2017.11.004

Tanno, Y., Kato, S., Takahashi, S., Tamaki, S., and Shinomura, T. (2020). Light dependent accumulation of β-carotene enhances photo-acclimation of *Euglena gracilis*. *J. Photochem. Photobiol. B. Biol.* 209:111950. doi: 10.1016/j.jphotobiol.2020.111950

Tevatia, R., Allen, J., Rudrappa, D., White, D., Clemente, T. E., Cerutti, H., et al. (2015). The taurine biosynthetic pathway of microalgae. *Algal Res.* 9, 21–26. doi: 10.1016/j.algal.2015.02.012

Tevatia, R., Payne, S., Allen, J., White, D., and Blum, P. (2019). A synthetic cdo/csad taurine pathway in the green unicellular alga *Chlamydomonas reinhardtii*. *Algal Res.* 40:101491. doi: 10.1016/j.algal.2019.101491

Tossavainen, M., Ilyass, U., Ollilainen, V., Valkonen, K., and Romantschuk, M. (2019). Influence of long term nitrogen limitation on lipid, protein and pigment production of *Euglena gracilis* in photoheterotrophic cultures. *PeerJ* 7:6624. doi: 10.7717/peerj.6624

Wan, Q. L., Meng, X., Fu, X., Chen, B., Yang, J., Yang, H., et al. (2019). Intermediate metabolites of the pyrimidine metabolism pathway extend the lifespan of *C. elegans* through regulating reproductive signals. *Aging* 11:102033. doi: 10.18632/aging.102033

Wang, J., Zhang, X., Shi, M., Gao, L., Niu, X., Te, R., et al. (2014). Metabolomic analysis of the salt-sensitive mutants reveals changes in amino acid and fatty acid composition important to long-term salt stress in *Synechocystis* sp. PCC 6803. *Funct. Integrat. Genomics* 14, 431–440. doi: 10.1007/s10142-014-0370-7

Watanabe, M., and Suzuki, T. (2002). Involvement of reactive oxygen stress in cadmium-induced cellular damage in *Euglena gracilis*. *Compar. Biochem. Physiol. Toxicol. Pharmacol. Cbp* 131, 491–500. doi: 10.1016/S1532-0456(02)00036-4

Watanabe, S., Matsumoto, M., Hakomori, Y., Takagi, H., Shimada, H., and Sakamoto, A. (2014). The purine metabolite allantoin enhances abiotic stress tolerance through synergistic activation of abscisic acid metabolism. *Plant Cell Environ.* 37, 1022–1036. doi: 10.1111/pce.12218

Xia, J., Sinelnikov, I. V., Han, B., and Wishart, D. S. (2015). MetaboAnalyst 3.0-making metabolomics more meaningful. *Nucleic Acids Res.* 43, 251–257. doi: 10.1093/nar/gkv380

Yang, L., Chen, J., Qin, S., Zeng, M., and Wang, J. (2018). Growth and lipid accumulation by different nutrients in the microalga *Chlamydomonas reinhardtii*. *Biotechnol. Biofuels*. 11:40. doi: 10.1186/s13068-018-1041-z

Yanming, W., Tuulikki, S. N. L., Heiko, R., Wiebe, M. G., and Adrianna, I. (2018). *Euglena gracilis* growth and cell composition under different temperature, light and trophic conditions. *PLoS ONE*. 13:e0195329. doi: 10.1371/journal.pone.0195329

Zakryś, B., Milanowski, R., and Karnkowska, A. (2017). Evolutionary origin of Euglena. *Oxygen Transport Tissue*. 979, 3–17. doi: 10.1007/978-3-319-54910-1_1

Zhang, T., Zhang, S., Chen, L., Ding, H., Wu, P., Zhang, G., et al. (2020). UHPLC-MS/MS-Based nontargeted metabolomics analysis reveals biomarkers related to the freshness of chilled chicken. *Foods* 9:1326. doi: 10.3390/foods9091326

Zhou, Z., Sun, B., Nie, A., Yu, D., and Bian, M. (2020). Roles of Aminoacyl-tRNA synthetases in cancer. *Front. Cell Dev. Biol.* 8:599765. doi: 10.3389/fcell.2020.599765

Conflict of Interest: The authors declare that the research was conducted in the absence of any commercial or financial relationships that could be construed as a potential conflict of interest.

frontiers in Bioengineering and Biotechnology

ORIGINAL RESEARCH
published: 25 October 2021
doi: 10.3389/fbioe.2021.650178

Transcription Factors From *Haematococcus pluvialis* Involved in the Regulation of Astaxanthin Biosynthesis Under High Light-Sodium Acetate Stress

Chaogang Wang[1,2], Kunpeng Wang[1,2], Jingjing Ning[1,2], Qiulan Luo[3], Yi Yang[4], Danqiong Huang[1,2] and Hui Li[1,2]*

[1] Shenzhen Key Laboratory of Marine Bioresource and Eco-Environmental Science, College of Life Sciences and Oceanography, Shenzhen University, Shenzhen, China, [2] Guangdong Technology Research Center for Marine Algal Bioengineering, College of Life Sciences and Oceanography, Shenzhen University, Shenzhen, China, [3] School of Life Science and Food Engineering, Hanshan Normal University, Chaozhou, China, [4] Department of Biochemistry and Molecular Biology, Health Sciences Center of Shenzhen University, Shenzhen, China

OPEN ACCESS

Edited by:
Chengwei Liang, Qingdao University of Science and Technology, China

Reviewed by:
Zhengquan Gao, Shandong University of Technology, China
Changhong Yao, Sichuan University, China

***Correspondence:**
Chaogang Wang
charlesw@szu.edu.cn

Specialty section:
This article was submitted to Bioprocess Engineering, a section of the journal Frontiers in Bioengineering and Biotechnology

Received: *06 January 2021*
Accepted: *06 May 2021*
Published: *25 October 2021*

Citation:
Wang C, Wang K, Ning J, Luo Q, Yang Y, Huang D and Li H (2021) Transcription Factors From Haematococcus pluvialis Involved in the Regulation of Astaxanthin Biosynthesis Under High Light-Sodium Acetate Stress. Front. Bioeng. Biotechnol. 9:650178. doi: 10.3389/fbioe.2021.650178

The microalgae *Haematococcus pluvialis* attracts attention for its ability to accumulate astaxanthin up to its 4% dry weight under stress conditions, such as high light, salt stress, and nitrogen starvation. Previous researches indicated that the regulation of astaxanthin synthesis might happen at the transcriptional level. However, the transcription regulatory mechanism of astaxanthin synthesis is still unknown in *H. pluvialis*. Lacking studies on transcription factors (TFs) further hindered from discovering this mechanism. Hence, the transcriptome analysis of *H. pluvialis* under the high light-sodium acetate stress for 1.5 h was performed in this study, aiming to discover TFs and the regulation on astaxanthin synthesis. In total, 83,869 unigenes were obtained and annotated based on seven databases, including NR, NT, Kyoto Encyclopedia of Genes and Genomes Orthology, SwissProt, Pfam, Eukaryotic Orthologous Groups, and Gene Ontology. Moreover, 476 TFs belonging to 52 families were annotated by blasting against the PlantTFDB database. By comparing with the control group, 4,367 differentially expressed genes composing of 2,050 upregulated unigenes and 2,317 downregulated unigenes were identified. Most of them were involved in metabolic process, catalytic activity, single-organism process, single-organism cellular process, and single-organism metabolic process. Among them, 28 upregulated TFs and 41 downregulated TFs belonging to 27 TF families were found. The transcription analysis showed that TFs had different transcription modules responding to the high light and sodium acetate stress. Interestingly, six TFs belonging to MYB, MYB_related, NF-YC, Nin-like, and C3H families were found to be involved in the transcription regulation of 27 astaxanthin synthesis-related genes according to the regulatory network. Moreover, these TFs might affect astaxanthin synthesis by directly regulating *CrtO*, showing that *CrtO* was the hub gene in astaxanthin synthesis. The present study provided new insight into a global view of TFs and their correlations to astaxanthin synthesis in *H. pluvialis*.

Keywords: *Haematococcus pluvialis*, transcription factor, astaxanthin biosynthesis, regulatory network, high light-sodium acetate stress

INTRODUCTION

Haematococcus pluvialis, which belonged to Chlorophata, Chlorophyceae, Volvocales, and Haematococcaceae, was paid close attention to its ability to accumulate astaxanthin up to its 4% cellular dry weight. Under favorite environment, *Haematococcus* cells is a green cell swimming with its flagellum, while generating a thick cell wall and produce astaxanthin under stress conditions, such as high light, salt stress, and nitrogen starvation (Lemoine and Schoefs, 2010; Shah et al., 2016; Zhao et al., 2020). However, the regulatory mechanism of astaxanthin biosynthesis causing by abiotic stresses is still unknown.

Previous researches showed that *H. pluvialis* accumulated huge astaxanthin under high light and sodium acetate stresses, with the observation that the transcription activity of genes related to astaxanthin biosynthesis increased quickly (Huang et al., 2006; Raman et al., 2008). As well known, light is the most important contributor to microalgae growth. Normally, the light intensity suitable for growth is 25–50 50 μmol m^{-2} $s^{-1,}$ and it would cause the accumulation of astaxanthin when more than 100 100 μmol m^{-2} s^{-1} depending on the light tolerance of different *H. pluvialis* strains (Steinbrenner and Linden, 2001; Steinbrenner and Linden, 2003; Su et al., 2014). The sodium acetate was also noticed because it helped the growth of *H. pluvialis* and improved the cell density. Specially, sodium acetate has been reported to contribute to the accumulation of astaxanthin under high light (He et al., 2018; Jeon et al., 2006). The transcription levels of astaxanthin synthesis-related genes were improved to accelerate the astaxanthin synthesis under environmental stresses. According to previous reports, astaxanthin biosynthesis in *H. pluvialis* started from isopentenyl pyrophosphate, gradually formed phytoene, β-carotene, and then finally produced astaxanthin by β-carotene hydroxylase and β-carotene ketolase (Lemoine and Schoefs, 2010; Uri et al., 2019). Increasing astaxanthin yield under stresses, astaxanthin biosynthesis-related enzymes such as phytoene synthase (PSY), phytoene desaturase (PDS), zeta-carotene desaturase (ZDS), beta-carotene ketolase (BKT), and beta-carotene hydroxylase (crtR-B) transcribed at a high level within 24 h, suggesting that the regulation of astaxanthin synthesis might happen at the transcriptional level (Steinbrenner and Linden, 2003; Lu et al., 2010; Gao et al., 2012a; Wen et al., 2015).

Responses to stresses in the plant could be achieved by the complex signal transduction, including the expression of transcription factors (TFs), promoter binding, and the regulation of functional genes. Hence, transcriptional regulation was closely related to the function of TFs and the *cis*-acting elements in the promoter. Till now, the research on the correlation between TFs and astaxanthin synthesis is still blank, although a lot of transcriptome data were published. The *cis*-acting elements in the *CrtO*, *BKT* promoter were obtained, including ABA, ABRE, C-repeat/DRE, G-box, MeJA-responsive element, and MBS (Meng et al., 2005; Gao et al., 2010; Wang et al., 2012). In addition, a little achievement was made when 59 TFs belonging to MYB, bHLH, bZIP, and C2H2 families were identified when treated with salicylic acid or jasmonic acid, suggesting that TFs might involve in hormone stress (Gao et al., 2015). A lot of research focused on astaxanthin biosynthesis and lipid biosynthesis but overlooked the function of TFs, leading to the failure of exposing the regulatory mechanism of astaxanthin biosynthesis.

In this study, *H. pluvialis* under high light-sodium acetate (HLS) stress was chosen to proceed with transcriptome analysis. Fortunately, many TFs were found at the early stage of HLS stress so that we could study the response patterns and the internal connection between TFs and astaxanthin biosynthesis-related genes. Totally, 83,869 unigenes were identified, among which 476 unigenes were annotated as TFs. After that, 69 differentially expressed transcription factors (DETFs) were obtained, and their transcription profiles of high light and sodium acetate stress responses were studied. Results revealed that their expression was changed along with different stresses. In addition, we finally constructed a TF–astaxanthin biosynthesis regulatory network obtaining six important TFs that might directly modulate key genes of astaxanthin biosynthesis, based on a combined analysis of DETFs, expression trends, and the analysis of the transcription factor binding site (TFBS). This is the first report to take a look inside the correlations between TFs and astaxanthin biosynthesis-related genes *via* gene expression trends and TFBS. Results in this study would not only help us understand the response of TFs to environmental stresses but also provide a new way to obtain key TFs involved in the modulation of astaxanthin biosynthesis.

MATERIALS AND METHODS

Algal Strains and Culture Conditions

Haematococcus pluvialis strain 192.80 was purchased from Sammlung von Algenkulturen Göttingen Culture Collection of Algae. It was cultured in MIX medium, with a 12:12-h light/dark cycle at 22°C (Luo et al., 2017). The light intensity for normal culture was 25 μmol m^{-2} s^{-1} while 550 μmol m^{-2} s^{-1} for the high light stress (HL). The final concentration of sodium acetate was 45 μM for the sodium acetate stress (HS). The alga was cultured until the cell concentration reached 4–5 × 10^5 cells/ml and then treated with HLS stress. *H. pluvialis* cells were treated with a light intensity of 550 μmol m^{-2} s^{-1} and 45-μM sodium acetate for HLS. Also, the *H. pluvialis* cells under a light intensity of 25 μmol m^{-2} s^{-1} were the control group.

Microscopy Observation of Algal Cells

Algal cells were treated with HLS stress when the cell concentration reached 4–5 × 10^5 cells/ml. After sampling at 0, 0.5, 1, 1.5, 2, 2.5, 3, 4, 5, 6, 7, 8, 9, 10, 11, and 12 h, the alga cells were observed using an Olympus BX61 microscope and an Olympus DP10 digital camera.

Total RNA Extraction and Quality Control

Total RNA was extracted according to the modified RNA isolation methods (Luo et al., 2017). The RNA quality and

quantity were checked by 1% agarose gel and spectrophotometer NanoDrop (BioPhotometer, Eppendorf, Hamburg, Germany).

Complementary DNA Library Construction and Transcriptome Sequencing

The eukaryotic messenger RNA was enriched with Oligo (dT) magnetic beads and then added with a fragmentation buffer. Random hexamers were used to finish single-stranded complementary DNA (cDNA) synthesis, deoxyribonucleotide triphosphates, and DNA polymerase I, and RNase H was then added to synthesize the second-strand cDNA. AMPure XP beads purified those fragments. After amplification by polymerase chain reaction (PCR), the products were purified by AMPure XP beads to construct the final cDNA library. Qubit2.0 was used to dilute the cDNA concentration to 1.5 ng/μl. Then, the insert size was checked with Agilent 2100. After that, the effective concentration of the cDNA library was accurately quantified by the quantitative PCR method, making sure that the effective concentration of 2 nM was reached. Finally, transcriptome sequencing was performed by Illumina HiSeq^{TM} (Illumina, Santiago, CA, United States). The transcriptome data has been uploaded to the National Center for Biotechnology Information (NCBI) website (accession number: SRR6816386).

Sequence Assembly and Gene Annotation

The assembled sequences were annotated with several protein databases, including NR (NCBI non-redundant protein sequences), NT (NCBI nucleotide sequences), Kyoto Encyclopedia of Genes and Genomes (KEGG) Ortholog (KO), SwissProt (a manually annotated and reviewed protein sequence database), Pfam (protein family), Eukaryotic Orthologous Groups (clusters of orthologous groups of proteins) (KOG), and Gene Ontology (GO). Cufflinks and HTSeq package in 2010 were used to calculate the fragments per kilobase of transcript, per million mapped reads value and read counts of each gene, respectively. Also, the differentially expressed genes (DEGs) were identified using the DEGSeq, with p-adjust < 0.05 and $|\log_2 FC| >= 1$ setting as the threshold to indicate significant differential expression.

Annotation and Classification of Transcription Factors

All the unigenes, including known genes and new genes, were blasted against plantTFDB[1] database to obtain TF data. Those TFs were classified according to the information in plantTFDB.

Validation of Gene Expression by Real-Time Quantitative Reverse Transcription Polymerase Chain Reaction

Haematococcus pluvialis cells were cultured until cell numbers reached 4–5 × 10^5 cells/ml, then treated with a light intensity of 25 μmol m^{-2} s^{-1} as control, 550 μmol m^{-2} s^{-1} as high light (HL), 25 μmol m^{-2} s^{-1} plus 45-mM sodium acetate as sodium acetate stress (HS), and 550 μmol m^{-2} s^{-1} plus 45-mM sodium acetate as HLS stress. The real-time quantitative reverse transcription (qRT)-PCR was performed using an SYBR Premix Ex Taq^{TM} II Kit (TaKaRa, Tokyo, Japan) in a 20-μl reaction system containing 10-μl 2 × SYBR Premix Ex Taq^{TM} II (TaKaRa, Tokyo, Japan), 0.8 μl each of the forward and reverse primers, 2-μl cDNA, 0.4-μl 50 × ROX Reference Dye, and 6-μl double distilled water. Reaction steps followed the program: 95°C for 30 s, followed by 40 cycles of 95°C for 5 s, 55°C for 31 s, and reading the fluorescence signal. Each qRT-PCR reaction was performed with three biological replicates. β-actin of *H. pluvialis* was used as internal control. All primers were designed by the Primer Premier 5.0 and are listed in **Supplementary Table 1**. The relative transcription level was calculated using the $2^{-\Delta\Delta CT}$ method.

Construction of Transcription Factor–Astaxanthin Synthesis Regulatory Network

Obtaining the target genes of TFs and considering the relationship between TFs and their target genes, we could generate the network reflecting the regulation between TFs and their target genes. Firstly, DETFs should obtain as a dataset. Then, DEGs related to astaxanthin synthesis were collected as another dataset. According to the TFBS information in the promoter of astaxanthin synthesis-related genes, we could calculate the correlation between TFs and astaxanthin synthesis-related genes by searching the JASPAR database. Finally, the network between TFs and target genes was obtained.

Statistical Analysis

All experiments were performed with biological triplicates from separate cultures. GraphPad Prism 5 was used for statistical analysis, and P-values of <0.05 were considered statistically significant.

RESULTS

Microscopic Observation and Transcription Analysis of *H. pluvialis* Under High Light-Sodium Acetate Stress

Under the HLS condition, the content of astaxanthin in algal cells was increased with the time course. *H. pluvialis* cells were turned red after HLS stress for 4 h and then the red getting darker along with the extension time of stress treatment (**Figure 1**). The transcription of *HpCrtR-B* and *Hpbkt1* was observed under HLS stress for 0.5 h, suggesting that they could respond to stress quickly. Totally, the expression level of *HpCrtR-B* and *Hpbkt1* was kept increasing, with the exception that their expression was downregulated after stressing for 4–5 h (**Figure 2**). Therefore, samples after 1.5 h stress treatment were selected for transcriptome analysis.

[1] http://planttfdb.cbi.pku.edu.cn/

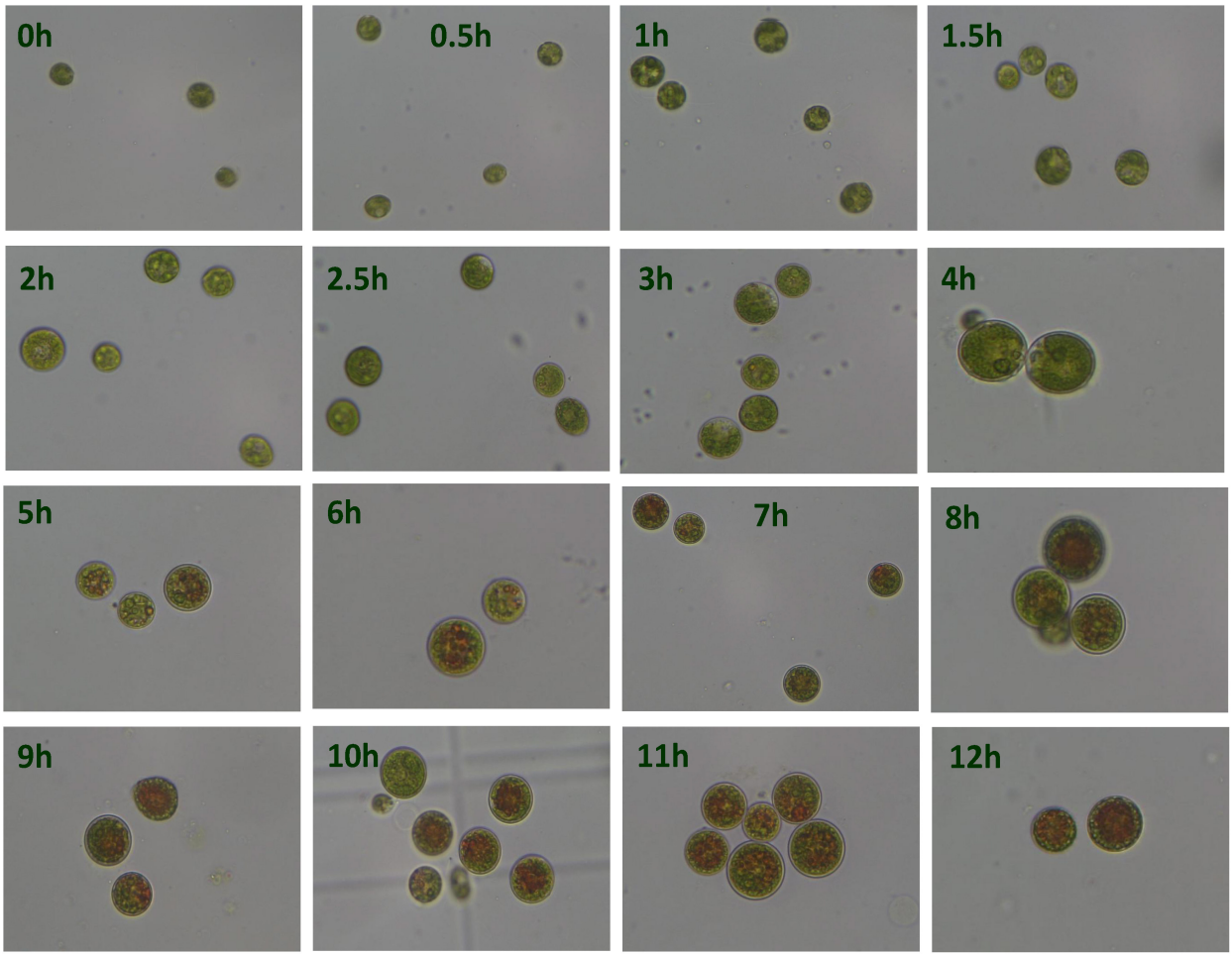

FIGURE 1 | Microscopic observation of *Haematococcus pluvialis* under high light-sodium acetate (HLS) stress.

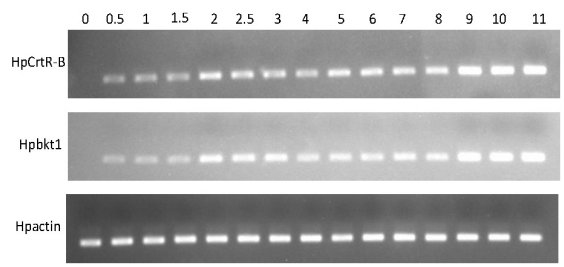

FIGURE 2 | Expression pattern of *HpCrtR-B* and *Hpbkt1* responding to HLS stress.

Transcriptome Sequencing and Assembly

Firstly, total RNA was extracted from *H. pluvialis* treated with HLS stress, and its quality was checked with Nanodrop and 1% agarose gel (**Figure 3**). The A260/280 and A260/230 were more than 2, and the RNA integrity number value was 7.0, showing that the quality of extraction RNA was great to conduct transcriptome sequencing.

Then, total RNA was reverse transcribed to cDNA and proceeded transcriptome sequencing. In total, the quality of Q20 was more than 94%, and the GC content was around 58.16% (**Table 1**). Here, 117,861 transcripts and 83,869 unigenes were obtained, with an average length of 615 and 747 bp, respectively. In unigenes, the N50 and N90 were 1,268 and 292 bp, respectively (**Table 2**).

Gene Annotation

All unigenes were blasted against seven databases, including NR, NT, KO, SwissProt, PFAM, KOG, and GO. As a whole, there were 23,928 unigenes (28.53%) annotated in at least one database; 1,969 unigenes (2.34%) were annotated in all databases. Specifically, 18,177 unigenes (21.67%), 18,162 unigenes (21.65%), 13,464 unigenes (16.05%), 9,931 unigenes (11.84%), 7,154 unigenes (8.52%), 6,158 unigenes (7.34%), and 5,767 unigenes (6.87%) were annotated in PFAM, GO, NR, SwissProt, KOG, KO, and NT, respectively. In addition, *H. pluvialis* shared 32.6% homology with *Volvox carteri* and 25.9% homology

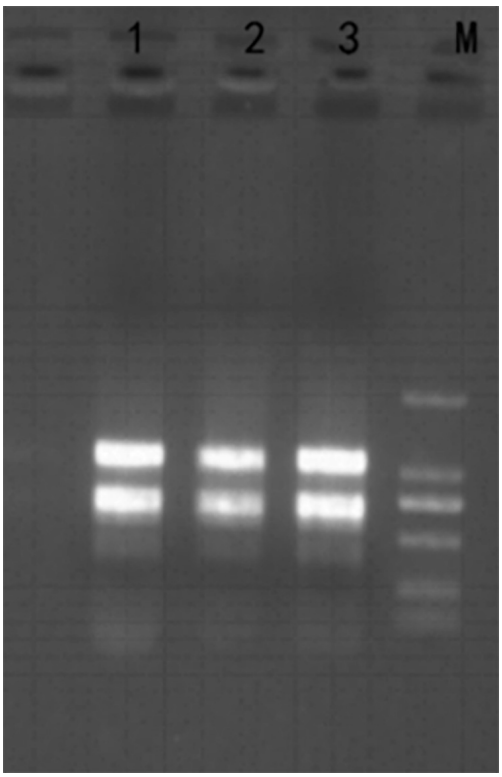

FIGURE 3 | Total RNA from *H. pluvialis* 192.80. Lane M was DL2000 marker, and lanes 1–3 represent three separate samples as replicates.

with *Chlamydomonas reinhardtii* (**Supplementary Figure 1**). A great number of unigenes associated with gene transcription, signal transduction, and TF activity were found in GO, KOG, and KEEG analyses, suggesting that gene transcription was active and TFs might be involved in the response of HLS stress.

Prediction and Classification of Transcription Factors

Transcription factors play a key role in a plant when responding to environmental stresses. However, few references were focused on TFs in *H. pluvialis* and hindered the research of transcriptional regulation to stresses. Hence, to understand their functions in transcriptional regulation, we predicted all the TFs in *H. pluvialis* by blasting against PlantTFDB. Totally, 476 TFs belonging to 52 families were predicted and annotated. According to the searching data, the top five families were C3H (8.6%), SET (8.6%), GNAT (7.98%), SNF2 (7.1%), and MYB (5.9%) (**Table 3**). It is well known that the C3H family is related to the regulation of light and photoperiod. In addition, TF families such as WRSKY, MYB, and AP2-EREBP are generally associated with abiotic stress responses in plants. Here, many TFs were found in *H. pluvialis* during an early stage of HLS stress, which might be related to transcription regulation to the stress response.

Differentially Expressed Genes Under High Light-Sodium Acetate Stress

To find out genes involving in early stress response, unigenes from the control group cultured under normal conditions were compared with that from the treatment group under HLS stress. As expected, results provided that they held 40,275 unigenes as common, whereas the control group had 12,803 different unigenes and the treatment group owned 10,724 different unigenes (**Supplementary Figure 2**). In addition, there were 4,367 DEGs composed of 2,050 upregulated unigenes and 2,317 downregulated unigenes (**Figure 4**).

The GO enrichment analysis showed that GO terms were significantly enriched in the treated group, indicating that the top five terms were metabolic process, catalytic activity, single-organism process, single-organism cellular process, and single-organism metabolic process (**Supplementary Figure 3**). Interestingly, 620 unigenes were involved in the catalytic function, and 12.6% unigenes were related to the binding process of iron and metal ions, showing that enzymatic catalysis

TABLE 1 | List of data output quality.

Sample	Raw Reads	Clean Reads	CleanBases	Error(%)	Q20(%)	Q30(%)	GC Content(%)
HLST1	50385816	47984828	6G	0.03	95.03	90.21	58.09
HLST2	52595368	50248474	6.28G	0.03	95.22	90.55	57.98
HLST3	53089534	50392078	6.3G	0.03	95.32	90.7	58.12
LLMT4	54231624	51614202	6.45G	0.03	95.17	90.38	58.36
LLMT5	62538310	59057482	7.38G	0.03	94.64	89.41	58.3
LLMT6	53201140	50665756	6.33G	0.03	95.06	90.21	58.12

Samples of HLST1, HLST2, and HLST3 were three biological replicates treated with HLS stress for 1.5 h. Samples of LLMT4, LLMT5, and LLMT6 were three biological replicates cultured in normal conditions as controls.

TABLE 2 | Length distribution of transcripts and unigenes.

Transcript length interval	200–500 bp	500–1,000 bp	1,000–2,000 bp	>2,000 bp	Total
Number of transcripts	69,950	22,470	16,350	9,091	117,861
Number of Unigenes	57,664	13,813	7,968	4,424	83,869

TABLE 3 | List of transcription factors (TFs).

Family name	Numbers	Family name	Numbers	Family name	Numbers
ABI3VP1	1	DDT	1	PBF-2-like	1
AP2-EREBP	20	E2F-DP	2	PHD	21
ARID	3	FHA	14	PLATZ	2
ARR-B	1	G2-like	2	RB	1
bHLH	3	GNAT	38	Rcd1-like	1
BSD	3	HB	4	RWP-RK	13
bZIP	17	HMG	9	SBP	9
C2C2-co-like	1	HSF	2	SET	41
C2C2-Dof	1	IWS1	3	Sigma70-like	1
C2C2-GATA	14	Jumonji	16	SNF2	34
C2C2-YABBY	1	LIM	2	SOH1	2
C2H2	22	MBF1	2	SWI/SNF-BAF60b	1
C3H	41	MED6	2	SWI/SNF-SWI3	2
CCAAT	12	MED7	1	TAZ	6
Coactivator p15	2	mTERF	3	TIG	8
CPP	6	MYB	28	TRAF	9
CSD	8	Orphans	34	TUB	2
WRKY	3				

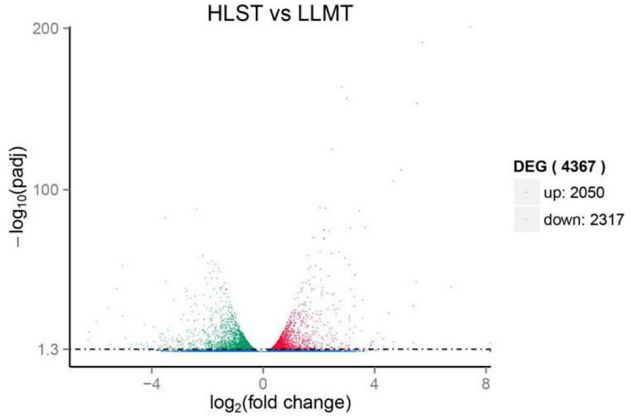

FIGURE 4 | Expression analysis of differentially expressed genes (DEGs). Y-axis represents statistical significance of DEGs. X-axis represents change fold of gene expression. Red and green dots represent upregulated genes and downregulated genes, respectively. Blue dots represent genes with no significant difference in expression level.

and metal ions might play important roles during the early stage of HLS stress. The KEEG enrichment showed that the upregulated DEGs were significantly enriched in KEGG terms. The top five terms were "Protein processing in endoplasmic reticulum," "Proteasome," "Non-alcoholic fatty liver disease," "Plant-pathogen interaction," and "Tuberculosis." As expected, 11 upregulated DEGs were involved in carotenoid biosynthesis, including LUT1, lcyB, crtL1, crtY, ZDS, crtQ, PDS, crtP, crtZ, crtB, and Z-ISO. Moreover, the downregulated DEGs were significantly enriched in KEGG terms of "Purine metabolism," "Pyrimidine metabolism," and "Biosynthesis of amino acids."

Obtainment of Differentially Expressed Transcription Factors

Although TFs played an important role in response to abiotic stresses, researches on transcriptome under stresses did not expose their functions in *H. pluvialis*. Among the 476 TFs, there were 28 upregulated TFs and 41 downregulated TFs when compared with the control group. The DETFs belonged to 27 TF families, such as SET (13%), GNAT (10%), and Orphans (10%) (**Table 4**). Among the upregulated DETFs, GNAT, and Orphans families owned the same numbers as four, whereas SET families had the most as eight among the downregulated DETFs. In addition, TFs from GNAT, MYB, Orphans, PHD, and bZIP families were found in both upregulated and downregulated TFs.

To validate the expression of the DETFs, total RNA was extracted from the *H. pluvialis* under normal culture conditions and HLS stress. A total of 26 DETFs were randomly selected to verify their expression. Most of them were confirmed that the expression of TFs in transcriptome analysis under HLS stress was credible (**Figures 5**, **6**). What attracted our attention was the expression of GNAT3 and HB, showing strong upregulation with more than eightfold, which was not previously reported before.

Transcription Factors Expression Profiles Under High Light Stress and Sodium Acetate Stress

In this research, 476 TFs were found, and 69 DETFs belonging to different TF families were obtained. Among them, TFs related to stress response were chosen for further study, helping us understand their function. Therefore, 14 DETFs were selected to analyze their transcription profiles under HL and HS from 0 to 6 h, respectively. TFs showed different transcription activities

TABLE 4 | Differentially expressed transcription factors (DETFs) and their classification.

	TF family	Numbers		TF family	Numbers
Down-regulated TFs	SET	8	Up-regulated TFs	GNAT	4
	SNF2	5		Orphans	4
	CCAAT	3		C2C2-GATA	2
	GNAT	3		CCAAT	2
	MYB	3		MYB	2
	Orphans	3		RWP-RK	2
	C2C2-GATA	2		TRAF	2
	C3H	2		bHLH	1
	Coactivator p15	2		bZIP	1
	PHD	2		C2C2-co-like	1
	AP2-EREBP	1		C2H2	1
	bZIP	1		CPP	1
	CSD	1		G2-like	1
	E2F-DP	1		HB	1
	MED7	1		MBF	1
	Rcd1-like	1		PHD	1
	Sigma7C0-like	1		SNF	1
	WRKY	1			
Total number		41			28

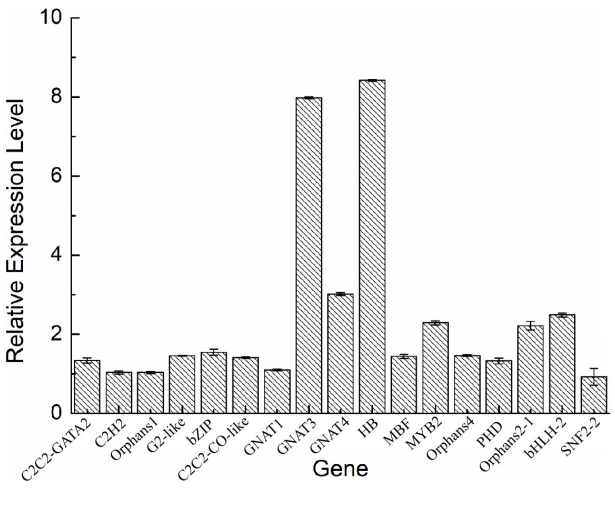

FIGURE 5 | Analysis of upregulated differentially expressed transcription factors (DETFs) by qRT-PCR.

under HL and HS, suggesting that they responded to stresses differentially, which might be due to their varied regulation pattern. In general, results showed that most of TFs were upregulated at the stress condition of HL or HS. TFs such as C2H2, COLIKE, G2like, ORPHANS-1, PHD, and RWP-RK-1 were sensitive to HL, and C2C2GATA, ORPHANS-3, and RWP-RK-2 were positive to HS. ORPHANS-2 could respond to both HL and HS. Interestingly, four TFs of ORPHANS families showed very different transcriptional profiles, in which ORPHANS-1 was positive to HL, ORPHANS-2 was normal sensitive to HL and HS, ORPHANS-3 was positive to HS, and the expression of ORPHANS was negative to HL and HS except that its expression increased 2.6-fold after HL at 1 h. The same appearance was found in RWP-RK families, in which RWP-RK-1 was positive to HL with a 4.2-fold increase, whereas RWP-RK-2 was positive to HS with a 6.5-fold increase (**Figure 7**). Those results implied that TFs could respond to different kinds of stresses, although they were from the same TF families.

Expression of Key Genes Associated With Astaxanthin Synthesis

Haematococcus pluvialis under HLS stress was sampled in 0, 1.5, 3, 6, 9, 12, 24, and 48 h and extracted total RNA to finish transcriptome analysis. Also, 24 key genes related to astaxanthin synthesis were found from transcriptome data. Totally, three *ipi*, four *ggps*, two *psy*, two *pds*, three *zds*, three *lcy*, four *bkt*, one *crtz*, and two *crtR-B* genes were found, and their expression trends showed three expression modes (**Supplementary Table 2**). The first mode included 13 genes (Ch_GLEAN_10009908, XLOC_015032, XLOC_030044, Ch_GLEAN_10009310, XLOC_03954, Ch_GLEAN_10006000, Ch_GLEAN_10011708, Ch_GLEAN_10007045, Ch_GLEAN_10009207, Ch_GLEAN_10010071, Ch_GLEAN_10010036, Ch_GLEAN_10011505, and XLOC_006571), showing their highest transcription level that happened after stress at 1.5 or 3 h. Especially, the transcription of *crtR-B* (Ch_GLEAN_10006000) was increased to 24-fold. The second mode had 11 genes (XLOC_013259, Ch_GLEAN_10007057, XLOC_038901, XLOC_051007, XLOC_048563, XLOC_042543, XLOC_048896, XLOC_048897, Ch_GLEAN_10005232, Ch_GLEAN_10010046, and XLOC_053142), showing that their highest expression level was reached at 24 or 48 h. Among them, the expression of *BKT* (XLOC_038901) and *CRTZ* (Ch_GLEAN_10005232) were upregulated up to 19.6- and 16.07-fold at 24 h, respectively. Moreover, the expression of *IPI* (XLOC_051007) and *PSY* (XLOC_042543 and XLOC_048563)

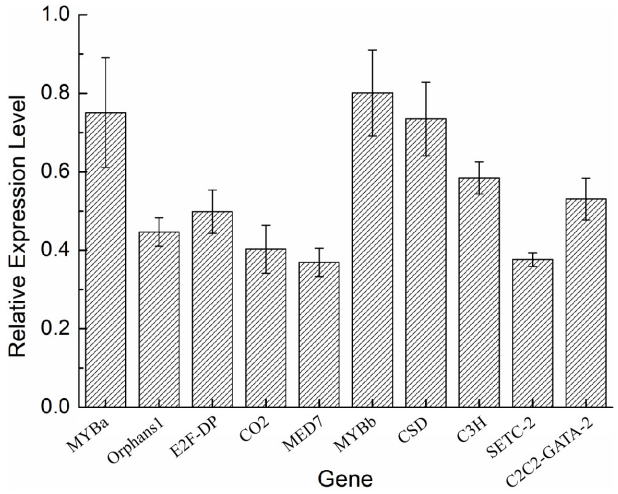

FIGURE 6 | Analysis of downregulated DETFs by quantitative reverse transcription (qRT)-PCR.

were significantly increased at both 3 and 48 h with similar levels (**Figure 8** and **Supplementary Table 3**).

Construction of Transcription Factor–Astaxanthin Synthesis Regulatory Network

It is well known that TFs are usually involved in the regulation of important functional genes to help cells defend against abiotic stresses. However, the correlations between TFs and astaxanthin synthesis have never been reported. Based on the transcriptome data, 27 astaxanthin synthesis-related genes were targeted to six TFs. Hence, both DETFs and astaxanthin synthesis-related genes were taken into consideration with their targeting information to generate a valuable regulatory network (**Figure 9**). According to the regulatory network, six important TFs were found, suggesting that they might be involved in regulating 27 astaxanthin synthesis-related genes. Those TFs belong to MYB, MYB_related, NF-YC, Nin-like, and C3H families, among which there were four upregulated genes and two downregulated genes. Four TFs, including MYB, Nin-like, and C3H, were positive to *CrtO*, whereas two TFs such as MYB_related and NF-YC were negative to *CrtO*. Moreover, all of them could affect other astaxanthin synthesis-related genes by directly regulating *CrtO*, showing that *CrtO* was the hub gene of astaxanthin synthesis. NF-YC could also regulate the expression of CCDs. Furthermore, astaxanthin synthesis-related genes also existed in mutual modulation. For example, most of the astaxanthin synthesis-related genes were positive to each other. Nevertheless, both ZEP and CYP97C1 were negative to *CrtO* and CCDs (**Figure 9**).

DISCUSSION

Haematococcus pluvialis always attracts researchers because of its special ability to accumulate so much astaxanthin in many stress conditions such as high light and high salt (Domínguez-Bocanegra et al., 2004; He et al., 2007; Raman et al., 2008; Lemoine and Schoefs, 2010; Su et al., 2014). Meanwhile, mining genes related with astaxanthin synthesis has succeeded helping us to clarify the synthetic pathway of astaxanthin in *H. pluvialis* (Steinbrenner and Linden, 2001; Lemoine and Schoefs, 2010; Uri et al., 2019). The secrets why *H. pluvialis* can accumulate so much astaxanthin are still unknown, urging us to study more, including transcriptome analysis. All results indicated that improving the transcription level of astaxanthin synthesis-related genes leads to a significant increase of astaxanthin products when treated with many kinds of stresses (Huang et al., 2006; Raman et al., 2008; Gao et al., 2012b; He et al., 2018; Zhao et al., 2020). The regulation of astaxanthin synthesis would happen at the transcriptional level. However, the regulatory mechanism of astaxanthin synthesis at the transcriptional level is still kept unclear, hindering us from further improving astaxanthin production. In recent years, promoters of astaxanthin synthesis-related genes such as *bkt*, *crtO*, and *crtR-B* were isolated, finding that the promoters owned plenty of *cis*-elements including G-box, I-box, AE-box, MBS, and so on (Meng et al., 2005; Gao et al., 2010; Lu et al., 2010; Wang et al., 2012), and could respond to high light and sodium acetate (Wang et al., 2016). However, it is a pity that the research on TFs binding to these *cis*-elements made little progress.

To construct the regulatory network including astaxanthin synthesis-related genes and TFs, we tried to obtain dataset and expression trends of TFs and astaxanthin synthesis-related genes from the *H. pluvialis* transcriptome data treated with HLS stress for 1.5 h. Many research showed that the transcriptional of astaxanthin synthesis-related genes and astaxanthin production kept increasing under many kinds of stresses (Raman et al., 2008; Gao et al., 2012a; Wen et al., 2015). In these cases, the transcription of astaxanthin synthesis-related genes such as *psy*, *pds*, *bkt*, and *chy* could significantly increase after stressed for 4–8 h (Steinbrenner and Linden, 2001, 2003; Gao et al., 2012a). In this research, the transcription of astaxanthin synthesis-key genes such as *bkt* and *crtR-B* could be observed after stress for 0.5 h and notably increased after 2.5 h, although astaxanthin accumulation was detected at 4 h. Hence, we believed that their transcriptional regulation would have happened in an early stage of stress. Finally, 476 TFs belonging to 59 TF families were found in the transcriptome data of *H. pluvialis* under HLS stress for 1.5 h, indicating that a large number of TFs involved in the transcriptional regulation and stress response at an early stage of stress. This is the first report providing the largest TFs in the amount and variety in *H. pluvialis*.

Transcriptome data of our research found a great number of genes involving in cell process, metabolic process, single-organism process, catalytic activity, and binding, with active metabolite synthesis and inactive protein synthesis. DEGs mainly enriched in metabolic process, catalytic activity, single-organism process, single-organism cellular process, and single-organism metabolic process, which is similar to previous reports (Gao et al., 2012a, 2015; Li et al., 2017; He et al., 2018). It was no doubt that the most concerned synthetic pathway was carotenoid synthesis, and results showed that most of the upregulated DEGs

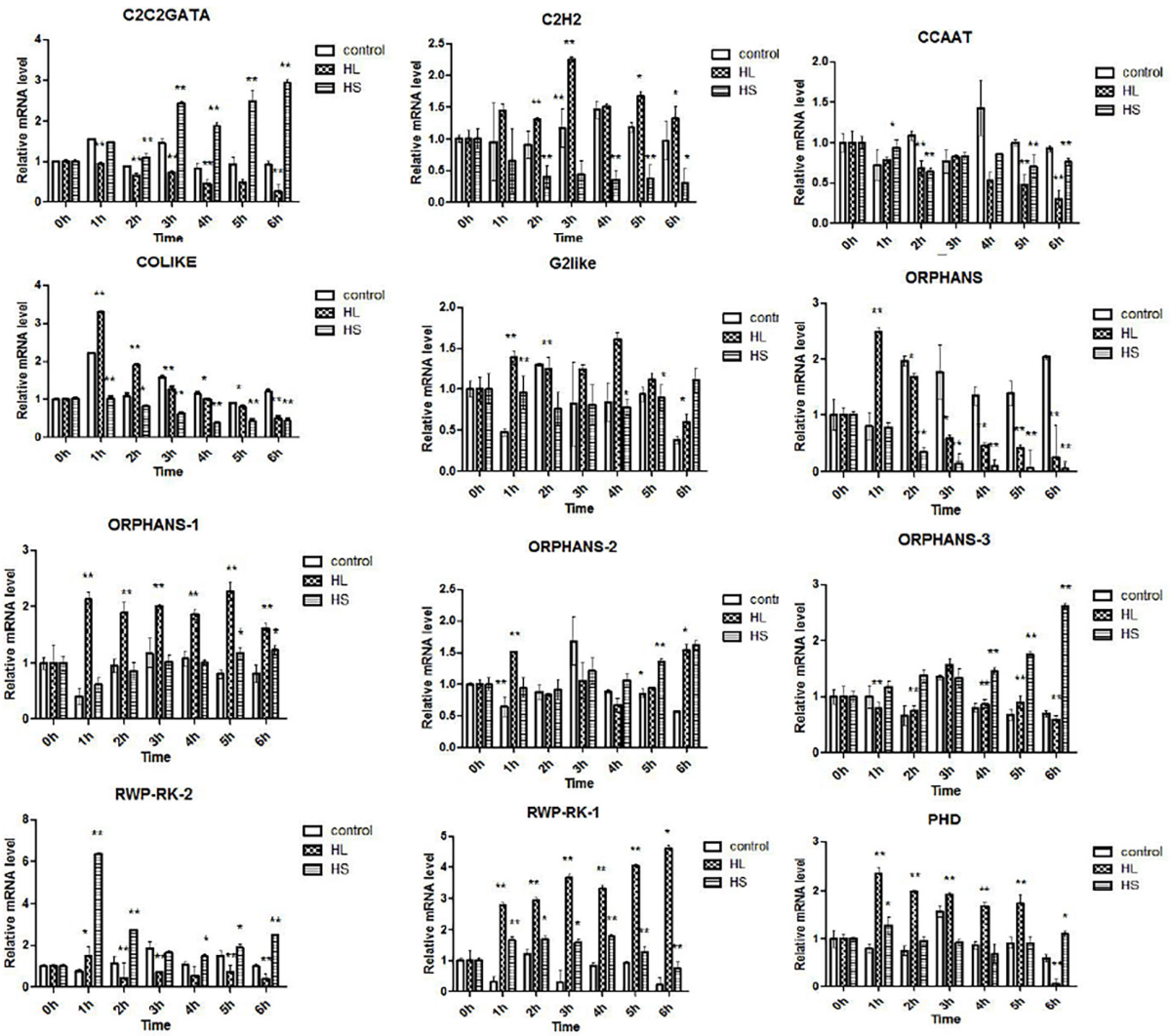

FIGURE 7 | Transcription profiles of transcription factors (TFs) under high light and sodium acetate stress. Control represents control group, HL represents high light stress, and HS represents sodium acetate stress. *Indicates significant difference at level of 0.05, and **indicates significant difference at level of 0.01.

were involved in lipid substances and carotenoid biosynthesis, whereas the downregulated DEGs were significantly enriched in DNA replication and photosynthesis. Moreover, our results provided more details indicating that astaxanthin synthesis-related genes were distributed into three expression trends with the transcription peak at 1.5–3, 24–48 h, or two peaks at 1.5–3 and 24–48 h. To understand the regulatory mechanism of astaxanthin synthesis in *H. pluvialis*, we should pay more attention to the time point of 1.5–3 and 24–48 h, which would be the important time point for regulation under HLS stress. Although so much transcriptome data were reported to study the correlation between astaxanthin synthesis and fatty acid synthesis and the transcriptional profiles of genes associated with them (He et al., 2018), little research on the transcription regulation was reported, especially the important TFs. Indeed, only 59 TFs could not support systematic analysis on the correlation between TFs and astaxanthin synthesis, which lead to no report until now (Gao et al., 2015). As we knew, TFs play important roles in responding to environmental stresses so that their expression is also affected by stresses. Previous research showed that *H. pluvialis* could respond to different environmental stresses by increasing the transcription activity of astaxanthin synthesis-related genes (Huang et al., 2006; Raman et al., 2008). As showed in our results, the transcription activity of TFs such as C2H2, COLIKE, G2like, ORPHANS, and PHD significantly improved under HL or HS. Interestingly, our results also indicated that TFs showed very different transcription profiles under HL or HS, although they were from the same TF families. For example, four TFs from ORPHANS showed very different transcriptional profiles, in which ORPHANS-1 was positive to HL, ORPHANS-2 was normal sensitive to HL and HS, and ORPHANS-3 was positive to HS, whereas the ORPHANS

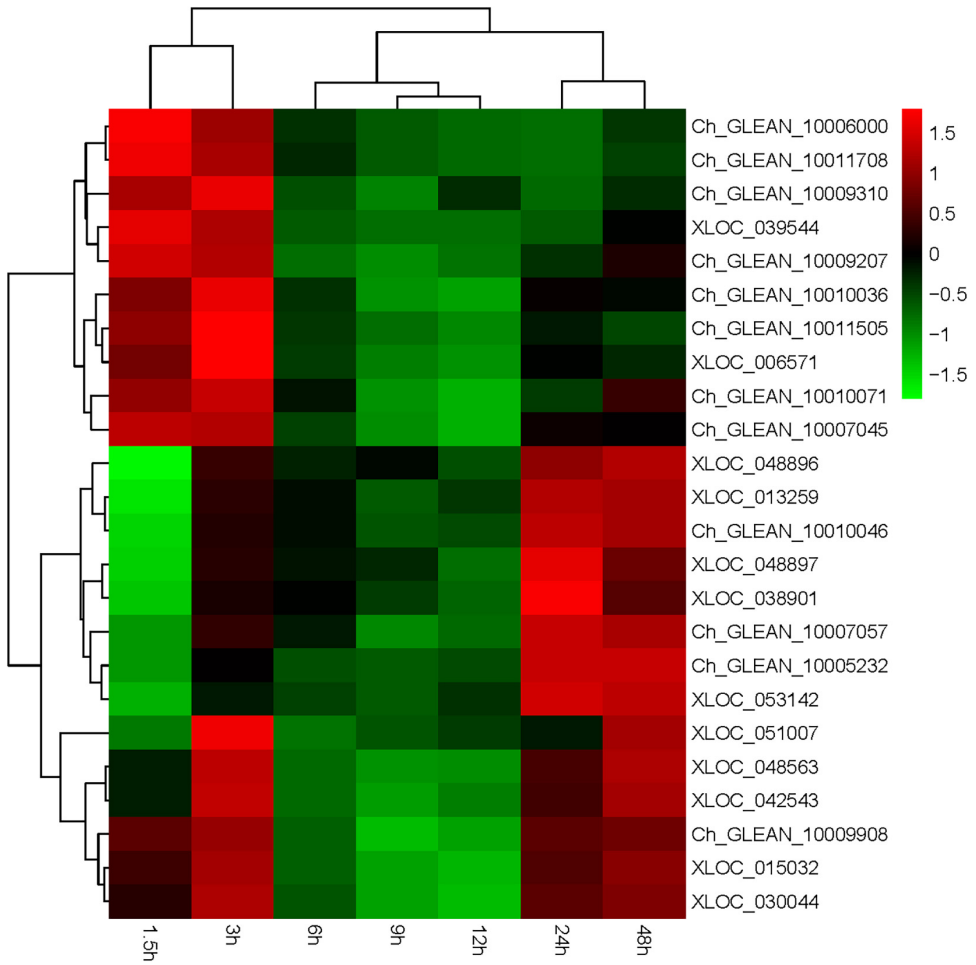

FIGURE 8 | Expression of astaxanthin synthesis-related genes from 0 to 48 h.

was negative to HL and HS. These phenomena might explain why *H. pluvialis* quickly responded to different environmental stresses. In addition, the TFs found in this research have not been reported elsewhere. So, further clarifying their functions would surely contribute to the study on the stress response mechanism of *H. pluvialis*.

In the present study, it was gratifying that up to 476 TFs and 79 DETFs were found from the *H. pluvialis* at the early stage of stress, providing the possibility to explore the correlation between TFs and astaxanthin synthesis. By constructing co-expression regulatory networks, we could find the important functional genes and identify hub genes in expression regulatory networks (Hollender et al., 2014; Zhao et al., 2018). Here, the TF–astaxanthin synthesis regulatory network pointed out that TFs modulated astaxanthin synthesis at the transcriptional level by regulating the transcription of *CrtO*, indicating that *CrtO* was at the core of astaxanthin synthesis, which is evidenced by many references proposing that β-carotene ketolase was the key enzyme in astaxanthin synthesis (Lemoine and Schoefs, 2010; Uri et al., 2019). In addition, six important TFs were involved in regulating astaxanthin synthesis-related genes, among which four TFs were positive, whereas two TFs were negative, showing that their regulation was multidimensional at the transcriptional level. Research on plant TFs confirmed that MYB TFs involved in plant stress resistance and flavonoid synthesis could bind to the MBS *cis*-element in the promoter, which was found in astaxanthin synthesis-related genes with high frequency (Meng et al., 2005; Gao et al., 2010; Wang et al., 2012). Also, the TFs of NF-YC, Nin-like, and C3H were also involved in drought stress and salt stress. Interestingly, we noticed that ZEP and CYP97C were negative to astaxanthin synthesis by affecting *CrtO* and CCDs. ZEP could convert zeaxanthin to violaxanthin, which would further produce abscisate so that downregulation of ZEP was observed in many kinds of abiotic stresses (Gao et al., 2015; He et al., 2018). Therefore, inhibiting ZEP expression might improve astaxanthin production. However, CYP97C1 was reported to be upregulated under high light and downregulated under SA and JA stresses (Gao et al., 2015; He et al., 2018). So, further researches might conduct to classify the role of CYP97C1. Hence, our findings provide a new clue on the astaxanthin synthesis.

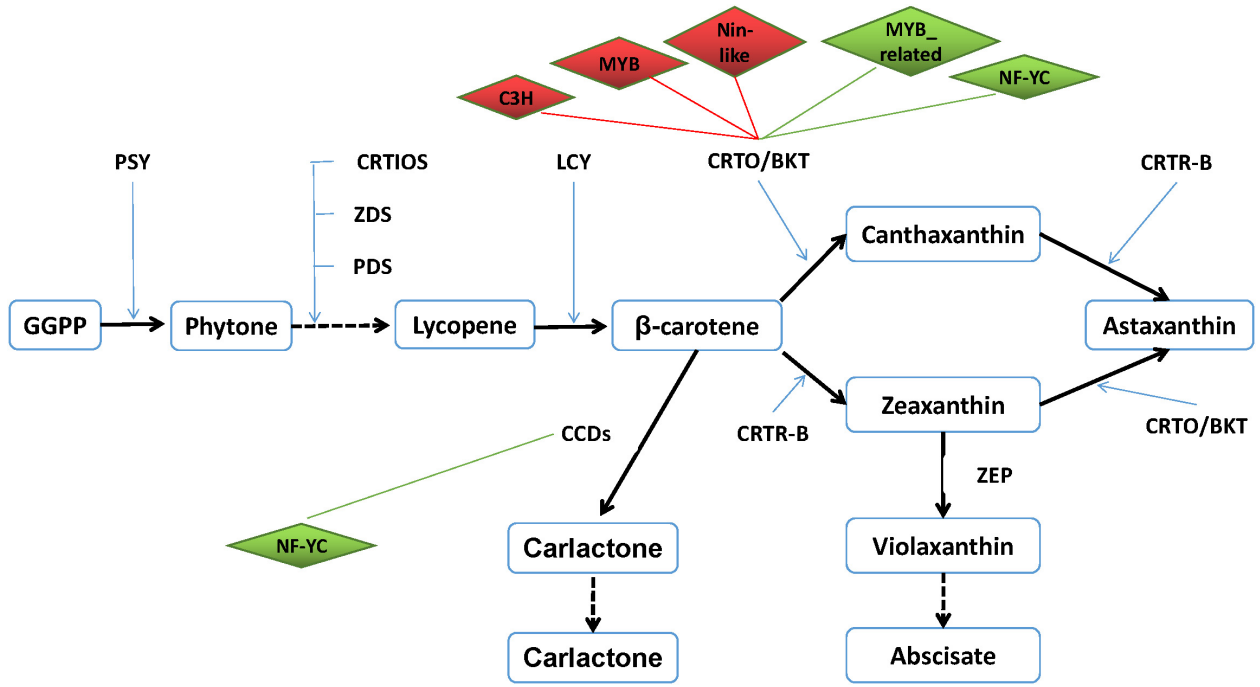

FIGURE 9 | Transcription factor–astaxanthin synthesis regulatory network. Diamond represents transcription factor. Upregulated TF is marked in red, whereas downregulated TF is in green. Rectangle represents astaxanthin synthesis-related gene. Line in red means their relationship is positive, whereas line in green means their relationship is negative.

The present studies provided the TF dataset of *H. pluvialis*, helping us to make clear the TF function in responding to environmental stresses. By constructing the TF–astaxanthin synthesis regulatory network, we could obtain their correlations and find important TFs involved in the transcription regulation under HLS stress, providing a theoretical foundation for artificial control of astaxanthin synthesis.

CONCLUSION

In conclusion, our transcriptome data found 83,869 unigenes, among which there were 4,367 DEGs composed of 2,050 upregulated unigenes and 2,317 downregulated unigenes in *H. pluvialis* under HLS stress for 1.5 h. Most of DEGs were involved in metabolic process, catalytic activity, single-organism process, single-organism cellular process, and single-organism metabolic process at the early stage of stress. In addition, 476 TFs belonging to 52 families were identified and 69 DETFs including 28 upregulated TFs and 41 downregulated TFs. The TFs such as C2H2, COLIKE, and others showed different transcription profiles under HL or HS during 6 h, showing that they were involved in response to the environmental stresses during the early stage of stress. Finally, there were six TFs belonging to MYB, MYB_related, NF-YC, Nin-like, and C3H families that might be involved in the transcription regulation of 27 astaxanthin synthesis-related genes. Moreover, four TFs, including MYB, Nin-like, and C3H were positive to *CrtO*, whereas two TFs such as MYB_related and NF-YC were negative to *CrtO*. In brief, these TFs could affect astaxanthin synthesis by directly regulating *CrtO*. The present study provides new insight into the global view of TFs and their correlations with astaxanthin synthesis in *H. pluvialis*.

DATA AVAILABILITY STATEMENT

The data presented in the study are deposited in the NCBI repository, accession number SRR6816386.

AUTHOR CONTRIBUTIONS

KW and JN performed the experiments. KW, JN, QL, and CW collected the data and carried out all the analyses. CW and YY initiated the preparation of the manuscript. CW and HL conceptualized the idea and revised the manuscript. All authors have read and approved the final manuscript.

FUNDING

This work was supported financially by the National Key Research and Development Plan Special Project for Synthetic

Biology (2018YFA0902500), the National Natural Science Foundation of China (31972815 and 31470389), Guangdong Natural Science Foundation (2019A1515011701), and the Shenzhen Scientific Project (JCYJ201908081142 16058).

SUPPLEMENTARY MATERIAL

The Supplementary Material for this article can be found online at: https://www.frontiersin.org/articles/10.3389/fbioe.2021.650178/full#supplementary-material

REFERENCES

Domínguez-Bocanegra, A. R., Legarreta, I. G., Jeronimo, F. M., and Campocosioet, A. T. (2004). Influence of environmental and nutritional factors in the production of astaxanthin from Haematococcus pluvialis. *Bioresour. Technol.* 92, 209–214. doi: 10.1016/j.biortech.2003.04.001

Gao, Z., Li, Y., Wu, G., Li, G., Sun, H., Deng, S., et al. (2015). Transcriptome analysis in Haematococcus pluvialis: astaxanthin induction by salicylic acid (SA) and jasmonic acid (JA). *PLoS One* 10:e0140609. doi: 10.1371/journal.pone.0140609

Gao, Z. Q., Meng, C. X., and Ye, N. H. (2010). Three 5-flanking regions of crtO encoding – carotene oxygenase in Haematococcus pluvialis. *Bull. Mar. Sci.* 12, 59–64.

Gao, Z. Q., Meng, C. X., Zhang, X. W., Xu, D., Miao, X. X., Wang, Y. T., et al. (2012a). Induction of salicylic acid (SA) on transcriptional expression of eight carotenoid genes and astaxanthin accumulation in Haematococcus pluvialis. *Enzyme Microb. Technol.* 51, 225–230. doi: 10.1016/j.enzmictec.2012.07.001

Gao, Z. Q., Meng, C. X., Zhang, X. W., Xu, D., Zhao, Y. F., Wang, Y. T., et al. (2012b). Differential expression of carotenogenic genes, associated changes on astaxanthin production and photosynthesis features induced by JA in H. pluvialis. *PLoS One* 7:e42243. doi: 10.1371/journal.pone.0042243

He, B. G., Hou, L. L., Dong, M. M., Shi, J. W., Huang, X. Y., Ding, Y. T., et al. (2018). Transcriptome analysis in Haematococcus pluvialis: astaxanthin induction by high light with acetate and Fe2+. *Int. J. Mol. Sci.* 19:175. doi: 10.3390/ijms19010175

He, P., Duncan, J., and Barber, J. (2007). Astaxanthin accumulation in the green alga Haematococcus pluvialis: effects of cultivation parameters. *J. Integr. Plant Biol.* 49, 447–451. doi: 10.1111/j.1744-7909.2007.00468.x

Hollender, C. A., Kang, C., Darwish, O., Geretz, A., Matthews, B. F., Slovin, J., et al. (2014). Floral transcriptomes in woodland strawberry uncover developing receptacle and anther gene networks. *Plant Physiol.* 165, 1062–1075. doi: 10.1104/pp.114.237529

Huang, J. C., Chen, F., and Sandmann, G. (2006). Stress-related differential expression of multiple beta-carotene ketolase genes in the unicellular green alga Haematococcus pluvialis. *J. Biotechnol.* 122, 176–185. doi: 10.1016/j.jbiotec.2005.09.002

Jeon, Y. C., Cho, C. W., and Yun, Y. S. (2006). Combined effects of light intensity and acetate concentration on the growth of unicellular microalga Haematococcus pluvialis. *Enzyme Microb. Technol.* 39, 490–495. doi: 10.1016/j.enzmictec.2005.12.021

Lemoine, Y., and Schoefs, B. (2010). Secondary ketocarotenoid astaxanthin biosynthesis in algae: a multifunctional response to stress. *Photosynth. Res.* 106, 155–177. doi: 10.1007/s11120-010-9583-3

Li, K., Cheng, J., Lu, H. X., Yang, W. J., Zhou, J. H., and Cen, K. F. (2017). Transcriptome-based analysis on carbon metabolism of Haematococcus pluvialis mutant under 15% CO2. *Bioresour. Technol.* 233, 313–321. doi: 10.1016/j.biortech.2017.02.121

Lu, Y. D., Peng, J., Liu, S. F., Gan, Q., Cui, H., and Song, Q. (2010). Methyl jasmonate- or gibberellins A3-induced astaxanthin accumulation is associated with up-regulation of transcription of β-carotene ketolase genes (bkts) in microalga Haematococcus pluvialis. *Bioresour. Technol.* 101, 6468–6474. doi: 10.1016/j.biortech.2010.03.072

Luo, Q. L., Wang, K. P., Xiao, K., Wang, C. G., and Hu, Z. L. (2017). A rapid and high-quality method for total rna isolation from Haematococcus pluvialis. *Genet. Mol. Res.* 16:gmr16029614. doi: 10.4238/gmr16029614

Meng, C. X., Teng, C. Y., Jiang, P., Qin, S., and Tseng, C. K. (2005). Cloning and characterization of β-carotene ketolase gene promoter in Haematococcus pluvialis. *Acta Biochem. Biophys. Sin.* 37, 270–275. doi: 10.1111/j.1745-7270.2005.00033.x

Raman, V., Lakshmanan, V., Ravi, S., and Gokare, A. R. (2008). Regulation of carotenoid biosynthetic genes expression and carotenoid accumulation in the green alga Haematococcus pluvialis under nutrient stress conditions. *J. Exp. Bot.* 59, 1409–1418. doi: 10.1093/jxb/ern048

Shah, M. M. R., Liang, Y., Cheng, J. J., and Daroch, M. (2016). Astaxanthin-producing green microalga Haematococcus pluvialis: from single cell to high value commercial products. *Front. Plant Sci.* 7:531. doi: 10.3389/fpls.2016.00531

Steinbrenner, J., and Linden, H. (2001). Regulation of two carotenoid biosynthesis genes coding for phytoene synthase and carotenoid hydroxylase during stress-induced astaxanthin formation in the green alga Haematococcus pluvialis. *Plant Physiol.* 125, 810–817. doi: 10.1104/pp.125.2.810

Steinbrenner, J., and Linden, H. (2003). Light induction of carotenoid biosynthesis genes in the green alga Haematococcus pluvialis : regulation by photosynthetic redox control. *Plant Mol. Biol.* 52, 343–356. doi: 10.1023/A:1023948929665

Su, Y. X., Wang, J. X., Shi, M. L., Niu, X. F., Yu, X. H., Gao, L. J., et al. (2014). Metabolomic and network analysis of astaxanthin-producing Haematococcus pluvialis under various stress conditions. *Bioresour. Technol.* 170, 522–529. doi: 10.1016/j.biortech.2014.08.018

Uri, P., Aliza, Z., Sammy, B., and Lital, D. (2019). A hypothesis about the origin of carotenoid lipid droplets in the green algae Dunaliella and Haematococcus. *Planta* 249, 31–47. doi: 10.1007/s00425-018-3050-3

Wang, C. G., Hu, Z. L., Zhao, C. N., and Mao, X. M. (2012). Isolation of the β-carotene ketolase gene promoter from Haematococcus pluvialis and expression of ble in transgenic Chlamydomonas. *J. Appl. Phycol.* 24, 1303–1310. doi: 10.1007/s10811-011-9781-1

Wang, C. G., Peng, X., Wang, J., Lei, A., Li, H., and Hu, Z. (2016). A β-carotene ketolase gene (bkt1) promoter regulated by sodium acetate and light in a model green microalga Chlamydomonas reinhardtii. *Algal Res.* 20, 61–69. doi: 10.1016/j.algal.2016.09.020

Wen, Z., Liu, Z., Hou, Y., Liu, C., Gao, F., Zheng, Y., et al. (2015). Ethanol induced astaxanthin accumulation and transcriptional expression of carotenogenic genes in Haematococcus pluvialis. *Enzyme Microb. Technol.* 78, 10–17. doi: 10.1016/j.enzmictec.2015.06.010

Zhao, X., Li, C., Wan, S., Zhang, T., and Shan, S. (2018). Transcriptomic analysis and discovery of genes in the response of arachis hypogaea to drought stress. *Mol. Biol. Rep.* 45, 119–131. doi: 10.1007/s11033-018-4145-4

Zhao, Y., Hou, Y. Y., Chai, W. J., Liu, Z. Y., Wang, X., He, C. Q., et al. (2020). Transcriptome analysis of Haematococcus pluvialis of multiple defensive systems against nitrogen starvation. *Enzyme Microb. Tech.* 134:109487. doi: 10.1016/j.enzmictec.2019.109487

Conflict of Interest: The authors declare that the research was conducted in the absence of any commercial or financial relationships that could be construed as a potential conflict of interest.

Publisher's Note: All claims expressed in this article are solely those of the authors and do not necessarily represent those of their affiliated organizations, or those of the publisher, the editors and the reviewers. Any product that may be evaluated in this article, or claim that may be made by its manufacturer, is not guaranteed or endorsed by the publisher.

Advantages of publishing in Frontiers

OPEN ACCESS
Articles are free to read for greatest visibility and readership

FAST PUBLICATION
Around 90 days from submission to decision

HIGH QUALITY PEER-REVIEW
Rigorous, collaborative, and constructive peer-review

TRANSPARENT PEER-REVIEW
Editors and reviewers acknowledged by name on published articles

Frontiers
Avenue du Tribunal-Fédéral 34
1005 Lausanne | Switzerland

Visit us: www.frontiersin.org
Contact us: frontiersin.org/about/contact

REPRODUCIBILITY OF RESEARCH
Support open data and methods to enhance research reproducibility

DIGITAL PUBLISHING
Articles designed for optimal readership across devices

FOLLOW US
@frontiersin

IMPACT METRICS
Advanced article metrics track visibility across digital media

EXTENSIVE PROMOTION
Marketing and promotion of impactful research

LOOP RESEARCH NETWORK
Our network increases your article's readership